Midwest States' Regional Pooled Fund Research Program
Fiscal Year 2006-2007 (Year 17)
Research Project Number SPR-3 (017)
NDOR Sponsoring Agency Code RPFP-07-03

PERFORMANCE LIMITS FOR 152-MM (6-IN.) HIGH CURBS PLACED IN ADVANCE OF THE MGS USING MASH-08 VEHICLES PART I: VEHICLE-CURB TESTING AND LS-DYNA ANALYSIS

Submitted by

Ling Zhu, M.S.E.M.
Graduate Research Assistant

Ronald K. Faller, PhD., P.E.
Research Assistant Professor

John D. Reid, Ph.D.
Professor

Dean L. Sicking, PhD., P.E.
MwRSF Director and Professor

Robert W. Bielenberg, M.S.M.E., E.I.T.
Research Associate Engineer

Karla A. Lechtenberg, M.S.M.E, E.I.T.
Research Associate Engineer

Christopher D. Benner
Former Undergraduate Research Assistant

MIDWEST ROADSIDE SAFETY FACILITY
University of Nebraska-Lincoln
527 Nebraska Hall
Lincoln, Nebraska 68588-0529
(402) 472-0965

Submitted to

MIDWEST STATES' REGIONAL POOLED FUND PROGRAM
Nebraska Department of Roads
1500 Nebraska Highway 2
Lincoln, Nebraska 68502

MwRSF Research Report No. TRP-03-205-09

May 6, 2009

TECHNICAL REPORT DOCUMENTATION PAGE

1. Report No. TRP-03-205-09	2.	3. Recipient's Accession No.	
4. Title and Subtitle Performance Limits for 152-mm (6-in.) High Curbs Placed in Advance of the MGS using MASH-08 Vehicles Part I: Vehicle-Curb Testing and LS-DYNA Analysis		5. Report Date May 6, 2009 6.	
7. Author(s) Zhu, L., Reid, J.D., Faller, R.K., Sicking, D.L., Bielenberg, R.W., Lechtenberg, K.A., and Benner, C.D.		8. Performing Organization Report No. TRP-03-205-09	
9. Performing Organization Name and Address Midwest Roadside Safety Facility (MwRSF) University of Nebraska-Lincoln 527 Nebraska Hall Lincoln, Nebraska 68588-0529		10. Project/Task/Work Unit No. 11. Contract © or Grant (G) No. SPR-3(017)	
12. Sponsoring Organization Name and Address Midwest States' Regional Pooled Fund Program Nebraska Department of Roads 1500 Nebraska Highway 2 Lincoln, Nebraska 68502		13. Type of Report and Period Covered Final Report 2006-2009 14. Sponsoring Agency Code RPFP-07-03	
15. Supplementary Notes Prepared in cooperation with U.S. Department of Transportation, Federal Highway Administration			
16. Abstract (Limit: 200 words) Although curbs have been discouraged on high-speed roads based on previous research, the use of curbs is often required for certain situations. There exists a need to examine the use of curbs in conjunction with the Midwest Guardrail System (MGS) in order to determine effective curb placement guidelines. Four vehicle crash tests were performed to investigate vehicle behaviors after traversing a 152-mm (6-in.) AASHTO Type B curb. Two tests with 2270P pickup trucks, one test with the 1100C passenger car, and one test with the 2000P pickup truck, were performed. All of the vehicles were tested at a target speed of 100 km/h (62.1 mph) and at a target angle of 25 degrees. Test data was collected by both low- and high-speed video cameras and transducers. An analysis was performed on vehicle trajectories with respect to the MGS height to determine the critical lateral offset locations for further investigation within the curb-MGS combination study. .			
17. Document Analysis/Descriptors Highway Safety, Roadside Appurtenances, Longitudinal Barriers, Guardrail, MGS, Curb, MASH-08, Crash Test, Compliance Test		18. Availability Statement No restrictions. Document available from: National Technical Information Services, Springfield, Virginia 22161	
19. Security Class (this report) Unclassified	20. Security Class (this page) Unclassified	21. No. of Pages 207	22. Price

SPECIAL EXECUTIVE SUMMARY

Year 17 Project No. RPFP-07-03

Performance Limits for 6-inch (152-mm) High Curbs Placed in Advance of the MGS Using 350 Update (MASH-08) Vehicles

In the Spring of 2008, the members of the Midwest Pooled Fund Program requested a change in project scope. That change is summarized in this Special Executive Summary and is not contained in the following report. The report itself documents the work completed on the project up until the occurrence for the change in scope. However, the report does contain the details used to justify the recommendations given in this summary.

In a letter dated April 28, 2008, the Midwest Roadside Safety Facility (MwRSF) sought additional guidance from Pooled Fund Program members on the following three issues.

1. What test level should be used in this crash testing program?
2. Is barrier placement more common 0.15 to 1.22 m (½ to 4 ft) or 1.22 to 2.44 m (4 to 8 ft) behind a curb?
3. Are both 0.15 to 1.22 m (½ to 4 ft) and 1.22 to 2.44 m (4 to 8 ft) placement ranges important?

All respondents favored using the TL-3 criteria and only one respondent indicated that the 0 to 4 ft (1.22 m) offset was more important than 1.22 to 2.44 m (4 to 8 ft) offset. Further, two-thirds of the responding states indicated that there was no need for placement in the 0.15 to 1.22 m (½ to 4 ft) offset range.

Based upon this input, MwRSF proposed several changes in the scope of this project. Recall that the original research objective was to develop general guidelines for the safe placement of the MGS behind a 152-mm (6-in.) high, AASHTO Type B curb. The new objective will be to determine if the MGS can be safely placed between 1.22 to 2.44 m (4 and 8 feet) from the face of a curb.

Full-scale vehicle crash testing and computer simulations of vehicle-to-curb impacts clearly showed that when a guardrail was placed 1.22 m (4 ft) or more behind a curb, vehicle override was the primary concern. Testing and simulation also indicated that the risk of vehicle override increased as the barrier was placed farther from the curb and as the size and height of the impacting vehicle was increased. Therefore, the critical test used to verify the safety performance of guardrail installed between 1.22 to 2.44 m (4 and 8 feet) behind a curb involved a 2270P vehicle impacting an MGS placed 2.44 m (8 feet) behind the face of a curb. Modeling has shown that the MGS must be mounted 787 mm (31 in.) above the ground or 940 mm (37 in.) above the pavement surface in order to maximize the potential for the barrier to capture a vehicle under these impact conditions. It is proposed that this crash test be conducted to determine if the MGS can safely contain a vehicle impacting under these critical conditions.

If the MGS proves to be capable of containing the 2270P vehicle under all of these critical impact conditions, then the only remaining concern will be the potential for a small car to under-ride the MGS when installed 1.22 m (4 feet) behind the curb. Full-scale vehicle crash testing of a small car impacting a curb has shown that, at this location, the small car's front bumper is near its normal height relative to the surrounding terrain and is moving upward. Therefore, it can be concluded that the small car would have little chance of underriding the MGS when installed 1.22 meters (4 feet) behind the curb and mounted 787 mm (31 in.) above the surrounding terrain. Provided that the 2270P test is successful, it may be possible to use the results of the full-scale vehicle-to-curb impact testing to garner FHWA approval for using the MGS placed 1.22 to 2.44 m (4 to 8 ft) behind the curb. The MwRSF will therefore request FHWA approval using the MGS in this range, provided the first full-scale crash test is successful. If the full-scale crash test fails or FHWA does not accept the noted arguments, the

MwRSF will seek further input from the Pooled Fund Program members. If FHWA approves our request, existing funds will be more than sufficient to complete the project.

MwRSF sought and obtained Pooled Fund approval of this revised crash testing plan.

ORIGINAL ABSTRACT OF *CRITICAL OFFSET OF THE MIDWEST GUARDRAIL SYSTEM BEHIND A CURB* (M.S. THESIS OF LING ZHU)

Although curbs are discouraged on high-speed roads because of their potential to cause drivers to lose control in a crash and to cause the errant vehicle to vault or underride any barrier behind the curb, the use of curbs is often required for certain situations. A need exists to examine the use of curbs in conjunction with the Midwest Guardrail System (MGS) in order to determine effective curb placement guidelines.

Among the curbs that could possibly be used in combination with the guardrail, the 152-mm (6-in.) high, AASHTO Type B curb is believed to present the worst impact scenario. Few physical test data of the vehicle-to-curb impact event have been previously performed and thus, four vehicle crash tests were performed to investigate vehicle behaviors after hitting a 152-mm (6-in.) AASHTO Type B curb. Two tests with 2270P pickup trucks, one with an 1100C passenger car, and one with a 2000P pickup truck, were performed. All of the vehicles were tested at a speed of 100 km/h (62.1 mph) and at an angle of 25 degrees.

Nonlinear finite element simulation was performed to replicate the 2000P pickup test. Evaluation of the pickup was conducted to assist the MGS-Curb project and to identify the weaknesses in the model. Results of simulation showed the current 2000P model can accurately predict the vehicle's trajectory within 2.24 m (7.35 ft) behind the curb.

Investigation of vehicle and W-beam guardrail interaction was performed to determine the critical override/underride impact scenario of the MGS. It was concluded that the MGS can capture the pickup when the top edge of the pickup bumper is lower than the top hump of MGS.

Then, analysis was performed on vehicle trajectories with respect to the MGS height to determine the critical offset locations. A safe installation offset range was summarized and

recommends two different MGS installation options. LS-DYNA simulations were performed to verify the results from the trajectory analysis.

DISCLAIMER STATEMENT

This report was funded in part through grant[s] from the Federal Highway Administration [and Federal Transit Administration], U.S. Department of Transportation. The contents of this report reflect the views and opinions of the authors who are responsible for the facts and the accuracy of the data presented herein. The contents do not necessarily reflect the official views or policies of the state highway departments participating in the Midwest States' Regional Pooled Fund Program nor the Federal Highway Administration, U.S. Department of Transportation. This report does not constitute a standard, specification, regulation, product endorsement, or an endorsement of manufacturers.

ACKNOWLDGEMENTS

The authors wish to acknowledge several sources that made a contribution to this project: (1) the Midwest States' Regional Pooled Fund Program funded by the Connecticut Department of Transportation, Illinois Department of Transportation, Iowa Department of Transportation, Kansas Department of Transportation, Minnesota Department of Transportation, Missouri Department of Transportation, Nebraska Department of Roads, Ohio Department of Transportation, South Dakota Department of Transportation, Wisconsin Department of Transportation, and Wyoming Department of Transportation for sponsoring this project; and (2) MwRSF personnel for constructing the barriers and conducting the crash tests.

Acknowledgment is also given to the following individuals who contributed to the completion of this research project.

Midwest Roadside Safety Facility

D.L. Sicking, Ph.D., P.E., Professor and MwRSF Director
J.R. Rohde Ph.D., P.E., Associate Professor
J.C. Holloway, M.S.C.E., E.I.T., Research Manager
S.K. Rosenbaugh, M.S.C.E., E.I.T., Research Associate Engineer
C.L. Meyer, B.S.M.E., E.I.T., Research Engineer II
A.T. Russell, B.S.B.A., Laboratory Mechanic II
K.L. Krenk, B.S.M.A, Field Operations Manager
A.T. McMaster, Laboratory Mechanic I
Undergraduate and Graduate Research Assistants

Connecticut Department of Transportation

Dionysia Oliveira, Transportation Engineer 3

Illinois Department of Transportation

David Piper, P.E., Highway Policy Engineer

Iowa Department of Transportation

David Little, P.E., Assistant District Engineer
Deanna Maifield, P.E., Methods Engineer
Chris Poole, P.E., Litigation/Roadside Safety Engineer

Kansas Department of Transportation

Ron Seitz, P.E., Bureau Chief
Rod Lacy, P.E., Assistant Bureau Chief
Scott King, P.E., Road Design Leader

Minnesota Department of Transportation

Michael Elle, P.E., Design Standard Engineer

Missouri Department of Transportation

Joseph G. Jones, P.E., Engineering Policy Administrator

Nebraska Department of Roads

Amy Starr, P.E., Research Engineer
Phil TenHulzen, P.E., Design Standards Engineer
Jodi Gibson, Research Coordinator

Ohio Department of Transportation

Dean Focke, P.E., Road Safety Engineer

South Dakota Department of Transportation

David Huft, Research Engineer
Bernie Clocksin, Lead Project Engineer

Wisconsin Department of Transportation

John Bridwell, P.E., Standards Development Engineer
Erik Emerson, P.E., Standards Development Engineer

Wisconsin Department of Transportation

William Wilson, P.E., Standards Engineer

Federal Highway Administration

John Perry, P.E., Nebraska Division Office
Danny Briggs, Nebraska Division Office

TABLE OF CONTENTS

Page
TECHNICAL REPORT DOCUMENTATION PAGE i
SPECIAL EXECUTIVE SUMMARY ii
ORIGINAL ABSTRACT OF *CRITICAL OFFSET OF THE MIDWEST GUARDRAIL SYSTEM BEHIND A CURB* (M.S. THESIS OF LING ZHU) v
DISCLAIMER STATEMENT vii
ACKNOWLDGEMENTS viii
TABLE OF CONTENTS x
List of Figures xiii
List of Tables xix
1 INTRODUCTION 1
1.1 Problem Statement 1
1.2 Objective 2
1.3 Scope 2
2 LITERATURE REVIEW 4
2.1 Curb Configuration 4
2.2 Vehicle Impact on Curb 5
2.2.1 Olsen, et al. 6
2.2.2 Holloway, et al. 7
2.2.3 Ross, et al. 8
2.2.4 Plaxico, et al. 10
2.3 Vehicle Impact on Curb and W-beam Guardrail Combination 10
2.3.1 Plaxico, et al. 10
2.3.2 Polivka, et al. 11
2.4 Literature Summary 12
3 TEST CONDITIONS 13
3.1 Test Introduction 13
3.2 Test Facility 13
3.3 Vehicle Tow and Guidance System 13
3.4 Test Vehicles 14
3.5 Curb Setup 22
3.6 Data Acquisition Systems 30
3.6.1 Accelerometers 30
3.6.2 Rate Transducers 31
3.6.3 High-Speed Photography 32
3.6.4 Pressure Tape Switches 32
4 CRASH TEST NO. 1 (MGSC-1, 2270P) 38
4.1 Introduction 38
4.2 Test Description 38
4.3 System and Component Damage 39
4.4 Vehicle Damage 39
4.5 Trajectory Results 39
4.6 Occupant Risk Values 40
4.7 Discussion 40

5 CRASH TEST NO. 2 (MGSC-2, 2270P) 52
5.1 Introduction 52
5.2 Test Description 52
5.3 System and Component Damage 52
5.4 Vehicle Damage 53
5.5 Trajectory Results 53
5.6 Occupant Risk Values 54
5.7 Discussion 54
6 CRASH TEST NO. 3 (MGSC-3, 1100C) 66
6.1 Introduction 66
6.2 Test Description 66
6.3 System and Component Damage 67
6.4 Vehicle Damage 67
6.5 Trajectory Results 67
6.6 Occupant Risk Values 68
6.7 Discussion 68
7 CRASH TEST NO. 4 (MGSC-4, 2000P) 81
7.1 Introduction 81
7.2 Test Description 81
7.3 System and Component Damage 82
7.4 Vehicle Damage 82
7.5 Trajectory Results 82
7.6 Occupant Risk Values 83
7.7 Discussion 83
8 TEST TRAJECTORY DATA ANALYSIS 95
8.1 Verification of Video Analysis Data 95
8.2 Processed Longitudinal Distance (PLD) Coordinate 98
8.3 Processed Curb-Lateral Distance (CLD) Coordinate 101
9 PICKUP-CURB IMPACT SIMULATION AND VALIDATION 104
9.1 Introduction 104
9.2 LS-DYNA Model Description and Results 104
9.3 Tire Performance Analysis 108
9.4 Roll Movement Analysis 111
9.5 Pitch Movement Analysis 114
9.6 Yaw Movement Analysis 118
9.7 Bumper Trajectory Analysis 119
9.8 Summary 119
10 CRITICAL VEHICLE-MGS IMPACT POINT ANALYSIS 121
10.1 Introduction 121
10.2 Pickup-MGS Critical Override Impact Point 121
10.2.1 Comparison of 2000P and 2270P Bumpers 121
10.2.2 Analysis of Previous Full-Scale Pickup W-Beam Tests 124
10.2.3 Analysis of Pickup and W-beam Critical Impact Height 129
10.2.4 LS-DYNA Simulation Verification 132
10.3 Discussion 134
10.4 Small Car-MGS Critical Impact Point 136

11 DETERMINATION OF MGS CRITICAL OFFSET BEHIND CURB 138
11.1 Introduction 138
11.2 Trajectory of Critical Bumper Impact Point 138
11.3 MGS Critical Offset Behind Curb 140
12 MGS-CURB COMBINATION LS-DYNA SIMULATION 145
12.1 Simulation No. 1 147
12.2 Simulation No. 2 150
12.3 Simulation No. 3 154
12.4 Additional Simulations 155
12.5 Simulation Summary 155
13 SUMMARY AND CONCLUSIONS 160
14 FUTURE RESEARCH 164
15 REFERENCES 165
APPENDIX A - VEHICLE-CURB TEST SETUP (ENGLISH UNITS) 167
APPENDIX B - RAW TEST RESULTS (ENGLISH UNITS) 171
APPENDIX C - ACCELOROMETER AND RATE TRANSDUCER DATA 184
APPENDIX D - TRANSFORMATION OF BUMPER CRITICAL IMPACT POINT TRAJECTORY FROM C.G. TARGET TRAJECTORY 201
APPENDIX E - VEHICLE BUMPER CRITICAL IMPACT POINT TRAJECTORIES (ENGLISH UNITS) 204

List of Figures

Page
Figure 1. Typical AASHTO Curbs 4
Figure 2. NPG-5 System Setup 11
Figure 3. Test Vehicle, Test MGSC-1 15
Figure 4. Test Vehicle, Test MGSC-2 16
Figure 5. Test Vehicle Dimensions, Tests MGSC-1 and MGSC-2 17
Figure 6. Test Vehicle, Test MGSC-3 18
Figure 7. Test Vehicle Dimensions, Test MGSC-3 19
Figure 8. Test Vehicle, Test MGSC-4 20
Figure 10. Vehicle Target Locations, Tests MGSC-1 and MGSC-2 23
Figure 11. Vehicle Target Locations, Test MGSC-3 24
Figure 12. Vehicle Target Locations, Test MGSC-4 25
Figure 13. System Layout 26
Figure 14. Curb Detail 27
Figure 15. Bill of Bars 28
Figure 16. 152-mm (6-in.) AASHTO Type B Curb Construction and Test Layout 29
Figure 17. Location of Cameras, Test MGSC-1 34
Figure 18. Location of Cameras, Test MGSC-2 35
Figure 19. Location of Cameras, Test MGSC-3 36
Figure 20. Location of Cameras, Test MGSC-4 37
Figure 21. Impact Location, Test MGSC-1 41
Figure 22. Sequential Photographs, Test MGSC-1 42
Figure 23. Additional Sequential Photographs, Test MGSC-1 43
Figure 24. Additional Sequential Photographs, Test MGSC-1 44
Figure 25. Vehicle Final Position and Trajectory, Test MGSC-1 45
Figure 26. System Damage, Test MGSC-1 46
Figure 27. Vehicle Damage, Test MGSC-1 47
Figure 28. C.G. Target Displacement vs. Time, Test MGSC-1 (2270P) 48
Figure 29. C.G. Target Displacement vs. Raw Longitudinal Distance, Test MGSC-1 (2270P) 48
Figure 30. Bumper Target Displacement vs. Time, Test MGSC-1 (2270P) 49
Figure 31. Bumper Target Displacement vs. Raw Longitudinal Distance, Test MGSC-1 (2270P) 49
Figure 32. C.G. Target Trajectory vs. Raw Longitudinal Distance, Test MGSC-1 (2270P) 50
Figure 33. C.G. Target Trajectory vs. Raw Longitudinal Distance, Test MGSC-1 (2270P) 50
Figure 34. Bumper Target Trajectory vs. Time, Test MGSC-1 (2270P) 51
Figure 35. Bumper Target Trajectory vs. Raw Longitudinal Distance, Test MGSC-1 (2270P) 51
Figure 36. Impact Location, Test MGSC-2 55
Figure 37. Sequential Photographs, Test MGSC-2 56
Figure 38. Additional Sequential Photographs, Test MGSC-2 57
Figure 39. Additional Sequential Photographs, Test MGSC-2 58
Figure 40. Vehicle's Final Position and Trajectory, Test MGSC-2 59
Figure 41. System Damage, Test MGSC-2 60
Figure 42. Vehicle Damage, Test MGSC-2 61
Figure 43. C.G. Target Displacement vs. Time, Test MGSC-2 (2270P) 62

Figure 44. C.G. Target Displacement vs. Raw Longitudinal Distance, Test MGSC-2 (2270P) .. 62
Figure 45. Bumper Target Displacement vs. Time, Test MGSC-2 (2270P) 63
Figure 46. Bumper Target Displacement vs. Raw Longitudinal Distance,
Test MGSC-2 (2270P) 63
Figure 47. C.G. Target Trajectory vs. Time, Test MGSC-2 (2270P) 64
Figure 48. C.G. Target Trajectory vs. Raw Longitudinal Distance, Test MGSC-2 (2270P) 64
Figure 49. Bumper Target Trajectory vs. Time, Test MGSC-2 (2270P)..... 65
Figure 50. Bumper Target Trajectory vs. Raw Longitudinal Distance, Test MGSC-2 (2270P) .. 65
Figure 51. Impact Location, Test MGSC-3 70
Figure 52. Sequential Photographs, Test MGSC-3..... 71
Figure 53. Additional Sequential Photographs, Test MGSC-3..... 72
Figure 54. Additional Sequential Photographs, Test MGSC-3..... 73
Figure 55. Vehicle Final Position and Trajectory, Test MGSC-3 74
Figure 56. System Damage, Test MGSC-3 75
Figure 57. Vehicle Damage, Test MGSC-3..... 76
Figure 58. C.G. Target Displacement vs. Time, Test MGSC-3 (1100C) 77
Figure 59. C.G. Target Displacement vs. Raw Longitudinal Distance, Test MGSC-3 (1100C).. 77
Figure 60. Bumper Target Displacement vs. Time, Test MGSC-3 (1100C)..... 78
Figure 61. Bumper Target Displacement vs. Raw Longitudinal Distance,
Test MGSC-3 (1100C)..... 78
Figure 62. C.G. Target Trajectory vs. Time, Test MGSC-3 (1100C)..... 79
Figure 63. C.G. Target Trajectory vs. Raw Longitudinal Distance, Test MGSC-3 (1100C)..... 79
Figure 64. Bumper Target Trajectory vs. Time, Test MGSC-3 (1100C) 80
Figure 65. Bumper Target Trajectory vs. Raw Longitudinal Distance,Test MGSC-3 (1100C)... 80
Figure 66. Impact Location, Test MGSC-4 84
Figure 67. Sequential Photographs, Test MGSC-4..... 85
Figure 68. Additional Sequential Photographs, Test MGSC-4..... 86
Figure 69. Additional Sequential Photographs, Test MGSC-4..... 87
Figure 70. Vehicle Final Position and Trajectory, Test MGSC-4 88
Figure 71. System Damage, Test MGSC-4 89
Figure 72. Vehicle Damage, Test MGSC-4..... 90
Figure 73. C.G. Target Displacement vs. Time, Test MGSC-4 (2000P)..... 91
Figure 74. Bumper Target Displacement vs. Time, Test MGSC-4 (2000P) 91
Figure 75. C.G. Target Displacement vs. Raw Longitudinal Distance, Test MGSC-4 (2000P) .. 92
Figure 76. Bumper Target Displacement vs. Raw Longitudinal Distance,
Test MGSC-4 (2000P) 92
Figure 77. C.G. Target Trajectory vs. Time, Test MGSC-4 (2000P) 93
Figure 78. C.G. Target Trajectory vs. Raw Longitudinal Distance, Test MGSC-4 (2000P) 93
Figure 79. Bumper Target Trajectory vs. Time, Test MGSC-4 (2000P)..... 94
Figure 80. Bumper Target Trajectory vs. Raw Longitudinal Distance, Test MGSC-4 (2000P) .. 94
Figure 81. Illustration of Bumper Target Trajectory Reconstruction 95
Figure 82. Bumper Target Trajectory Reconstruction, Test MGSC-1 96
Figure 83. Bumper Target Trajectory Reconstruction, Test MGSC-2 97
Figure 84. Bumper Target Trajectory Reconstruction, Test MGSC-3 97
Figure 85. Bumper Target Trajectory Reconstruction, Test MGSC-4 98
Figure 86. Setup of PLD Coordinate System..... 99

Figure 87. C.G. Target Vertical Displacement vs. Processed Longitudinal Distance 100
Figure 88. Bumper Target Vertical Displacement vs. Processed Longitudinal Distance..... 100
Figure 89. Setup of CLD Coordinate System 101
Figure 90. C.G. Target Displacement in CLD Coordinates..... 102
Figure 91. Bumper Target Displacement in CLD Coordinates 102
Figure 92. C.G. Target Trajectory in CLD Coordinates 103
Figure 93. Bumper Target Trajectory in CLD Coordinates..... 103
Figure 94. 2000P-Curb Impact LS-DYNA Model 105
Figure 95. Curb and Ground LS-DYNA Model 106
Figure 96. Overhead Sequential of 2000P-Curb Impact..... 107
Figure 97. Tire Deformation Comparison 109
Figure 98. Left-Rear Tire Does Not Impact the Curb in the Simulation 110
Figure 99. C.G. Roll Displacement Comparison 112
Figure 100. Cargo Box Presented Large Deformation in the Simulation..... 113
Figure 101. C.G. Pitch Movement Comparison 114
Figure 102. Vehicle Post-Curb-Impact Trajectory Comparison-Side View..... 115
Figure 103. Vehicle Post-Curb-Impact Trajectory Comparison-Front View 116
Figure 104. Illustration of Simplified Pitch Movement Model 118
Figure 105. C.G. Yaw Displacement Comparison 118
Figure 106. Pickup Model's Bumper Trajectory 120
Figure 107. 2000P Pickup Bumper Trajectory Comparison..... 120
Figure 108. Bumper Comparison – 2000P and 2270P 123
Figure 109. Only Middle Metallic Portion Actually Functions as a Bumper..... 123
Figure 110. Geometric Dimension of Standard MGS Guardrail 125
Figure 111. NPG-2 Bumper Impact Height..... 126
Figure 112. NPG-3 Bumper Impact Height..... 127
Figure 113. NPG-4 Bumper Impact Height..... 127
Figure 114. 2214MG-1 Bumper Impact Height 128
Figure 115. 2214MG-2 Bumper Impact Height 128
Figure 116. MIW-1 Bumper Impact Height 128
Figure 117. MIW-2 Bumper Impact Height 128
Figure 118. Pickup-MGS Critical Override Impact Height..... 129
Figure 119. Illustration of Pre-Impact Condition 130
Figure 120. Schematic of Guardrail Rotation during Impact 130
Figure 121. Bumper Deformation in Test MIW-1 (Failed) 131
Figure 122. Bumper Deformation in Test NPG-4 (Passed)..... 131
Figure 123. LS-DYNA Simulation of the Pickup-MGS Critical Override Impact Point..... 133
Figure 124. Pickup-W-beam Guardrail Override Critical Impact Point, 2000P and 2270P..... 133
Figure 125. Vehicle's Front Suspension Extended Due to the Slope 135
Figure 126. W-beam Rail Trapped Between the Front Wheel and the Bumper..... 135
Figure 127. Vehicle's Front Wheel Damage 135
Figure 128. Small Passenger Car and MGS Impact, Test 2214MG-3..... 137
Figure 129. Illustration of the Transformation of the Bumper Critical Impact Point Trajectory from the Bumper Target Trajectory 139
Figure 130. Pickup Bumper Critical Override Impact Point Trajectories 142
Figure 131. Small Passenger Car Critical Underride Impact Point Trajectory..... 143

Figure 132. Safe Zone Illustration for MGS Option I Installation behind Curb..... 144
Figure 133. Safe Zone Illustration for MGS Option II Installation behind Curb 144
Figure 134. MGS-Curb and 2000P Crash Simulation Setup 146
Figure 135. MGS-Curb Simulation Procedure Illustration..... 147
Figure 136. Simulation No. 1 Test Location - 1.22m (4 ft) 148
Figure 137. Vehicle-MGS Impact Position, Simulation No. 1 148
Figure 138. 2000P and MGS-Curb Impact Overhead Sequential, Simulation No. 1 149
Figure 139. 2000P and MGS-Curb Impact Downstream Sequential, Simulation No. 1 149
Figure 140. 2000P and MGS-Curb Impact Side Sequential, Simulation No. 1..... 150
Figure 141. Simulation No. 2 Test Location—1.1m (3.61 ft) 151
Figure 142. Vehicle-MGS Impact Position, Simulation No. 2 152
Figure 143. Guardrail Deformed Ahead of Vehicle 152
Figure 144. 2000P and MGS-Curb Impact Overhead Sequential, Simulation No. 2 153
Figure 145. 2000P and MGS-Curb Impact Downstream Sequential, Simulation No. 2 153
Figure 146. 2000P and MGS-Curb Impact Side Sequential, Simulation No. 2..... 154
Figure 147. Simulation No. 3 Test Location - 0.8 m (2.63 ft) 156
Figure 148. Pickup-MGS Impact Position, Simulation No. 3 156
Figure 149. 2000P and MGS-Curb Impact Overhead Sequential, Simulation No. 3 157
Figure 150. 2000P and MGS-Curb Impact Downstream Sequential, Simulation No. 3 157
Figure 151. 2000P and MGS-Curb Impact Side Sequential, Simulation No. 3..... 158
Figure A-1. System Layout (English Units) 168
Figure A-2. Curb Detail (English Units)..... 169
Figure A-3. Bill of Bars (English Units)..... 170
Figure B-1. C.G. Target Vertical Displacement vs. Time, Test MGSC-1 (2270P)..... 172
Figure B-2. C.G. Target Vertical Displacement vs. Raw Longitudinal Distance,
Test MGSC-1 (2270P) 172
Figure B-3. Bumper Target Vertical Displacement vs. Time, Test MGSC-1 (2270P) 173
Figure B-4. Bumper Target Vertical Displacement vs. Raw Longitudinal Distance,
Test MGSC-1 (2270P) 173
Figure B-5. C.G. Target Trajectory vs. Raw Longitudinal Distance, Test MGSC-1 (2270P) ... 174
Figure B-6. Bumper Target Trajectory vs. Raw Longitudinal Distance,
Test MGSC-1 (2270P) 174
Figure B-7. C.G. Target Vertical Displacement vs. Time, Test MGSC-2 (2270P)..... 175
Figure B-8. C.G. Target Vertical Displacement vs. Raw Longitudinal Distance,
Test MGSC-2 (2270P) 175
Figure B-9. Bumper Target Vertical Displacement vs. Time, Test MGSC-2 (2270P) 176
Figure B-10. Bumper Target Vertical Displacement vs. Raw Longitudinal Distance,
Test MGSC-2 (2270P) 176
Figure B-11. C.G. Target Trajectory vs. Raw Longitudinal Distance, Test MGSC-2 (2270P) . 177
Figure B-12. Bumper Target Trajectory vs. Raw Longitudinal Distance,
Test MGSC-2 (2270P) 177
Figure B-13. C.G. Target Vertical Displacement vs. Time, Test MGSC-3 (1100C) 178
Figure B-14. C.G. Target Vertical Displacement vs. Raw Longitudinal Distance,
Test MGSC-3 (1100C)..... 178
Figure B-15. Bumper Target Vertical Displacement vs. Time, Test MGSC-3 (1100C) 179

Figure B-16. Bumper Target Vertical Displacement vs. Raw Longitudinal Distance, Test MGSC-3 (1100C) 179
Figure B-17. C.G. Target Trajectory vs. Raw Longitudinal Distance, Test MGSC-3 (1100C) . 180
Figure B-18. Bumper Target Trajectory vs. Raw Longitudinal Distance, Test MGSC-3 (1100C) 180
Figure B-19. C.G. Target Vertical Displacement vs. Time, Test MGSC-4 (2000P) 181
Figure B-20. C.G. Target Vertical Displacement vs. Raw Longitudinal Distance, Test MGSC-4 (2000P) 181
Figure B-21. Bumper Target Vertical Displacement vs. Time, Test MGSC-4 (2000P) 182
Figure B-22. Bumper Target Vertical Displacement vs. Raw Longitudinal Distance, Test MGSC-4 (2000C) 182
Figure B-23. C.G. Target Trajectory vs. Raw Longitudinal Distance, Test MGSC-4 (2000P) . 183
Figure B-24. Bumper Target Trajectory vs. Raw Longitudinal Distance, Test MGSC-4 (2000P) 183
Figure C-1. Graph of Longitudinal Deceleration, Test MGSC-1 (2270P) 185
Figure C-2. Graph of Longitudinal Occupant Impact Velocity, Test MGSC-1 (2270P) 185
Figure C-3. Graph of Longitudinal Occupant Displacement, Test MGSC-1 (2270P) 186
Figure C-5. Graph of Lateral Occupant Impact Velocity, Test MGSC-1 (2270P) 187
Figure C-7. Graph of Roll, Pitch, and Yaw Angular Displacements, Test MGSC-1 (2270P) ... 188
Figure C-8. Graph of Longitudinal Deceleration, Test MGSC-2 (2270P) 189
Figure C-9. Graph of Longitudinal Occupant Impact Velocity, MGSC-2 (2270P) 189
Figure C-10. Graph of Longitudinal Occupant Displacement, Test MGSC-2 (2270P) 190
Figure C-11. Graph of Lateral Deceleration, Test MGSC-2 (2270P) 190
Figure C-12. Graph of Lateral Occupant Impact Velocity, Test MGSC-2 (2270P) 191
Figure C-13. Graph of Lateral Occupant Displacement, Test MGSC-2 (2270P) 191
Figure C-14. Graph of Roll, Pitch, and Yaw Angular Displacements, Test MGSC-2 (2270P) . 192
Figure C-15. Graph of Longitudinal Deceleration, Test MGSC-3 (1100C) 193
Figure C-16. Graph of Longitudinal Occupant Impact Velocity, Test MGSC-3 (1100C) 193
Figure C-17. Graph of Longitudinal Occupant Displacement, Test MGSC-3 (1100C) 194
Figure C-18. Graph of Lateral Deceleration, Test MGSC-3 (1100C) 194
Figure C-19. Graph of Lateral Occupant Impact Velocity, Test MGSC-3 (1100C) 195
Figure C-20. Graph of Lateral Occupant Displacement, Test MGSC-3 (1100C) 195
Figure C-21. Graph of Roll, Pitch, and Yaw Angular Displacements, Test MGSC-3 (1100C). 196
Figure C-22. Graph of Longitudinal Deceleration, Test MGSC-4 (2000P) 197
Figure C-23. Graph of Longitudinal Occupant Impact Velocity, Test MGSC-4 (2000P) 197
Figure C-24. Graph of Longitudinal Occupant Displacement, Test MGSC-4 (2000P) 198
Figure C-25. Graph of Lateral Deceleration, Test MGSC-4 (2000P) 198
Figure C-26. Graph of Lateral Occupant Impact Velocity, Test MGSC-4 (2000P) 199
Figure C-27. Graph of Lateral Occupant Displacement, Test MGSC-4 (2000P) 199
Figure C-28. Graph of Roll, Pitch, and Yaw Angular Displacements, Test MGSC-4 (2000P) . 200
Figure D-1. Illustration of the Transition of bumper Critical Point Trajectory for C.G. Target Trajectory 201
Figure D-2. Transition Comparison of the 2270P Pickup Critical Point Trajectory, Test MGSC-1 202
Figure D-3. Transition Comparison of the 2270P Pickup Critical Point Trajectory, Test MGSC-2 203

Figure D-4. Transition Comparison of the 2000P Pickup Critical Point Trajectory, Test (MGSC-4) 203
Figure E-1. Pickup Bumper Critical Override Impact Point Trajectories 205
Figure E-2. Small Passenger Car Critical Underride Impact Point Trajectory..... 206
Figure E-3. Safe Zone Illustration for MGS Option I Installation behind Curb..... 207
Figure E-4. Safe Zone Illustration for MGS Option II Installation behind Curb 207

List of Tables

Page
Table 1. Summary of Initial Parameters for Bumper Target Trajectory Reconstruction 96
Table 2. Summary of Parameters for Raw-to-PLD Transition 99
Table 3. 2000P and 2270P Comparison (as shown in Figure 108).....122
Table 4. Available Full Scale Tests of W-beam Guardrail and Pickup 125
Table 5. Height Comparison of Bumper Top Edge and W-beam Top Corrugation.....126
Table 6. Summary of Parameters for Bumper Critical Point Trajectory Transition.....139
Table 7. Vehicle-Curb Test Summary 163
Table D-1. Summary of Parameters for Bumper Critical Point Trajectory Transition 202

1 INTRODUCTION

1.1 Problem Statement

Highway design policy typically discourages the use of curbs on high-speed roadways because of their potential to cause drivers to lose control in a crash. Curbs can also affect the interaction of errant vehicles with roadside barriers by causing vaulting or underride of the barrier. However, the use of curbs is often required because of restricted right-of-way, drainage considerations, access control, and other curb functions. Often, there is a desire to offset the guardrail from the curb to reduce the propensity for snow plows to gouge and/or damage the W-beam rail sections or to allow for placement of sidewalks and other roadside features.

When curbs are required, the offset of the barrier from the curb has been shown to be critical in the performance of the system. Previous work with standard W-beam guardrail has shown that only a 102-mm (4-in.) high curb with the toe of the curb placed at the front face of the guardrail is capable of meeting National Cooperative Highway Research Program (NCHRP) Report No. 350 safety requirements (1). However, taller curbs are often required at the roadway edge for improved hydraulic drainage control. Recently, the Midwest Pooled Fund Program member states sponsored the development of the Midwest Guardrail System (MGS). The MGS has proven to be far more robust than standard W-beam guardrail systems, and it is believed that the MGS system would provide more flexibility when used in conjunction with curbs than the current W-beam guardrail. Thus, a need existed to examine the use of curbs in conjunction with the MGS in order to determine effective curb placement guidelines.

The recent development and testing of the MGS has demonstrated that this system can be used with a 152-mm (6-in.) tall, American Association of State Highway and Transportation Officials (AASHTO) Type B curb positioned 152 mm (6 in.) in front of the face of the guardrail

element (2-3). Although the current guardrail-to-curb configuration provided increased hydraulic flow for roadway runoff, as well as reduced guardrail maintenance arising from snow plowing operations, Ohio and other state departments of transportation (DOTs) often desire to locate roadside curbs farther away from the front of the guardrail. Although standard guardrail systems cannot perform adequately in this situation for most test levels, the MGS would likely provide adequate performance to a Test Level 2 (TL-2), and possibly for Test Level 3 (TL-3). As such, there exists a need to determine the performance limits of a 152-mm (6-in.) high curb located farther away from the front face of the MGS.

1.2 Objective

The objectives of this research were to: (1) determine pickup truck and small passenger car trajectories after impacting a 152-mm (6-in.) curb; (2) analyze the vehicle's post-impact trajectory; (3) investigate the interaction between the MGS and the vehicle and find the critical override impact scenario for the pickup truck and the critical underride impact scenario for the small passenger car; (4) evaluate the reliability of the current LS-DYNA pickup model for MGS-curb impacts; and (5) determine the offset limit for the MGS system behind a 152-mm (6-in.) curb potentially capable of meeting TL-3 criteria of the Manual for Assessing Safety Hardware (MASH) (4).

1.3 Scope

The research objectives were achieved through the completion of several tasks. First, a detailed literature review was conducted on curb configurations, previous curb and vehicle impact studies, and previous curb and W-beam guardrail combination studies. Next, a series of vehicle-to-curb physical tests were performed, including the 2270P and 1100C test vehicles required by MASH and the 2000P pickup truck of the NCHRP Report No. 350 guidelines. The

target impact condition for each test utilized an impact speed of 100.0 km/h (62.1 mph) and impact angle of 25 degrees. The test results were documented. Next, an LS-DYNA simulation was performed to replicate the 2000P vehicle impacting a curb. By comparing the simulation results with the physical test, an evaluation of the current pickup model was performed to assist the MGS-curb project and to identify the weaknesses of the current model. Next, the test results were analyzed. An investigation was conducted to determine the critical override/underride impact scenarios between the vehicle and the MGS. Next, the trajectory of the vehicle's critical impact component was compared with the MGS height to find out the critical override locations for the pickup and the critical underride locations for the small passenger car. Next, a series of LS-DYNA simulations was conducted to verify the critical locations obtained from the trajectory analysis. Finally, conclusions and recommendations were made for further study of the installation of MGS behind curbs and the improvement of the current pickup model.

2 LITERATURE REVIEW

2.1 Curb Configuration

Configurations of commonly used curbs were summarized by the American Association of State Highway and Transportation Officials (AASHTO) (5), including both vertical and sloping curbs, as shown in Figure 1

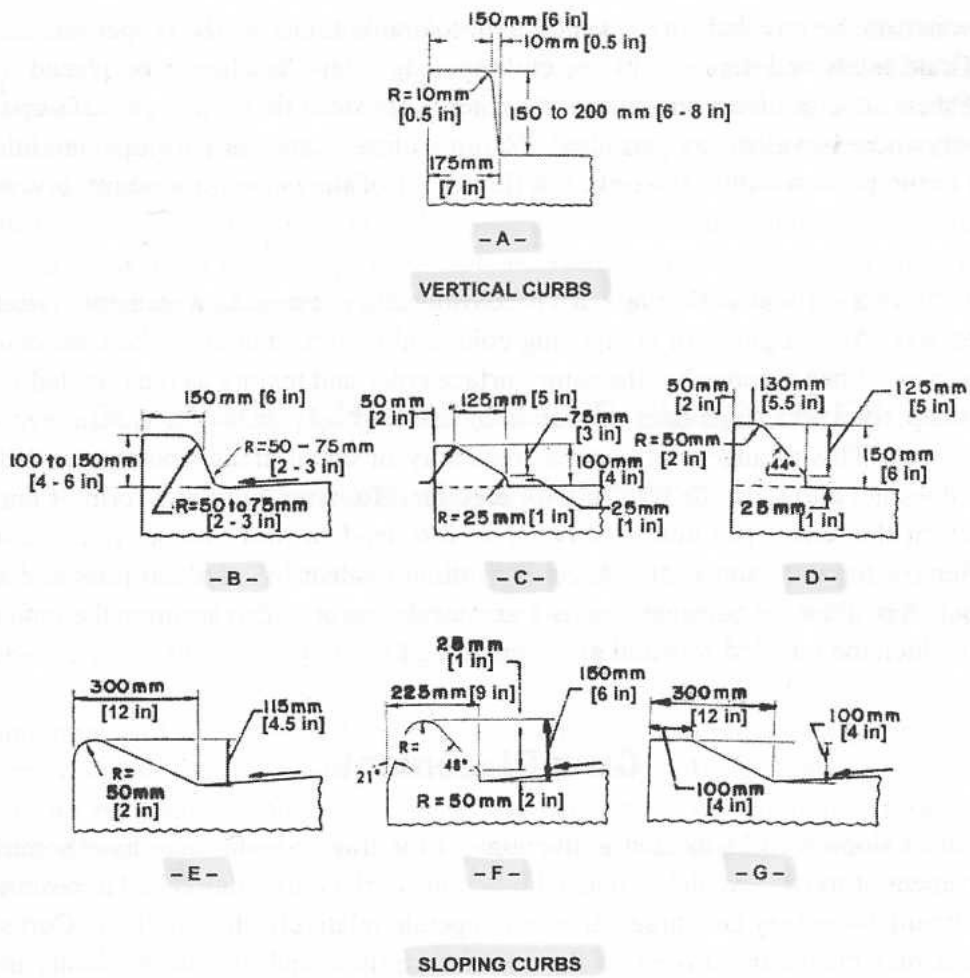

Figure 1. Typical AASHTO Curbs

Vertical curbs may be either vertical, or nearly vertical, and are intended to discourage vehicles from leaving the roadway, as designated by Type A shown in Figure 1. They range from 152 to 203 mm (6 to 8 in.) in height. Vertical curbs should not be used along freeways or other

high-speed roadways because an out-of-control vehicle may overturn or become airborne as a result of an impact with such a curb.

Sloping curbs are designed so vehicles can cross them when the need arises. Sloping curbs are low with flat sloping faces, as such Types B through G shown in Figure 1. For example, curbs Types B, C, and D are considered to be mountable under emergency conditions although such curbs may scrape the undersides of some vehicles. When the slope of the curb face is steeper than 1V:1H, vehicles can mount the curb more readily when the height of the curb is limited to 102 mm (4 in.) and preferably less. However, when the face slope is between 1V:1H and 1V:2H, the height should be limited to 152 mm (6 in.).

Vertical curbs should not be used along freeways or other high-speed arterials, but if a curb is needed, it should be of the sloping type and should not be located closer to the traveled way than the outer edge of the shoulder. Since curbs are not adequate to prevent a vehicle from leaving the roadway, a suitable traffic barrier should be provided where redirection of vehicles is needed. When using curbs in conjunction with traffic barriers, consideration should be given to the type and height of the barrier. Curbs placed in front of traffic barriers can result in unpredictable impact trajectories. If a curb is used in conjunction with a traffic barrier, the height of a vertical curb should be limited to 102 mm (4 in.), or it should be of the sloping type and ideally located flush with or behind the face of the barrier. Curbs should not be used with concrete median barriers (6).

2.2 Vehicle Impact on Curb

Because vertical curbs can cause severe vehicle instabilities and vehicle damage at high speeds and are usually restricted to low speed facilities, sloping curbs were selected for this project. Meanwhile, the AASHTO Type B curb has the steepest slope among the sloping curbs.

Thus, it is believed that the Type B curb presents the worst impact scenario among all of the sloping curbs. Previous researchers also proved that the AASHTO Type B curb resulted in worse vehicle impact performance than observed for the other sloping curbs (7). In addition, a high curb was found to provide a worse impact behavior than a low curb. Therefore, a 152-mm (6-in.) high, AASHTO Type B curb was selected for this project due to its high potential for creating a worst-case impact scenario. If the test results are found to be satisfactory, then shorter heights and other types of sloping curbs would also be acceptable and would not require additional testing.

2.2.1 Olsen, et al.

In 1974, Olsen and other researchers at Texas Transportation Institute (TTI), investigated the effects of curbs on vehicle attitude using both full-scale tests and simulations. Highway Vehicle-Object Simulation Model (HVOSM) was used to conduct the simulation. Three curbs (AASHTO Types C, E, and H) were selected for the detailed study. All of the results were presented in NCHRP Report No. 150 (7).

Eighteen full-scale tests were conducted on curb Types C and E. A series of nine tests were conducted on each curb at 48.3 km/h (30 mph), 72.4 km/h (45 mph), and 96.6 km/h (60 mph) with 5, 12.5, and 20 degree encroachment angles. Twelve curb impacts were simulated on each of the curb Types C, E, and H. The simulations included impacts of 48.3 km/h (30 mph), 72.4 km/h (45 mph), and 96.6 km/h (60 mph) at 5, 12.5, and 20 degrees and a 120.7-km/h (75-mph) impact at 5, 10, and 15 degrees.

The results of the study are summarized as follows. First, 152-mm (6-in.) tall curbs with configurations similar to that of AASHTO Types C, E, or H will not redirect a vehicle at speeds above 72.4 km/h (45 mph) and encroachment angles greater than approximately 5 degrees.

Second, curbs similar to Types C, E, and H can produce, under certain speed and angle impact conditions, vehicle ramping to a height at which the vehicle will vault a 686-mm (27-in.) tall guardrail located behind the curb. The guardrail offset distance necessary to restrain the vehicle is dependent primarily on the exit angle, speed, and curb geometry. Guardrail height and placement behind a curb should be determined by analysis of expected impact conditions. Third, 152-mm (6-in.) curbs can cause a vehicle to impact a 686-mm (27-in.) tall guardrail (W-beam at a 610-mm (2-ft) offset) at a point below the lower edge of the rail face, thus creating the possibility of snagging. Consideration should be given to the use of a rub rail on guardrail located behind a 152-mm (6-in.) curb. Lastly, impacting 152-mm (6 in.) tall curbs can be expected to produce minor or no injury. An automobile travelling at a highway speed will cross the curb with ease, and the vehicle path can be expected to deviate only slightly from the initial encroachment path.

2.2.2 Holloway, et al.

In 1993, Holloway, and other researchers at the Midwest Roadside Safety Facility (MwRSF), investigated three commonly used Nebraska Department of Roads (NDOR) mountable/sloping curbs for relative safety through a combination of full-scale testing and computer simulation using HVOSM (8-9). Two full-scale crash tests were performed on a 152-mm (6-in.) wedge shaped curb, and eight crash tests were performed on a 152-mm (6-in.) Type I mountable curb. The Type I curb is similar to the Type B curb but with a smoother slope. The crash tests were conducted with an 817-kg (1,800-lb) (1984 Dodge Colt) and a 2,043-kg (4,500-lb) (1986 Ford LTD) test vehicles at impact speeds of 72.4 km/h (45 mph), 80.5 km/h (50 mph), and 88.5 km/h (55 mph) and impact angles of 5, 12.5, and 20 degrees.

The results showed that Nebraska's mountable curbs do not have a potential for causing loss of vehicle control nor vehicle destabilization when impacted in a tracking condition. It was also determined that the performance of W-beam guardrail can be adversely affected when used in conjunction with roadside curbs.

The results of HVOSM simulations indicated that the 817-kg (1,800-lb) small vehicle may underride a W-beam guardrail if the guardrail is placed within 1 m (3.28 ft) of the 152-mm (6-in.) lip curb. Also, the simulations indicated that the 2,043-kg (4,500-lb) vehicle had a slight potential to underride a W-beam guardrail located within 1 m (3.28 ft) of the curb and to vault the guardrail located within a region of 0.61 to 3 m (2 to 9.84 ft) behind the curb.

The simulations with the AASHTO Type I curb indicated that impact with the curb could cause underride of a W-beam guardrail placed within 0.61 m (2 ft) of the curb. For the small car impact, a potential for vaulting existed if the guardrail was placed 0.46 m (1.5 ft) to 3.0 m (9.84 ft) behind the curb. For the large car impacts, a potential for vaulting existed if the guardrail was placed 0.46 m (1.5 ft) to 3.7 m (12.1 ft) behind the curb.

2.2.3 Ross, et al.

NCHRP Report No. 318 (10) concluded by full-scale testing and simulation that the AASHTO Type B curb posed no appreciable hazard to occupants of a small car for the conditions evaluated. Those conditions were tracking impacts with the curb at various encroachment angles and speeds up to 96.5 km/h (60 mph). However, AASHTO Type B has a propensity of overturning a small car for non-tracking impacts. Type B curbs caused damage to small passenger cars in high-speed impacts, such as flat tires and bent rims.

Five tests were conducted on 152-mm (6-in.) AASHTO Type B curbs using a 1985 Fiat Uno-45 small passenger car, with a weight of 704 kg (1,550 lbs). In all 5 tests, the vehicle

remained upright and stable. The damage to the vehicles was minimal. Damage to the curb was not found, except for minor scuff marks.

Test 7043-9A had an impact speed of 53.1 km/h (33 mph) and an angle of 5 degrees. The left side of the vehicle easily crossed over the curb, and the vehicle continued forward straddling the curb until it left the test site. No noticeable damage to the vehicle was found.

Test 7043-9B had an impact speed of 73.4 km/h (45.6 mph) and an angle of 5 degrees. The left side of the vehicle easily crossed over the curb, and the vehicle continued forward straddling the curb until it left the test site. There was no damage to the vehicle, except the left-front rim was slightly dented.

Test 7043-9C had an impact speed of 48.3 km/h (30 mph) and an angle of 15 degrees. All four tires crossed the curb, and all four briefly lost contact with the ground as they bounced up on the curb. There was no damage to the vehicle, except the left-front rim was slightly dented.

Test 7043-9D had an impact speed of 75.3 km/h (46.8 mph) and an angle of 15 degrees. The left-front tire deflated as it rode up onto the curb. All four tires crossed the curb and briefly lost contact with the ground as they bounced up on the curb. There was no major damage to the vehicle. However, the left-front tire was cut, and the rim bent severely. Also, the left-rear and right-front rims were dented.

Test 7043-9E had an impact speed of 101.4 km/h (63 mph) and an angle of 15 degrees. The left-front tire deflated as it rode up onto the curb. All four tires crossed the curb and briefly lost contact with the ground as they bounced up on the curb. The left-front strut on the vehicle was pushed back 76 mm (3 in.), and the left-front tire was severely damaged with the rim bent. The right-front tire was deflated with the rim bent, and the left-rear rim was dented.

2.2.4 Plaxico, et al.

In 2002, Plaxico (11) investigated pickup truck and 152-mm (6-in.) curb impacts using LS-DYNA simulations. A series of simulations were performed using a 2,000-kg (4,409-lb) pickup truck impacting AASHTO Types B, C, D, and G curbs at impact angles of 5, 15, and 25 degrees and impact speeds of 70 km/h (43.5 mph) and 100 km/h (62.1 mph).

For a 152-mm (6-in.) AASHTO Type B curb, simulation results showed that the 2000P pickup truck smoothly traversed the curb. The trajectory of the pickup truck bumper was continually increasing from the time of the first wheel impact until 3.3 m (10.8 ft) behind the curb. Furthermore, the height of the bumper exceeded the standard height of a strong-post guardrail (i.e., 685 mm (27 in.)) when the lateral position of the bumper was in the range of 1.5 m (4.92 ft) to almost 5 m (16.4 ft) behind the curb. It also showed that underride of the guardrail was not likely for the 2000P pickup truck.

2.3 Vehicle Impact on Curb and W-beam Guardrail Combination

Due to the objective of this specific project, only 152-mm (6-in.) sloping curb and W-beam guardrail combinations were reviewed.

2.3.1 Plaxico, et al.

An investigation of a vehicle's impact with a curb and guardrail combination was performed by Plaxico using LS-DYNA simulation (11). The simulation results showed that when the guardrail was positioned at a 0-m (0-ft) offset from the curbs, rollover of the vehicle was possible for each curb-barrier scenario involving the AASHTO Types B, C, D, and G curbs due to excessive pitch of the vehicle during redirection. Although the vehicle did not roll over in the simulations, the amount of damage to the front-impact side wheel during impact and the position

of the front wheels during redirection became critical factors regarding vehicle stability when the pitch angle of the vehicle was excessive during redirection.

For the case of 100 km/h (62.1 mph) and 25 degrees impact, the bumper trajectory continuously increased after wheel impact with the curb until the vehicle reached a lateral distance of approximately 6 m (19.7 ft) behind the curb. Furthermore, the bumper remained higher than the guardrail for a lateral distance of approximately 8 m (26.3 ft) with the maximum trajectory occurring at a lateral distance between 4 m (13.1 ft) and 6 m (19.7 ft).

2.3.2 Polivka, et al.

The only full-scale crash test of the MGS and curb combination was performed by MwRSF in test no. NPG-5 (2-3). A 152-mm (6-in.) AASHTO Type B curb was constructed such that the center of the curb's front face was placed 152 mm (6 in.) in front of the front face of the guardrail. The top mounting height of the guardrail remained at 787 mm (31 in.), which was measured from the gutter line to the top of the W-beam rail, as shown in Figure 2.

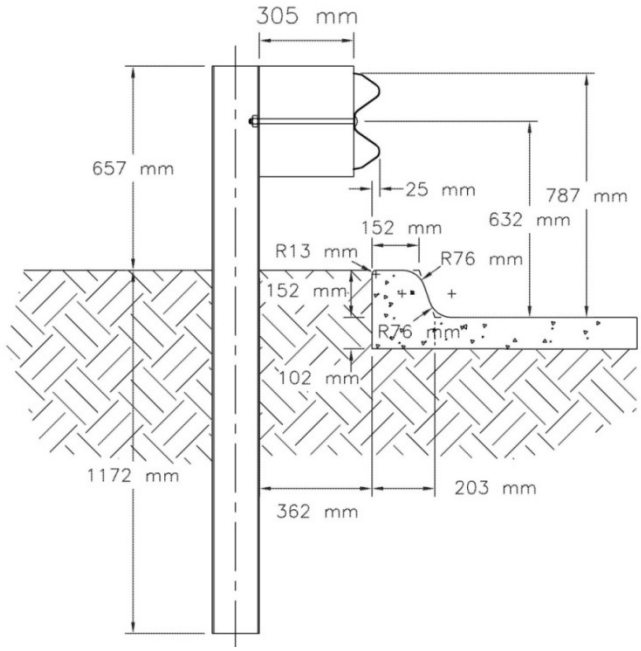

Figure 2. NPG-5 System Setup

A 1,986-kg (4,378-lb) pickup truck impacted the MGS installed over a concrete curb at a speed of 96.6 km/h (60.1 mph) and at an angle of 25.8 degrees. The pickup truck struck the curb first and then was contained and smoothly redirected by the MGS system. The vehicle did not penetrate nor ride over the guardrail and remained upright during and after the collision. Vehicle roll, pitch, and yaw angular displacements were noted and were deemed acceptable according to the TL-3 safety performance criteria found in NCHRP Report No. 350.

2.4 Literature Summary

The 152-mm (6-in.) AASHTO Type B curb was selected for this MGS-Curb combination investigation, since vertical curbs are restricted from high-speed roadways and 152-mm (6-in.) Type B curbs present a worse-case impact scenario over the other sloping curbs. Previous researchers proved that the sloping curbs (including AASHTO Type B) could not redirect errant vehicles at an impact angle larger than 5 degrees. However, damage was found on the wheels of small passenger cars during high-speed impacts with 152-mm (6-in.) AASHTO Type B curbs.

Placement of curbs in front of the guardrail can produce, under certain speed and encroachment angles, vehicle ramping high enough to allow the bumper height to equal or exceed the height of a typical guardrail. For a given type of curb and guardrail, the offset of the barrier away from the curb has been shown to be critical in the performance of the curb-guardrail combination system. The tests indicated that there was very little potential for a regular passenger car to vault over the guardrail. It also showed that underride of the guardrail was not likely for 2000P pickup truck.

3 TEST CONDITIONS

3.1 Test Introduction

According to the literature review, a vehicle's post-curb-impact trajectory is affected by several variables: the size and suspension characteristics of the vehicle, its impact speed, and the angle and shape of the curb itself (6). However, most of the previous research on vehicle-to-curb impacts used old sedans, which are quite different from today's vehicles. Some LS-DYNA simulations were conducted for 2000P pickup truck impacts into curbs, but no physical test was available to validate the simulation results. Thus, physical testing was needed of the 2270P, 1100C, and 2000P vehicles impacting a 152-mm (6-in.) AASHTO Type B curb at 100 km/h (62.1 mph) and 25 degrees in order to obtain accurate vehicle trajectories after curb impact.

3.2 Test Facility

The testing facility is located at the Lincoln Air Park on the northwest (NW) side of the Lincoln Municipal Airport and is approximately 8.0 km (5 mi.) NW of the University of Nebraska-Lincoln.

3.3 Vehicle Tow and Guidance System

A reverse cable tow system with a 1:2 mechanical advantage was used to propel the test vehicle. The distance traveled and the speed reached by the tow vehicle was one-half that of the test vehicle. The test vehicle was released from the tow cable before impact with the curb. A digital speedometer on the tow vehicle increases the accuracy of the test vehicle impact speed.

A vehicle guidance system developed by Hinch (12) was used to steer the test vehicle. A guide-flag, attached to the left-front wheel and the guide cable, was sheared off before impact with the curb system. The 9.5-mm (0.375-in.) diameter guide cable was tensioned to approximately 15.6 kN (3,500 lbs), and supported laterally and vertically every 30.48 m (100 ft)

by hinged stanchions. The hinged stanchions stood upright while holding up the guide cable, but as the vehicle was towed down the line, the guide-flag struck and knocked each stanchion to the ground. For tests MGSC-1, MGSC-2, MGSC-3 and MGSC-4, the vehicle guidance system was 166 m (546 ft) long.

3.4 Test Vehicles

For test nos. MGSC-1 and MGSC-2, a 2003 Dodge Ram 1500 (½ ton) Quad Cab pickup truck was used as the test vehicle. The test inertial and gross static weights were both 2,253 kg (4,966 lbs). The test vehicle is shown in Figures 3 and 4, and vehicle dimensions are shown in Figure 5.

For test no. MGSC-3, a 2002 Kia Rio passenger car was used as the test vehicle. The test inertial and gross static weights were 1,079 kg (2,378 lbs) and 1,154 kg (2,544 lbs), respectively. The test vehicle is shown in Figure 6, and vehicle dimensions are shown in Figure 7.

For test no. MGSC-4, a 1999 Chevrolet C2500 (¾ ton) pickup was used as the test vehicle. The test inertial and gross static weights were both 2,032 kg (4,479 lbs). The test vehicle is shown in Figure 8, and vehicle dimensions are shown in Figure 9.

The Suspension Method (13) was used to determine the vertical component of the center of gravity (C.G.) for the pickup truck and the small car. This method is based on the principle that the C.G. of any freely suspended body is in the vertical plane through the point of suspension. The vehicle was suspended successively in three positions, and the respective planes containing the C.G. were established. The intersection of these planes pinpointed the location of the center of gravity. The longitudinal component of the C.G. was determined using the measured axle weights. The locations of the final longitudinal location of centers of gravity are shown in Figures 5, 7, and 9.

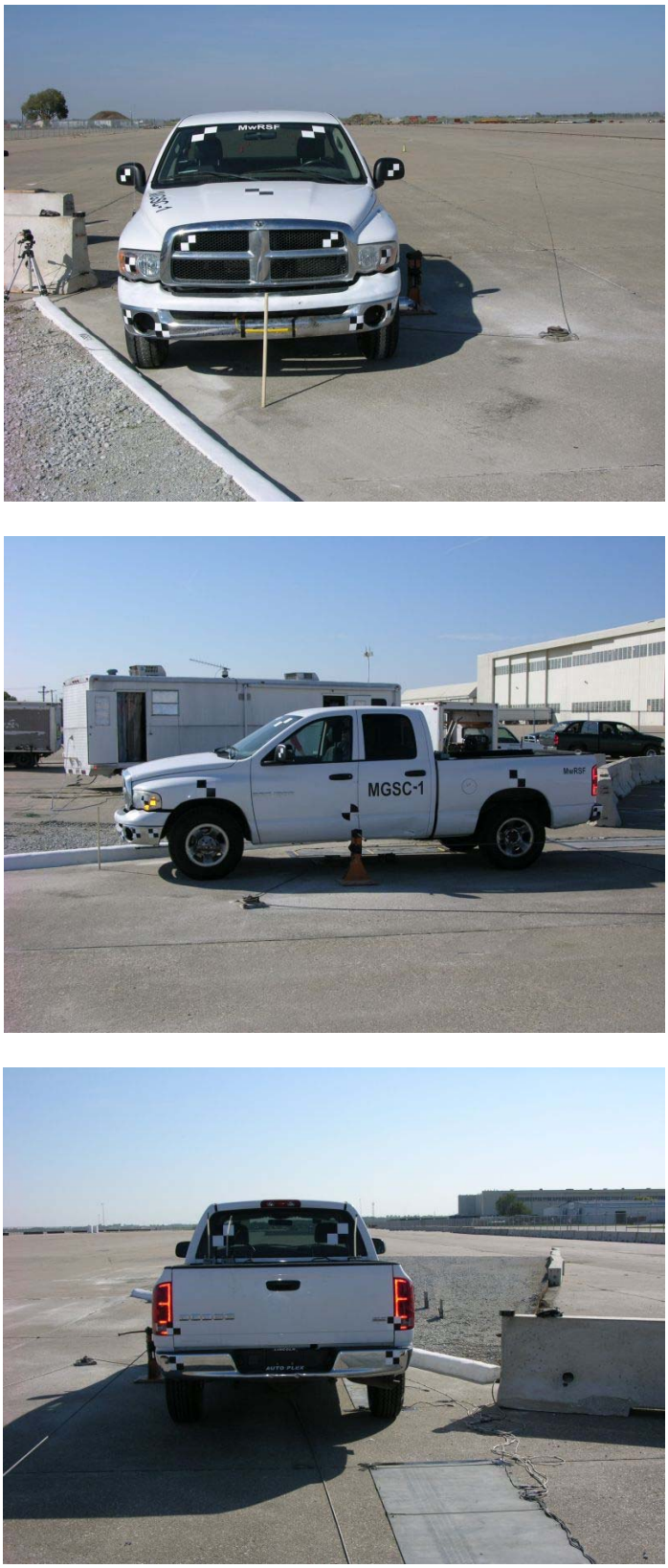

Figure 3. Test Vehicle, Test MGSC-1

Figure 4. Test Vehicle, Test MGSC-2

Date:	10/11&12/07	Test Number:	MGSC-1&2	Model:	Ram 1500 Q.C.
Make:	Dodge	Vehicle I.D.#:	1D7HA18N83J526581		
Tire Size:	265/70 R17	Year:	2003	Odometer:	139905

*(All Measurements Refer to Impacting Side)

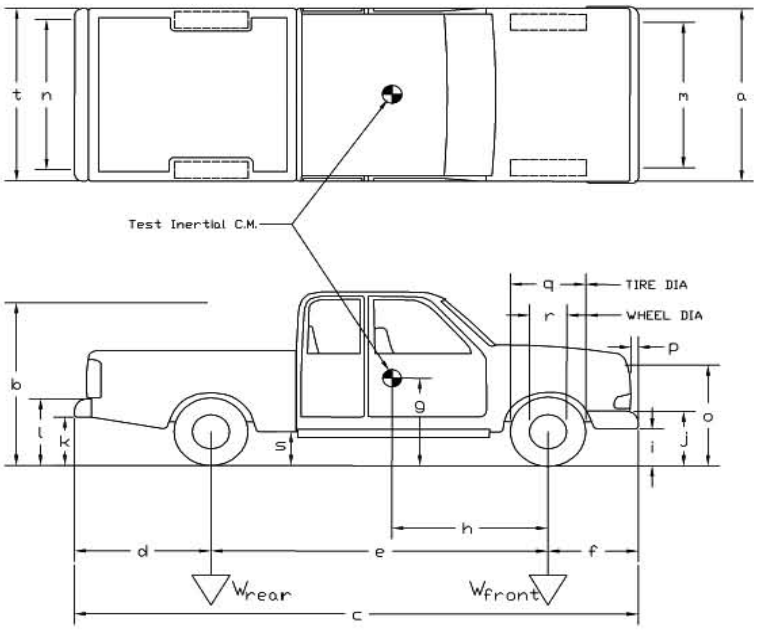

Vehicle Geometry -- mm (in.)

a	1994	(78.503)	b	1924	(75.748)
c	5829	(229.488)	d	1149	(45.236)
e	3562	(140.236)	f	1118	(44.016)
g	718	(28.268)	h	1575	(62.008)
i	394	(15.512)	j	686	(27.008)
k	546	(21.496)	l	756	(29.764)
m	1727	(67.992)	n	1721	(67.756)
o	1168	(45.984)	p	89	(3.504)
q	800	(31.496)	r	470	(18.504)
s	394	(15.512)	t	1969	(77.52)
Wheel Center Height Front				387	(15.236)
Wheel Center Height Rear				391	(15.394)
Wheel Well Clearance (FR)				908	(35.748)
Wheel Well Clearance (RR)				978	(38.504)
Frame Height (FR)				457	(17.992)
Frame Height (RR)				641	(25.236)
Engine Type				8 CYL. GAS	
Engine Size				4.7L	
Transmition Type:				Automatic	

Weights kg (lbs)	Curb		Test Inertial		Gross Static			RWD
W-front	1295	(2855)	1252	(2760)	1252	(2760)	Front GVWR	3650
W-rear	1042	(2297)	1001	(2207)	1001	(2207)	Rear GVWR	3900
W-total	2337	(5152)	2253	(4967)	2253	(4967)	Total GVWR	6650

Note any damage prior to test: Repaired SR-8 test vehicle, some cosmetic damage

Figure 5. Test Vehicle Dimensions, Tests MGSC-1 and MGSC-2

Figure 6. Test Vehicle, Test MGSC-3

Date:	10/23/2007	Test Number:	MGSC-3	Model:	Rio Sedan
Make:	Kia	Vehicle I.D.#:	KNADC123326172817		
Tire Size:	P175/65R14	Year:	2002	Odometer:	64654

Tire Inflation Pressure: 32 psi

*(All Measurements Refer to Impacting Side)

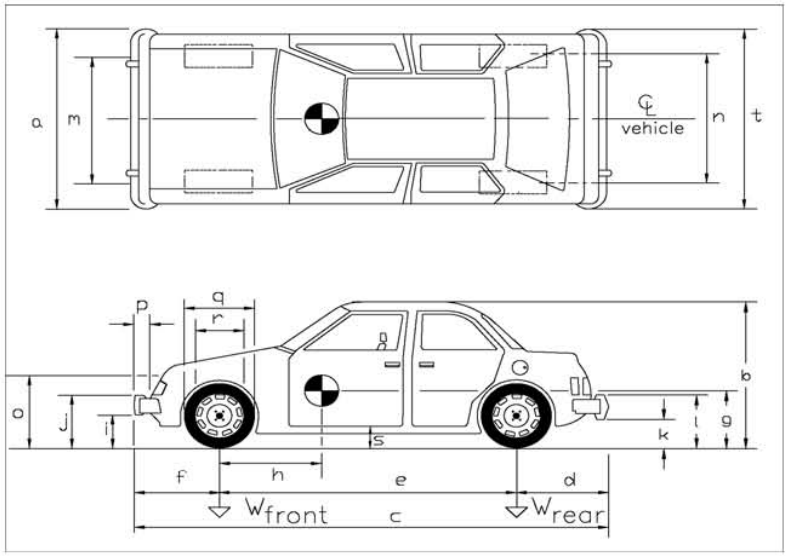

Vehicle Geometry -- mm (in.)

a	1632	(64.252)	b	1410	(55.512)
c	4216	(165.984)	d	997	(39.252)
e	2413	(95.0)	f	806	(31.732)
g	457	(17.992)	h	978	(38.504)
i	241	(9.488)	j	495	(19.488)
k	305	(12.008)	l	546	(21.496)
m	1429	(56.26)	n	1442	(56.772)
o	540	(21.26)	p	76	(2.992)
q	572	(22.52)	r	387	(15.236)
s	292	(11.496)	t	1619	(63.74)

Wheel Center Height Front	270	(10.63)
Wheel Center Height Rear	279	(10.984)
Wheel Well Clearance (FR)	622	(24.488)
Wheel Well Clearance (RR)	610	(24.016)
Frame Height (FR)	#####	NA
Frame Height (RR)	#####	NA
Engine Type	4cyl. GAS	
Engine Size	1.6L	

Mass Distribution

LF	682	RF	733
LR	507	RR	456

Weights kg (lbs)

	Curb		Test Inertial		Gross Static	
W-front	654	(1442)	642	(1415)	683	(1506)
W-rear	396	(873)	437	(963)	471	(1038)
W-total	1050	(2315)	1079	(2379)	1154	(2544)

Transmition Type:

Automatic (Manual)

(FWD) RWD 4WD

GVWR Ratings

Front	1808
Rear	1742
Total	(3315)

Dummy Data

Type: Hybrid 2

Mass: 166lbs

Seat Position: Full Rearward

Note any damage prior to test:

Figure 7. Test Vehicle Dimensions, Test MGSC-3

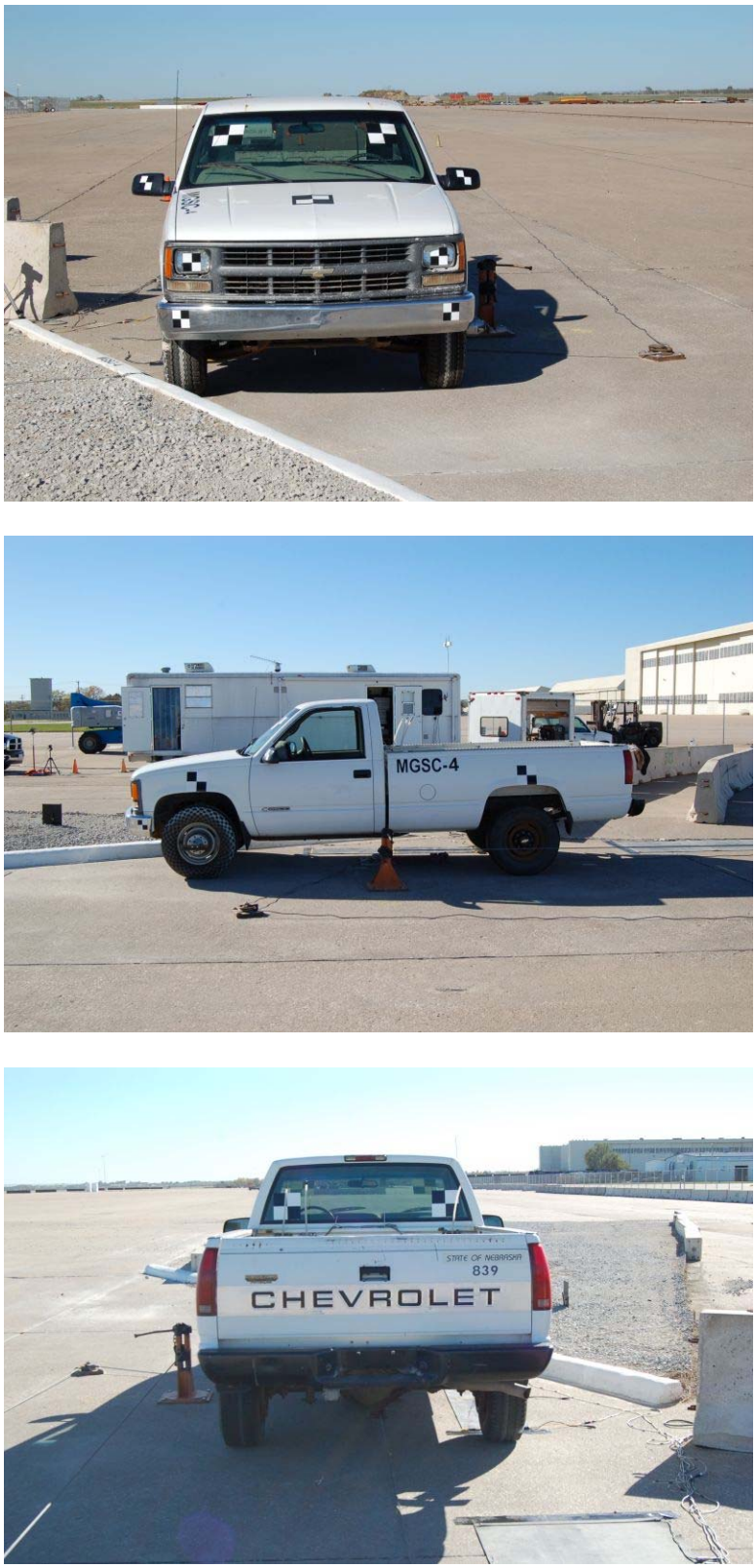

Figure 8. Test Vehicle, Test MGSC-4

Date:	10/23/2007	Test Number:	MGSC-4	Model:	2000p/C2500
Make:	Chevrolet	Vehicle I.D.#:	1GCGC24R5ZR705991		
Tire Size:	LT245/75 R16	Year:	1999	Odometer:	201350

*(All Measurements Refer to Impacting Side)

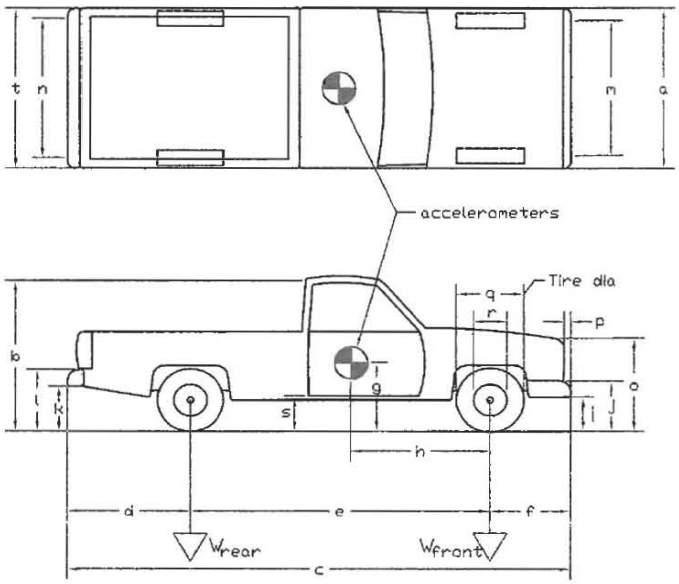

Vehicle Geometry -- mm (in.)

a	1873	(73.74)	b	1854	(72.992)
c	5544	(218.268)	d	1302	(51.26)
e	3340	(131.496)	f	864	(34.016)
g	667	(26.26)	h	1575	(62.008)
i	451	(17.756)	j	673	(26.496)
k	616	(24.252)	l	800	(31.496)
m	1594	(62.756)	n	1626	(64.016)
o	1067	(42.008)	p	89	(3.504)
q	724	(28.504)	r	438	(17.244)
s	483	(19.016)	t	1848	(72.756)
Wheel Center Height Front				362	(14.252)
Wheel Center Height Rear				359	(14.134)
Wheel Well Clearance (FR)				895	(35.236)
Wheel Well Clearance (RR)				959	(37.756)
Frame Height (FR)				387	(15.236)
Frame Height (RR)				699	(27.52)
Engine Type				8 CYL. GAS	
Engine Size				5.7L	

GVWR		
	F	4100
	R	6000
	Tot.	8600

Transmition Type:

Automatic

RWD

Weights kg (lbs)	Curb		Test Inertial		Gross Static	
W-front	1196	(2637)	1179	(2599)	1179	(2599)
W-rear	912	(2011)	853	(1881)	853	(1881)
W-total	2107	(4645)	2032	(4480)	2032	(4480)

Note any damage prior to test: None

Figure 9. Test Vehicle Dimension, Test MGSC-4

Black and white, checkered targets were placed on the vehicle to aid in the analysis of the high-speed digital video, as shown in Figures 10 through 12. One target was placed on each wheel center, one target was placed directly above each of the wheels, one was placed both on the vehicle's bumper front and side, and another was placed at the vehicle's C.G. on both the driver and passenger sides. In addition, targets were placed on the top of the vehicle. One target was placed at the vehicle's center of gravity, two were placed on the windshield, one was placed on the hood of the vehicle, one was placed on the vehicle's top, and one was placed on the top of the vehicle's trunk, aligned with the centerline of the vehicle top view. For the trucks, two targets were placed in the bed, aligned with the centerline of the vehicle. Also, targets were placed on the vehicle's front side.

The front wheels of each test vehicle were aligned for camber, caster, and toe-in values of zero so the vehicles would track properly along the guide cable. One 5B flash bulb was mounted on the dashboard of each vehicle to pinpoint the time of impact with the curb on the high-speed AOS videos. The flash bulbs were fired by a pressure tape switch mounted on the front face of the bumper. Another pressure tape was mounted on the front side of the curb to indicate the impact time. A remote-controlled brake system was installed in the test vehicle so the vehicle could be brought safely to a stop after the test.

3.5 Curb Setup

The 10.7-m (35-ft) long test installation consisted of 152-mm (6-in.) high AASHTO Type B curb doweled into the existing concrete apron. Design details are shown in Figures 13 through 15. The corresponding English-unit drawings are shown in Appendix A. Photographs of the test installation are shown in Figure 16.

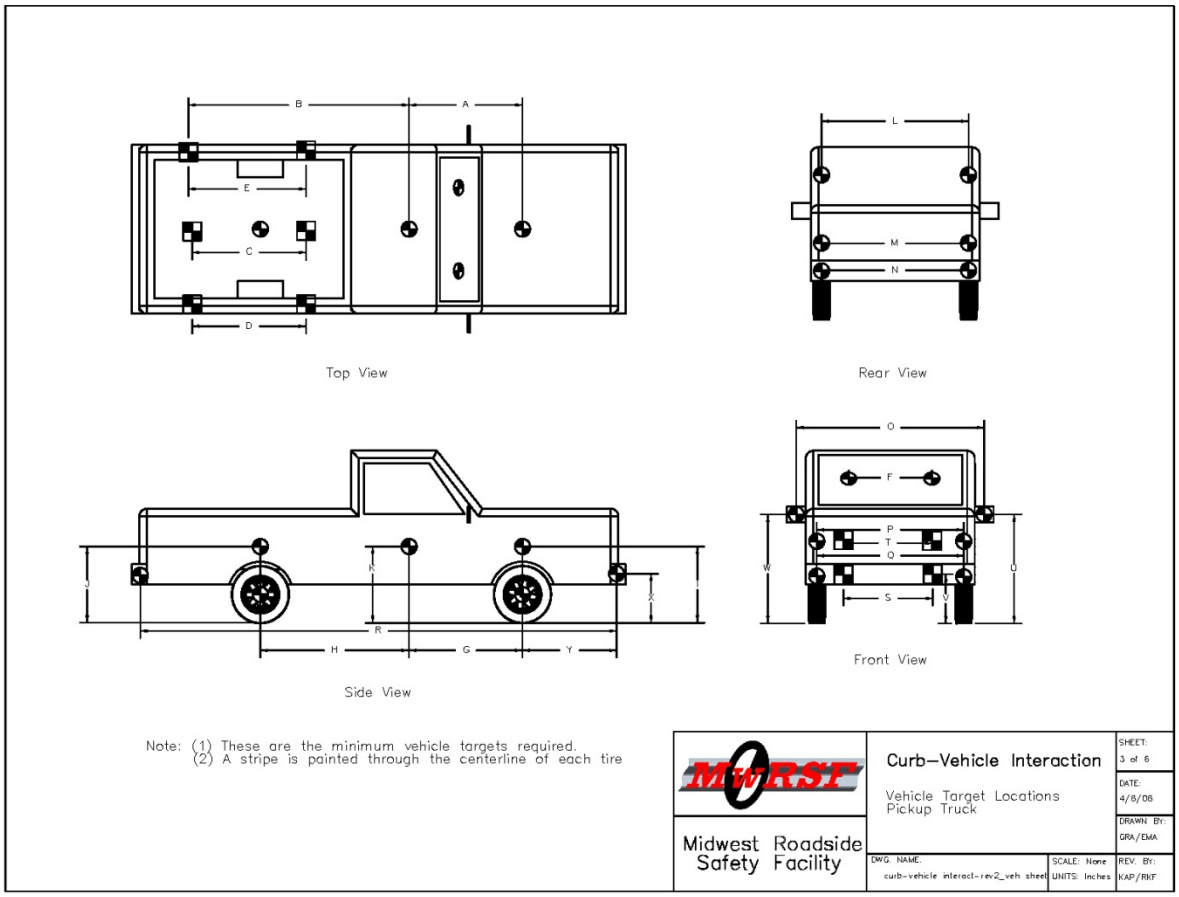

Location	mm	in.	Location	mm	in.
A	1870	73.6	**N**	1570	61.8
B	2718	107	**O**	2238	88.1
C	1219	48	**P**	1753	69
D	1626	64	**Q**	1788	70.4
E	1626	64	**R**	5205	204.9
F	1092	43	**S**	1295	51
G	1575	62	**T**	940	37
H	1988	78.3	**U**	NA	NA
I	1016	40	**V**	452	17.8
J	1086	42.8	**W**	NA	NA
K	718	28.3	**X**	521	20.5
L	1092	43	**Y**	571.5	22.5
M	1613	63.5			

Figure 10. Vehicle Target Locations, Tests MGSC-1 and MGSC-2

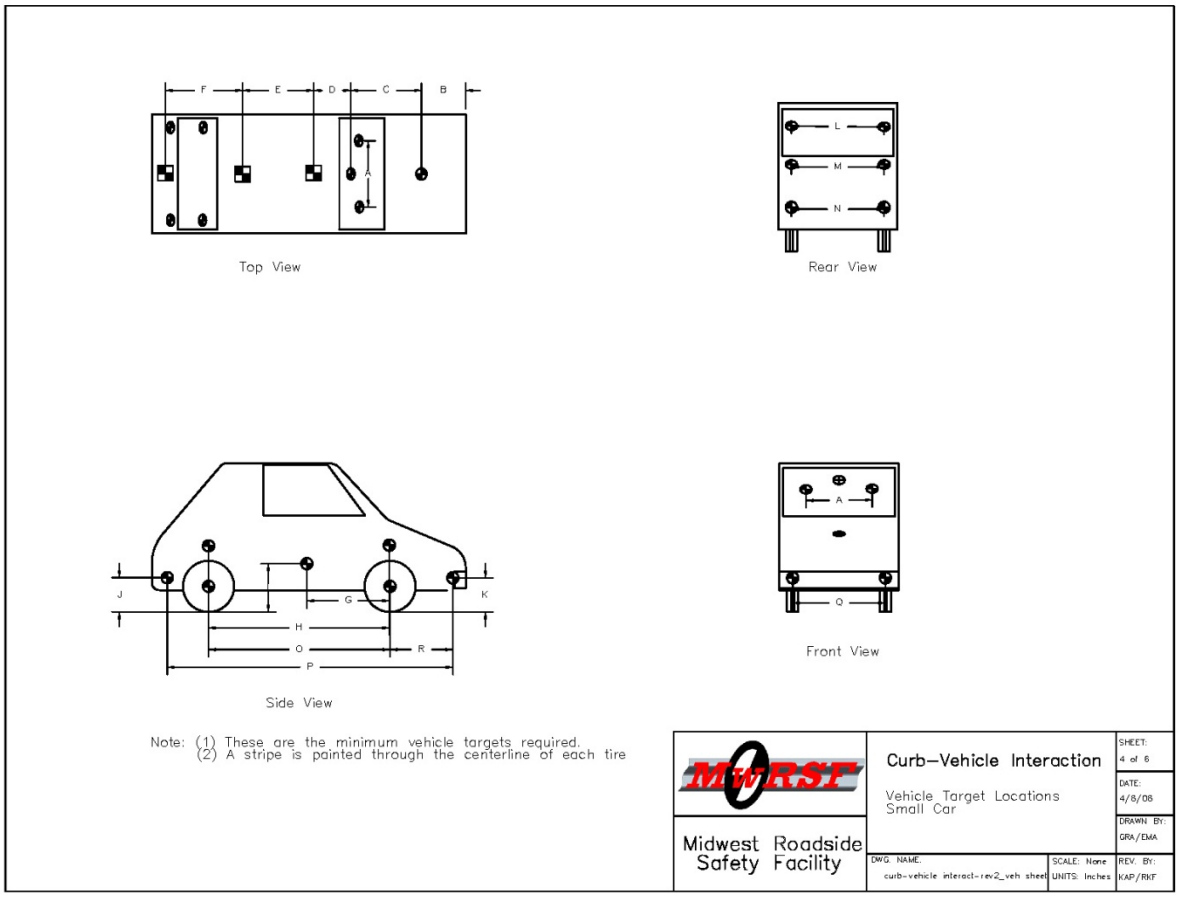

Location	mm	in.	Location	mm	in.
A	806	31.75	**N**	870	34.25
B	676	26.6	**O**	2413	95
C	1089	42.9	**P**	3327	131
D	270	10.6	**Q**	NA	NA
E	946	37.3	**R**	445	17.5
F	895	35.25			
G	978	38.5			
H	2413	95			
I	457	18			
J	NA	NA			
K	419	16.5			
L	826	32.5			
M	1238	48.75			

Figure 11. Vehicle Target Locations, Test MGSC-3

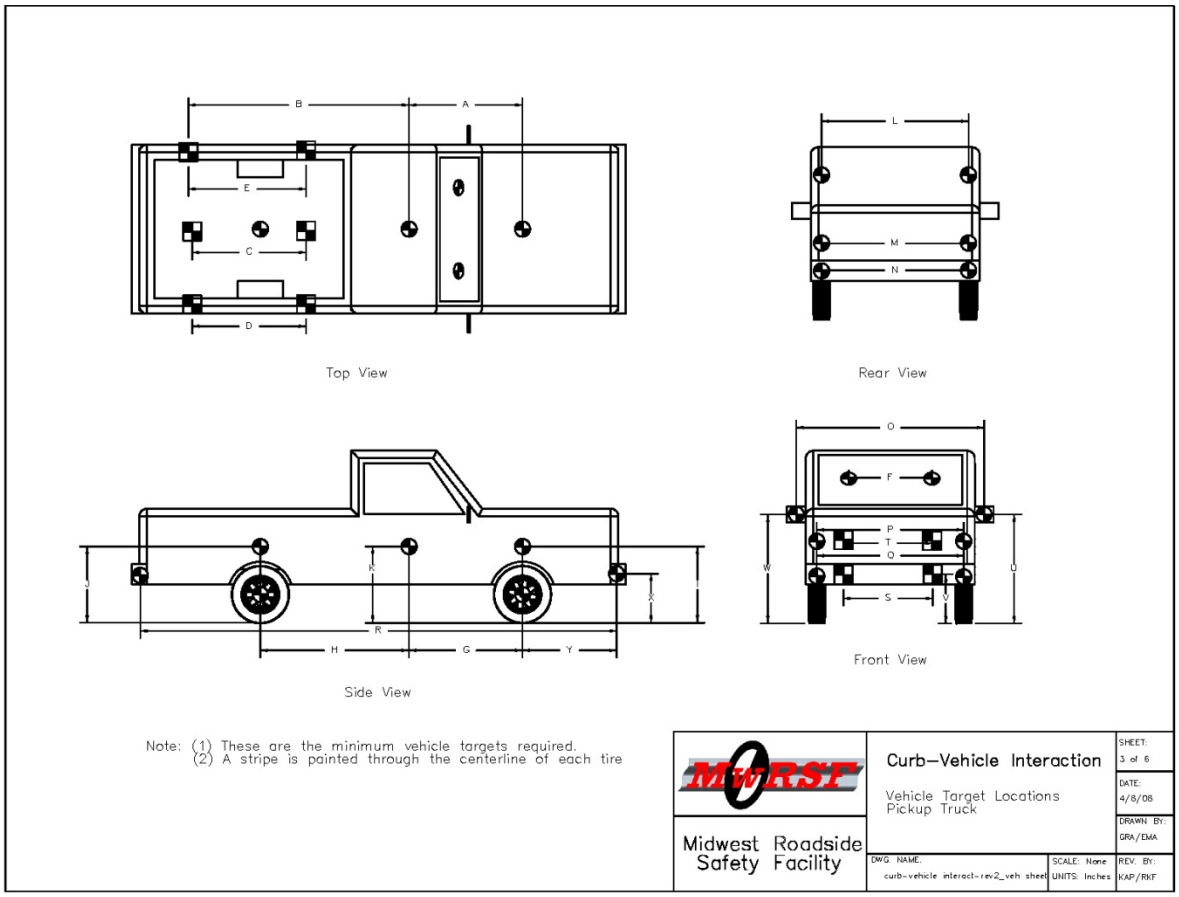

Location	mm	in.	Location	mm	in.
A	NA	NA	**N**	NA	NA
B	NA	NA	**O**	2159	85
C	NA	NA	**P**	1448	57
D	2153	84.75	**Q**	1575	62
E	2153	84.75	**R**	NA	NA
F	NA	NA	**S**	NA	NA
G	1575	62	**T**	NA	NA
H	1765	69.5	**U**	NA	NA
I	997	39.25	**V**	NA	NA
J	1060	41.75	**W**	NA	NA
K	667	26.25	**X**	572	22.5
L	1188	46.8	**Y**	572	22.5
M	NA	NA			

Figure 12. Vehicle Target Locations, Test MGSC-4

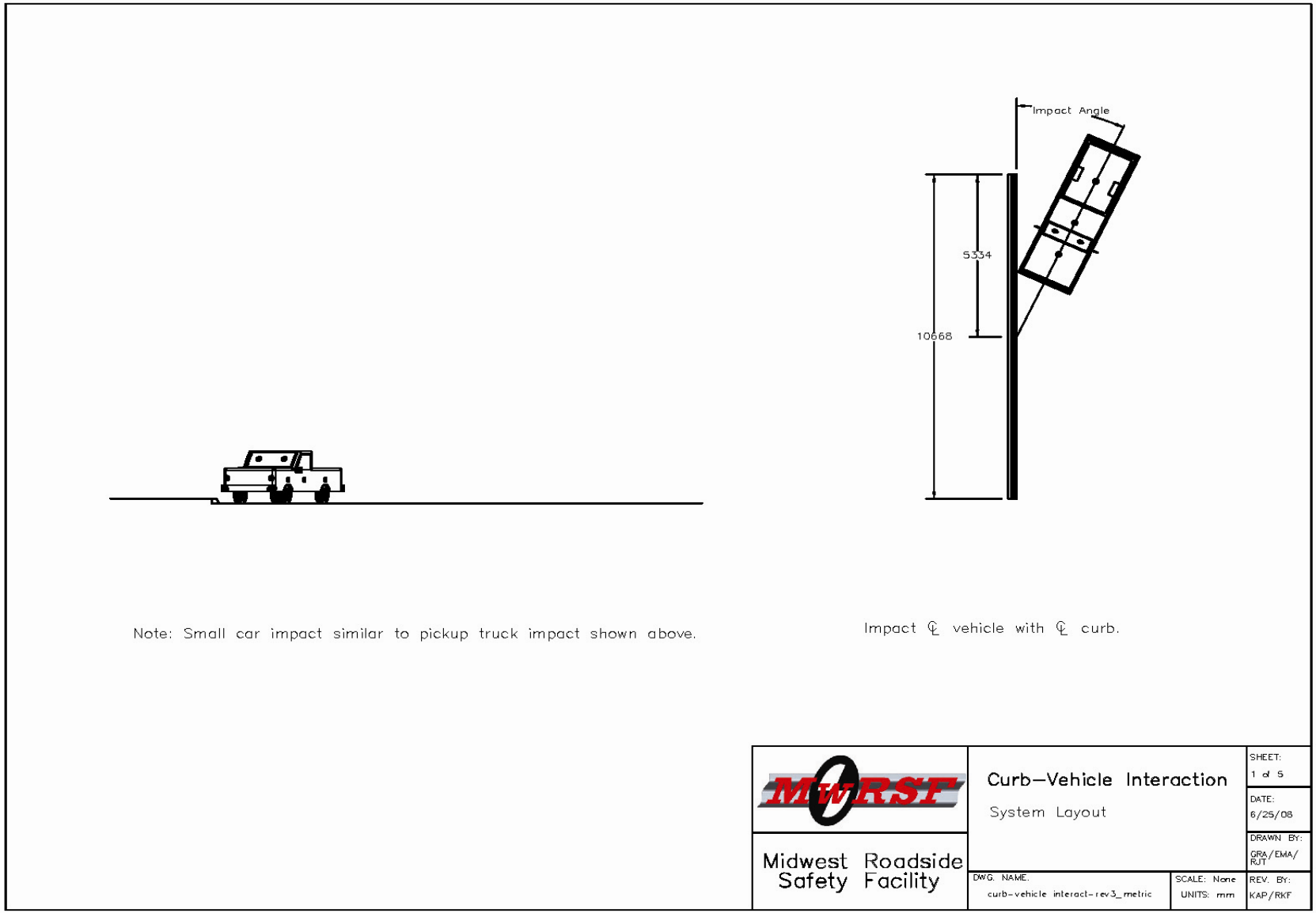

Figure 13. System Layout

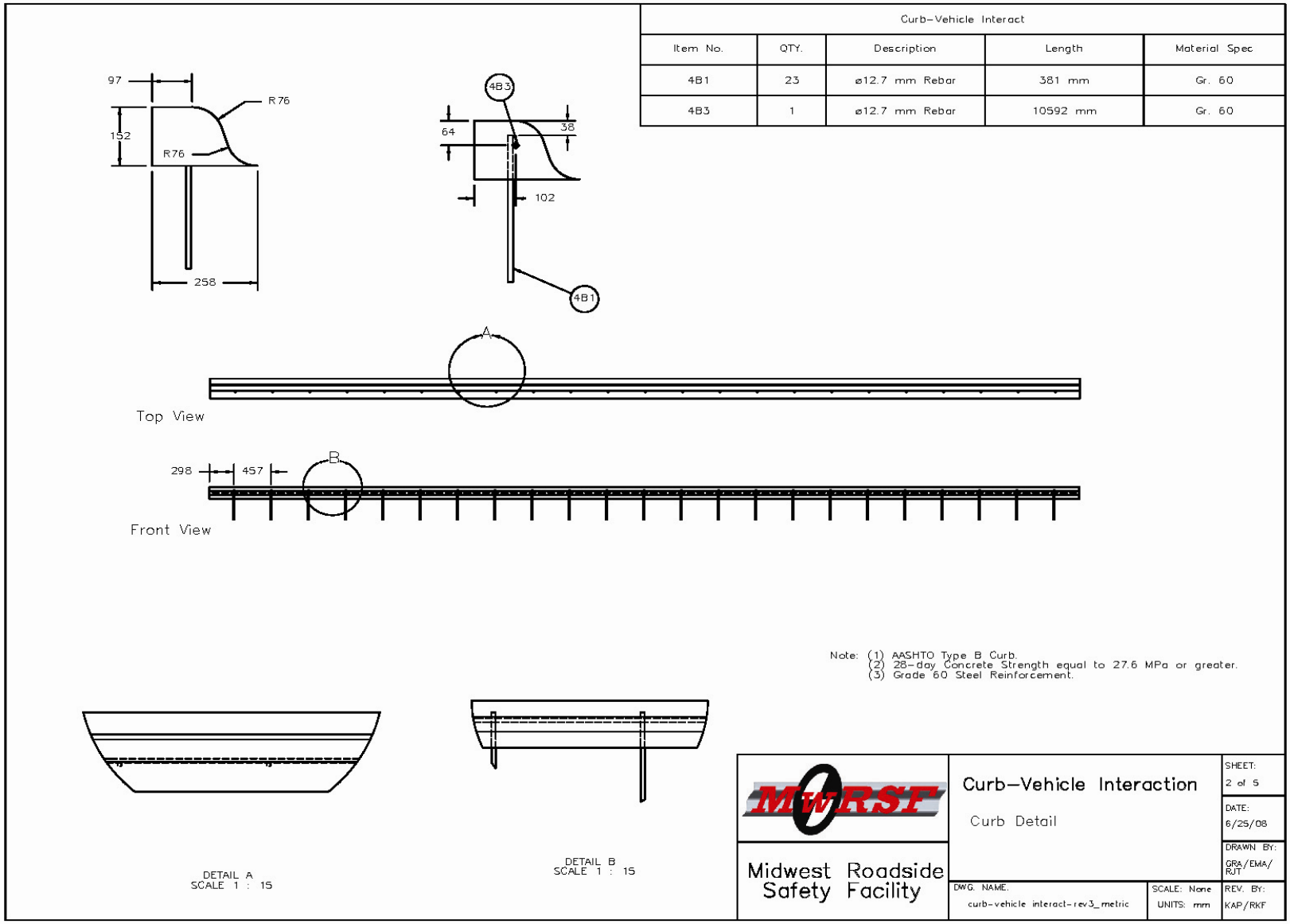

Figure 14. Curb Detail

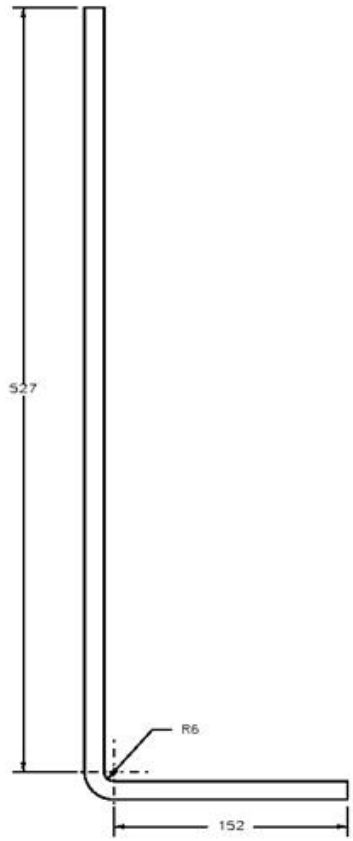

Curb–Vehicle Interact					
Item No.	Bend Dia.	Quantity	Length	Material Spec	Bar Size
4B1	–	32	381mm	Gr. 60	12.7mm
4B2	6.4mm	32	711mm	Gr. 60	12.7mm
4B3	–	3	10,592mm	Gr. 60	12.7mm

MWRSF

Midwest Roadside Safety Facility

Curb–Vehicle Interaction

Bill of Bars

SHEET: 6 of 6

DATE: 4/8/08

DRAWN BY: GRA/EMA

DWG. NAME: curb-vehicle interact-rev2_metric

SCALE: None

UNITS: mm

REV. BY: KAP/RKF

Figure 15**. Bill of Bars**

Figure 16. 152-mm (6-in.) AASHTO Type B Curb Construction and Test Layout

3.6 Data Acquisition Systems

3.6.1 Accelerometers

One triaxial piezoresistive accelerometer system with a range of ± 200 g's was used to measure the acceleration in the longitudinal, lateral, and vertical directions at a sample rate of 10,000 Hz. The environmental shock and vibration sensor/recorder system, Model EDR-4M6, was developed by Instrumented Sensor Technology (IST) of Okemos, Michigan and includes three differential channels as well as three single-ended channels. The EDR-4 was configured with 6 MB of RAM memory and a 1,500 Hz low-pass filter. "DYNAMax 1 (DM-1)" and "DADiSP" computer software programs were was used to analyze and plot the accelerometer data.

Another triaxial piezoresistive accelerometer system with a range of ± 200 g's was also used to measure the acceleration in the longitudinal, lateral, and vertical directions at a sample rate of 3,200 Hz. The environmental shock and vibration sensor/recorder system, Model EDR-3, was developed by Instrumental Sensor Technology (IST) of Okemos, Michigan. The EDR-3 was configured with 256 KB of RAM memory and a 1,120 Hz low-pass filter. "DYNAMax 1 (DM-1)" and "DADiSP" computer software programs were used to analyze and plot the accelerometer data.

An additional accelerometer system was used to measure the acceleration in the longitudinal, lateral, and vertical directions at a sample rate of 10,000 Hz, except for MGSC-3 test. The environmental shock and vibration sensor/recorder system, a two-Arm piezoresistive accelerometer, was developed by Endevco of San Juan Capistrano, CA. Three accelerometers were used to measure each of the longitudinal, lateral, and vertical accelerations independently. Data was collected using a Sensor Input Module (SIM), Model TDAS3-SIM-16M, which was

developed by Diversified Technical Systems, Inc. (DTS) of Seal Beach, CA. The SIM was configured with 16 MB SRAM memory and 8 sensor input channels with 250 kB SRAM/channel. The SIM was mounted on a TDAS3-R4 module rack. The module rack is configured with isolated power/event/communications, 10BaseT Ethernet and RS232 communication, and an internal back-up battery. Both the SIM and module rack are crashworthy. "DTS TDAS Control" and "DADiSP" computer software programs and a customized Microsoft Excel worksheet were used to analyze and plot the accelerometer data.

3.6.2 Rate Transducers

An Analog Systems 3-axis rate transducer with a range of 1,200 degrees/sec in each of the three directions (pitch, roll, and yaw) was used to measure the rates of motion of the test vehicle. The rate transducer was mounted inside the body of the EDR-4M6 and recorded data at 10,000 Hz to a second data acquisition board inside the EDR-4M6 housing. The raw data measurements were then downloaded, converted to the appropriate Euler angles for analysis, and plotted. "DYNAMax 1 (DM-1)" and "DADiSP" computer software programs were used to analyze and plot the rate transducer data.

ARS-1500 analog angular rate transducer was also used. The ARS-1500 has a range of 1,500 degrees/sec in each of the three directions (pitch, roll, and yaw) and was used to measure the rates of rotation of the test vehicle. The angular rate sensor was mounted on an aluminum block inside the test vehicle at the center of gravity and recorded data at 10,000 Hz to the SIM. The raw data measurements were then downloaded, converted to the proper Euler angles for analysis, and plotted. "DTS TDAS Control" and "DADiSP" computer software programs and a customized Microsoft Excel worksheet were used to analyzed and plot the rate transducer data.

3.6.3 High-Speed Photography

For test no. MGSC-1, four AOS VITcam high-speed digital video cameras, with operating speeds of 500 frames/sec, were used to film the crash test. Four JVC digital video cameras, with standard operating speeds of 29.97 frames/sec were also used to film the crash test. Camera details and a schematic of all eight camera locations are shown along with a schematic of the camera locations in Figure 17.

For test no. MGSC-2, four AOS VITcam high-speed digital video cameras, with operating speeds of 500 frames/sec, were used to film the crash test. Four JVC digital video cameras, with standard operating speeds of 29.97 frames/sec, were also used to film the crash test. Camera details and a schematic of all eight camera locations are shown in Figure 18.

For test nos. MGSC-3 and MGSC-4, four AOS VITcam high-speed digital video cameras, with operating speeds of 500 frames/sec, were used to film the crash tests. Four JVC digital video cameras, with standard operating speed of 29.97 frames/sec, were also used to film the crash tests. Camera details and a schematic of all eight camera locations are shown in Figures 19 and 20.

The AOS VITcam videos were analyzed using ImageExpress MotionPlus and Redlake Motion Scope software. Camera speed and camera divergence factors were considered in the analysis of the high-speed videos.

3.6.4 Pressure Tape Switches

For all tests, five pressure-activated tape switches, spaced at 2-m (6.56-ft) intervals, were used to determine the speed of the vehicle before impact. Each tape switch fired a strobe light which sent an electronic timing signal to the data acquisition system as the right-front tire of the test vehicle passed over it. The test vehicle speed was then determined from the electronic timing

mark data recorded using TestPoint software. Strobe lights and high-speed video analysis are used only as a backup in the event that vehicle speed cannot be determined from the electronic data.

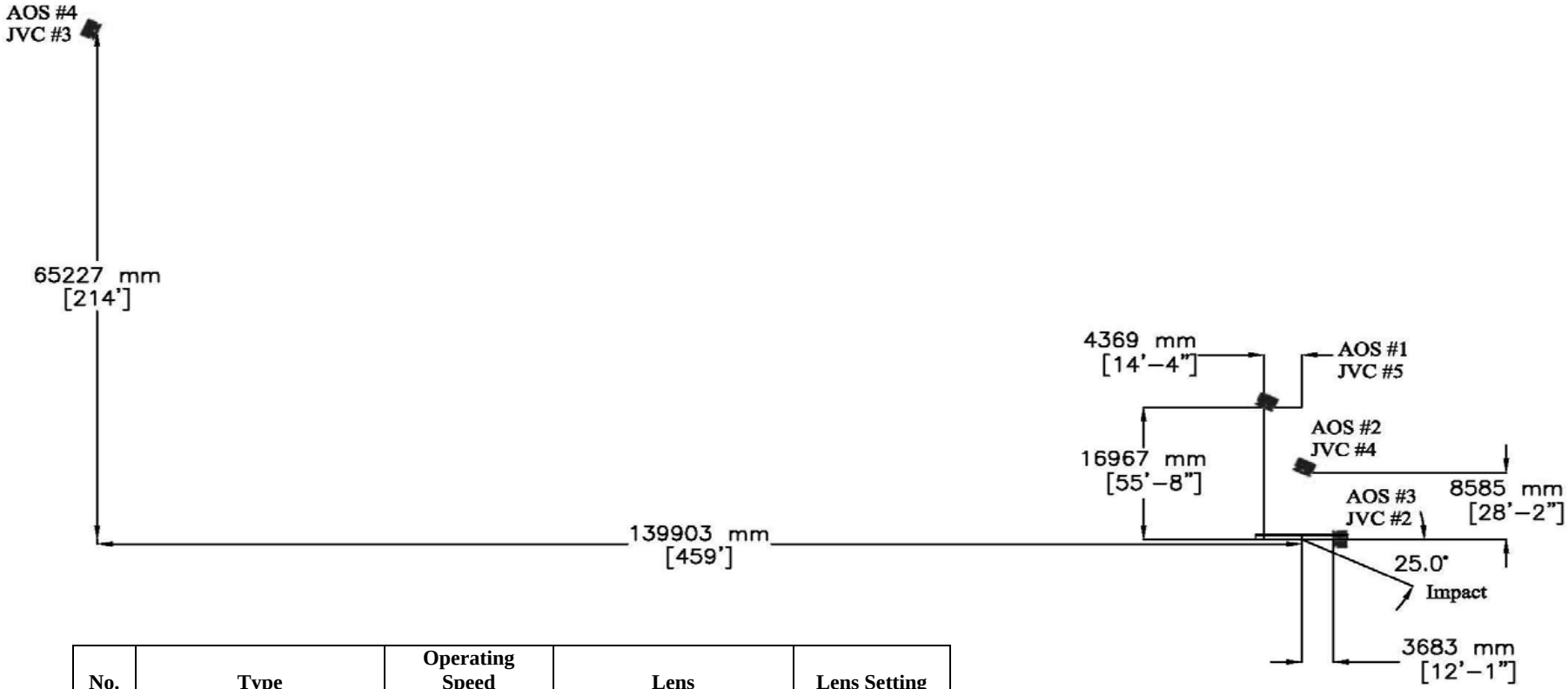

	No.	Type	Operating Speed (frames/sec)	Lens	Lens Setting
High-Speed Video	**1**	VITcam CTM	500	Kowa 8 mm fixed	NA
	2	VITcam CTM	500	Sigma 24-70	24
	3	VITcam CTM	500	Sigma 50mm fixed	NA
	4	VITcam CTM	500	Sigma 70-200	200
Digital Video	**2**	JVC-GZ-MC40u(Everio)	29.97	NA	NA
	3	JVC-GZ-MC40u(Everio)	29.97	NA	NA
	4	JVC-GZ-MC40u(Everio)	29.97	NA	NA
	5	JVC-GZ-MC27u(Everio)	29.97	NA	NA

Figure 17. Location of Cameras, Test MGSC-1

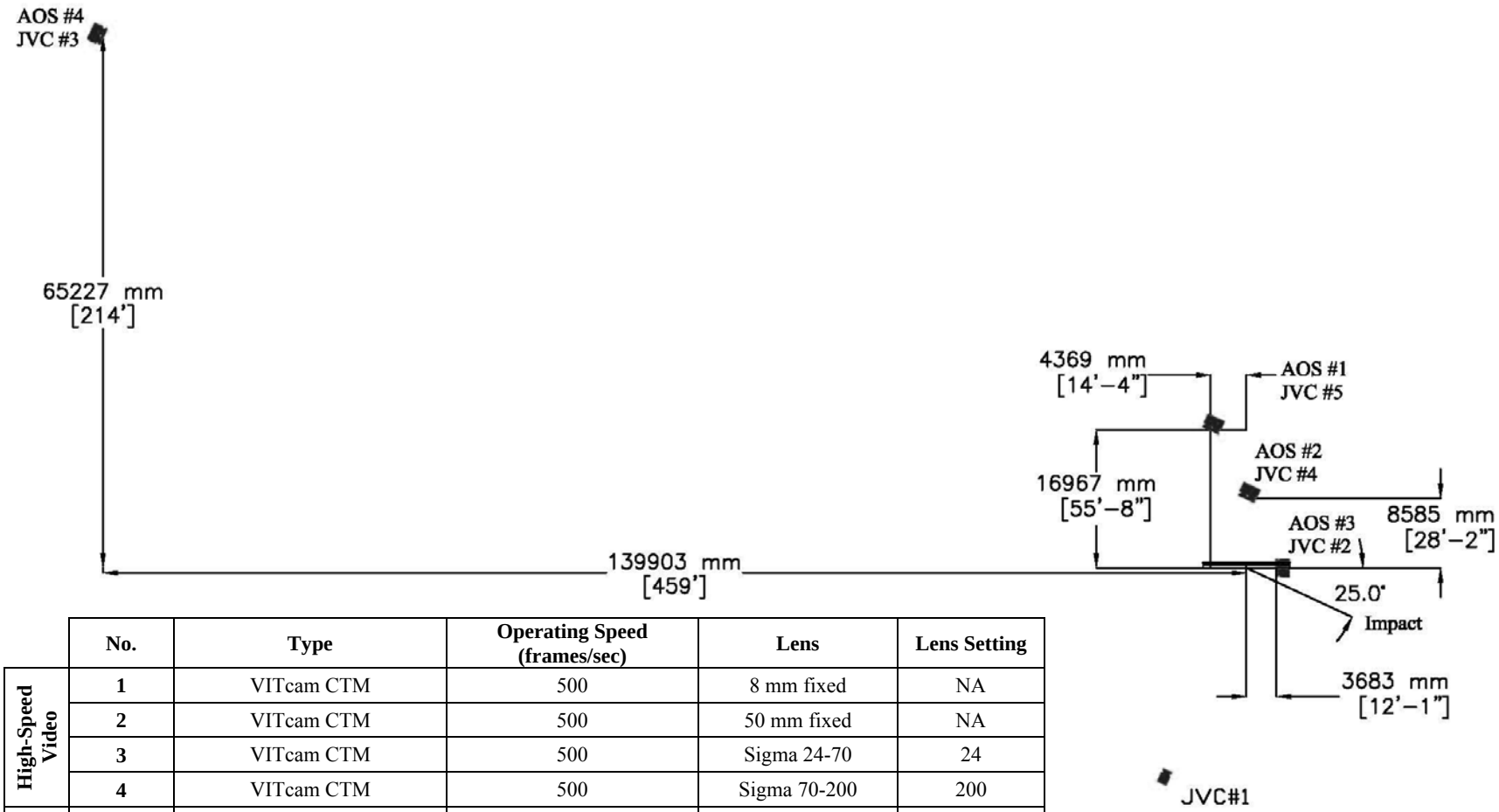

	No.	Type	Operating Speed (frames/sec)	Lens	Lens Setting
High-Speed Video	1	VITcam CTM	500	8 mm fixed	NA
	2	VITcam CTM	500	50 mm fixed	NA
	3	VITcam CTM	500	Sigma 24-70	24
	4	VITcam CTM	500	Sigma 70-200	200
Digital Video	1	JVC-GZ-MC500(Everio)	29.97	NA	NA
	2	JVC-GZ-MC40u(Everio)	29.97	NA	NA
	3	JVC-GZ-MC40u(Everio)	29.97	NA	NA
	4	JVC-GZ-MC40u(Everio)	29.97	NA	NA
	5	JVC-GZ-MC27u(Everio)	29.97	NA	NA

Figure 18. Location of Cameras, Test MGSC-2

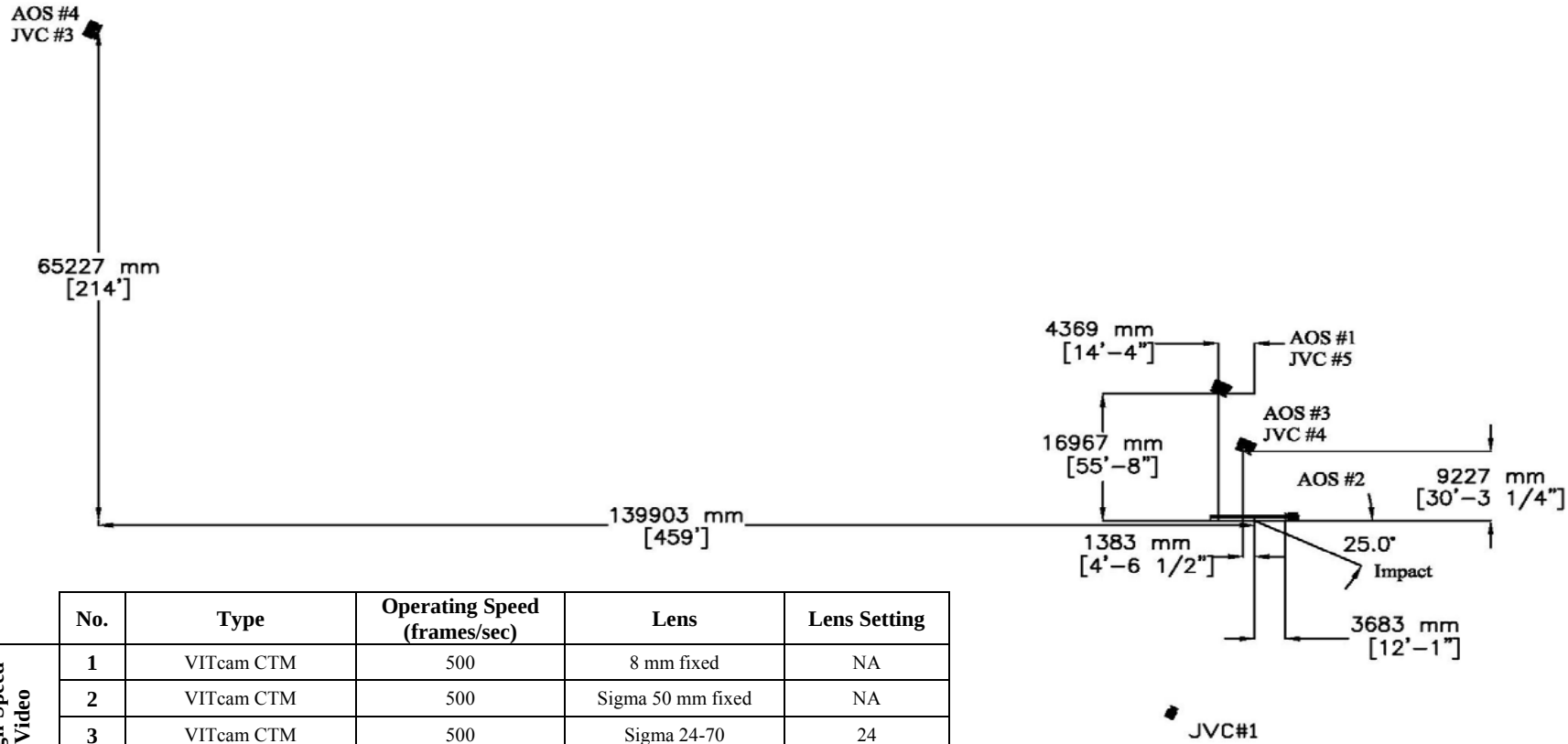

	No.	Type	Operating Speed (frames/sec)	Lens	Lens Setting
High-Speed Video	1	VITcam CTM	500	8 mm fixed	NA
	2	VITcam CTM	500	Sigma 50 mm fixed	NA
	3	VITcam CTM	500	Sigma 24-70	24
	4	VITcam CTM	500	Sigma 70-200	200
Digital Video	1	JVC-GZ-MC500(Everio)	29.97	NA	NA
	3	JVC-GZ-MC40u(Everio)	29.97	NA	NA
	4	JVC-GZ-MC40u(Everio)	29.97	NA	NA
	5	JVC-GZ-MC27u(Everio)	29.97	NA	NA

Figure 19. Location of Cameras, Test MGSC-3

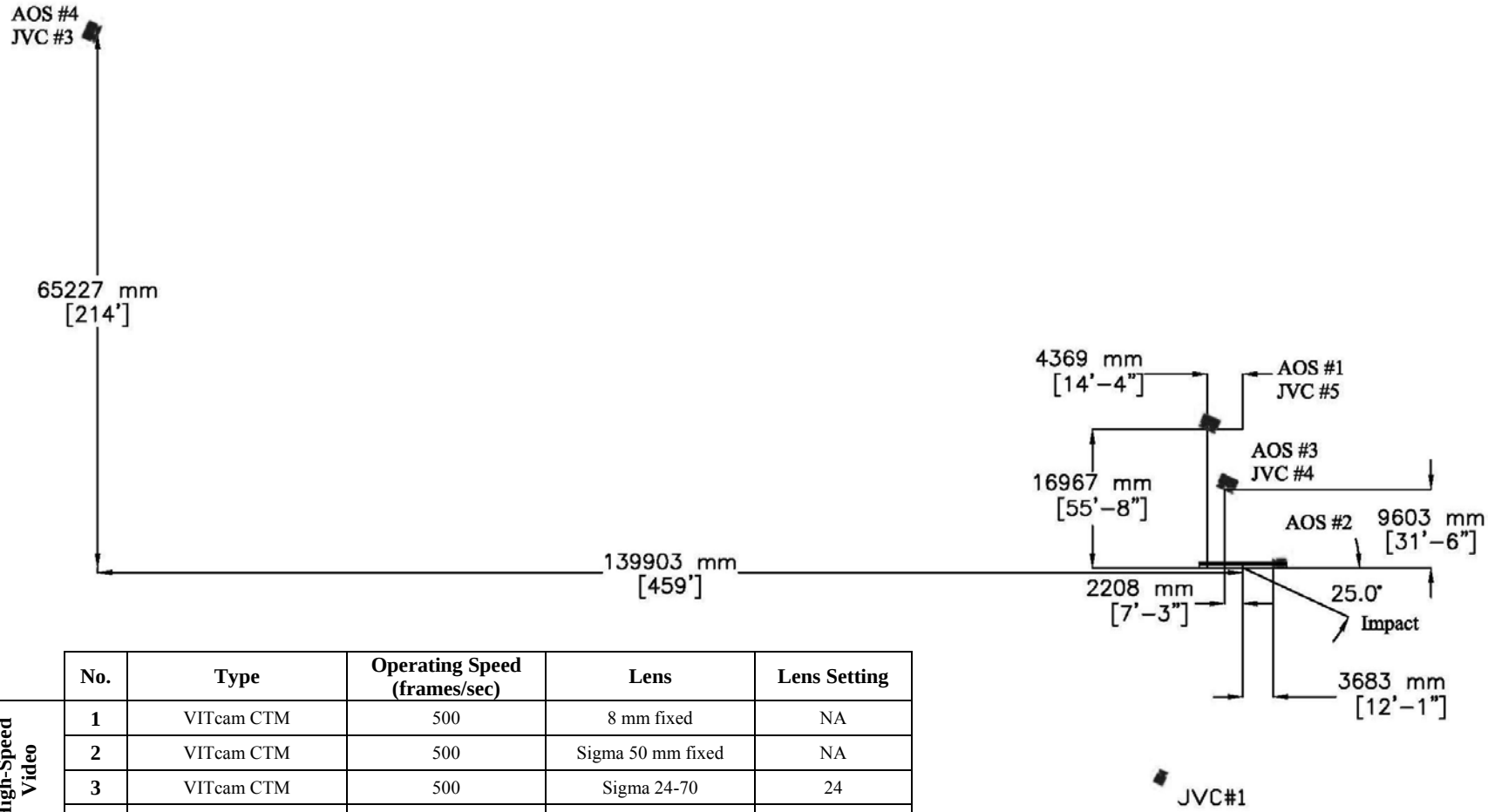

	No.	Type	Operating Speed (frames/sec)	Lens	Lens Setting
High-Speed Video	**1**	VITcam CTM	500	8 mm fixed	NA
	2	VITcam CTM	500	Sigma 50 mm fixed	NA
	3	VITcam CTM	500	Sigma 24-70	24
	4	VITcam CTM	500	Sigma 70-200	200
Digital Video	**1**	JVC-GZ-MC500(Everio)	29.97	NA	NA
	3	JVC-GZ-MC40u(Everio)	29.97	NA	NA
	4	JVC-GZ-MC40u(Everio)	29.97	NA	NA
	5	JVC-GZ-MC27u(Everio)	29.97	NA	NA

Figure 20. Location of Cameras, Test MGSC-4

4 CRASH TEST NO. 1 (MGSC-1, 2270P)

4.1 Introduction

The 2,253-kg (4,966-lb) Dodge Ram 1500 Quad Cab pickup truck impacted the 152-mm (6-in.) high, AASHTO Type B curb at a speed of 100.0 km/h (62.2 mph) and at an angle of 25 degrees with respect to the curb. The impact location is shown in Figure 21. The test sequential photographs are shown in Figures 22 through 24.

4.2 Test Description

The right-front tire first impacted the curb 3.23 m (10.6 ft) from the upstream end of the curb. After impact, the vehicle's front end pitched upward and rolled counter-clockwise. At 0.016 sec, the right-front suspension reached maximum compression. At 0.126 sec, the right-rear tire impacted the curb. At 0.134 sec, the left-front tire impacted the curb. At 0.140 sec, the right-rear tire reached maximum compression. At 0.176 sec after impact, the right-rear tire became airborne and then re-contacted the ground at 0.260 sec. At 0.192 sec, the pickup started to roll clockwise. At 0.264 sec, the compressed front suspension rebounded and reached its maximum extension. At 0.280 sec, the right-rear suspension started to unload from compression. At 0.308 sec, the pickup started to roll counter-clockwise. At 0.350 sec, the rear tires became airborne. At 0.390 sec, the vehicle's front end started to pitch downward. At 0.464 sec, the pickup started to yaw clockwise. At 0.728 sec, the vehicle's rear tires landed on the ground. At 0.890 sec, the vehicle's front suspensions were compressed to their lowest profile.

For this impact condition on the 152-mm (6-in.) high, AASHTO Type B curb, the heading angle of the vehicle was basically unaffected as the vehicle sustained nearly the same vehicle path after impacting the curb. The final vehicle position and trajectory are shown in Figure 25.

4.3 System and Component Damage

Damage to the curb system was negligible, as shown in Figure 26. No cracks or fractures were observed on the curb. Two contact marks were observed on the top and traffic-side faces of the curb. Tire marks and scrapes occurred at 3.23 mm (10.6 ft) and 7.32 m (24 ft) from the upstream end of the curb.

4.4 Vehicle Damage

Exterior vehicle damage was minor, as shown in Figure 27. Minor scrapes and scratches were found on the vehicle's tires due to the impact with the curb. No wheel deformations or suspension damages were observed. The remainder of the vehicle was intact.

4.5 Trajectory Results

For the purpose of this research study, the vehicle's post-impact trajectories were recorded by tracking C.G. and bumper target centers using high-speed video analysis. The vertical displacements of each target were plotted against both time and the raw longitudinal distance, as shown in Figures 28 through 31. The raw longitudinal distance was defined as a given target's longitudinal displacement starting at zero with respect to its initial target center location when the tire contacted the curb. As such, raw longitudinal distance measurements reported graphically for two different targets do not reference the same starting point and are out of phase. Adjustments to the noted plots will be made in Chapter 8 in order to bring target measurements into phase for further analysis.

The initial heights of the vehicle's C.G. and bumper targets were 711 mm (28 in.) and 527 mm (20.75 in.), respectively. Thus, the actual trajectories of the C.G. and bumper targets were obtained by coupling the raw, video-analysis, vertical displacement data with their initial

target heights, as shown in Figures 32 through 35. The results are also plotted in English-units in Appendix B.

4.6 Occupant Risk Values

The longitudinal and lateral occupant impact velocities from the EDR-3 transducer were determined to be -0.76 m/s (-2.50 ft/s) and -1.05 m/s (-3.44 ft/s), respectively. The maximum 0.010-sec average occupant ridedown deceleration in the longitudinal and lateral directions from the EDR-3 transducer were 3.33 g's and 4.65 g's, respectively. Results are shown graphically in Appendix C. The results from the rate transducer are shown graphically in Appendix C.

4.7 Discussion

The analysis of the test results for test MGSC-1 showed that the 152-mm (6-in.) high, AASHTO Type B curb system did not redirect the 2270P pickup at an impact speed of 100.0 km/h (62.2 mph) and an impact angle of 25 degrees. The 2270P pickup truck kept rising after impact until to a certain point at which the vehicle started to descend. The bumper target reached a maximum vertical displacement of 340 mm (14.4 in.) at 0.32 sec. after curb impact. The C.G. target reached a maximum vertical displacement of 439 mm (17.3 in.) at 0.57 sec. after curb impact. Both the C.G. and bumper targets had a monotonic descent after reaching the peak value due to the gravity. No damage was found on the curb. There were neither deformations nor damage to the pickup truck.

Figure 21. Impact Location, Test MGSC-1

0.000 sec

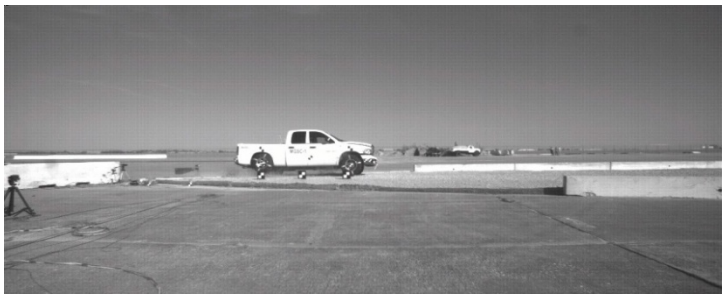

0.208 sec

0.376 sec

0.552 sec

0.704 sec

Figure 22. Sequential Photographs, Test MGSC-1

0.000 sec (right-front)

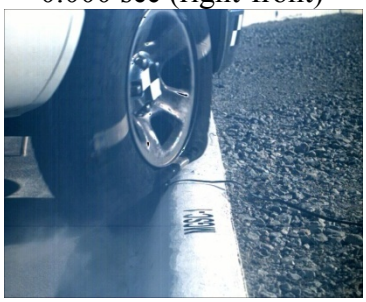
0.008 sec (right-front)

0.016 sec (right-front)

0.024 sec (right-front)

0.060sec (right-front)

0.124 sec (right-rear)

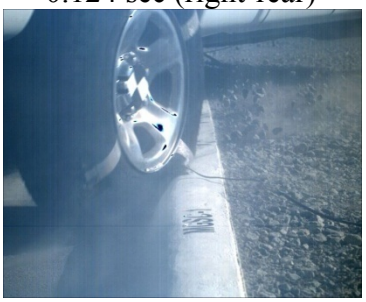
0.132 sec (right-rear)

0.140 sec (right-rear)

0.148 sec (right-rear)

0.164 sec (right-rear)

Figure 23. Additional Sequential Photographs, Test MGSC-1

0.000 sec

0.184 sec

0.328 sec

0.488 sec

0.672 sec

0.880 sec

Figure 24. Additional Sequential Photographs, Test MGSC-1

Figure 25. Vehicle Final Position and Trajectory, Test MGSC-1

Figure 26. System Damage, Test MGSC-1

Right-Front Tire

Right-Front Tire

Right-Rear Tire

Right-Rear Tire

Figure 27. Vehicle Damage, Test MGSC-1

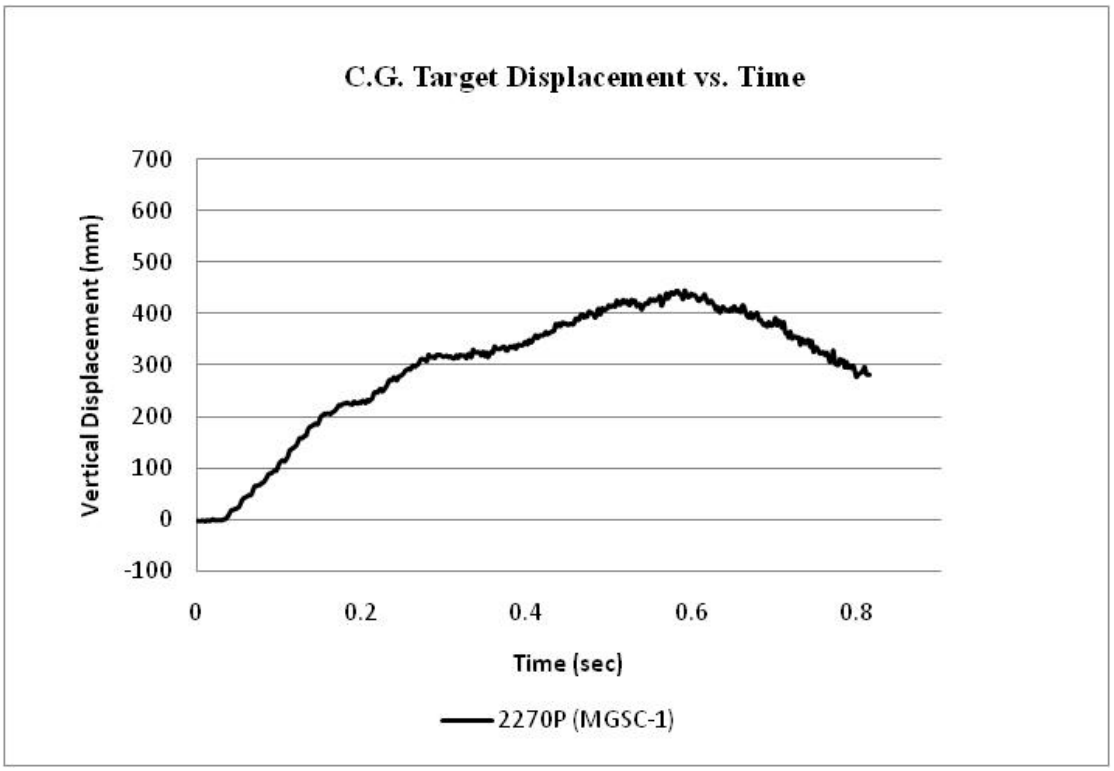

Figure 28. C.G. Target Displacement vs. Time, Test MGSC-1 (2270P)

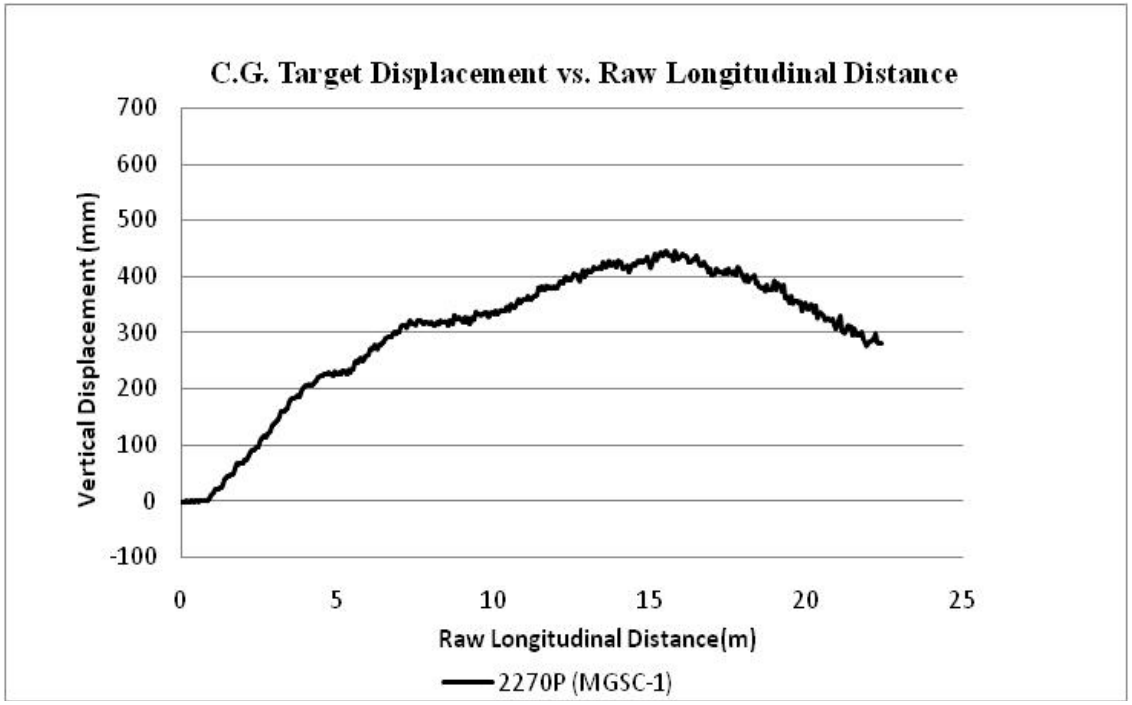

Figure 29. C.G. Target Displacement vs. Raw Longitudinal Distance, Test MGSC-1 (2270P)

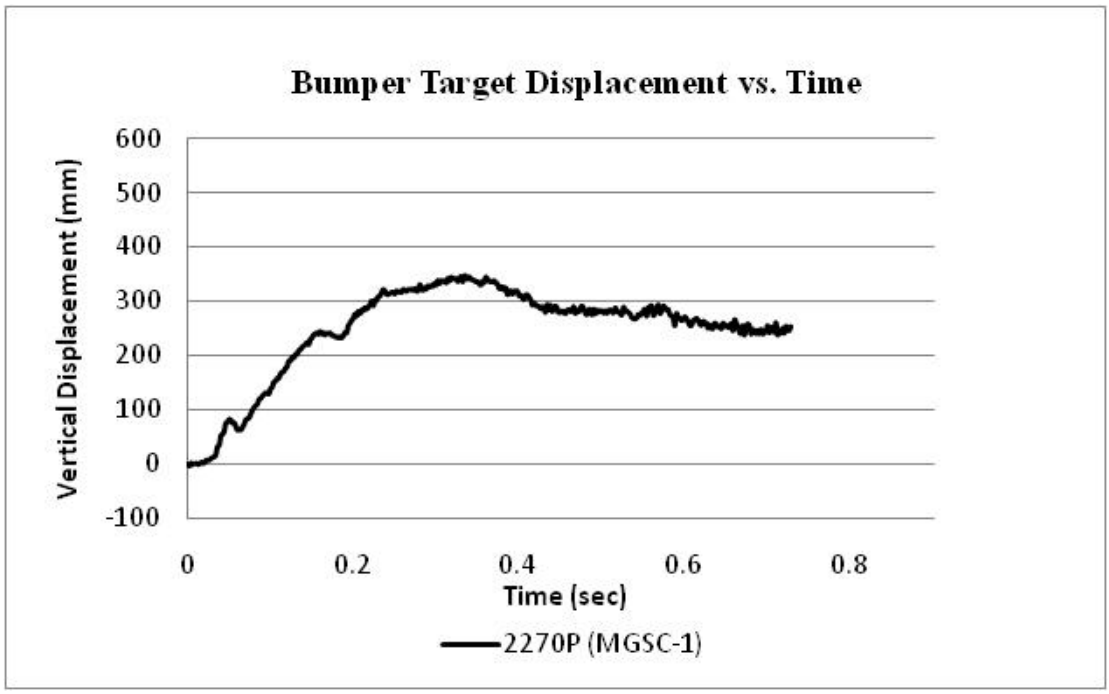

Figure 30. Bumper Target Displacement vs. Time, Test MGSC-1 (2270P)

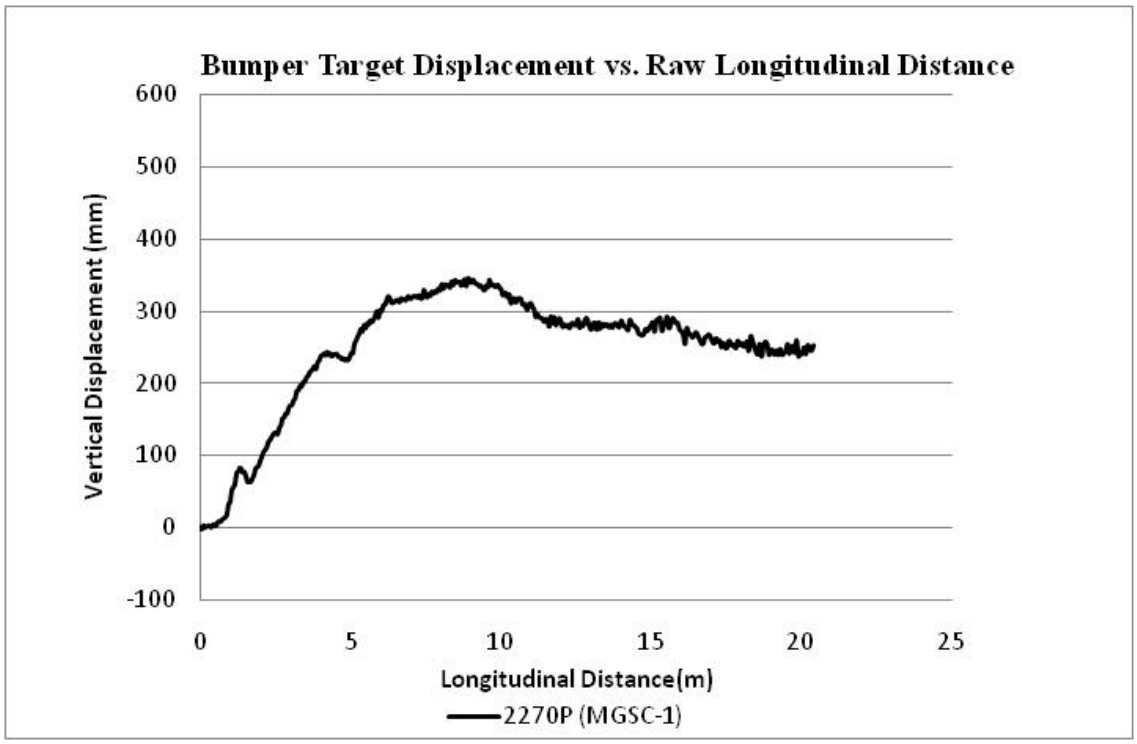

Figure 31. Bumper Target Displacement vs. Raw Longitudinal Distance, Test MGSC-1 (2270P)

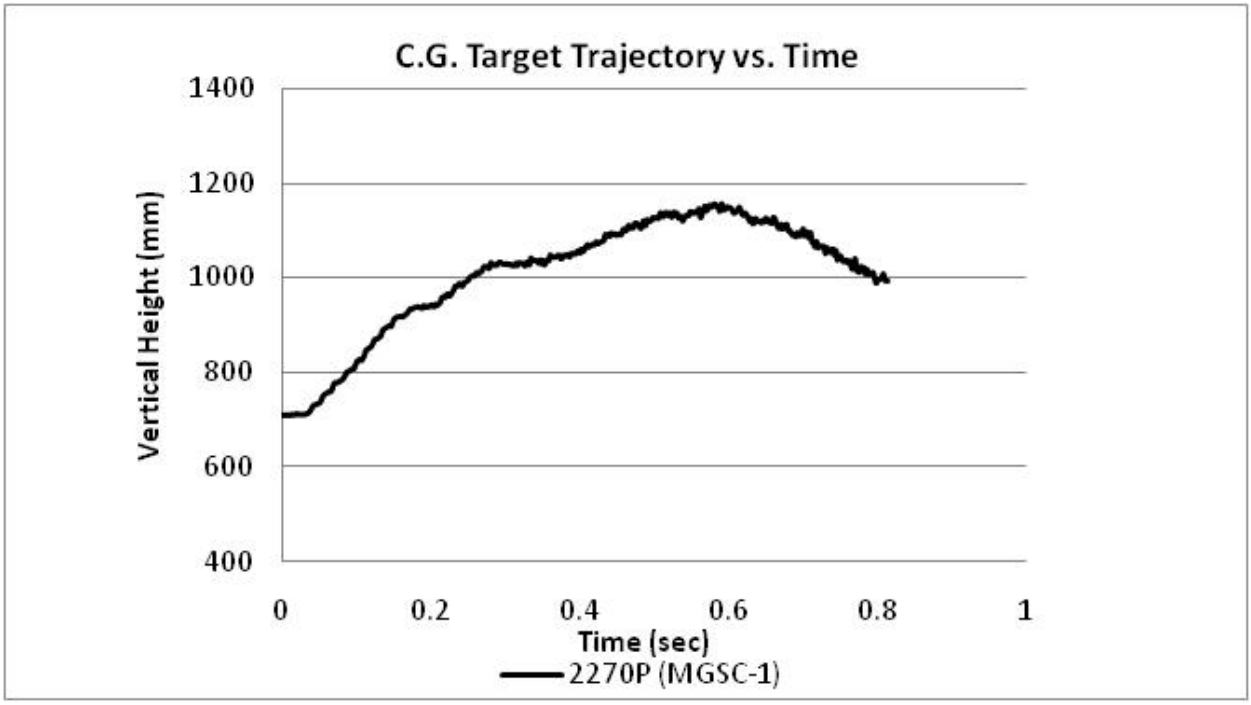

Figure 32. C.G. Target Trajectory vs. Raw Longitudinal Distance, Test MGSC-1 (2270P)

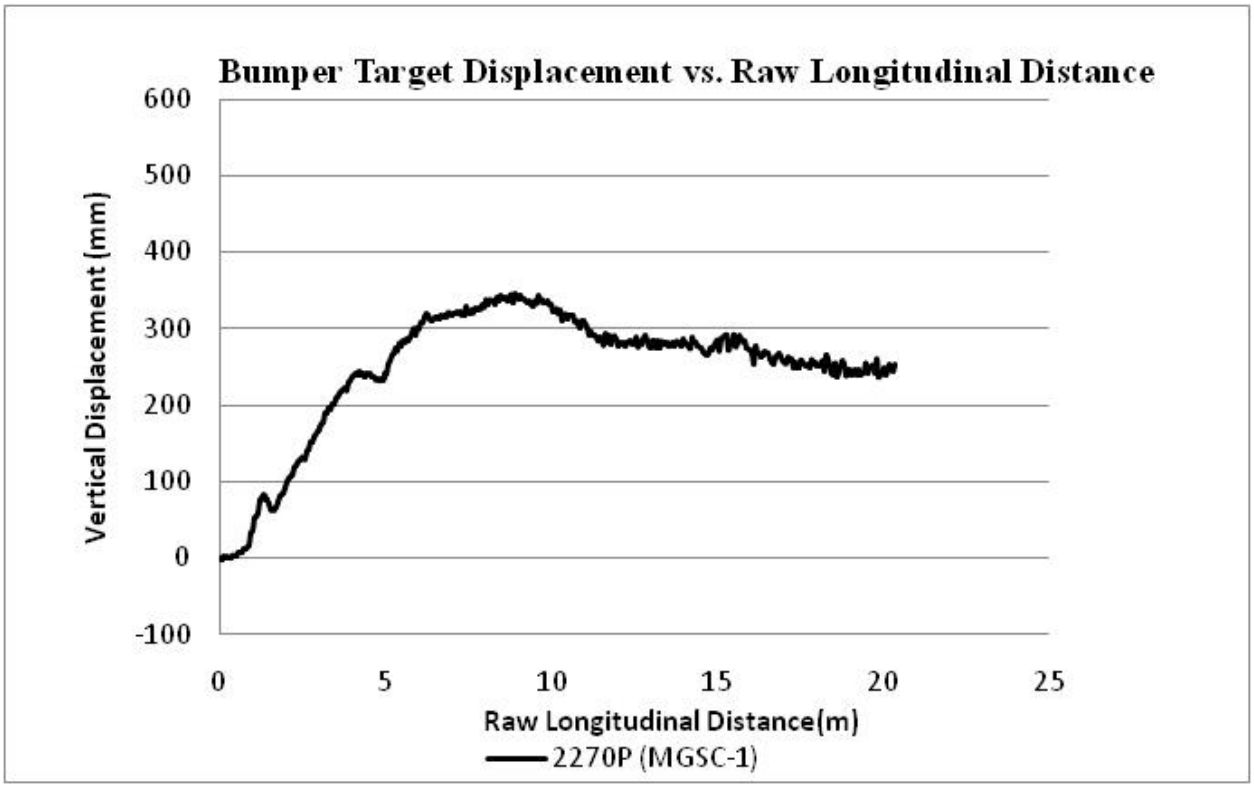

Figure 33. C.G. Target Trajectory vs. Raw Longitudinal Distance, Test MGSC-1 (2270P)

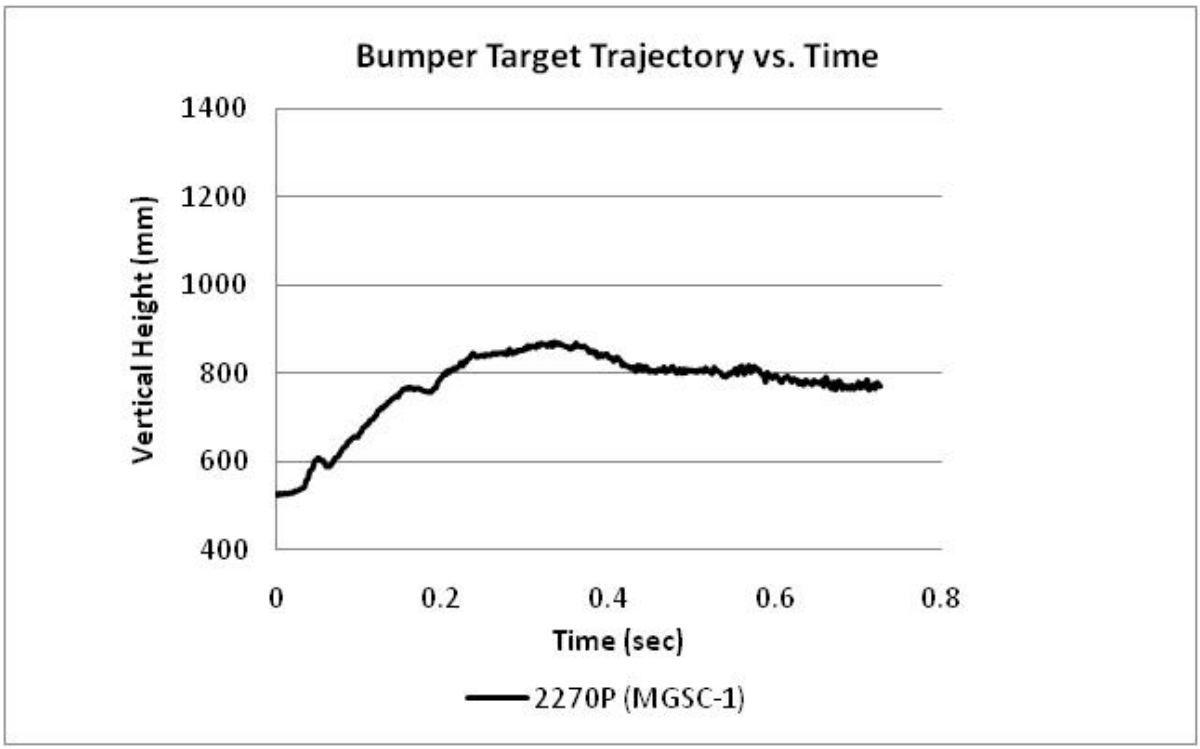

Figure 34. Bumper Target Trajectory vs. Time, Test MGSC-1 (2270P)

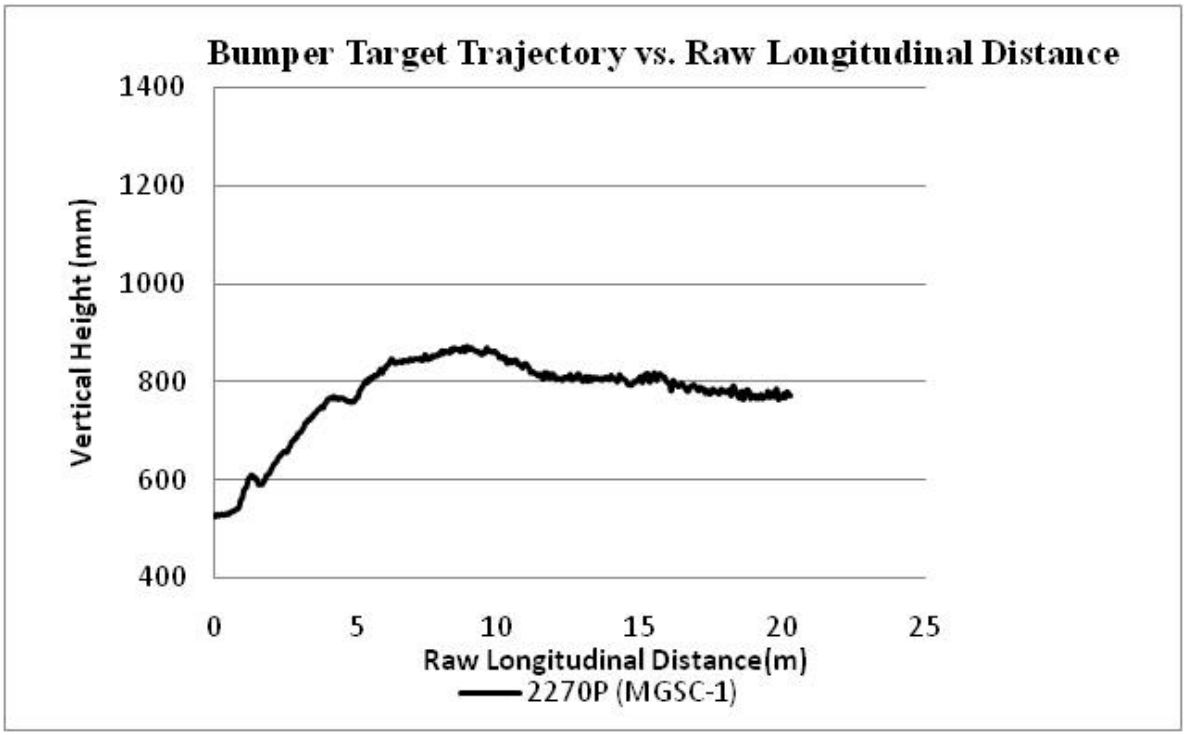

Figure 35. Bumper Target Trajectory vs. Raw Longitudinal Distance, Test MGSC-1 (2270P)

5 CRASH TEST NO. 2 (MGSC-2, 2270P)

5.1 Introduction

The 2,253-kg (4,966-lb) Dodge Ram 1500 Quad Cab pickup truck, which was the same truck used in test MGSC-1, impacted the 152-mm (6-in.) high, AASHTO Type B curb at a speed of 100.8 km/h (62.6 mph) and at an angle of 25 degrees with respect to the curb. The impact location is shown in Figure 36. The sequential photographs are shown in Figures 37 through 39.

5.2 Test Description

The right-front tire first impacted the curb at 3.23 m (10.6 ft) from the upstream end of the curb. After impact, the vehicle's front end pitched upward and rolled counter-clockwise. At 0.014 sec, the right-front suspension reached maximum compression. At 0.126 sec, the right-rear tire impacted the curb. At 0.132 sec, the left-front tire impacted the curb and caused the pickup's clockwise roll. At 0.138 sec, the right-rear suspension reached maximum compression. At 0.170 sec after impact, the right-rear tire became airborne and then re-contacted the ground at 0.258 sec. At 0.270 sec, the front suspension compression was released and reached its maximum extension. At 0.302 sec, the compressed right-rear suspension rebounded to its maximum extension. At 0.306 sec, the pickup started to roll counter-clockwise. At 0.346 sec, both of the pickup's rear tires became airborne. At 0.386 sec, the vehicle's front end started to pitch downward. At 0.456 sec, the pickup started to yaw clockwise. At 0.512 sec, the vehicle's right-rear tire contacted the ground. At 0.648 sec, the vehicle's left-rear tire landed on the ground.

For this impact condition on the 152-mm (6-in.) high AASHTO Type B curb, the heading angle of the vehicle was basically unaffected, as the vehicle maintained nearly the same vehicle path after hitting the curb. The final vehicle position and trajectory are shown in Figure 40.

5.3 System and Component Damage

Damage to the curb system was negligible, as shown in Figure 41. No cracks or fractures were observed on the curb. Two contact marks were observed on the top and traffic-side faces of the curb. Tire marks and scrapes occurred at a point 3.23 m (10.6 ft) and another point 7.32 m (24.0 ft) from the upstream end of the curb.

5.4 Vehicle Damage

Exterior vehicle damage was minor, as shown in Figure 42. Minor scrapes and scratches were found on the vehicle tires due to the impact with the curb. No wheel deformation or suspension damage was observed. The remainder of vehicle was intact.

5.5 Trajectory Results

For the purpose of this research study, the vehicle's post-impact trajectories were recorded by tracking the C.G. and bumper target centers using high-speed video analysis. The vertical displacement of each target was plotted against both time and the raw longitudinal distance, as shown in Figures 43 through 46. The raw longitudinal distance was defined as a given target's longitudinal displacement starting at zero with respect to its initial target center location when the tire contacted the curb. As such, raw longitudinal distance measurements reported graphically for two different targets do not reference the same starting point and are out of phase. Adjustments to the noted plots will be made in Chapter 8 in order to bring target measurements into phase for further analysis.

The initial heights of the vehicle's C.G. and bumper targets were 711 mm (28 in.) and 527 mm (20.75 in.), respectively. Thus, the actual trajectories of the C.G. and bumper targets were obtained by coupling the raw, film-analysis, vertical displacement data with their initial target heights, as shown in Figures 47 through 50. The results are also plotted in English-units in Appendix B.

5.6 Occupant Risk Values

The longitudinal and lateral occupant impact velocities from the EDR-3 transducer were determined to be -2.17 m/s (-7.13 ft/s) and 0.79 m/s (2.58 ft/s), respectively. The maximum 0.010-sec average occupant ridedown deceleration in the longitudinal and lateral directions from the EDR-3 transducer were 3.47 g's and 5.28 g's, respectively. Results are shown graphically in Appendix C. The results from the rate transducer are shown graphically in Appendix C.

5.7 Discussion

The analysis of the test results for test MGSC-2 showed that the 152-mm (6-in.) high, AASHTO Type B curb system did not redirect the 2270P pickup at an impact speed of 100.8 km/h (62.6 mph) and an impact angle of 25 degrees. The 2270P pickup truck kept rising after impact until a certain point at which the vehicle started to descend. The bumper target reached its first peak vertical displacement of 483 mm (19 in.) at 0.35 sec after curb impact. The C.G. target reached a maximum vertical displacement of 654 mm (25.7 in.) at 0.6 sec after curb impact. The C.G. target had a monotonic descent after the reaching the peak value due to gravity. However, the bumper target trajectory ascended again after the first peak and kept rising until out of video view. It should be noted that the results from test nos. MGSC-1 and MGSC-2 were substantially different, considering they used the same vehicle for testing. No damage was found on the curb. There were no deformation or damage to the pickup truck.

Figure 36. Impact Location, Test MGSC-2

0.000 sec

0.182 sec

0.322 sec

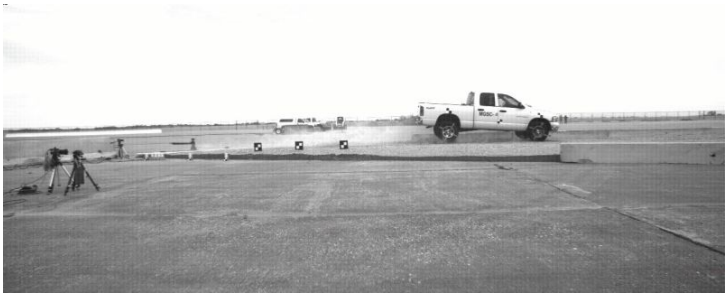

0.482 sec

0.722 sec

Figure 37. Sequential Photographs, Test MGSC-2

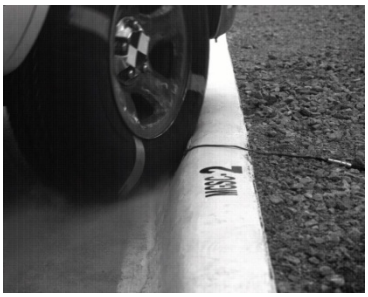

0.000 sec (right-front)

0.008 sec (right-front)

0.014 sec (right-front)

0.026 sec (right-front)

0.036sec (right-front)

0.128 sec (right-rear)

0.136 sec (right-rear)

0.144 sec (right-rear)

0.152 sec (right-rear)

0.162 sec (right-rear)

Figure 38. Additional Sequential Photographs, Test MGSC-2

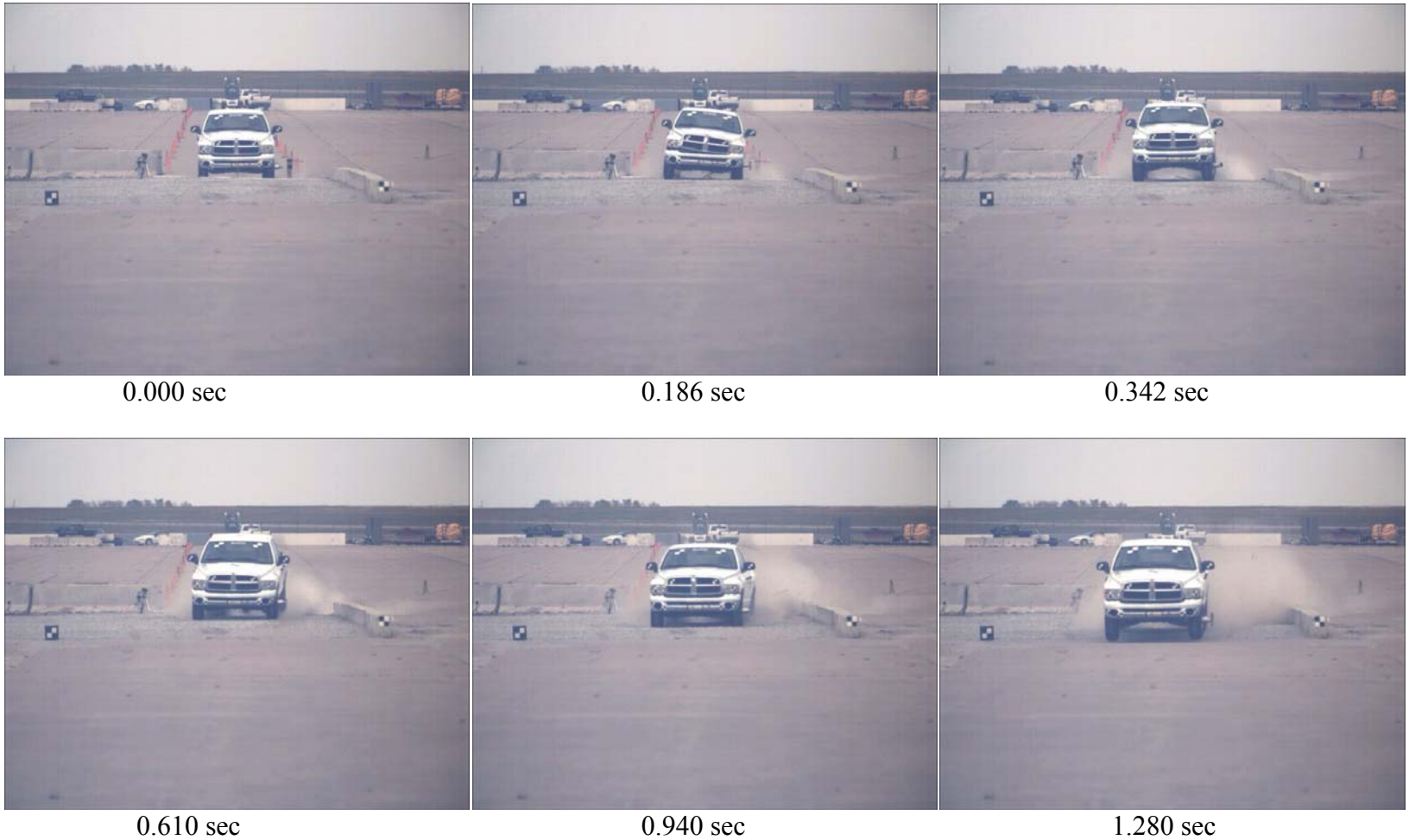

Figure 39. Additional Sequential Photographs, Test MGSC-2

Figure 40. Vehicle's Final Position and Trajectory, Test MGSC-2

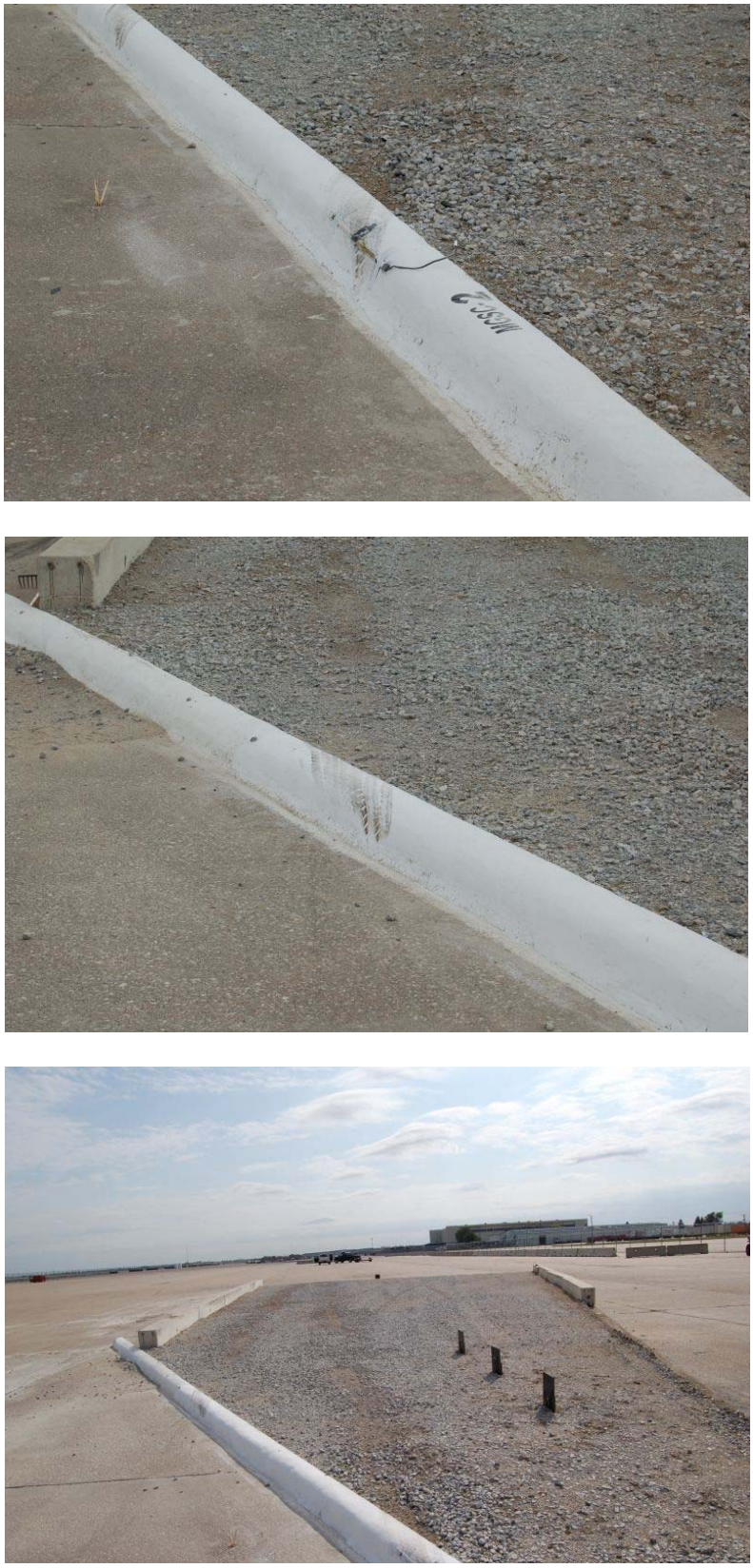

Figure 41. System Damage, Test MGSC-2

Right-Front Tire

Right-Front Tire (Close View)

Right-Rear Tire

Right-Rear Tire (Close View)

Figure 42. Vehicle Damage, Test MGSC-2

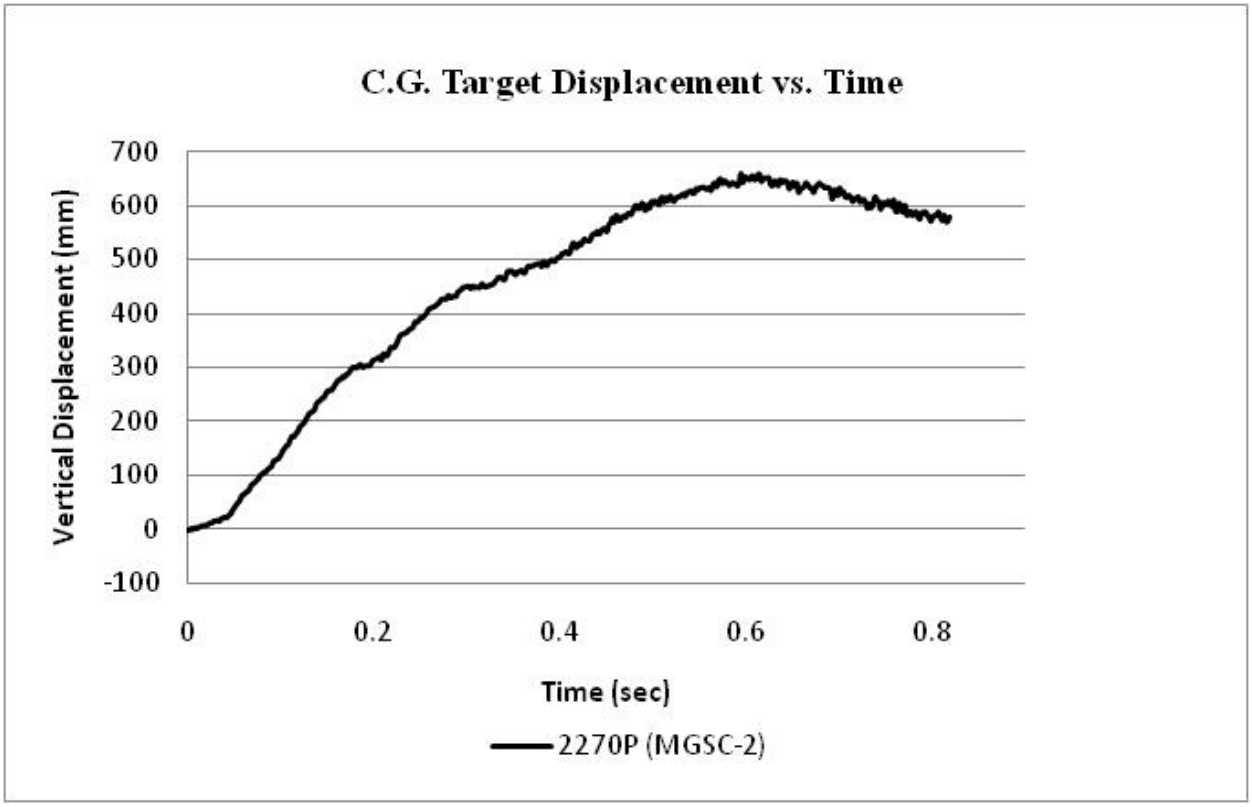

Figure 43. C.G. Target Displacement vs. Time, Test MGSC-2 (2270P)

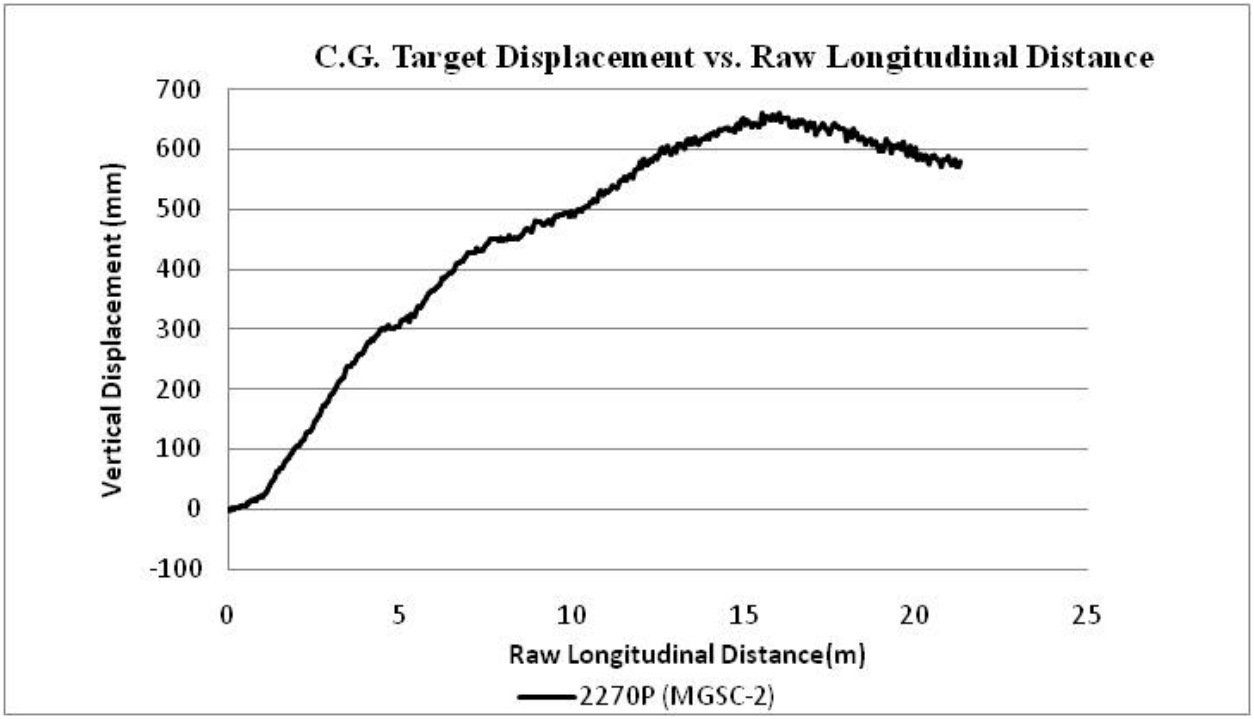

Figure 44. C.G. Target Displacement vs. Raw Longitudinal Distance, Test MGSC-2 (2270P)

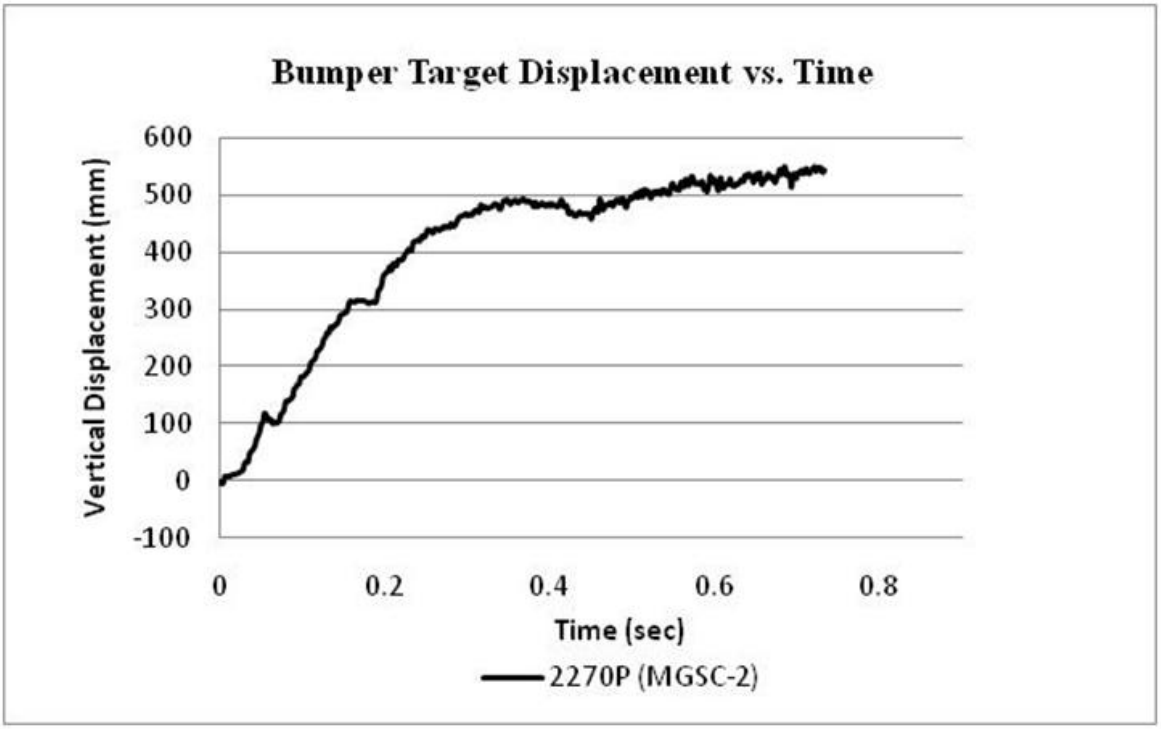

Figure 45. Bumper Target Displacement vs. Time, Test MGSC-2 (2270P)

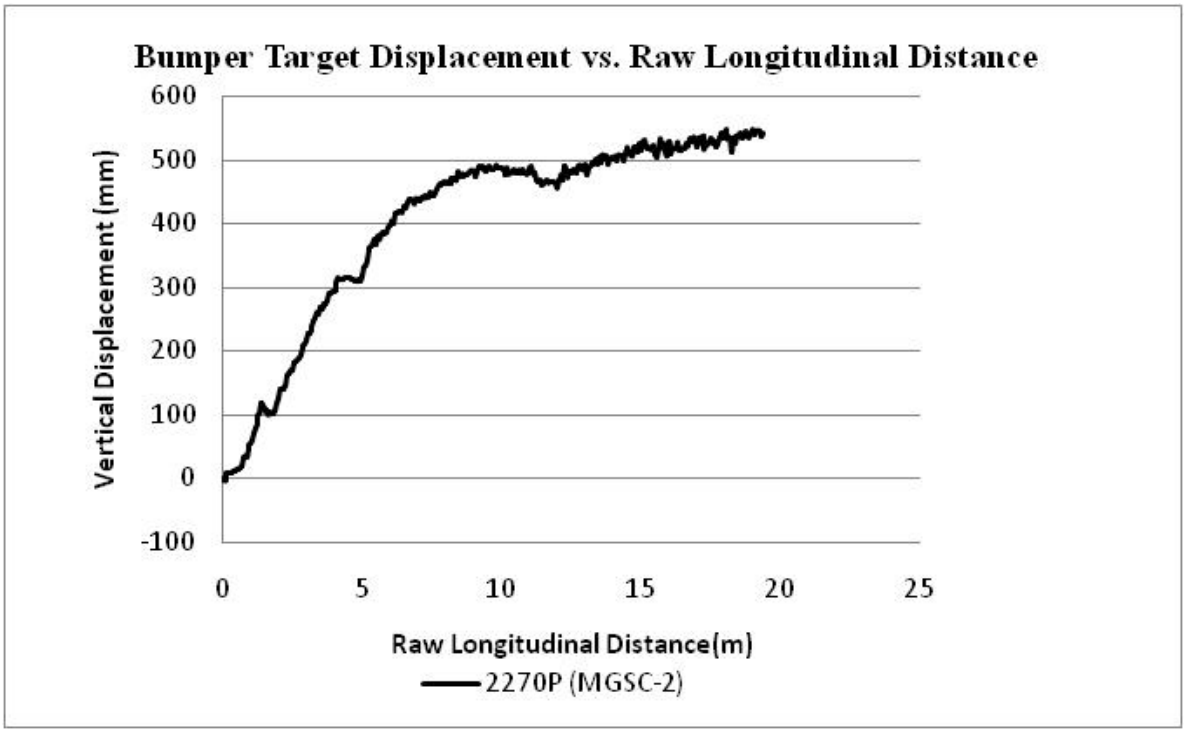

Figure 46. Bumper Target Displacement vs. Raw Longitudinal Distance, Test MGSC-2 (2270P)

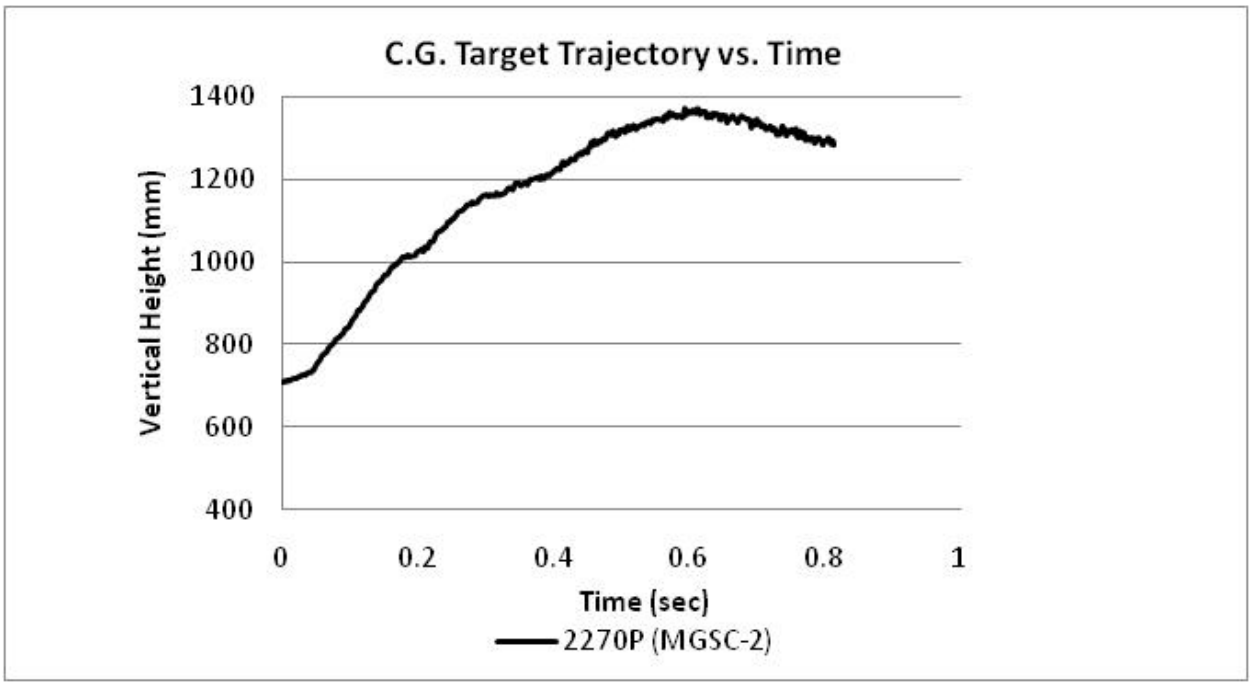

Figure 47. C.G. Target Trajectory vs. Time, Test MGSC-2 (2270P)

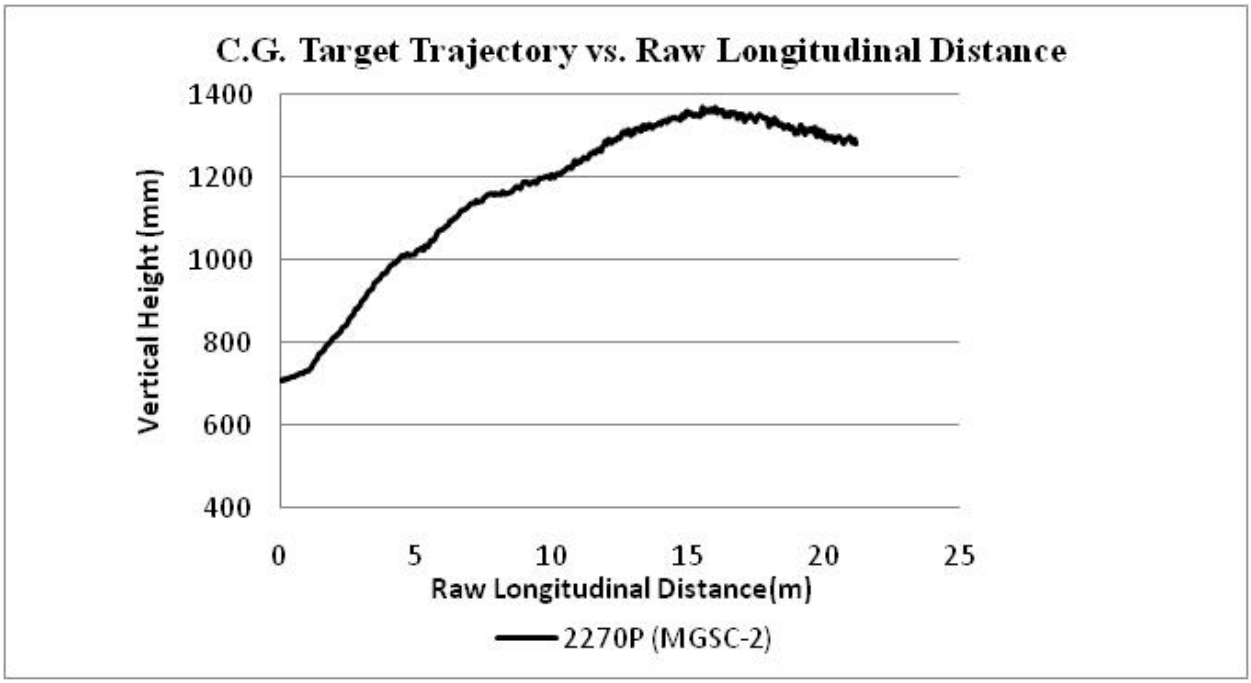

Figure 48. C.G. Target Trajectory vs. Raw Longitudinal Distance, Test MGSC-2 (2270P)

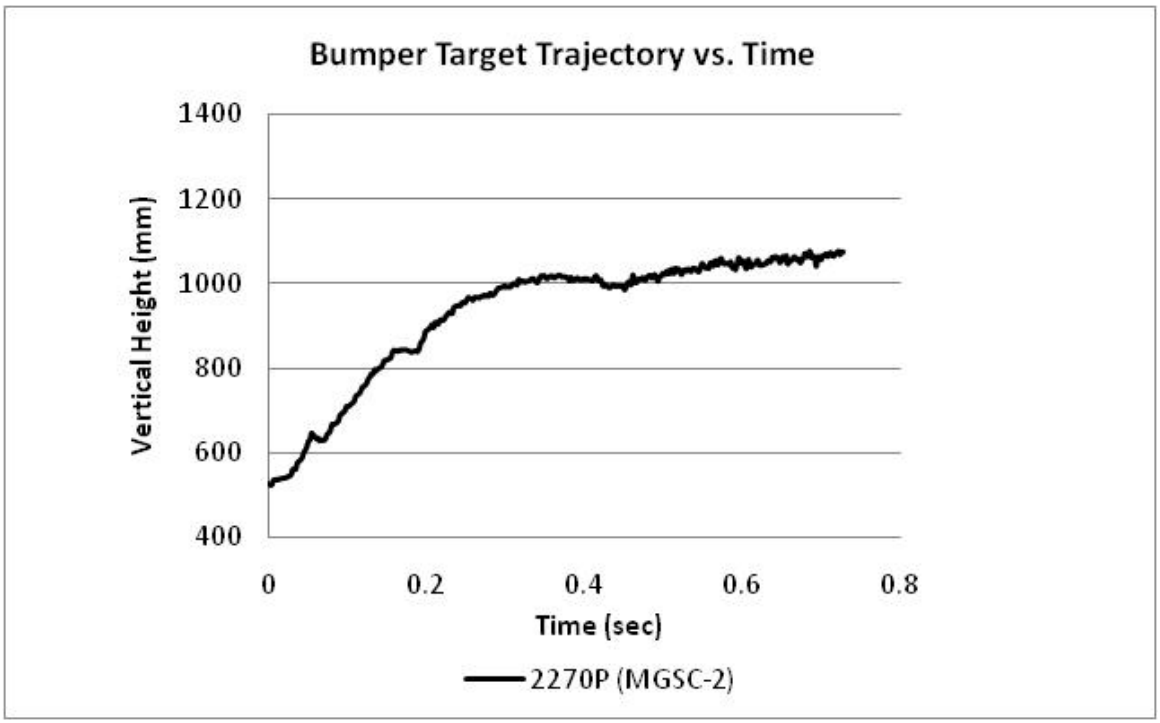

Figure 49. Bumper Target Trajectory vs. Time, Test MGSC-2 (2270P)

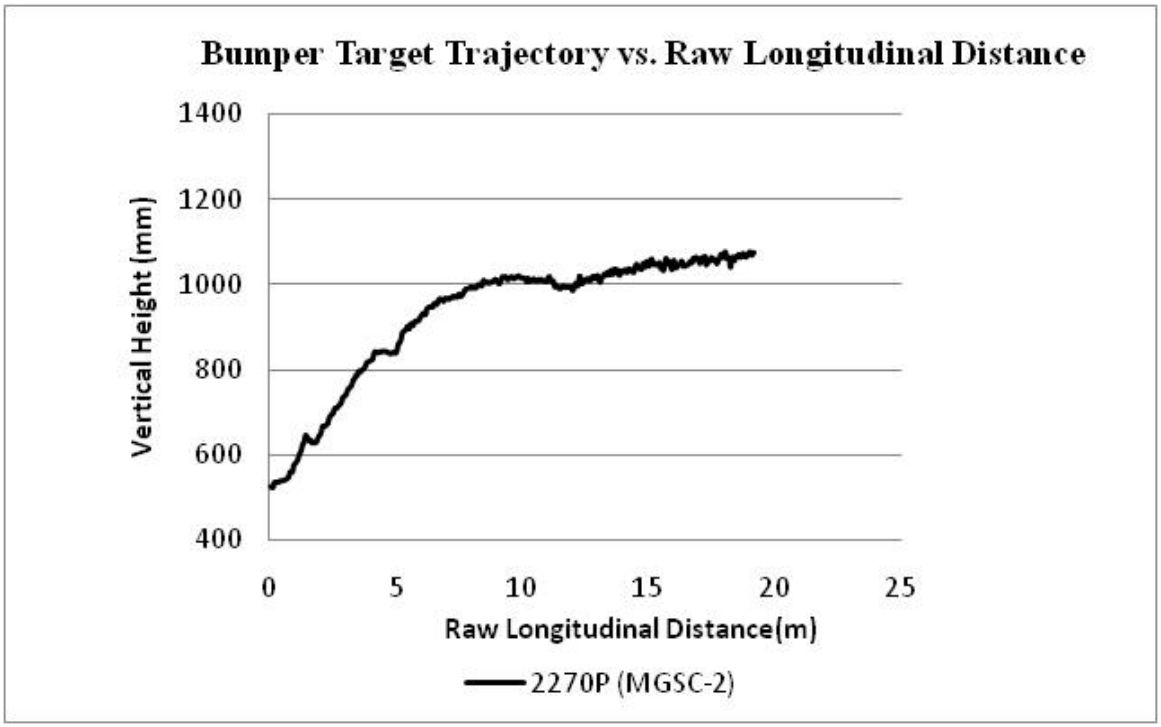

Figure 50. Bumper Target Trajectory vs. Raw Longitudinal Distance, Test MGSC-2 (2270P)

6 CRASH TEST NO. 3 (MGSC-3, 1100C)

6.1 Introduction

The 1,154-kg (2,544-lb) Kia Rio impacted the 152-mm (6-in.) high, AASHTO Type B curb at a speed of 99.1 km/h (61.6 mph) and at an angle of 25 degrees. The impact location is shown in Figure 51. The sequential photographs are shown in Figures 52 through 54.

6.2 Test Description

The vehicle's first impact occurred 3.4 m (11.2 ft) from the upstream end of the curb. Upon impact with the curb, the right-front wheel rim was bent, and the right-front tire deflated. The front end of the vehicle pitched upward after the impact. At 0.088 sec, the right-rear tire impacted the curb. At 0.172 sec, the left-front tire impacted the curb. At 0.182 sec, the left-rear tire left the ground in front of the curb and hit the curb at 0.212 sec. At 0.204 sec after impact, the right-front tire became airborne. At 0.374 sec, the vehicle started to roll counter-clockwise. At 0.360 sec, the front end of the vehicle started to pitch down. At 0.402 sec, the left-front tire left the ground and became airborne. At 0.440 sec, the left-rear tire became airborne. At 0.474 sec, the right-front tire re-contacted the ground. At 0.638 sec, the vehicle's left-front tire landed on the ground. At 0.736 sec, the vehicle started to yaw clockwise. At 0.770 sec, the vehicle's front suspensions were compressed to their lowest profile. At 1.856 sec, the vehicle started to yaw counter-clockwise and kept running on the bare wheel rims and flat tires.

For this impact condition on the 152-mm (6-in.) high AASHTO Type B curb, the heading angle of the small passenger car was basically unaffected by the curb impact. The final vehicle position and trajectory are shown in Figure 55.

6.3 System and Component Damage

Damage to the curb system was negligible, as shown in Figure 56. No cracks or fractures were observed on the curb. Two contact marks were observed on the top and traffic-side faces of the curb. Two tire marks, each of length 864 mm (34 in.), were found on the curb; one 3.4 m (11.2 ft) from the upstream end of the curb, and another 7.0 m (22.8 ft) from the downstream end of the curb.

6.4 Vehicle Damage

Exterior vehicle damage was moderate, as shown in Figure 57. The damage consisted of tire scratches, wheel deformations, and deflated tires. The right-front wheel rim was severely deformed due to the impact. The right-front tire was flat, with half of the tire off the rim. Scratches were found both on the right-front tire and the right-front rim. The right-rear wheel rim was severely dented where the impact occurred. The right-rear tire became flat but still remained on the rim. Scratches were found on both the right-rear tire and the right-rear wheel rim. Minor bends were found on the left-front wheel rim, but no major dents were found. The left-front tire was deflated but still remained on the rim. Scratches were found on both the left-front tire and the left-front wheel rim. A minor dent was found on the left-rear wheel rim where the impact occurred. The left-rear tire was still inflated. Scratches were found on the sidewall of the left-rear tire. No suspension damage was observed. The rest of vehicle was intact.

6.5 Trajectory Results

For the purpose of this research study, the vehicle's post-impact trajectories were recorded by tracking C.G. and bumper target centers using high-speed video analysis. The vertical displacements of each target were plotted against both time and the raw longitudinal distance, as shown in Figures 57 through 60. The raw longitudinal distance was defined as a

given target's longitudinal displacement starting at zero with respect to its initial target center location when the tire contacted the curb. As such, raw longitudinal distance measurements reported graphically for two different targets do not reference the same starting point and are out of phase. Adjustments to the noted plots will be made in Chapter 8 in order to bring target measurements into phase for further analysis.

The initial heights of the vehicle's C.G. and bumper targets were 406 mm (16 in.) and 381 mm (15 in.), respectively. Thus, the actual trajectories of the C.G. and bumper targets were obtained by coupling the raw, film-analysis, vertical displacement data with their initial target heights, as shown in Figures 61 through 64. The results are also plotted in English-units in Appendix B.

6.6 Occupant Risk Values

The longitudinal and lateral occupant impact velocities from the EDR-3 transducer were determined to be -1.69 m/s (-5.55 ft/s) and 0.05 m/s (0.16 ft/s), respectively. The maximum 0.010-sec average occupant ridedown deceleration in the longitudinal and lateral directions from the EDR-3 transducer were -2.44 g's and -1.38 g's, respectively. Results are shown graphically in Appendix C. The results from the rate transducer are shown graphically in Appendix C.

6.7 Discussion

The analysis of the test results for test MGSC-3 showed that the 152-mm (6-in.) high, AASHTO Type B curb system did not contain or redirect the 1100C small passenger car at an impact speed of 99.1 km/h (61.6 mph) and at an angle of 25 degrees. The impact caused tire and wheel damages to the small passenger car. Three tires deflated when the wheel rim bent. The 1100C small passenger car kept rising after impact until a certain point at which the vehicle then started descending. The bumper target reached its peak vertical displacement of 314 mm (12.4

in.) at 0.21 sec after curb impact. The C.G. target reached a maximum vertical displacement of 234 mm (9.2 in.) at 0.22 sec after curb impact. It was noticed that the C.G. and bumper targets had the peak values at almost the same time. After the peak, both the bumper and C.G. targets started to descend due to gravity. Oscillations of the C.G. and target trajectories were observed, which were the results of vehicle's suspension compressing on landing and then rebounding. No damage was found on the curb.

Figure 51. Impact Location, Test MGSC-3

0.00 sec

0.11 sec

0.27 sec

0.41 sec

0.61 sec

Figure 52. Sequential Photographs, Test MGSC-3

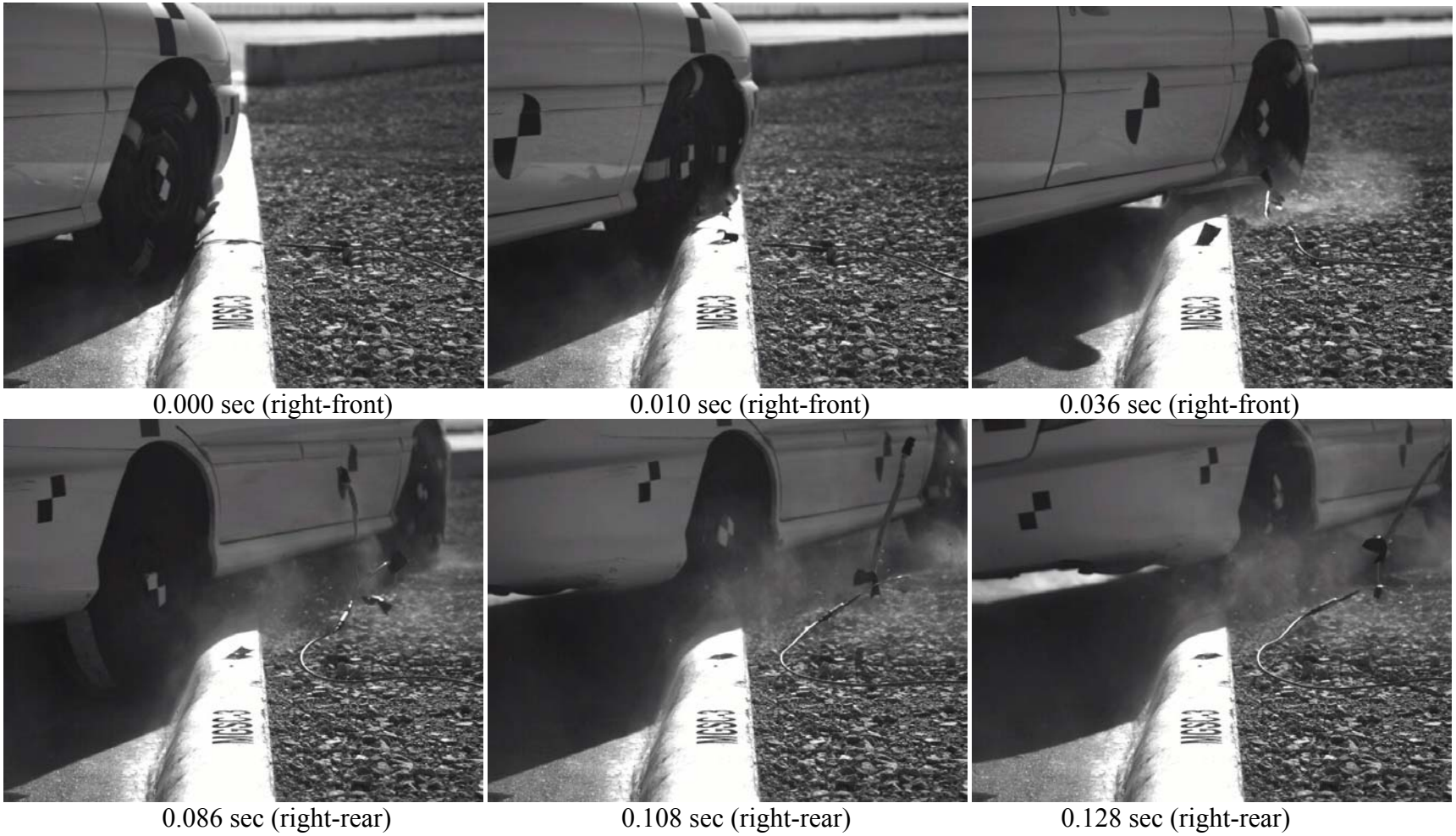

0.000 sec (right-front) 0.010 sec (right-front) 0.036 sec (right-front)

0.086 sec (right-rear) 0.108 sec (right-rear) 0.128 sec (right-rear)

Figure 53. Additional Sequential Photographs, Test MGSC-3

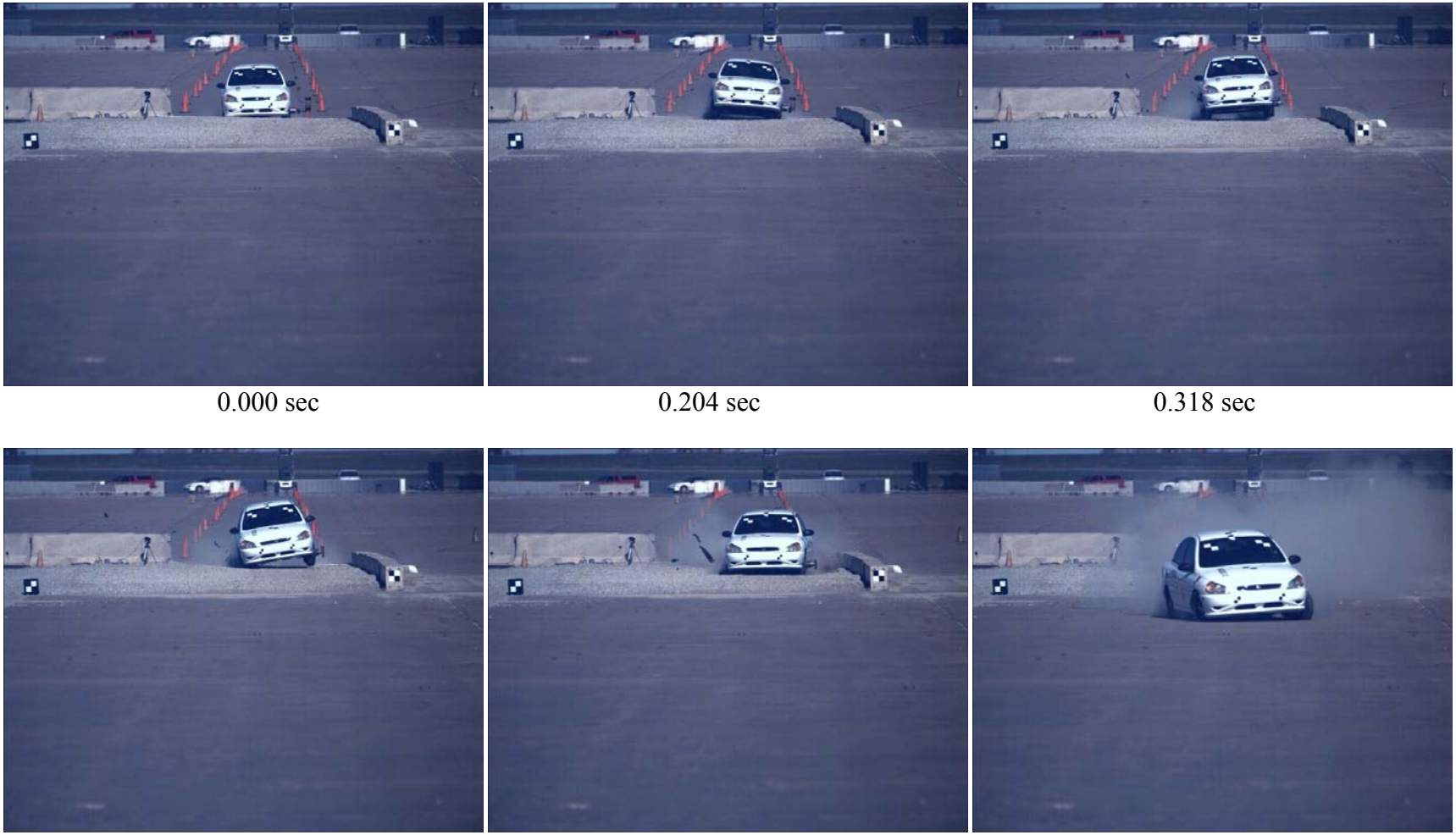

Figure 54. Additional Sequential Photographs, Test MGSC-3

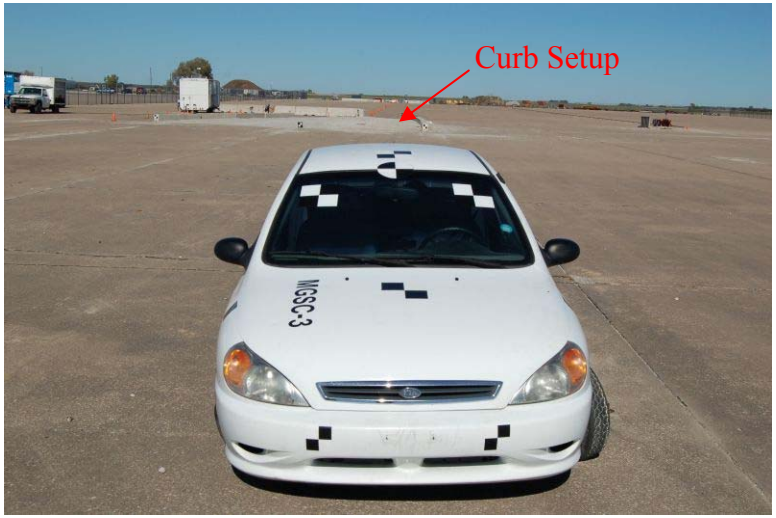

Figure 55. Vehicle Final Position and Trajectory, Test MGSC-3

Figure 56. System Damage, Test MGSC-3

Right-Front Tire

Right-Rear Tire

Left-Front Tire

Left-Rear Tire

Figure 57. Vehicle Damage, Test MGSC-3

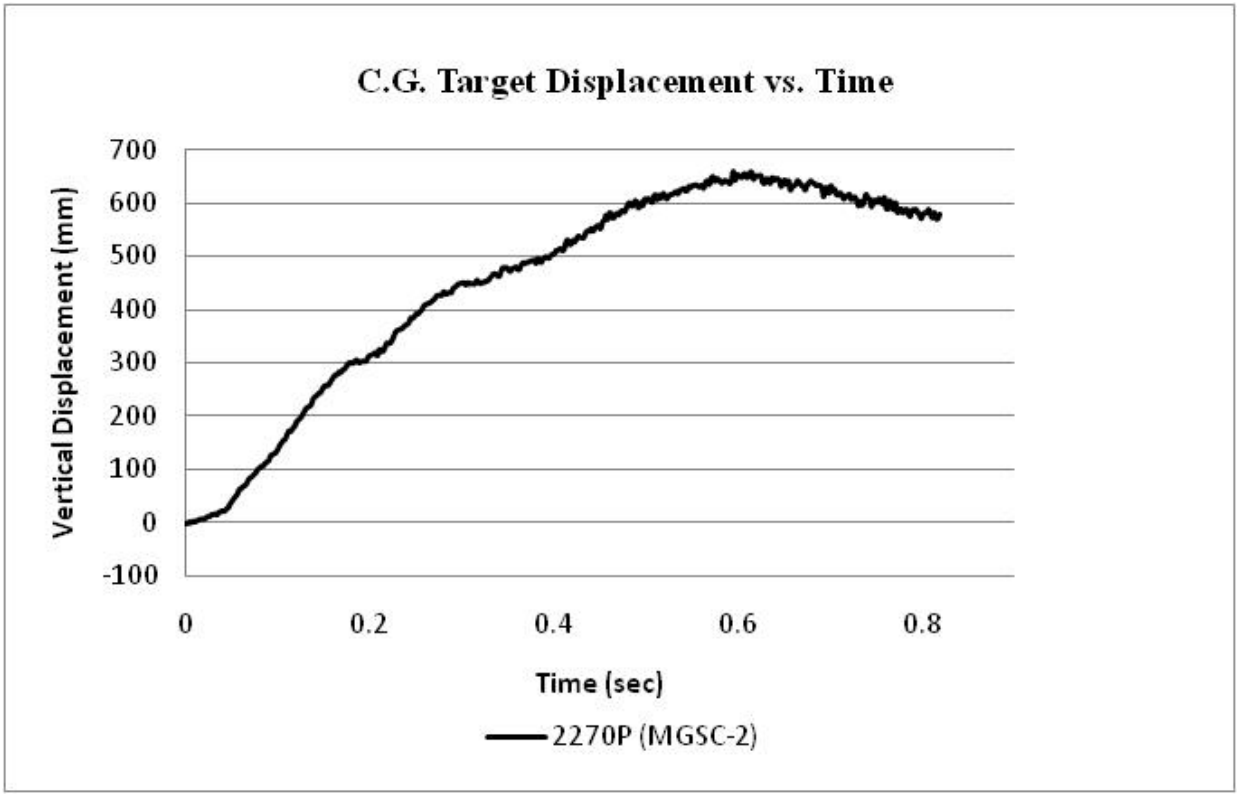

Figure 58. C.G. Target Displacement vs. Time, Test MGSC-3 (1100C)

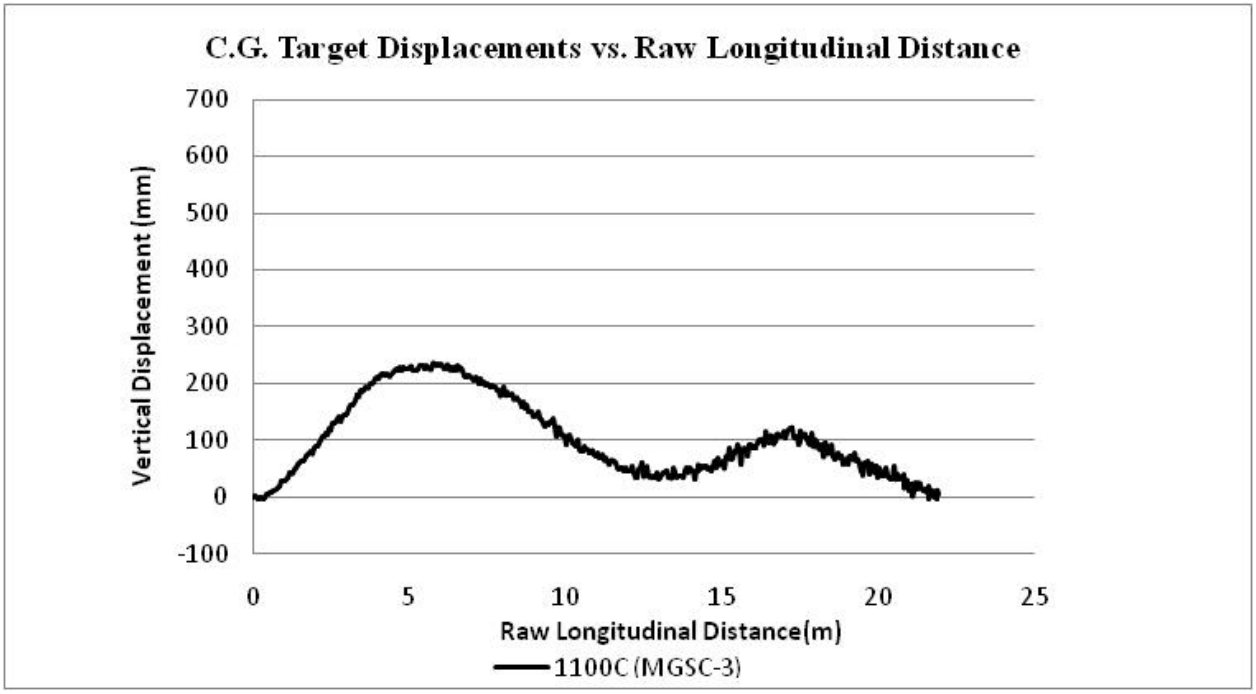

Figure 59. C.G. Target Displacement vs. Raw Longitudinal Distance, Test MGSC-3 (1100C)

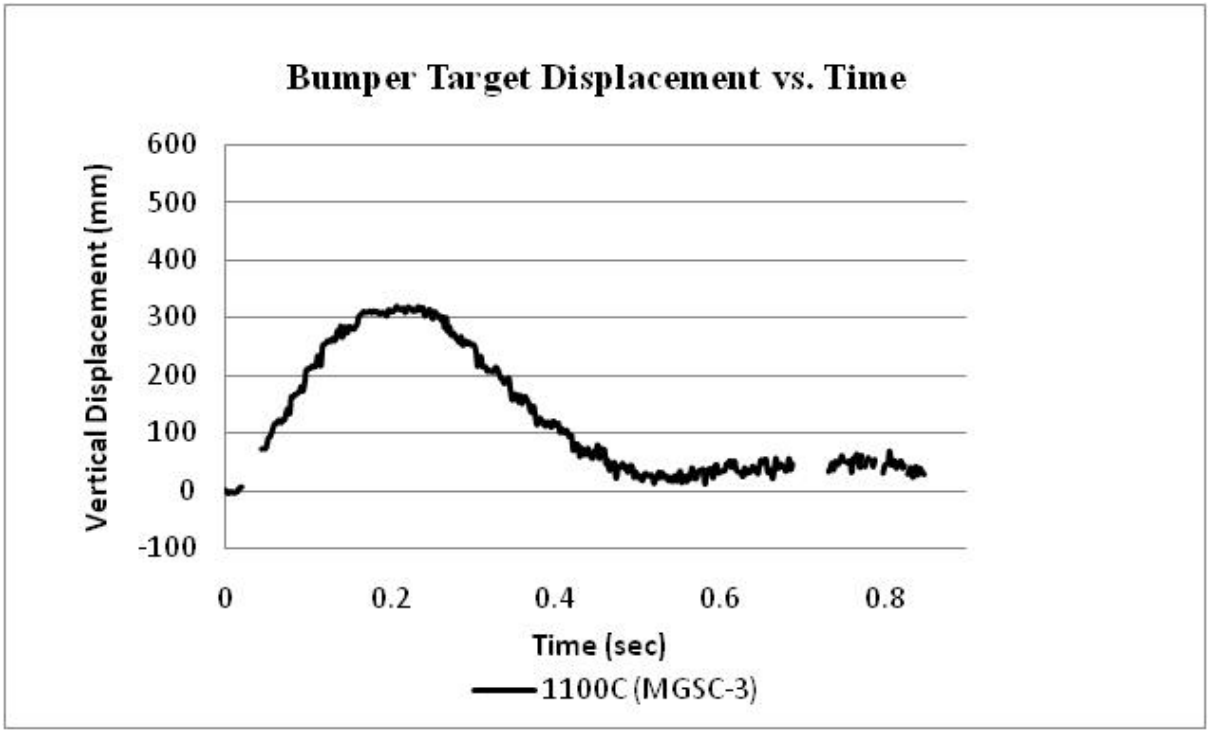

Figure 60. Bumper Target Displacement vs. Time, Test MGSC-3 (1100C)

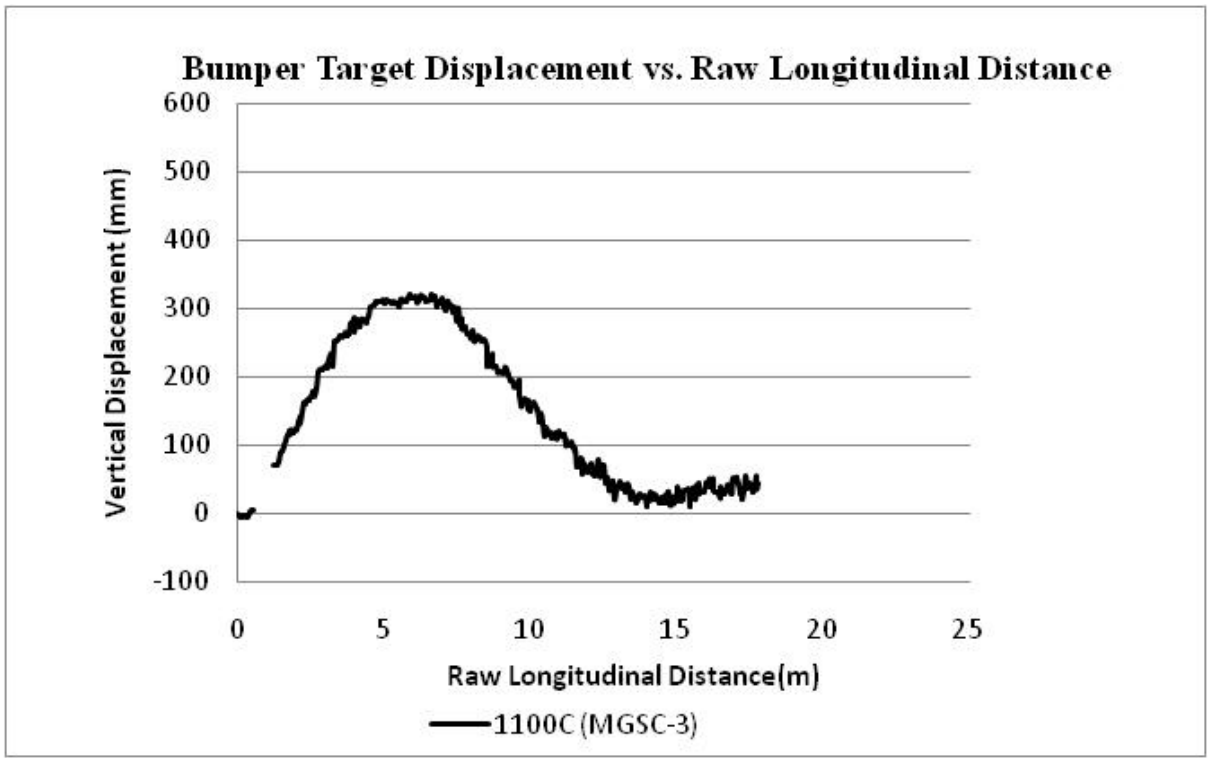

Figure 61. Bumper Target Displacement vs. Raw Longitudinal Distance, Test MGSC-3 (1100C)

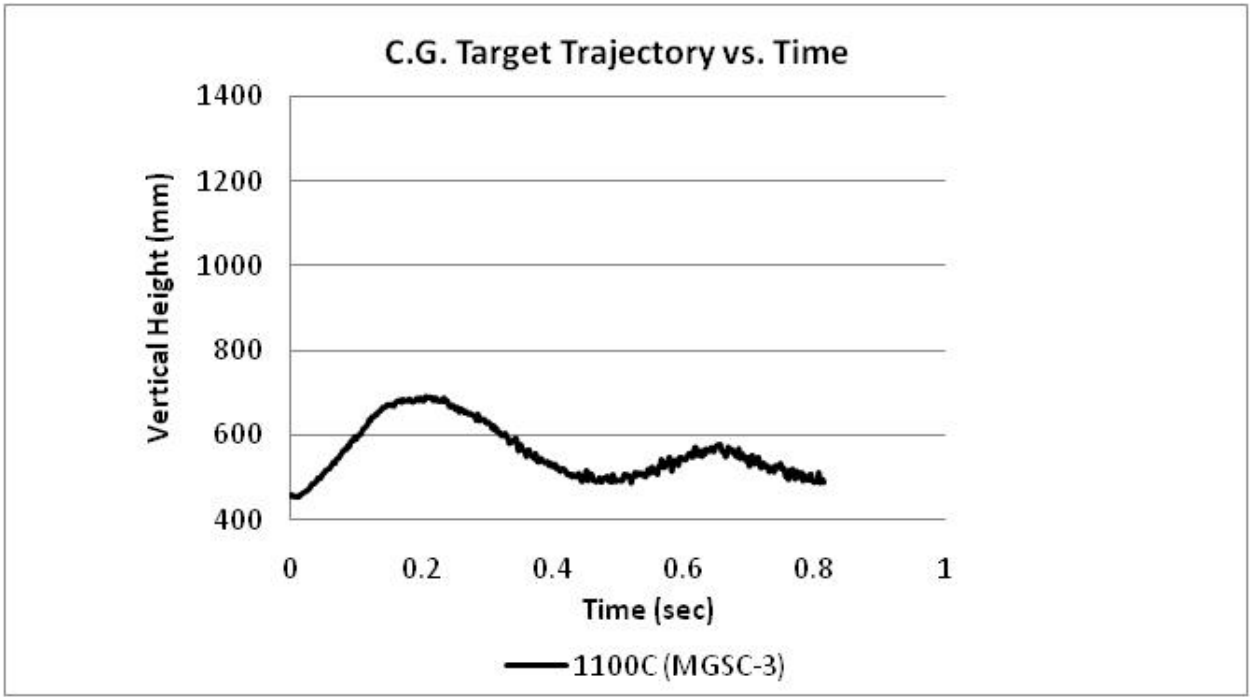

Figure 62. C.G. Target Trajectory vs. Time, Test MGSC-3 (1100C)

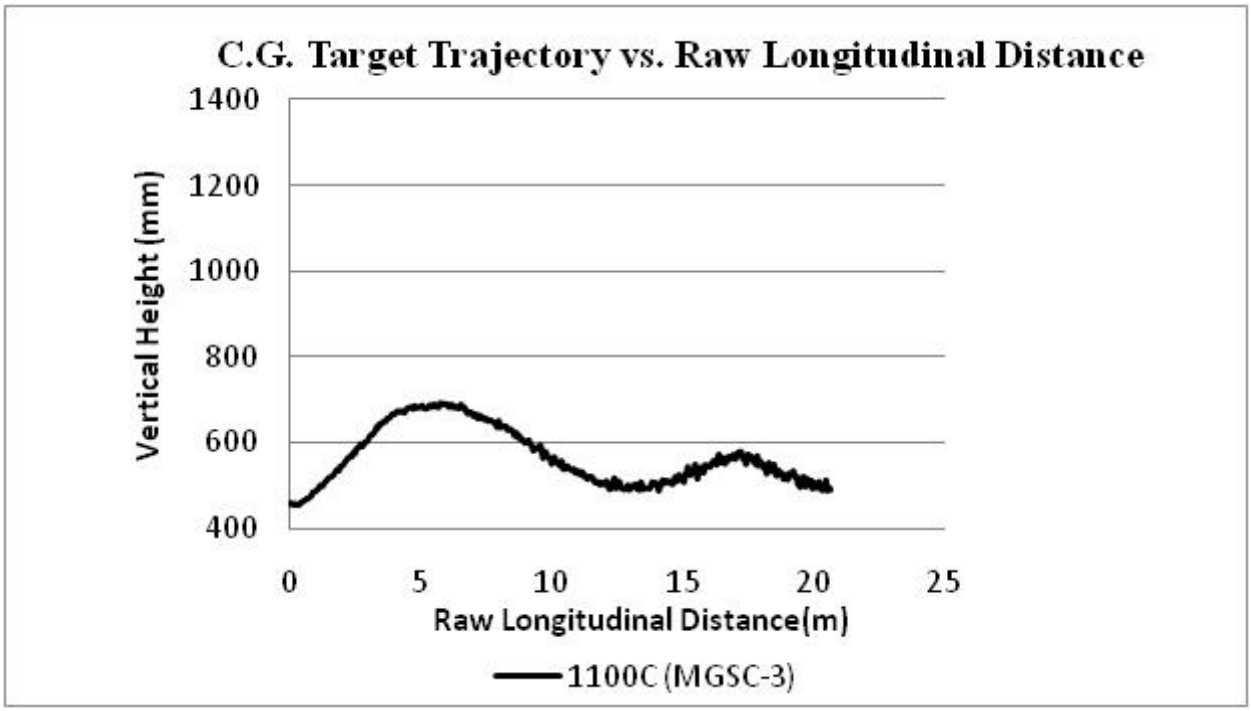

Figure 63. C.G. Target Trajectory vs. Raw Longitudinal Distance, Test MGSC-3 (1100C)

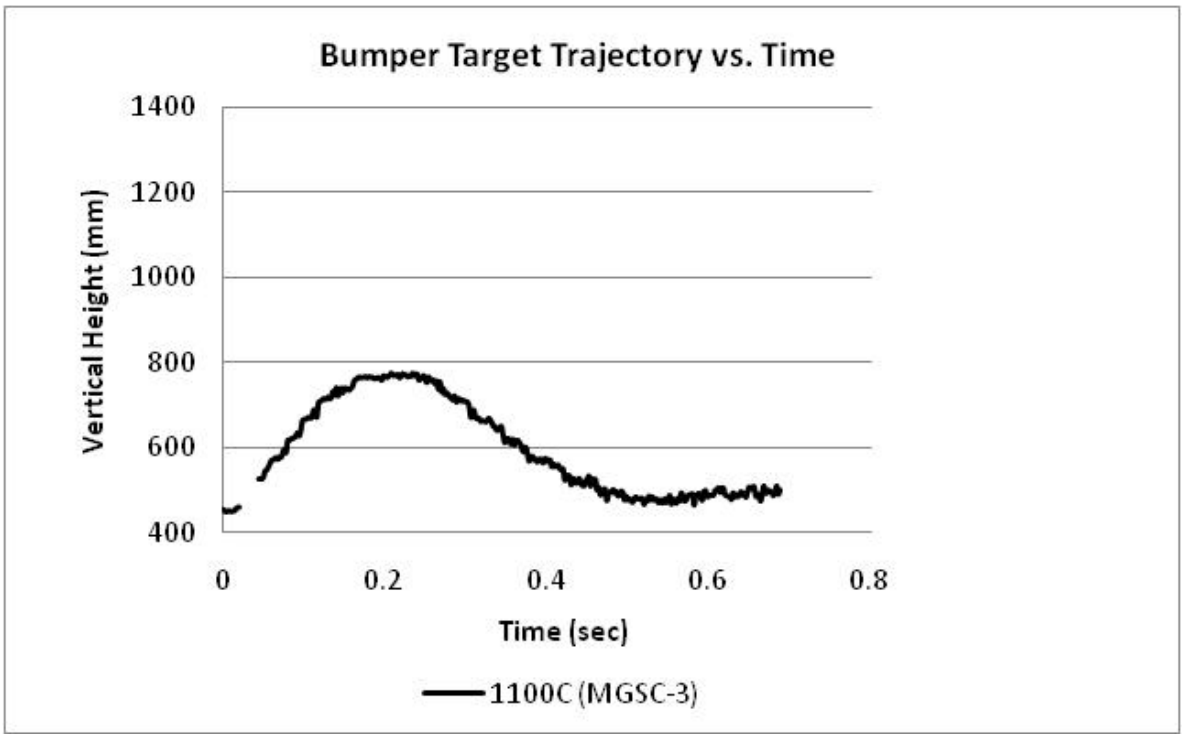

Figure 64. Bumper Target Trajectory vs. Time, Test MGSC-3 (1100C)

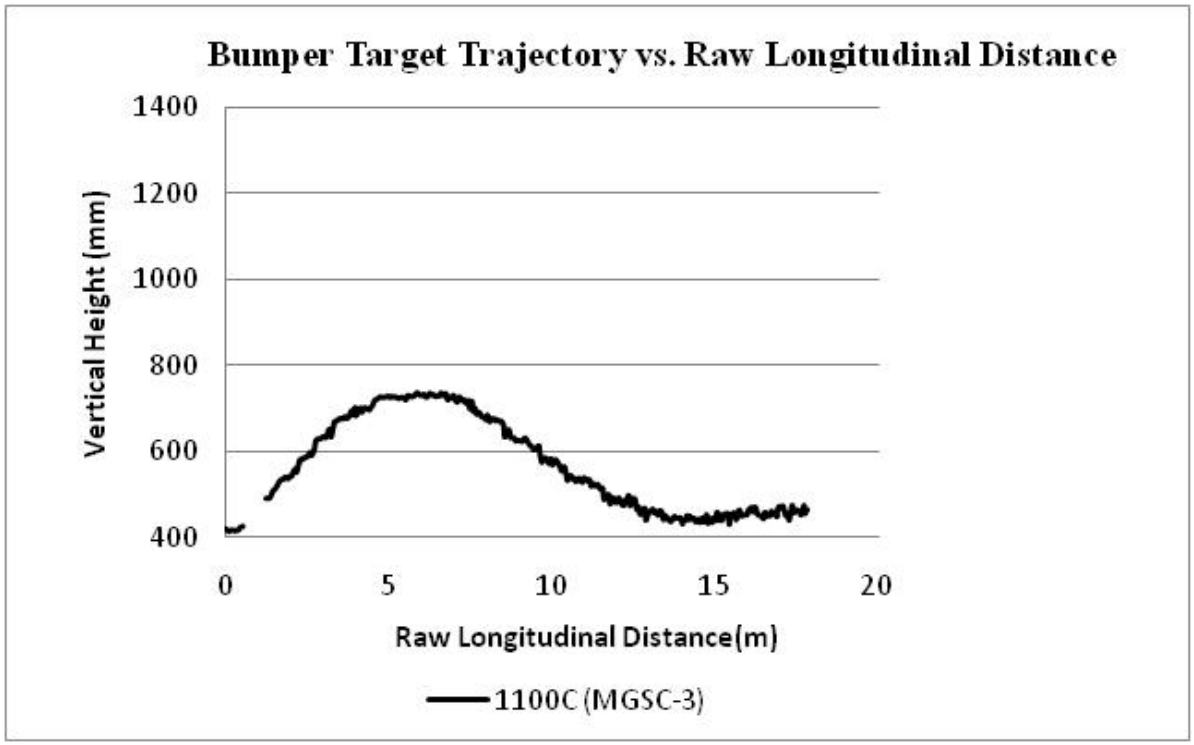

Figure 65. Bumper Target Trajectory vs. Raw Longitudinal Distance, Test MGSC-3 (1100C)

7 CRASH TEST NO. 4 (MGSC-4, 2000P)

7.1 Introduction

The 2,032-kg (4,479-lb) Chevrolet C2500 pickup truck impacted the AASHTO Type B curb at a speed of 100.6 km/h (62.5 mph) and at an angle of 25 degrees. The impact location is shown in Figure 66. Sequential photographs are shown in Figures 67 through 69.

7.2 Test Description

The right-front tire first impacted at 3.04 m (10 ft) from the upstream end of the curb. After impact, the vehicle pitched upward and rolled counter-clockwise. At 0.008 sec, the right-front suspension reached its maximum compression, and the tire became airborne at 0.030 sec. At 0.034 sec, the right-front suspension reached its maximum compression and the right-front tire hit the top of the vehicle's wheel well. At 0.068 sec, the right-front tire re-contacted the ground. At 0.116 sec, the right-rear tire impacted the curb. At 0.122 sec, the left-front tire impacted the curb, and the pickup started to roll clockwise due to the rise of the left-front tire. The right-rear suspension reached the maximum compression at 0.126 sec, and the tire bounced off the ground. At 0.242 sec, the left-rear tire impacted the curb and bounced off the ground. At 0.272 sec, the right-rear tire re-contacted the ground. At 0.280 sec, the left-rear tire became airborne. At 0.316 sec, the left-front tire re-contacted the ground. At 0.380 sec, the right-front tire landed on the ground. At 0.390 sec, the right-rear tire became airborne again due to the retraction of the right-rear suspension, resulting in the vehicle's pitch downward. At 0.716 sec, the left-rear tire landed on the ground. At 0.836 sec, the right-rear tire landed on the ground. At 1.148 sec, the rear-tires bounced off the ground again.

For this impact condition on the 152-mm (6-in.) high, AASHTO Type B curb, the heading angle of the vehicle was basically unaffected, as the vehicle maintained nearly the same

vehicle path after striking the curb. The final vehicle position and trajectory are shown in Figure 70.

7.3 System and Component Damage

Damage to the curb system was negligible, as shown in Figures 71. No cracks or fractures were observed on the curb. Two contact marks were observed on the top and traffic-side faces of the curb. Tire marks and scrapes occurred at 3.04 mm (10 ft) and 6.82 m (22.4 in.) from the upstream end of the curb.

7.4 Vehicle Damage

Exterior vehicle damage was minor, as shown in Figure 72. Minor scrapes and scratches were found on the tires of the vehicle due to the impact with the curb. A tire contact mark was found on the top of the right-front wheel well. No wheel deformation or suspension damage was observed. The rest of vehicle was intact.

7.5 Trajectory Results

For the purpose of this research study, the vehicle's post-impact trajectories were recorded by tracking the C.G. and bumper target centers using high-speed video analysis. The vertical displacements of each target were plotted against both time and the raw longitudinal distance, as shown in Figures 73 through 76. The raw longitudinal distance was defined as a given target's longitudinal displacement starting at zero with respect to its initial target center location when the tire contacted the curb. As such, raw longitudinal distance measurements reported graphically for two different targets do not reference the same starting point and are out of phase. Adjustments to the noted plots will be made in Chapter 8 in order to bring target measurements into phase for further analysis.

The initial heights of the vehicle's C.G. and bumper targets were 629 mm (24.75 in.) and 572 mm (22.5 in.), respectively. Thus, the actual trajectories of the C.G. and bumper targets were obtained by coupling the raw, film-analysis, vertical displacement data with their initial target heights, as shown in Figures 77 through 80. The results are also plotted in English-units in Appendix B.

7.6 Occupant Risk Values

The longitudinal and lateral occupant impact velocities from the EDR-3 transducer were determined to be -1.56 m/s (-5.12 ft/s) and -0.29 m/s (0.95 ft/s), respectively. The maximum 0.010-sec average occupant ride down deceleration in the longitudinal and lateral directions from the EDR-3 transducer were -1.79 g's and -3.80 g's, respectively. Results are shown graphically in Appendix C. The results from the rate transducer are shown graphically in Appendix C.

7.7 Discussion

The analysis of the test results for test MGSC-4 showed that the 152-mm (6-in.) high, AASHTO Type B curb system did not redirect the 2000P pickup at an impact speed of 100.6 km/h (62.5 mph) and at an impact angle of 25 degrees. The 2000P pickup truck kept rising after impact to a certain point at which the vehicle then started descending. The bumper target reached its peak vertical displacement of 207 mm (8.2 in.) at 0.3 sec after curb impact. The C.G. target reached a maximum vertical displacement of 264 mm (10.4 in.) at 0.64 sec after curb impact. The bumper target stayed at a high elevation between 3.4 sec and 8.9 sec. Then, the bumper had a significant descent. The C.G. target vibrated up and down before it reached its final peak value. Results showed that 2000P had a quite different post-curb-impact attitude compared to the 2270P. No damage was found on the curb. There was no deformation or damage to the pickup truck.

Figure 66. Impact Location, Test MGSC-4

0.000 sec

0.184 sec

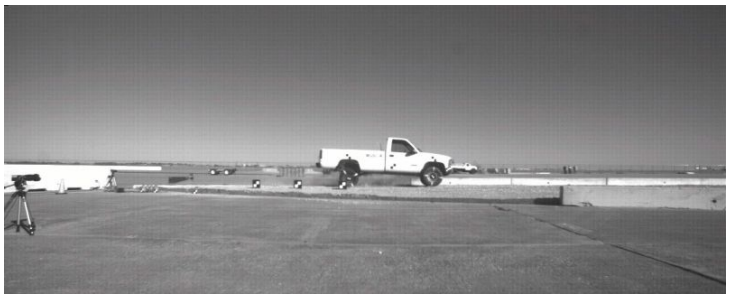

0.312 sec

0.486 sec

0.668 Sec

Figure 67. Sequential Photographs, Test MGSC-4

0.000 sec (right-front)

0.118 sec (right-rear)

0.004 sec (right-front)

0.124 sec (right-rear)

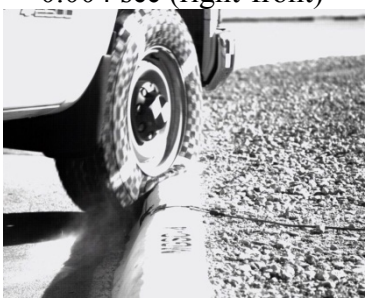

0.010 sec (right-front)

0.132 sec (right-rear)

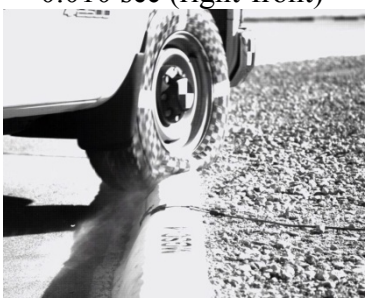

0.018 sec (right-front)

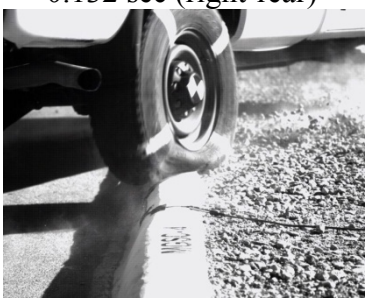

0.140 sec (right-rear)

0.026 sec (right-front)

0.150 sec (right-rear)

Figure 68. Additional Sequential Photographs, Test MGSC-4

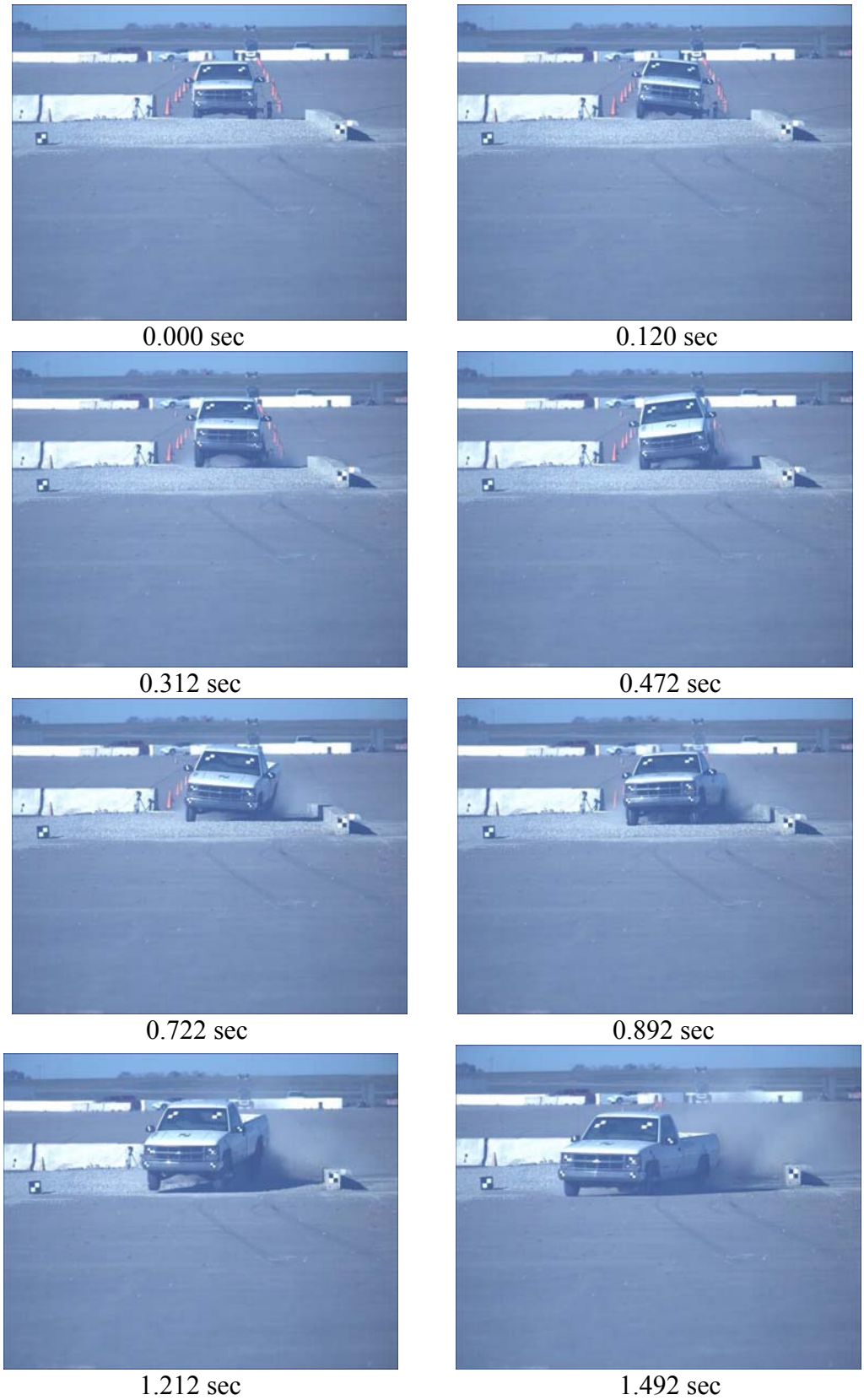

Figure 69. Additional Sequential Photographs, Test MGSC-4

Figure 70. Vehicle Final Position and Trajectory, Test MGSC-4

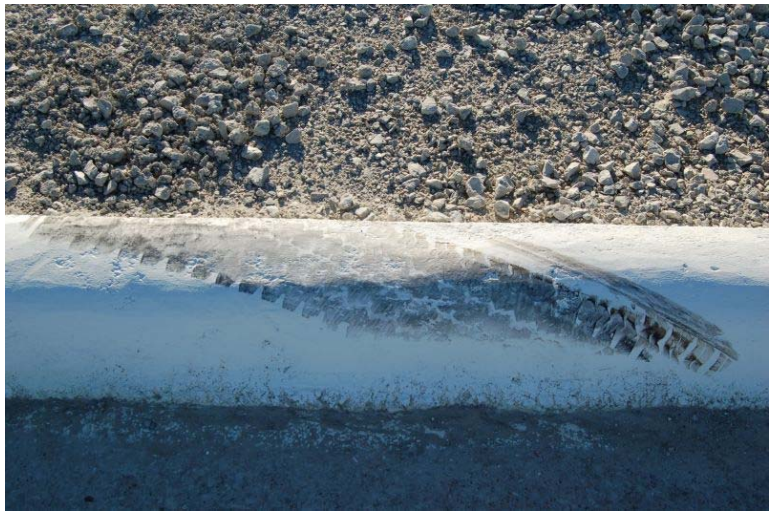

Figure 71. System Damage, Test MGSC-4

Right-Front Tire

Right-Rear Tire

Left-Front Tire

Left-Rear Tire

Figure 72. Vehicle Damage, Test MGSC-4

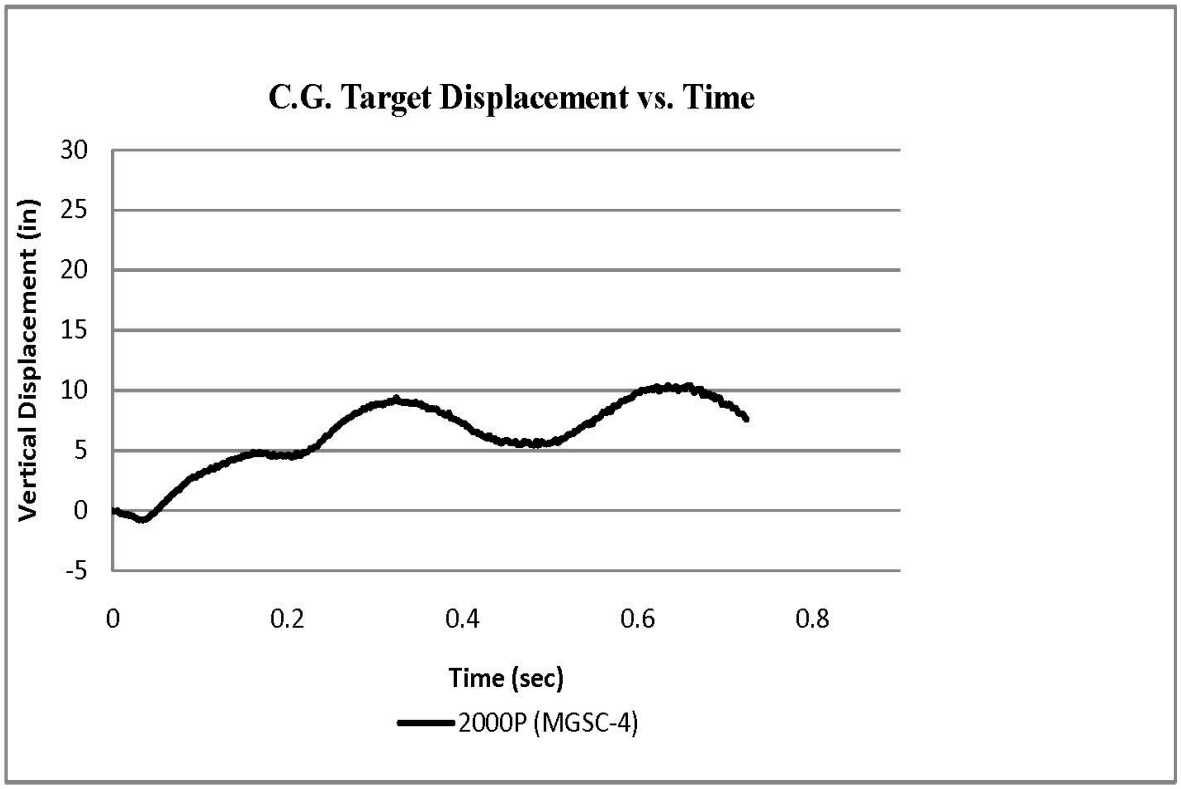

Figure 73. C.G. Target Displacement vs. Time, Test MGSC-4 (2000P)

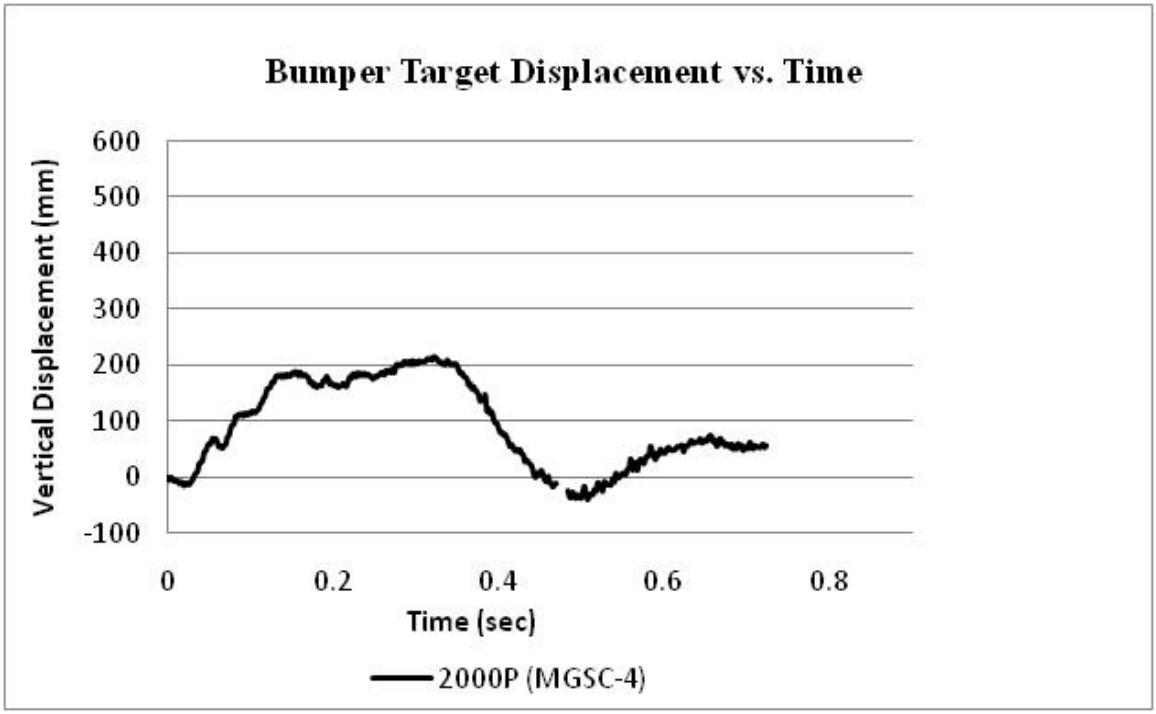

Figure 74. Bumper Target Displacement vs. Time, Test MGSC-4 (2000P)

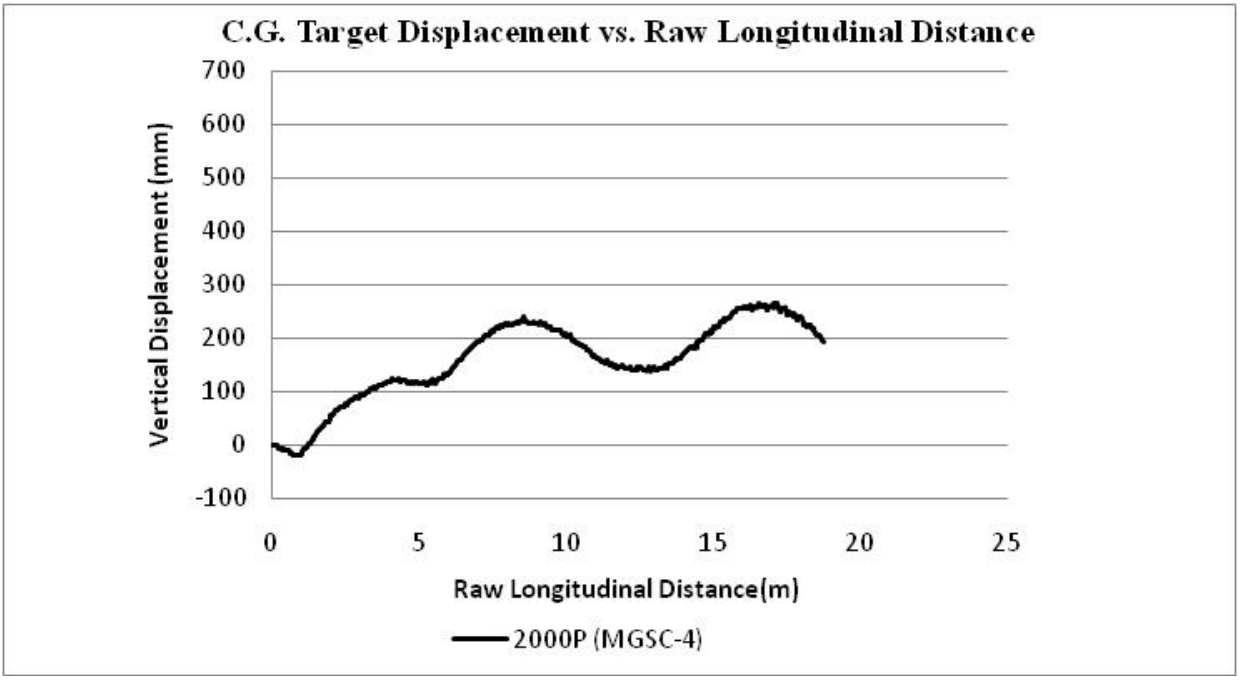

Figure 75. C.G. Target Displacement vs. Raw Longitudinal Distance, Test MGSC-4 (2000P)

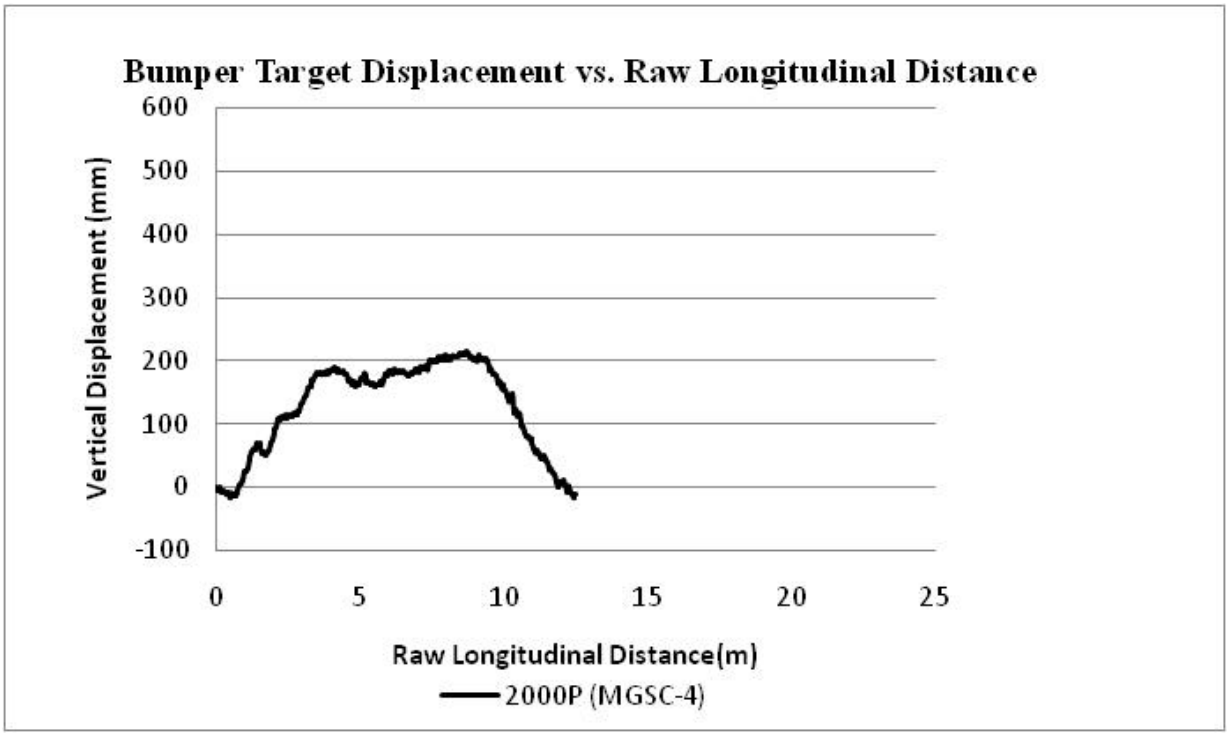

Figure 76. Bumper Target Displacement vs. Raw Longitudinal Distance, Test MGSC-4 (2000P)

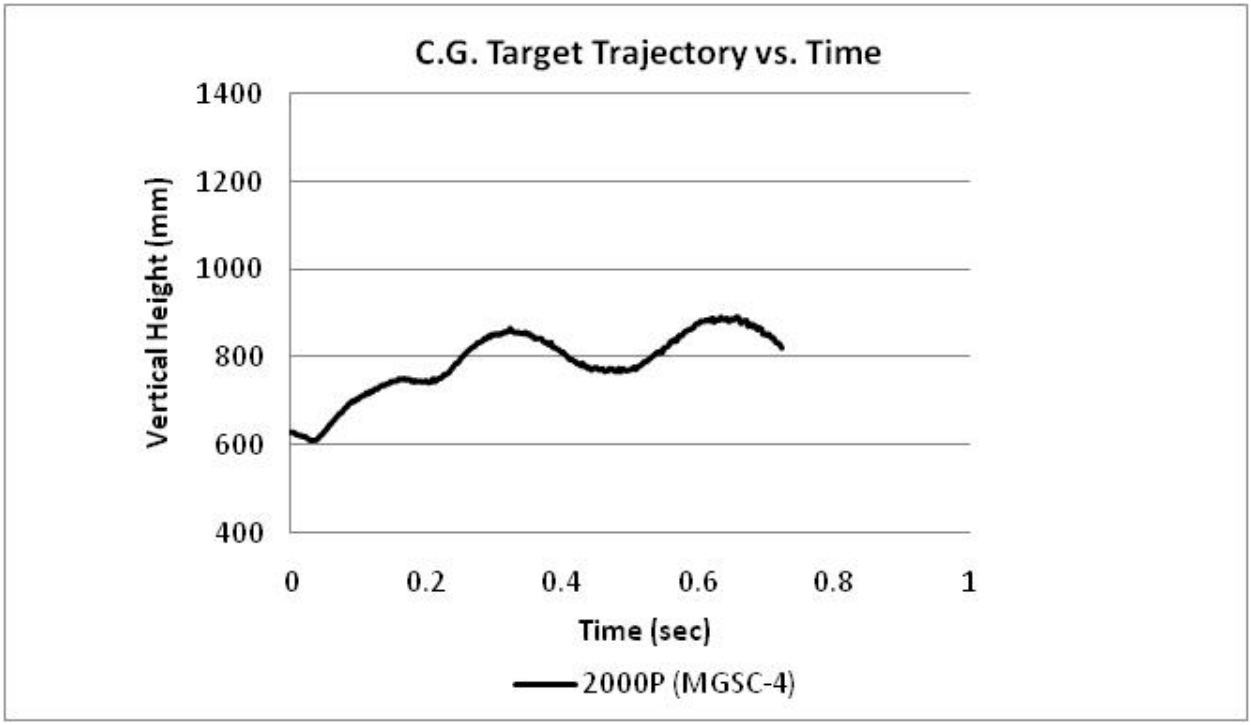

Figure 77. C.G. Target Trajectory vs. Time, Test MGSC-4 (2000P)

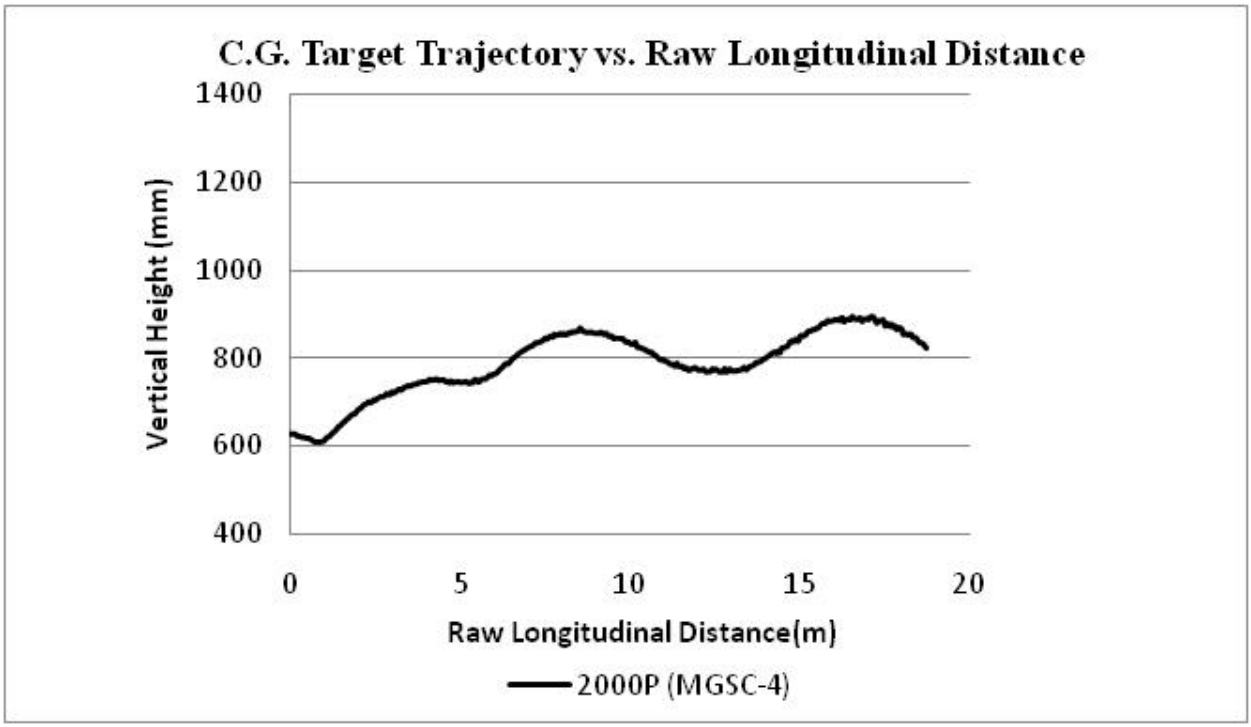

Figure 78. C.G. Target Trajectory vs. Raw Longitudinal Distance, Test MGSC-4 (2000P)

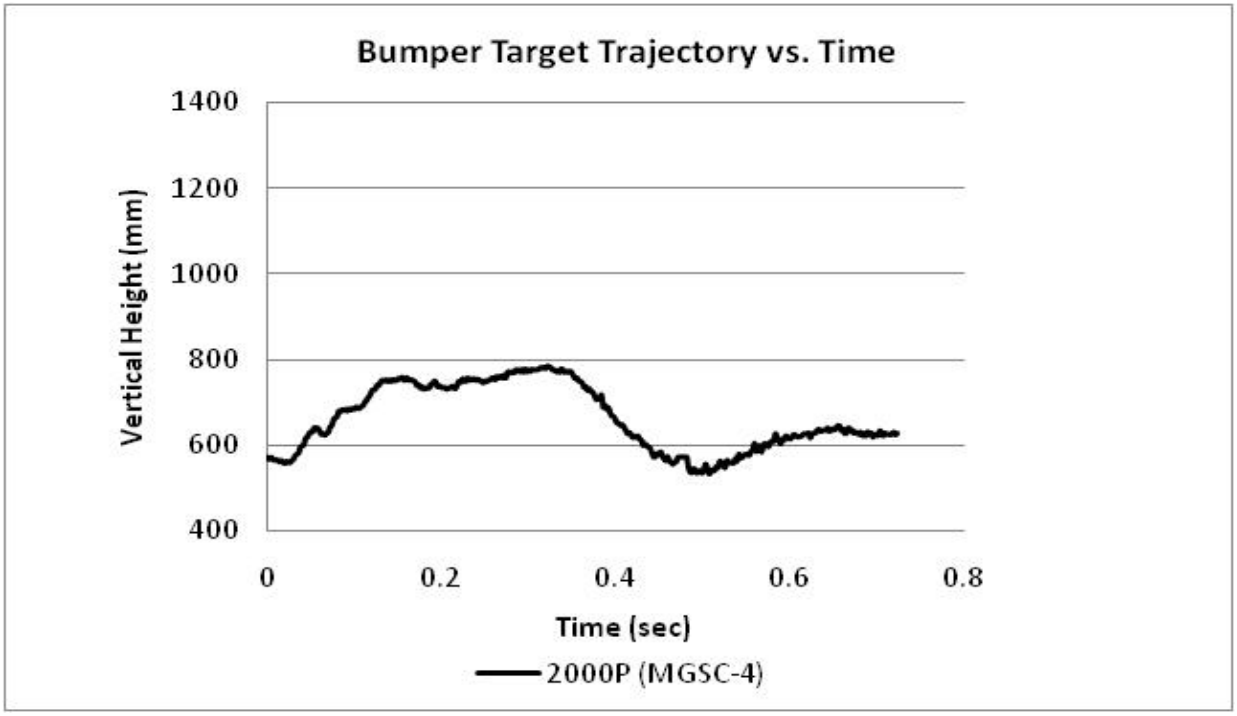

Figure 79. Bumper Target Trajectory vs. Time, Test MGSC-4 (2000P)

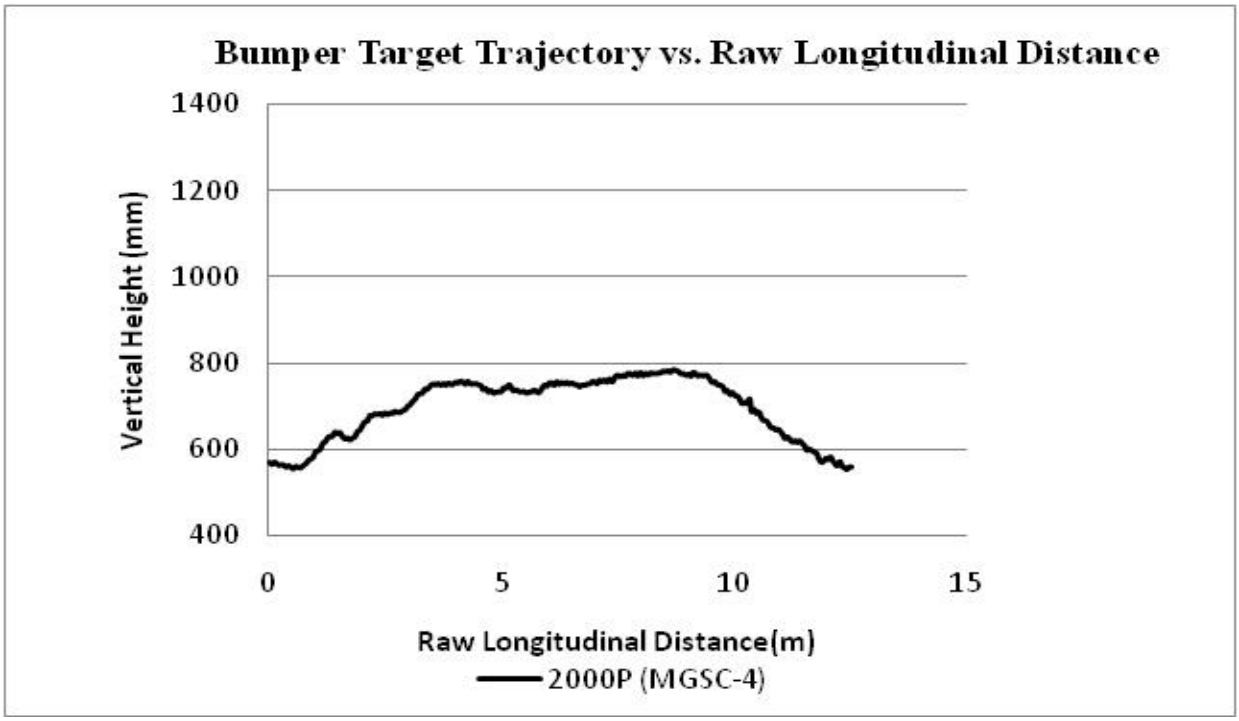

Figure 80. Bumper Target Trajectory vs. Raw Longitudinal Distance, Test MGSC-4 (2000P)

8 TEST TRAJECTORY DATA ANALYSIS

8.1 Verification of Video Analysis Data

The verification of the raw data from video analysis was conducted by reconstructing the bumper target trajectory from the C.G. target trajectory. The reconstruction was performed by coupling the video-analysis C.G. target trajectory with the pitch angular displacement collected from the rate transducers using Figure 81, Equation 8-1, and Table 1. The results showed that all four reconstructed bumper target trajectories agreed with the bumper target trajectories obtained from video analysis, as shown in Figures 82 through 85. It indicated that the C.G. data obtained from the video analysis was consistent with the bumper data obtained from the video analysis. It also proved the reliability of the transducer pitch data.

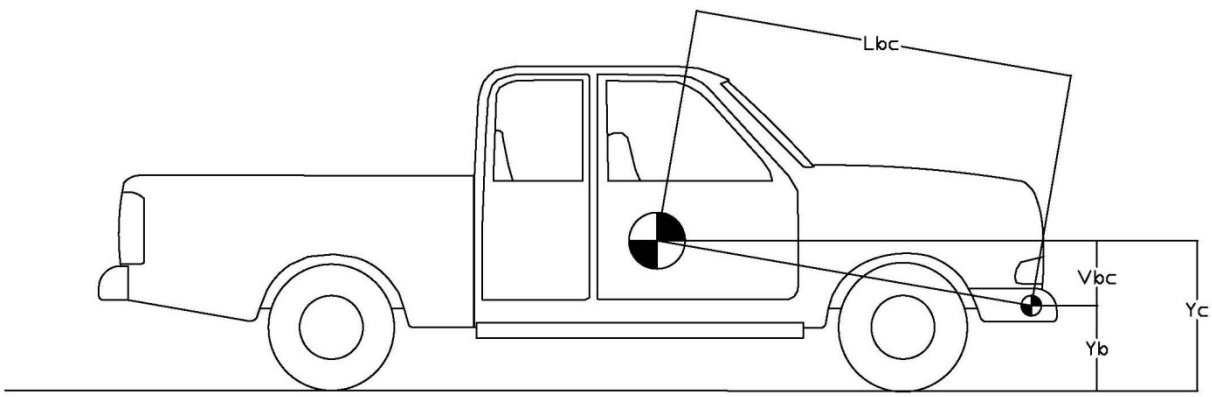

Figure 81. Illustration of Bumper Target Trajectory Reconstruction

$$Y_b = Y_c + V_{bc} + L_{bc} * sin(\Theta_p) \qquad \text{Eq. 8-1}$$

Y_b = Bumper Target Vertical Displacement

L_{bc} = Distance between C.G. Target and Bumper Target

V_{bc} = Initial Vertical Distance between C.G. Target Center and Bumper Target Center

Θ_p = Pitch Angle

Y_c = C.G. Target Vertical Displacement

Table 1. Summary of Initial Parameters for Bumper Target Trajectory Reconstruction

Test No.	MGSC-1	MGSC-2	MGSC-3	MGSC-4
V_{BC}	-184 mm (-7.25 in.)		0 mm (0 in.)	-57 mm (-2.25 in.)
L_{BC}	2,142 mm (84.31 in.)		1,530 mm (60.25 in.)	2,147 mm (84.53 in.)

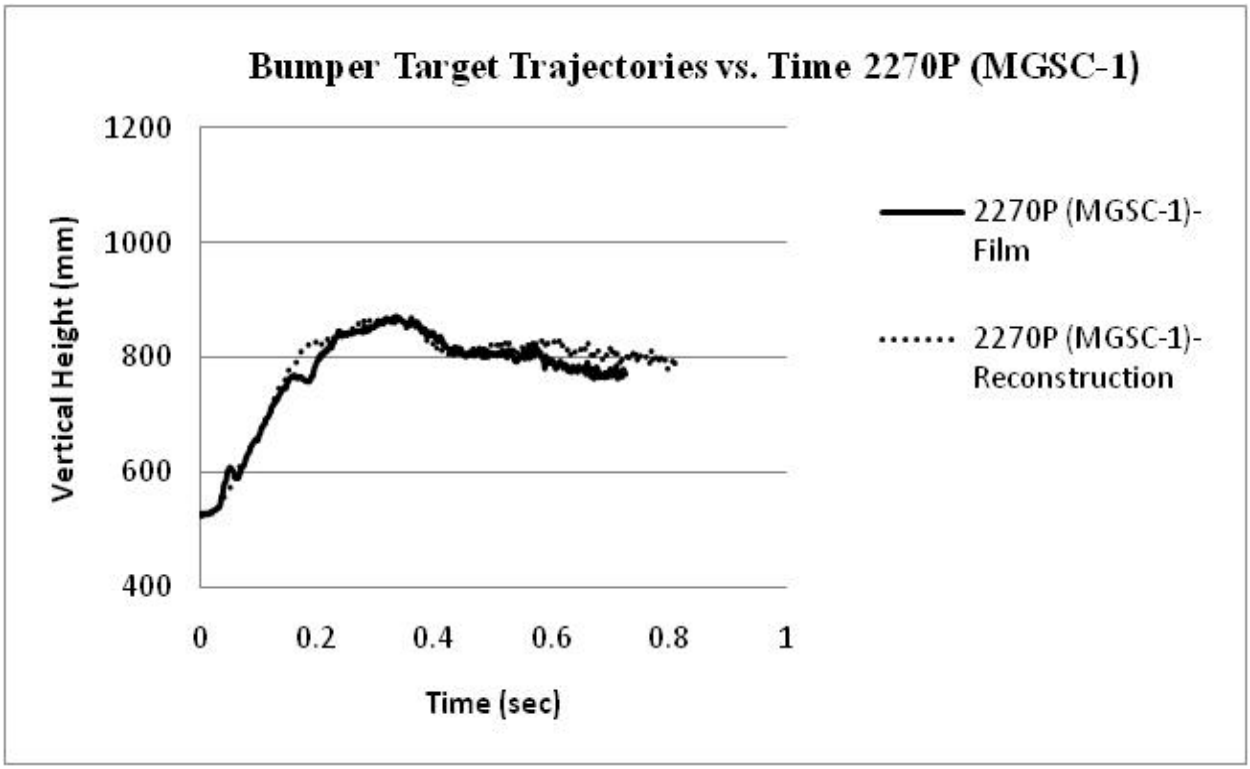

Figure 82. Bumper Target Trajectory Reconstruction, Test MGSC-1

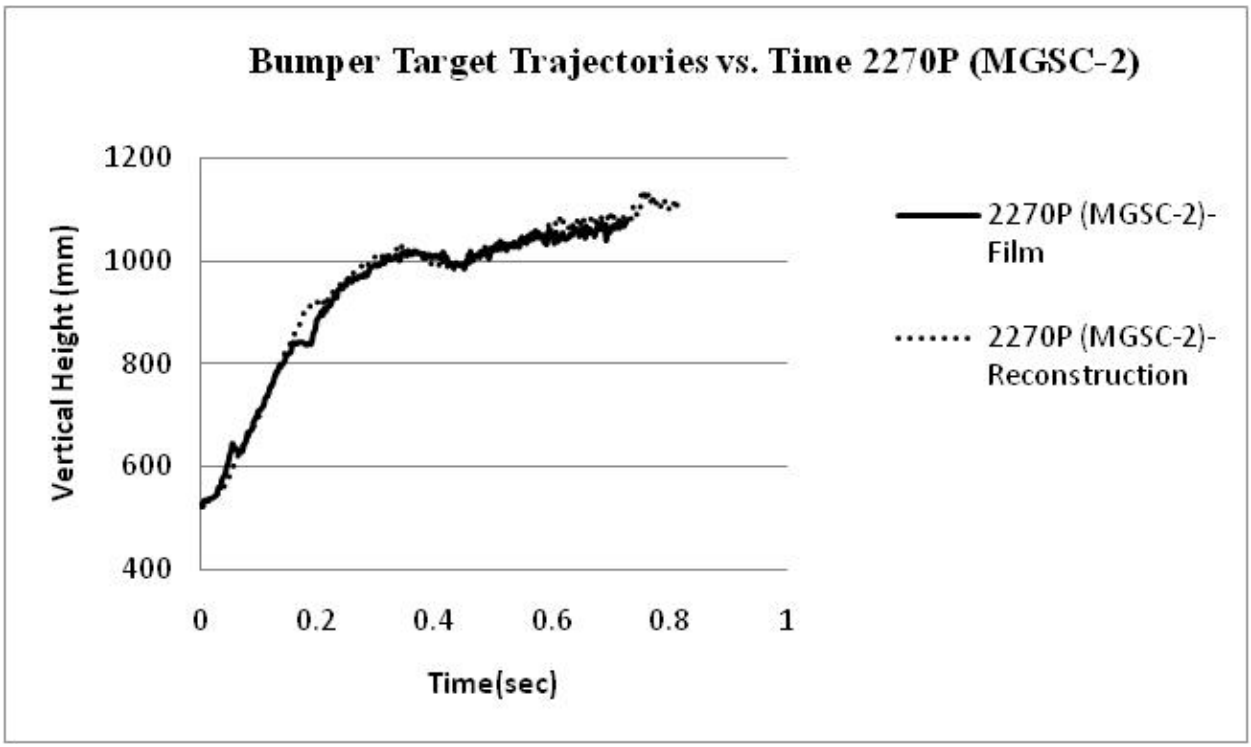

Figure 83. Bumper Target Trajectory Reconstruction, Test MGSC-2

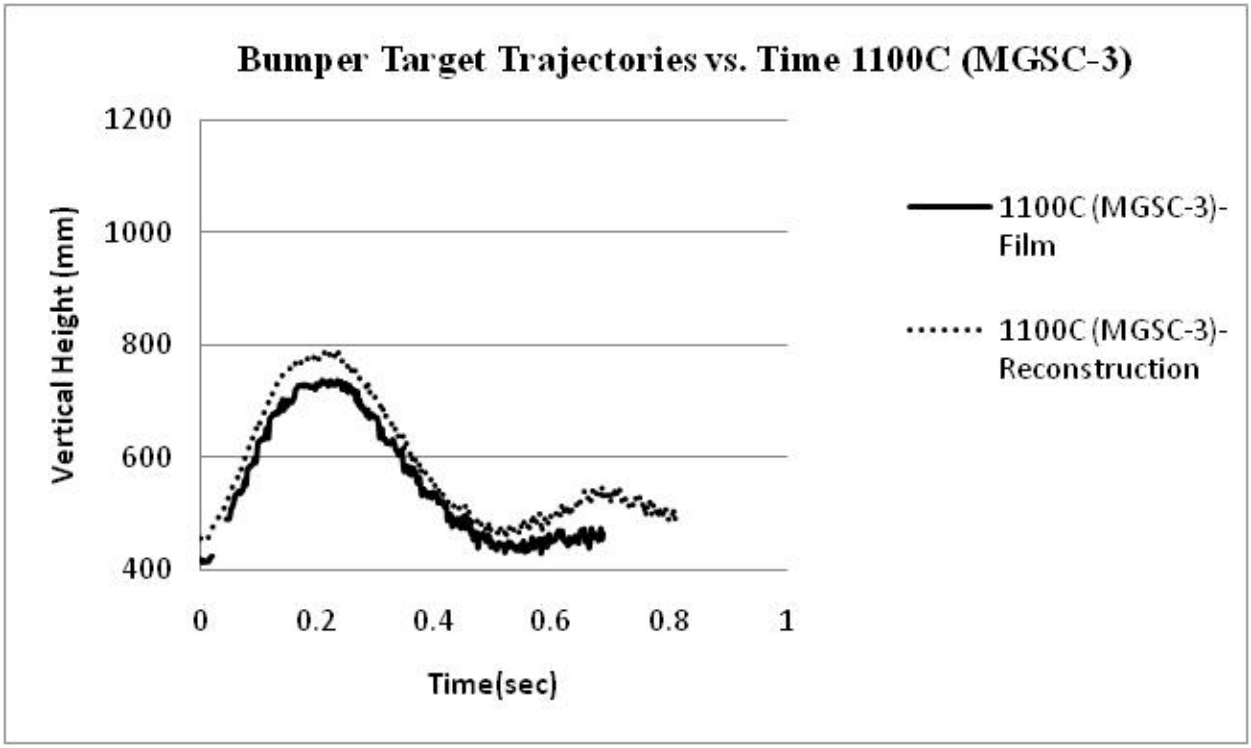

Figure 84. Bumper Target Trajectory Reconstruction, Test MGSC-3

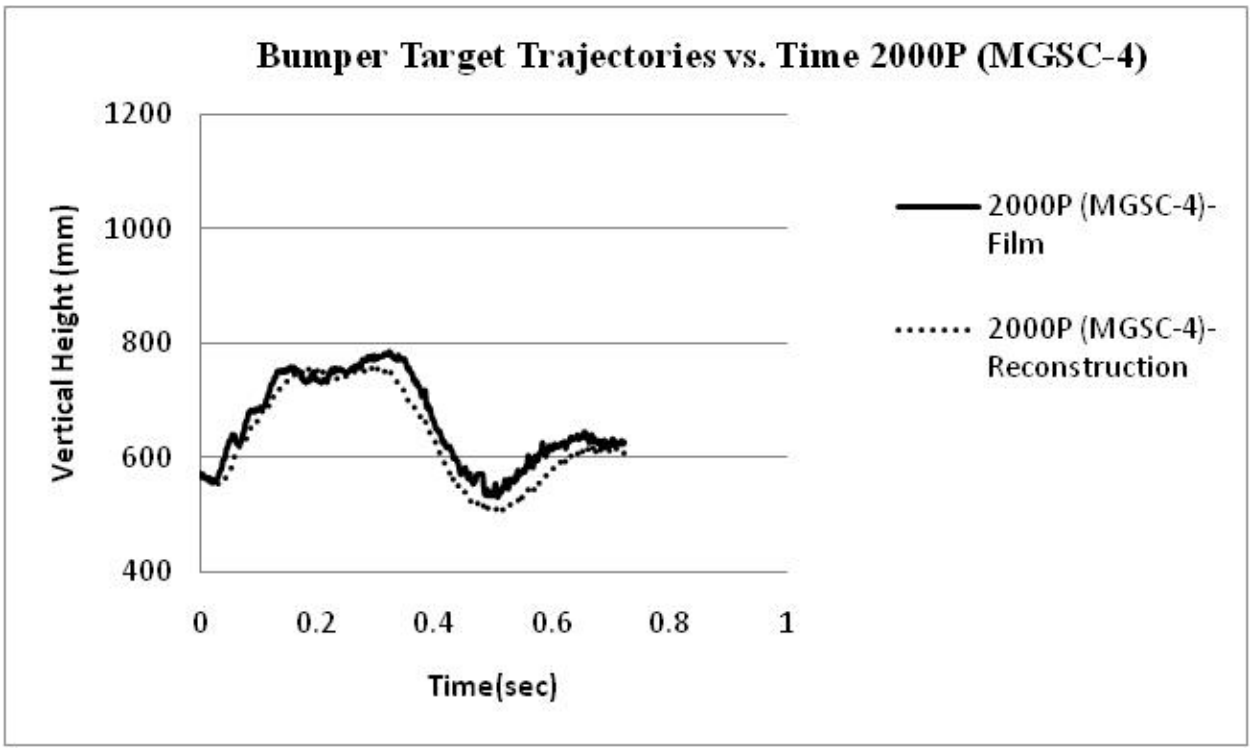

Figure 85. Bumper Target Trajectory Reconstruction, Test MGSC-4

8.2 Processed Longitudinal Distance (PLD) Coordinate

The raw longitudinal distance obtained from the video analysis is the displacement with respect to the target center's initial location at time zero, which varied across the different test vehicles. To bring the data into phase, a new coordinate system, called the Processed Longitudinal Distance (PLD) coordinate system, was setup to analyze the vehicle's trajectory with respect to the distance behind the curb. The setup of the PLD coordinate system is shown in Figure 86. In this system, the right-front corner of the tire is located on the front tangent edge of the curb's slope, defined as the zero point. The X-axis followed the initial impact direction, which was 25 degrees with respect to the curb. The Z-axis was perpendicular to the ground X-Y plane. The raw video data was transformed to the PLD by coupling the raw longitudinal coordinate data with each target's initial location in the PLD system using Equation 8-2 with the

information provided in Table 2. Vehicle trajectories in the PLD system are shown in Figures 87 and 88.

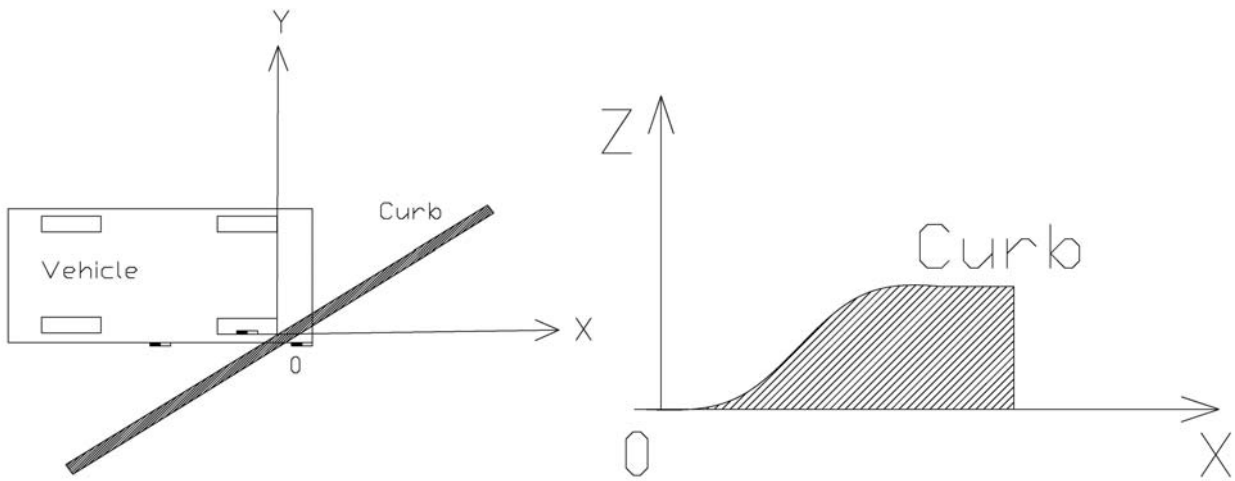

Top View Side View

Figure 86. Setup of PLD Coordinate System

$X_{pld} = X_{raw} + X_{ini}$ Eq. 8-2

X_{pld} = X coordinate in PLD system

X_{ini} = Target Center's initial X coordinate in PLD system

X_{raw} = Raw X coordinate from video analysis (Raw Longitudinal Distance)

Table 2. Summary of Parameters for Raw-to-PLD Transition

Test No.	MGSC-1	MGSC-2	MGSC-3	MGSC-4
X_{ini} of C.G. Target	-1.75 m (-5.75 ft)		-1.13 m (-3.7 ft)	-1.76 m (-5.77 ft)
X_{ini} of Bumper Target	0.38 m (1.26 ft)		0.33 m (1.07 ft)	0.39 m (1.28 ft)

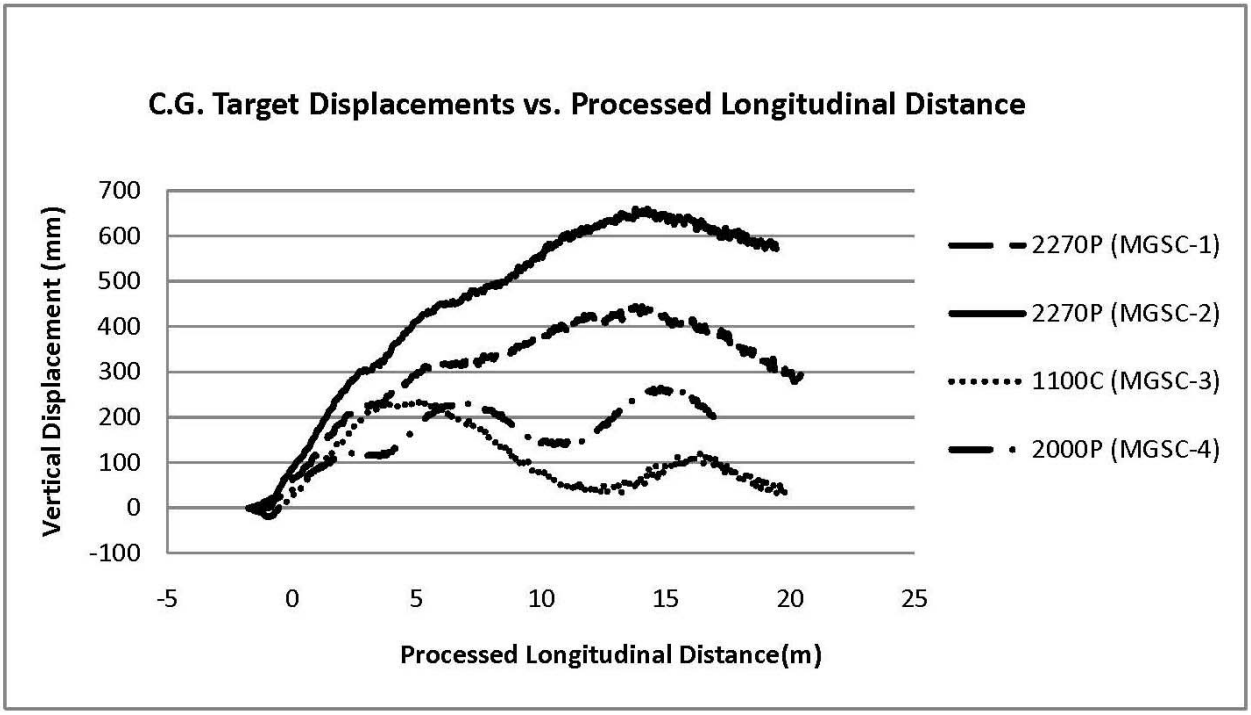

Figure 87. C.G. Target Vertical Displacement vs. Processed Longitudinal Distance

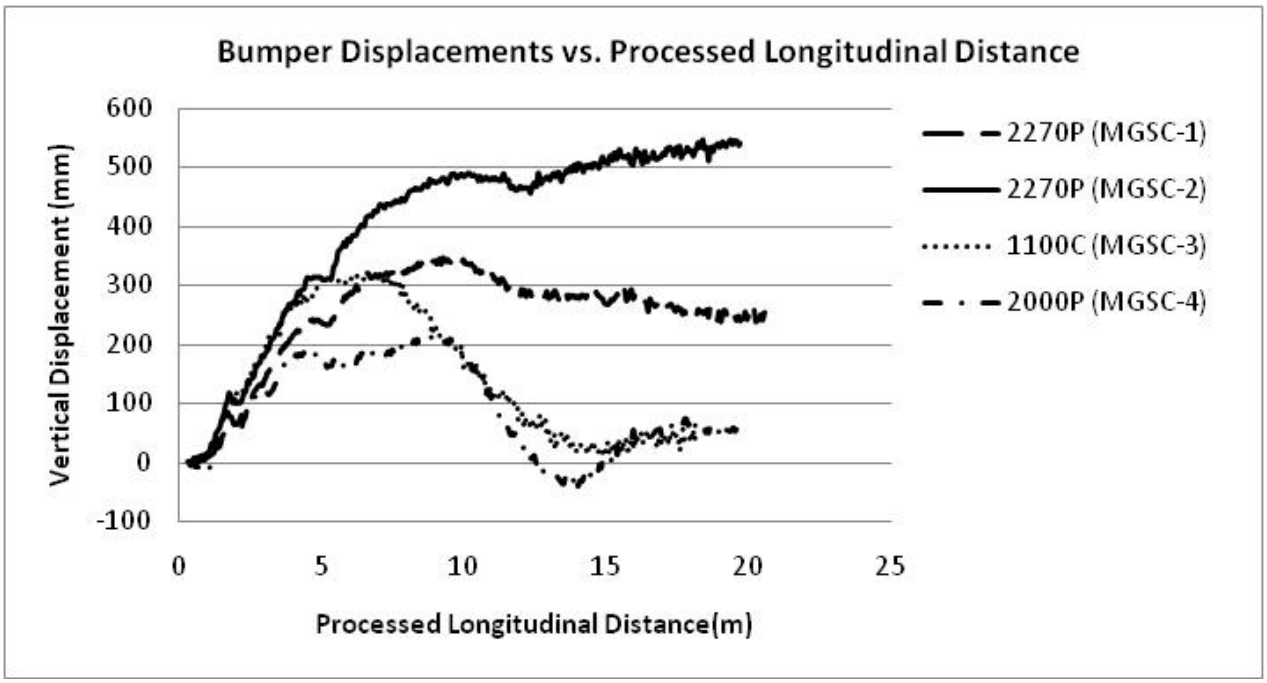

Figure 88. Bumper Target Vertical Displacement vs. Processed Longitudinal Distance

8.3 Processed Curb-Lateral Distance (CLD) Coordinate

An MGS installation would be constructed parallel with the curb. Thus, a new coordinate system (X'-Y'), was setup for the analysis of the MGS critical offset behind the curb, or to determine the Curb-Lateral Distance (CLD). The setup of the CLD coordinate system has the same zero point and Z-axis (i.e., Z' is parallel to Z) as the PLD system, but the X'-axis is normal to the curb, as shown in Figure 89. The transformation from the PLD coordinate system to the CLD coordinate system was conducted using Equation 8-3. After the coordinate transformation, the vertical displacements of the vehicle targets are shown in Figures 90 and 91. The target post-impact trajectories are shown in Figures 92 and 93.

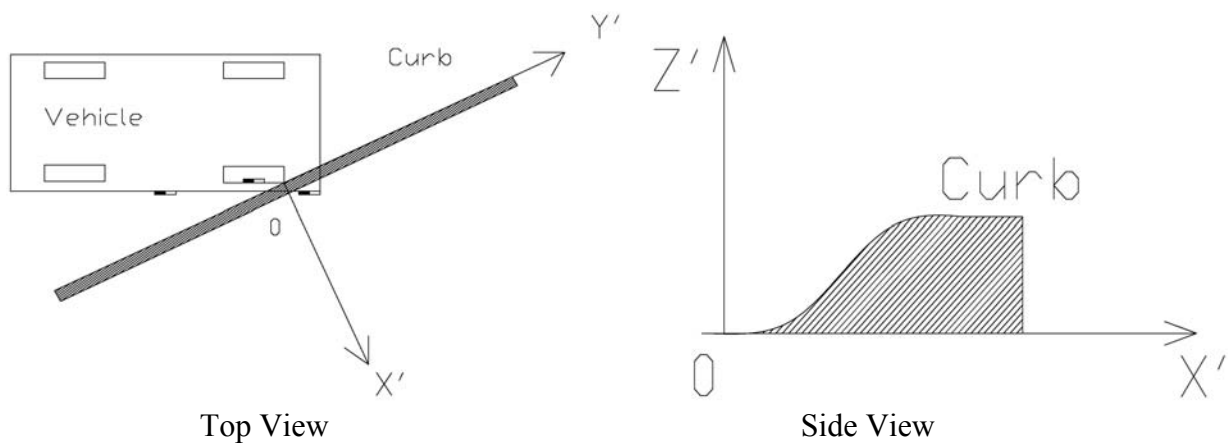

Figure 89. Setup of CLD Coordinate System

$$X'_{CLD} = X_{PLD} * \sin(25^\circ) \qquad \text{Eq. 8-3}$$

X'_{CLD} = X' coordinate in CLD system

X_{PLD} = X coordinate in PLD system

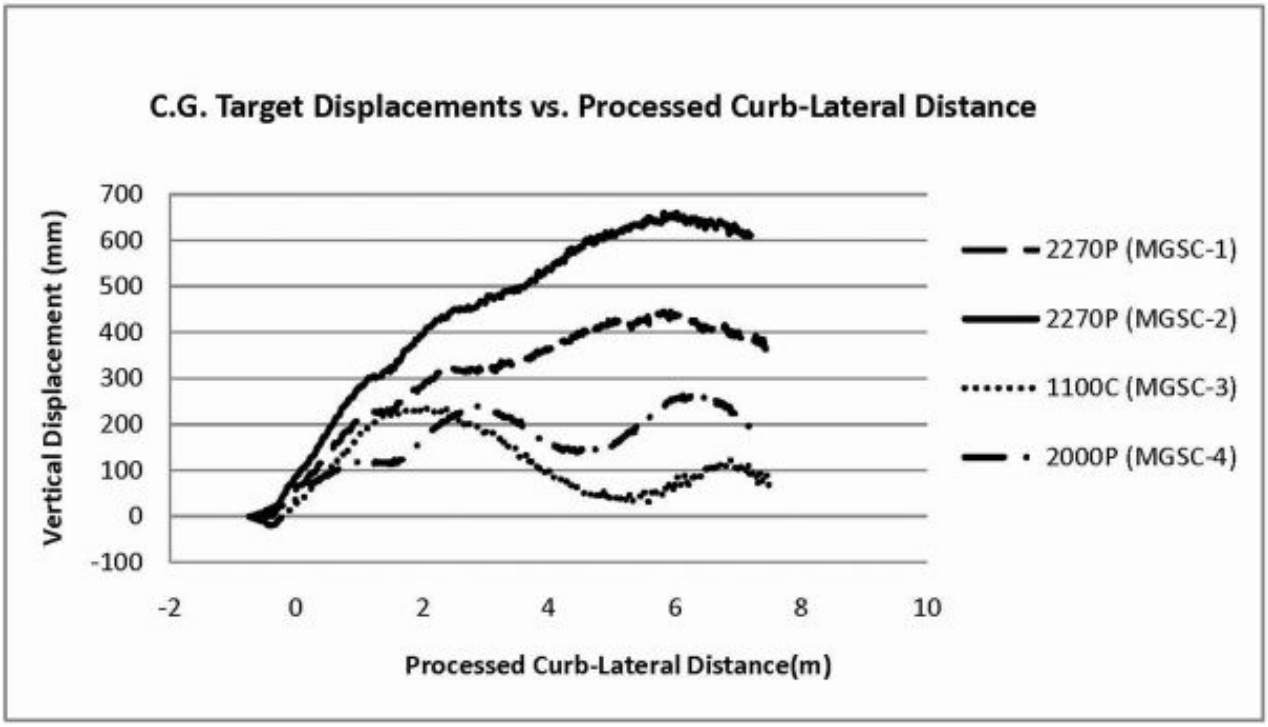

Figure 90. C.G. Target Displacement in CLD Coordinates

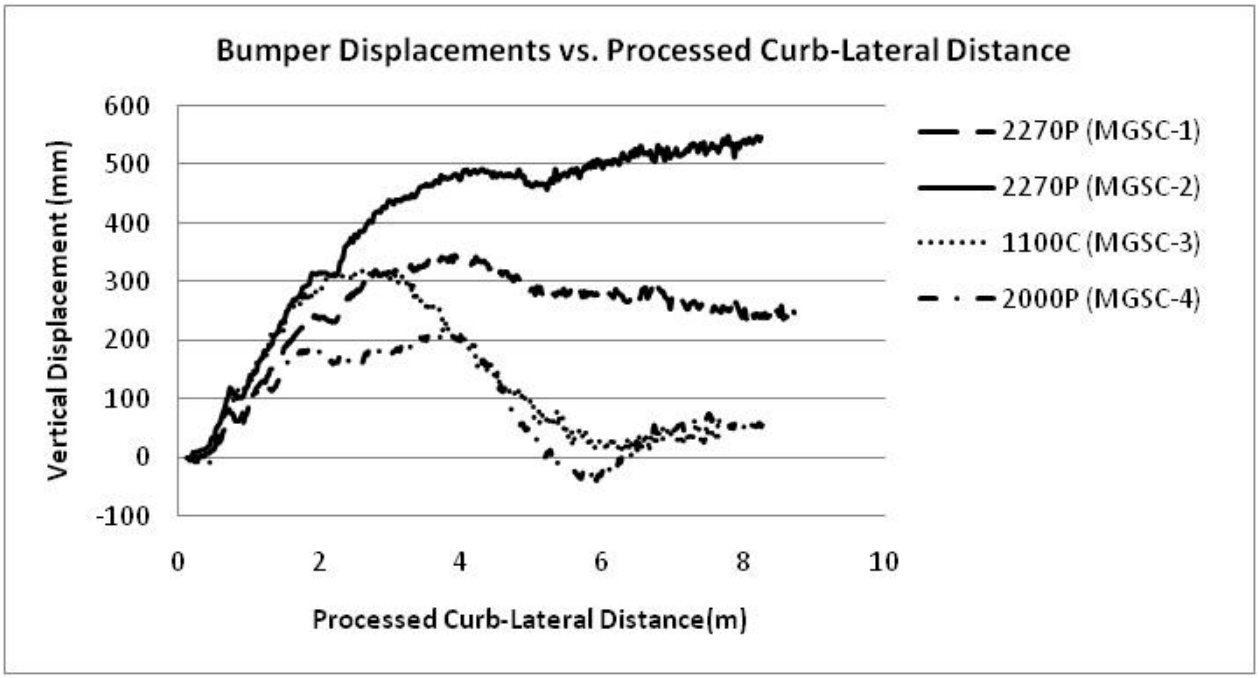

Figure 91. Bumper Target Displacement in CLD Coordinates

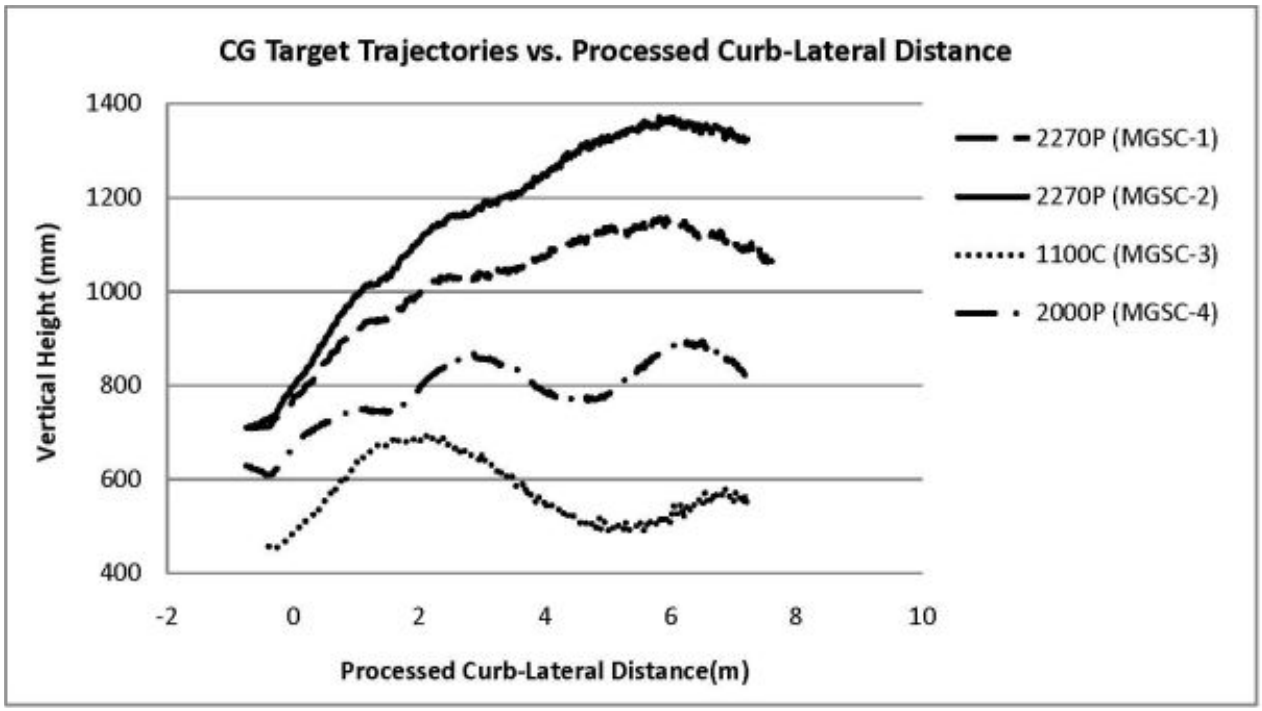

Figure 92. C.G. Target Trajectory in CLD Coordinates

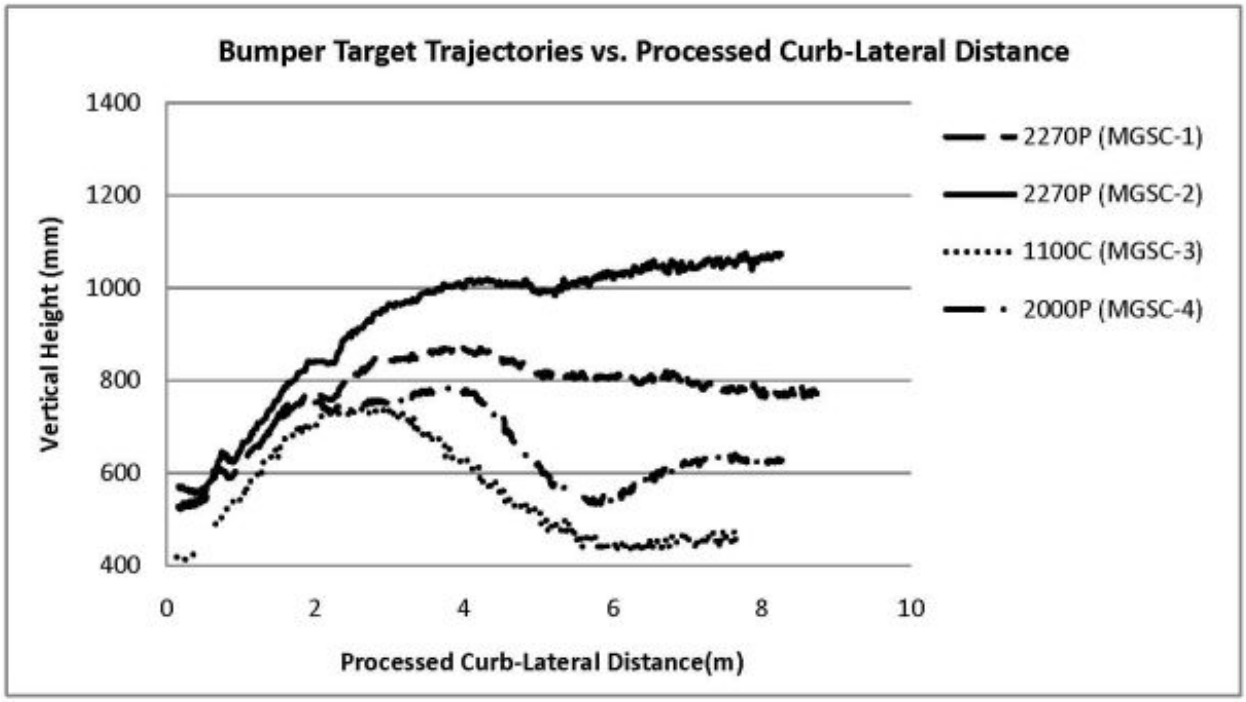

Figure 93. Bumper Target Trajectory in CLD Coordinates

9 PICKUP-CURB IMPACT SIMULATION AND VALIDATION

9.1 Introduction

To test the current 2000P pickup's reliability for studying curb impacts, an LS-DYNA simulation was performed. The simulation result was compared to a physical vehicle-to-curb impact test. Evaluation of the current pickup model was performed to assist the MGS-Curb project and to identify weaknesses in the current model.

9.2 LS-DYNA Model Description and Results

A 2000P pickup truck model struck a 152-mm (6-in.) AASHTO Type B curb at an impact speed of 100 km/h (62.1 mph) and an impact angle of 25 degrees, as shown in Figure 94.

A separate investigation was performed to compare different ground modeling methods in LS-DYNA. The ground and the curb were modeled with one continuous layer of rigid body solid elements, as shown in Figure 95, and the interaction between the tire and the ground/curb was processed using contact command *Contact-Automatic-Single-Surface. Considering the actual contact surface, a gap of half of the tire shell thickness was initially defined between the tire and the ground to match the real-life position, as shown in Figure 95.

The 2000P truck smoothly ran over the curb, as shown in Figure 96. The vehicle's heading direction was not affected by the curb impact, which was consistent with physical testing.

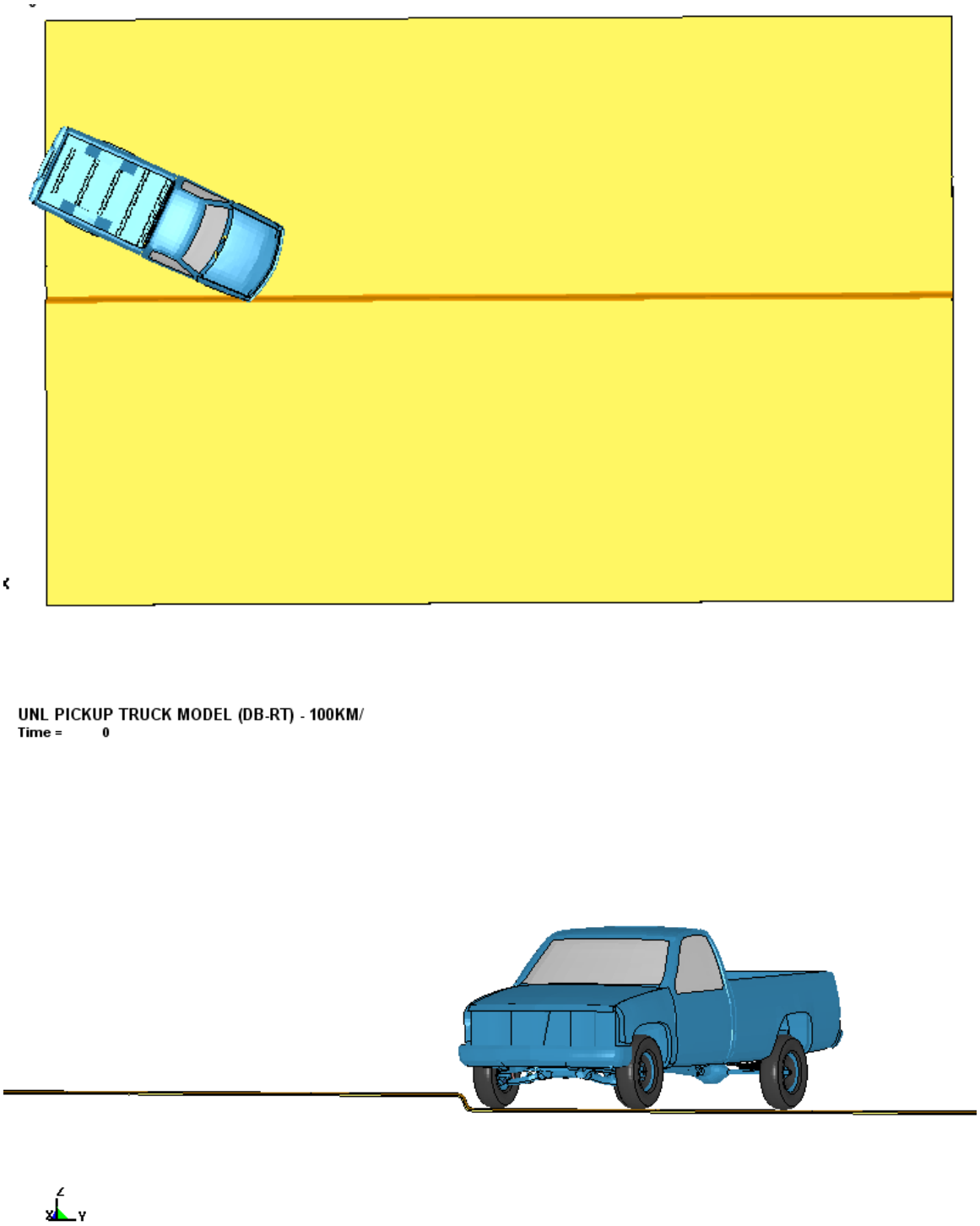

Figure 94. 2000P-Curb Impact LS-DYNA Model

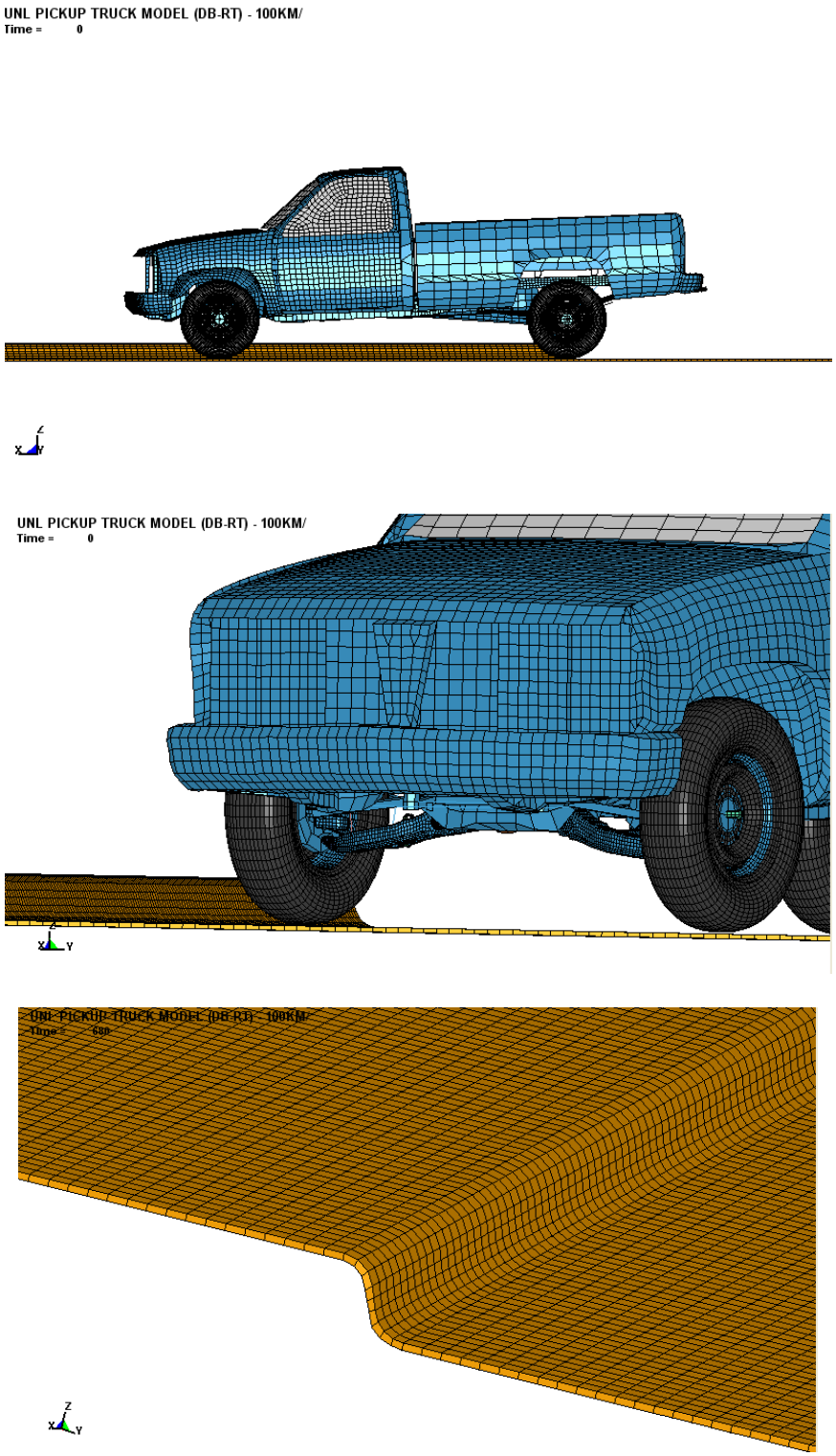

Figure 95. Curb and Ground LS-DYNA Model

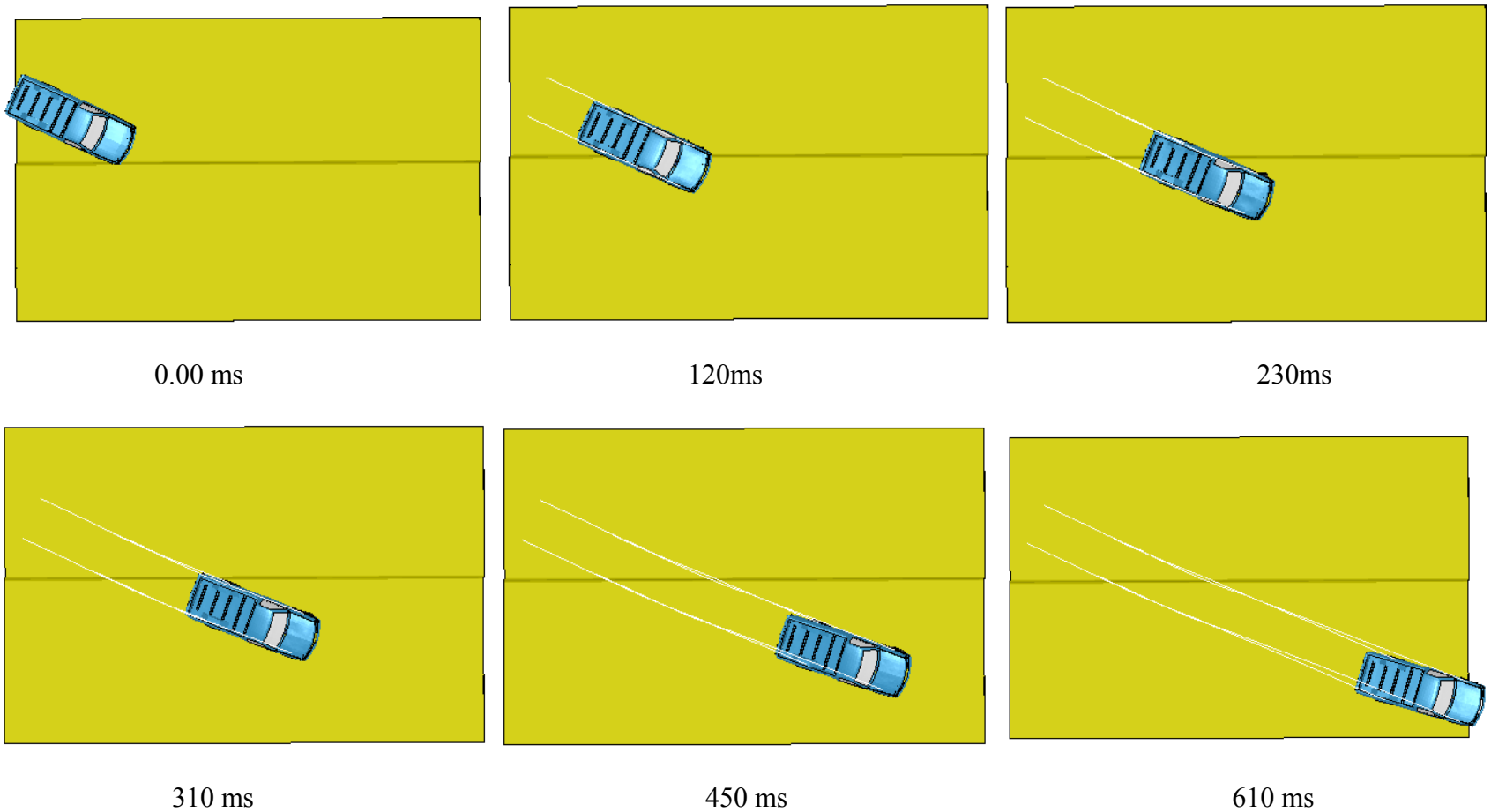

Figure 96. Overhead Sequential of 2000P-Curb Impact

9.3 Tire Performance Analysis

The tire model's accuracy was critical to the vehicle-curb impact simulation. The UNL-simplified tire model was used in the simulation (14). Vehicle tire model deformations upon impact presented an agreement with the physical test, as shown in Figure 97.

In the physical test, the vehicle's tires hit the curb in the order of right-front tire, right-rear tire, left-front tire, and left-rear tire. The right-rear tire and left-front tire impact the curb at almost the same time. The left-rear tire left the ground slightly in front of the curb, and later contacted it, as shown in the lower picture of Figure 98. In the simulation, only three tires impacted the curb, which were the right-front tire, right-rear tire, and left-front tire and were in the same order as the physical test. The right-rear tire and left-front tire impacted the curb almost at the same time as the physical test. The left-rear tire also became airborne in front of the curb, but the tire was too high to impact the curb, as shown in Figure 98.

The reason for the discrepancy may have to do with the tire rebound properties. The selected tire model was found to have less rebound performance during a separate tire-drop investigation. This might affect the vehicle's rebound after impact. Thus, the tire model needs further investigation and is left for future research.

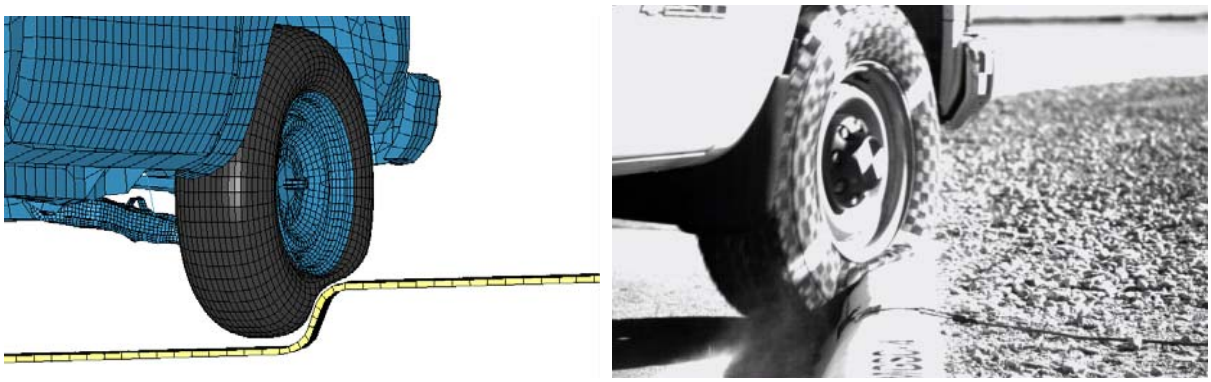

10 ms (right-front tire)

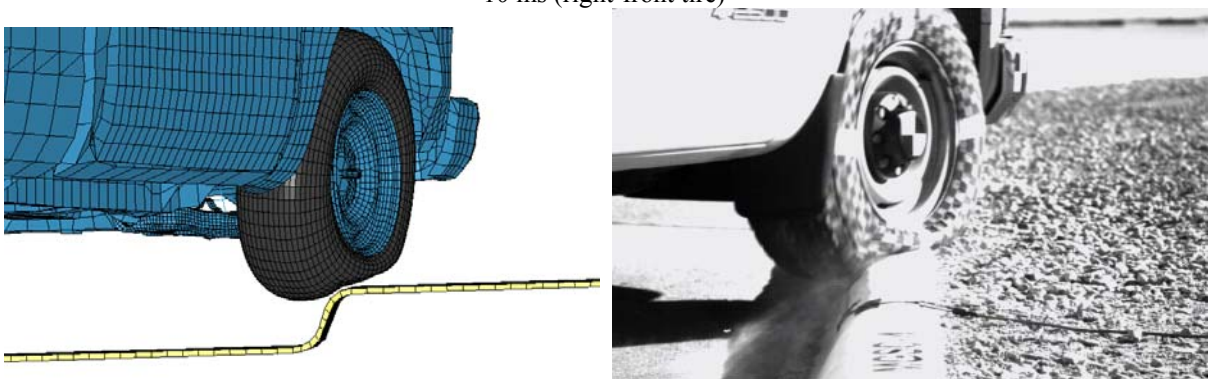

20 ms (rigit-front tire)

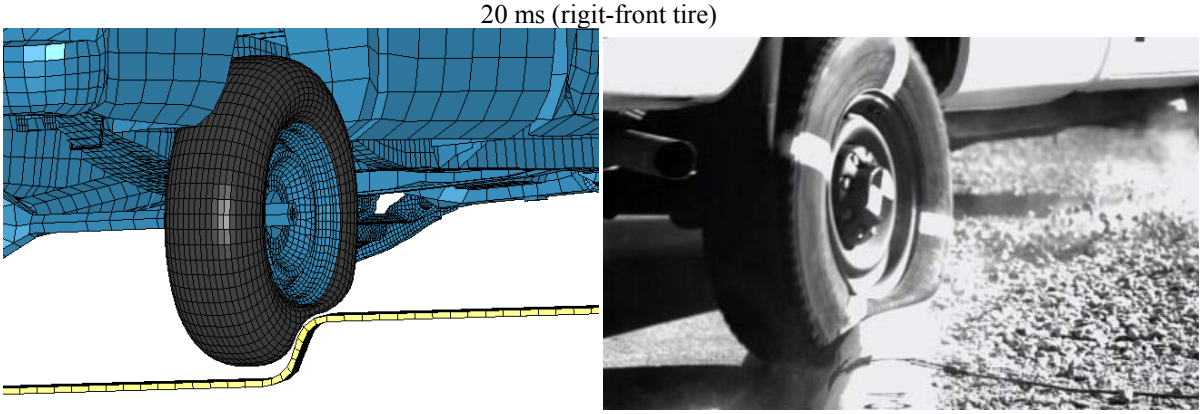

130 ms (right-rear tire)

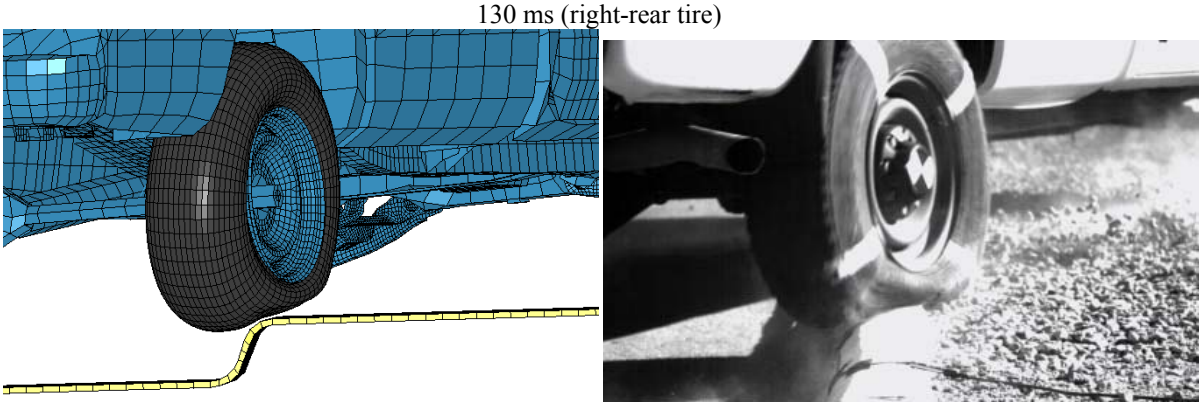

140 ms (right-rear tire)

Figure 97. Tire Deformation Comparison

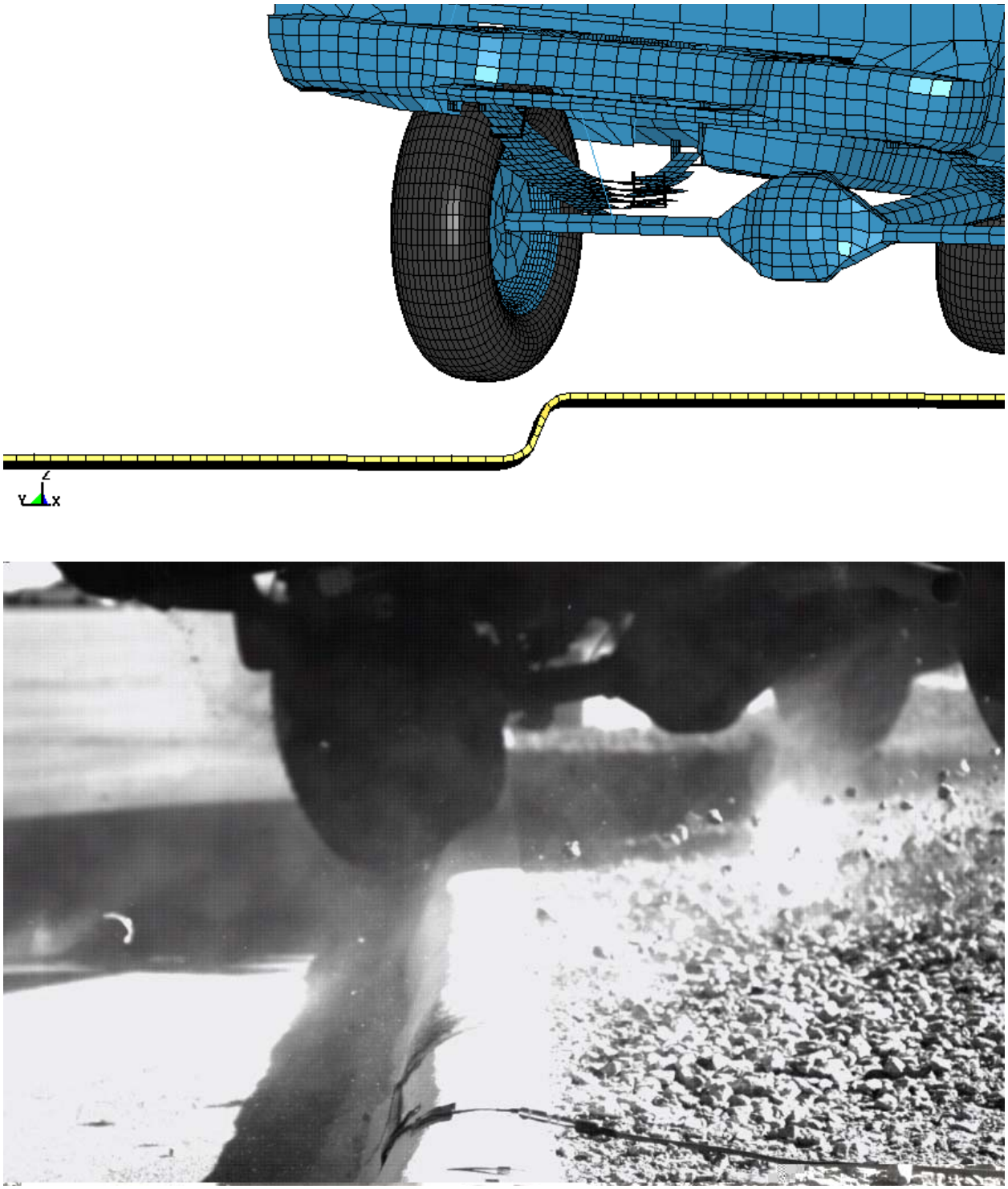

Figure 98. Left-Rear Tire Does Not Impact the Curb in the Simulation

9.4 Roll Movement Analysis

In the physical test, the pickup truck had a counter-clockwise roll motion due to the lift of the right-front tire, as shown before 150 ms in Figure 99. The curb impact of the left-front tire caused the vehicle to roll clockwise, which is shown as inflectional point "1" in Figure 99. The right-rear suspension was compressed due to the curb impact and started to rebound afterwards. The compression and the early stage of suspension rebound generated a resultant force to the vehicle, which rolled the vehicle counter-clockwise. This counter-clockwise roll motion counteracted the vehicle's clockwise roll movement and resulted in the relative flat portion, "2", as shown in Figure 99. Further, the curb impact of the left-rear tire, in combination with the later stage of rear suspension rebound, caused the vehicle to roll clockwise again, which made the roll curve become steeper between areas "2" and "3" in Figure 99.

For the simulation model, the roll movement curve was fairly straight after inflection point "1". No flat portion was observed in the simulation model, which implied that there was little counter-clockwise contribution from the right-rear suspension's compression and rebound. Actually, the right-rear suspension was also compressed and rebounded in the simulation model, which generated the counter-clockwise resultant force to the vehicle. However, the cargo box and the vehicle frame were twisted too much to transfer the counter-clockwise roll movement from the right-rear suspension to the cabin, where the C.G. was located. It was concluded from the roll motion comparison that the cargo box and frame models had less stiffness than the real-world pickup truck.

It was noticed that the front tires turned to the left upon impact in the simulation, which did not occur in the physical test, as shown in Figure 100. It implied that the joint stiffness in the

steering system needed future improvement. This tire rotation was not critical to the vehicle-curb analysis, but it did somewhat affect the vehicle's path after landing on the ground.

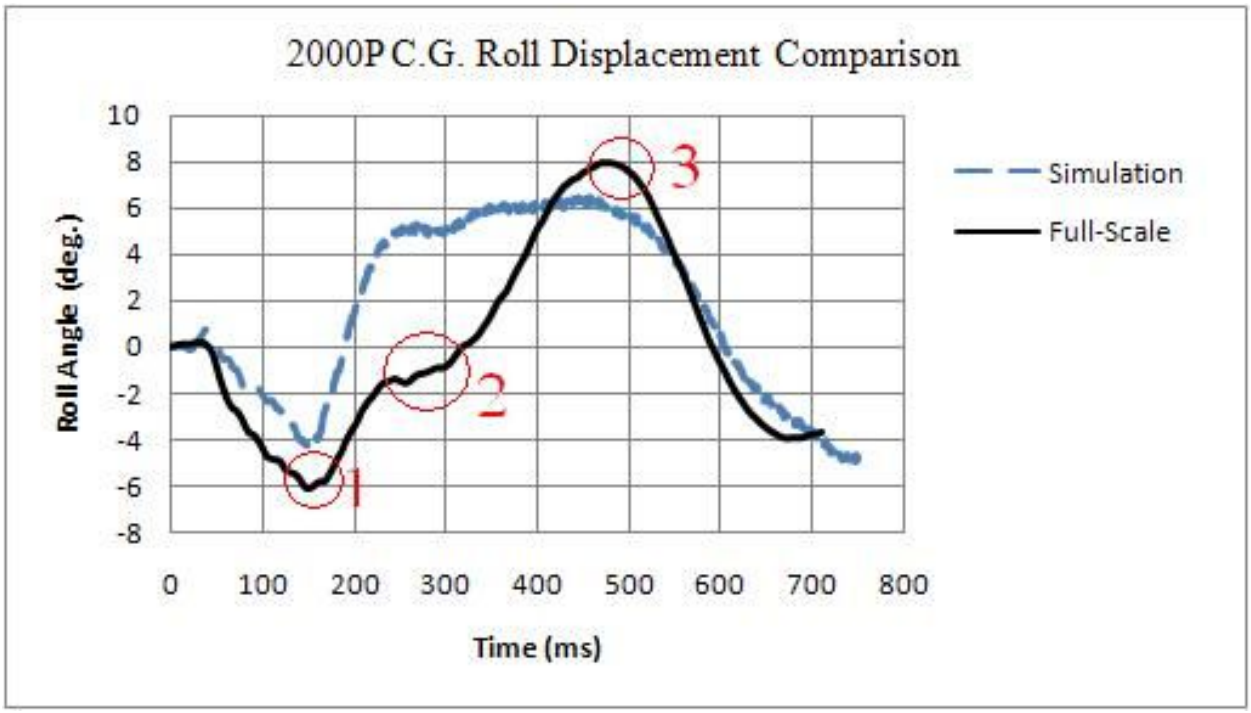

Figure 99. C.G. Roll Displacement Comparison

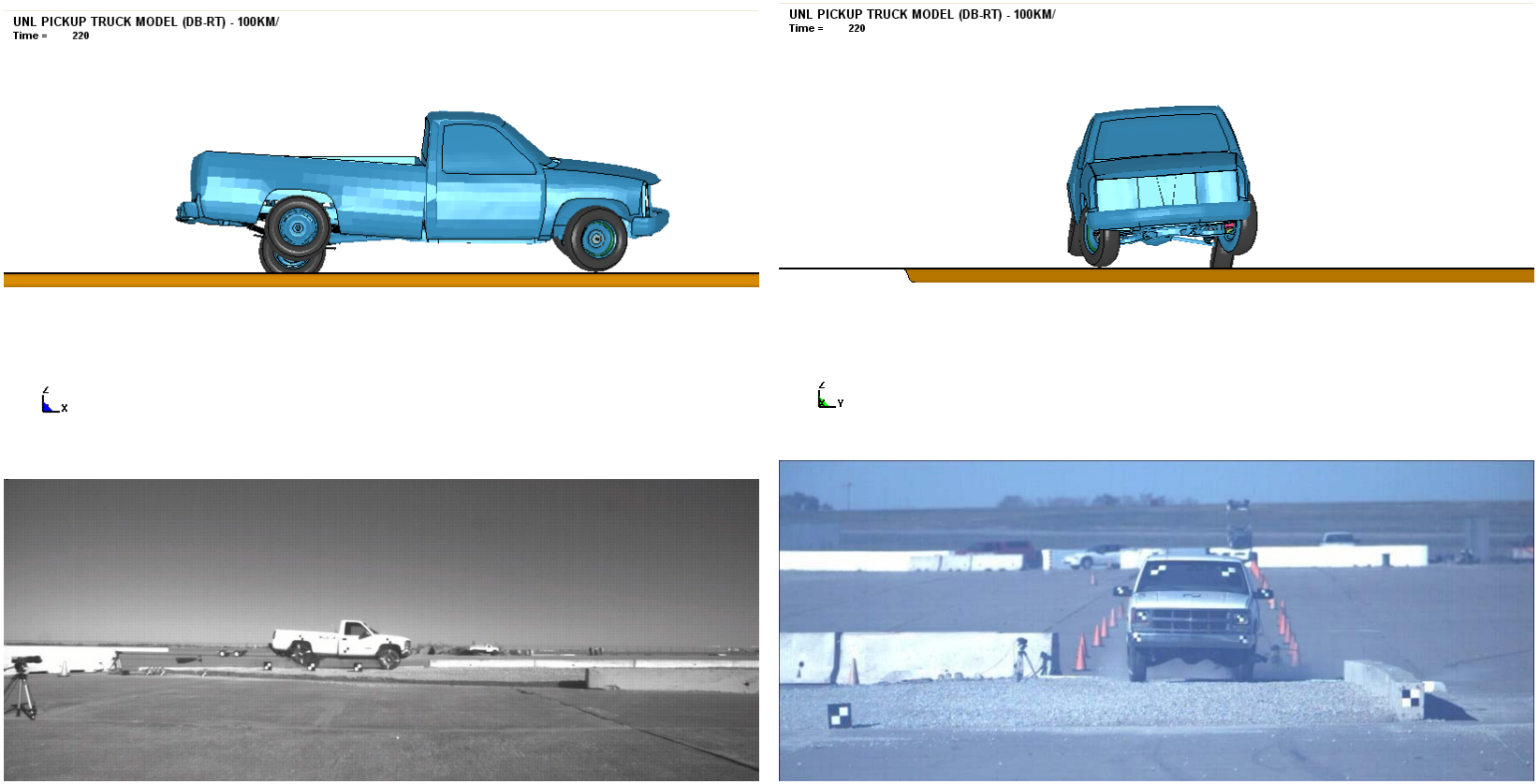

Time=220 ms

Figure 100. Cargo Box Presented Large Deformation in the Simulation

9.5 Pitch Movement Analysis

Both the simulation and physical test vehicles had a similar peak value for the pitch angle at about the same time, as shown in Figure 101. However, after reaching the peak value, the simulation result dramatically diverged from the physical test result. The pickup truck had a significant dive movement in the physical test, while the simulation was still fairly flat. This result was similar to the results observed during Plaxico's simulation effort (15).

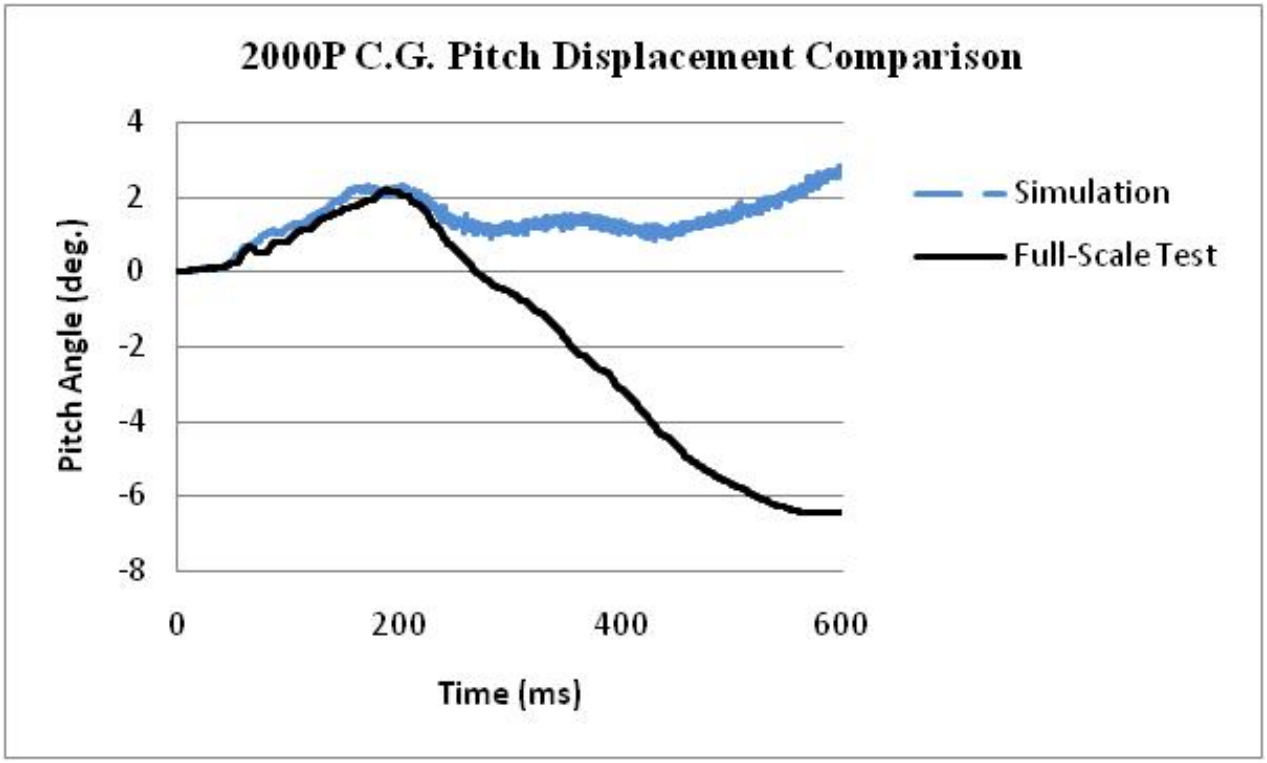

Figure 101. C.G. Pitch Movement Comparison

The vehicle's post-curb-impact attitude is compiled in Figures 102 and 103. The simulation agreed with the physical test at the early portion behind the curb, but it behaved quite differently later. There were multiple reasons that could cause the lower pitch-down movement in the model, such as inaccurate rear suspension and tire behaviors or inaccurate body-weight distribution over the vehicle.

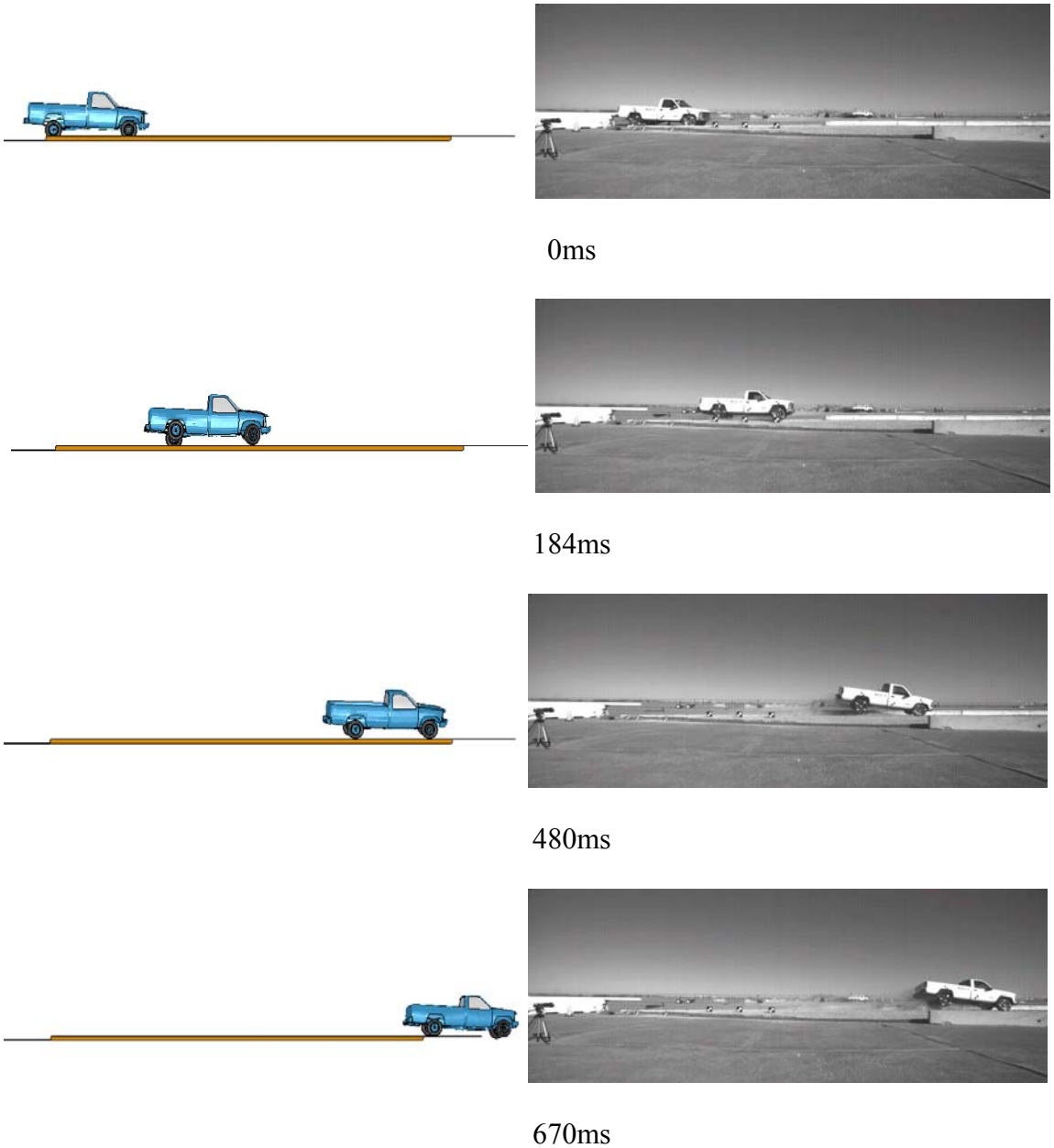

Figure 102. Vehicle Post-Curb-Impact Trajectory Comparison-Side View

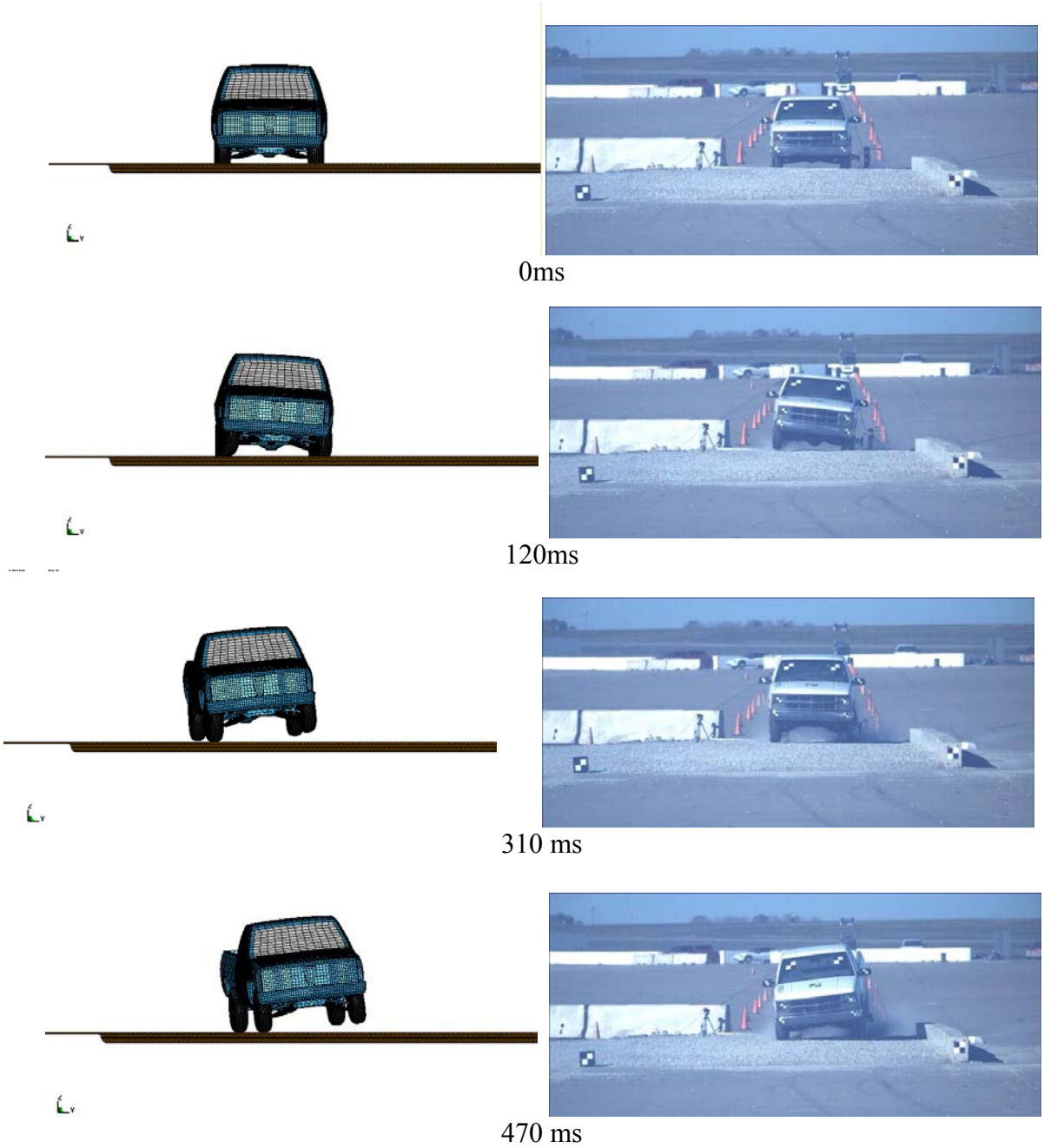

Figure 103. Vehicle Post-Curb-Impact Trajectory Comparison-Front View

The current rear suspension model was developed by T.J Paulson, and the suspension's loading force-deflection curve was proven to be accurate when compared with the physical test (16), but the rear suspension's unloading performance has not been tested yet. In real life, the

rear leaf suspension's unloading curve has a different path than its loading curve due to the friction between each layer of leaf springs. Considering that the rebound of the rear suspension affects the vehicle's pitch movement, future investigation is recommended to validate the rear suspension's unloading performance. Also, the damper's accuracy significantly affects vehicle-suspension rebound. The current damper is modeled with a simplified spring element. To capture the vehicle's behavior after curb impact, future efforts are needed to improve the current damper model.

Besides the rear suspension, the observed lower pitch movement was also likely caused by the inaccurate body-load distribution over the vehicle model. A simplified two-mass model was used as an analogy to analyze the vehicle's post-curb-impact pitch behavior, as shown in Figure 104. The front ball represented the vehicle's front sprung mass M1, and the rear ball represented the vehicle's rear unsprung mass M2. After curb impact, the front ball and the rear ball performed a parabolic movement. Each ball climbed up and started to drop after reaching the peak, but the rear ball always had a delay behind the front ball. Thus, the front ball was always higher than the rear ball before the peak value, and the rear ball was always higher than the front ball after the peak value. It was similar to the vehicle's pitch up before the peak and pitch down after the peak. The pitch angle was controlled by the relative weights of each ball. Usually, the more different M1 and M2 are, the larger the pitch angle will be. Thus, the simulation implied the rear mass M2 was too similar to the front mass M1, which made the pickup model have a smaller pitch-down angle than was observed in the physical test.

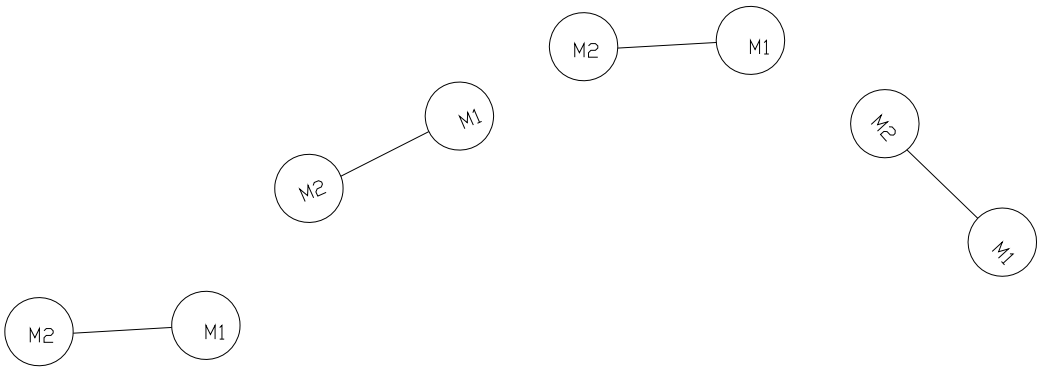

Figure 104. Illustration of Simplified Pitch Movement Model

9.6 Yaw Movement Analysis

Yaw movement was not critical to the MGS-Curb study. The pickup truck in the simulation yawed earlier than in the physical test, as shown in Figure 105. This means that the truck will strike the MGS at a higher impact angle in the simulation than in real life. This presents a worse impact scenario and gives a conservative estimation for MGS-Curb impact.

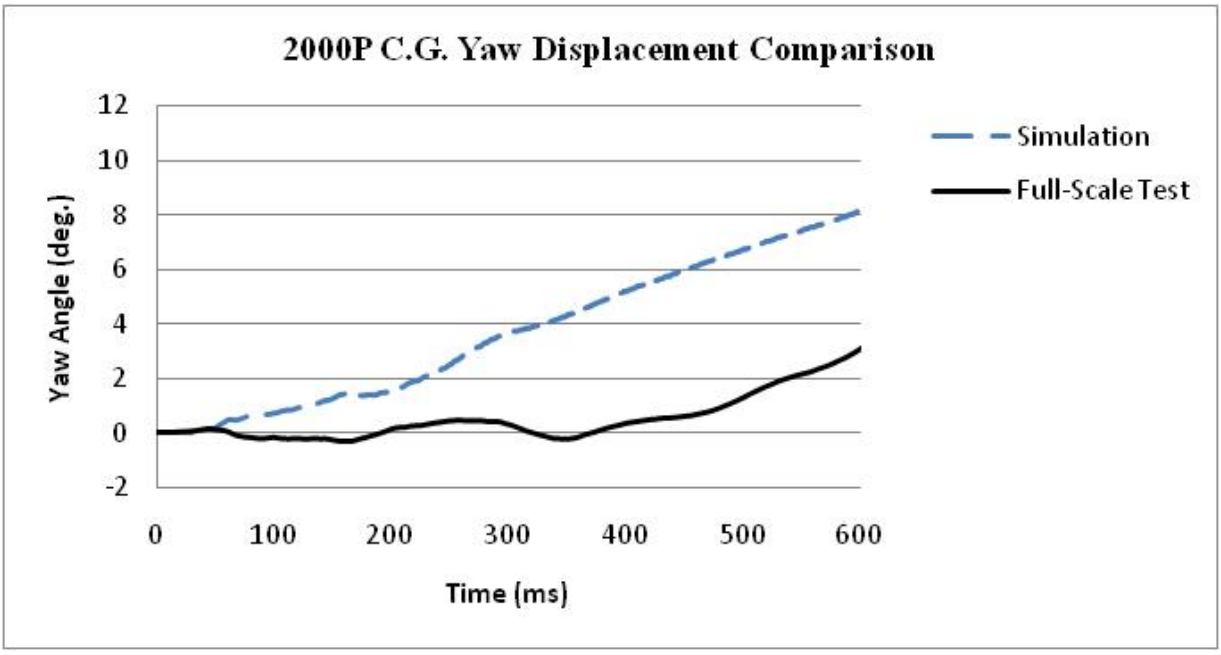

Figure 105. C.G. Yaw Displacement Comparison

9.7 Bumper Trajectory Analysis

As a critical component in the analysis of vehicle impacts MGS-Curb combinations, the pickup's bumper trajectory was tracked and plotted against the physical test data, as shown in Figures 106 and 107. Simulation results showed agreement with physical test data up until around 2.24 m (7.35 ft) behind the curb and reasonable agreement between 2.24 m (7.35 ft) and 3.95 m (13 ft). Thus, within 2.24 m (7.35 ft) behind the curb, the current UNL 2000P pickup model's bumper trajectory was fairly accurate and can be used to predict MGS-Curb combination performance.

9.8 Summary

Based on the comparison between vehicle-curb simulation and the physical test, it was shown that the truck model can accurately replicate the curb-impact tire deformation and accurately predict the bumper trajectory within a certain distance behind the curb.

However, it was also shown that the cargo box and frame models had less stiffness in the model than for real-world vehicles, which affects the vehicle's post-impact roll movement. Additionally, the truck model showed inaccurate post-impact pitch movement, which indicates the need for future investigation on the vehicle's rear suspension model.

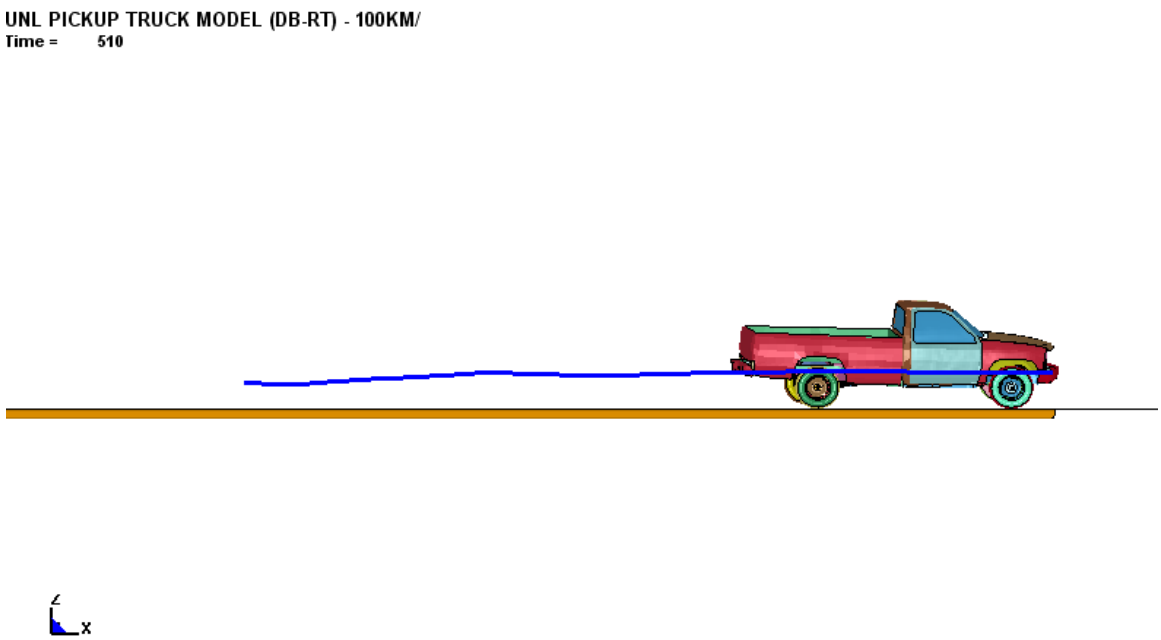

Figure 106. Pickup Model's Bumper Trajectory

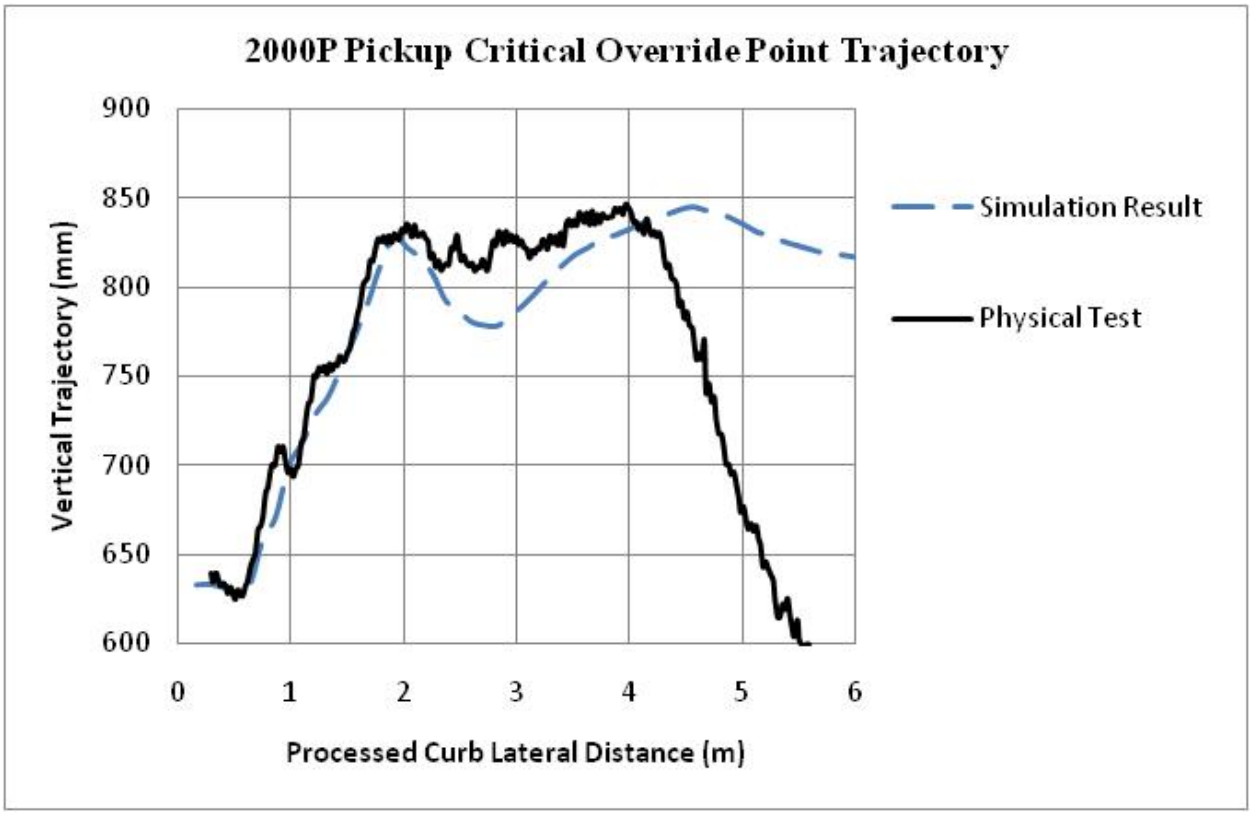

Figure 107. 2000P Pickup Bumper Trajectory Comparison

10 CRITICAL VEHICLE-MGS IMPACT POINT ANALYSIS

10.1 Introduction

The placement of curb in front of a W-beam guardrail affects the vehicle's attitude before its secondary impact with the guardrail. Previous research showed that pickup trucks might vault the guardrail and small passenger cars might underride the guardrail under certain conditions for curb-guardrail combinations.

10.2 Pickup-MGS Critical Override Impact Point

It is believed the pickup's bumper is the critical component during the override analysis, as it is usually the first part of the pickup that contacts the guardrail. Thus, to analyze the override impact, the bumper's trajectory is usually compared with the height of the W-beam guardrail. However, no previous research studies have defined the critical bumper to W-beam impact point that could result in the pickup truck vaulting. Furthermore, the vertical width of the 2000P's bumper is around 210 mm (8.27 in.), while the 2270P's vertical bumper width is around 290 mm (11.4 in.). The W-beam itself is around 311 mm (12.25 in.) wide. Thus, the obscurity of the critical-override-impact-point could result in substantial variance in the determination of MGS critical lateral offset. It is necessary to investigate the critical override impact point for pickup truck bumpers interacting with W beam guardrail.

10.2.1 Comparison of 2000P and 2270P Bumpers

The pickup-MGS critical impact point is defined as the highest impact point at which the W-beam rail can engage the pickup's bumper. The investigation began with reviewing previous full-scale pickup and W-beam guardrail crash tests. Because few available W-beam crash tests were performed with the 2270P vehicle, the estimation of the 2270P's critical override impact point had to be based on the 2000P crash tests.

First, a comparison of 2000P and 2270P bumpers was conducted. The 2270P bumper consists of 3 portions, including a bottom plastic portion, a middle metallic portion, and a top plastic portion, while the 2000P bumper only has one metallic portion, as shown in Figure 108. Physical tests proved both the bottom and top plastic portions were fairly weak and usually are easily damaged during impacts, as shown in Figure 109. Thus, only the middle metallic portion can actually function as a bumper and sustain resultant forces from the guardrail during impact. Comparison showed that the size of 2270P bumper's middle portion was similar to the 2000P bumper size (Table 3), which implied that the 2000P can be used as a reasonable reference to estimate 2270P's critical impact height.

Table 3. 2000P and 2270P Comparison (as shown in Figure 108)

	Bumper Bottom Edge Height (a)	**Bumper Top Edge Height (b)**	**C.G. Height**
2000P	451 mm (17.8 in.)	660 mm (26 in.)	667 mm (26.3 in.)
2270P	400 mm (15.7 in.)	635 mm (25 in.)	719 mm (28.3 in.)

Figure 108. Bumper Comparison – 2000P and 2270P

Figure 109. Only Middle Metallic Portion Actually Functions as a Bumper

10.2.2 Analysis of Previous Full-Scale Pickup W-Beam Tests

MwRSF has previously performed several W-beam guardrail and pickup truck crash tests, as shown in Table 4. Among those tests, tests NPG-2, MIW-1, and MIW-2 failed. Since the 2270P vehicle has a higher C.G. and is heavier than the 2000P, it is believed that if a guardrail failed to accommodate the 2000P, it would also fail with the 2270P.

The W-beam has two corrugations, which are the key components to engaging a vehicle during impact. The top corrugation centerline is 728 mm (28.7 in.) above the ground and the bottom is 534 mm (21 in.) above the ground, as shown in Figure 110. The positions of each pickup bumper and the W-beam corrugations in the previous full-scale tests are listed in Table 5 and are shown in Figures 111 through 117.

In all of the successful full-scale tests listed in Table 5, the top edge of the pickup's front bumper was always lower than the top corrugation of the W-beam rail, as shown in Figures 112 through 115. In all the unsuccessful full-scale tests, the top edge of the pickup's front bumper was at or above the W-beam's top corrugation height, as shown in Figures 111, 116, and 117. Thus, it was concluded from these full-scale tests that a conservative critical override impact height for the pickup truck and MGS guardrail would place the top edge of the bumper at the same height as the centerline of the W-beam's top corrugation, as shown in Figure 118. Normally, the centerline of the W-beam's top corrugation is 728 mm (28.7 in.) from the ground, as shown in Figure 110.

Table 4. Available Full Scale Tests of W-beam Guardrail and Pickup

Pickup Truck Types	MGS Guardrail Tests	Other W-Beam Guardrail Tests
2000P	NPG-3, NPG-4, NPG-5	MIW-1 (failed), MIW-2 (failed), 2214WB-1 (failed)
4 Wheel Drive	NPG-2 (failed)	NA
2270P	2214MG-2, 2214MG-1	2214WB-2

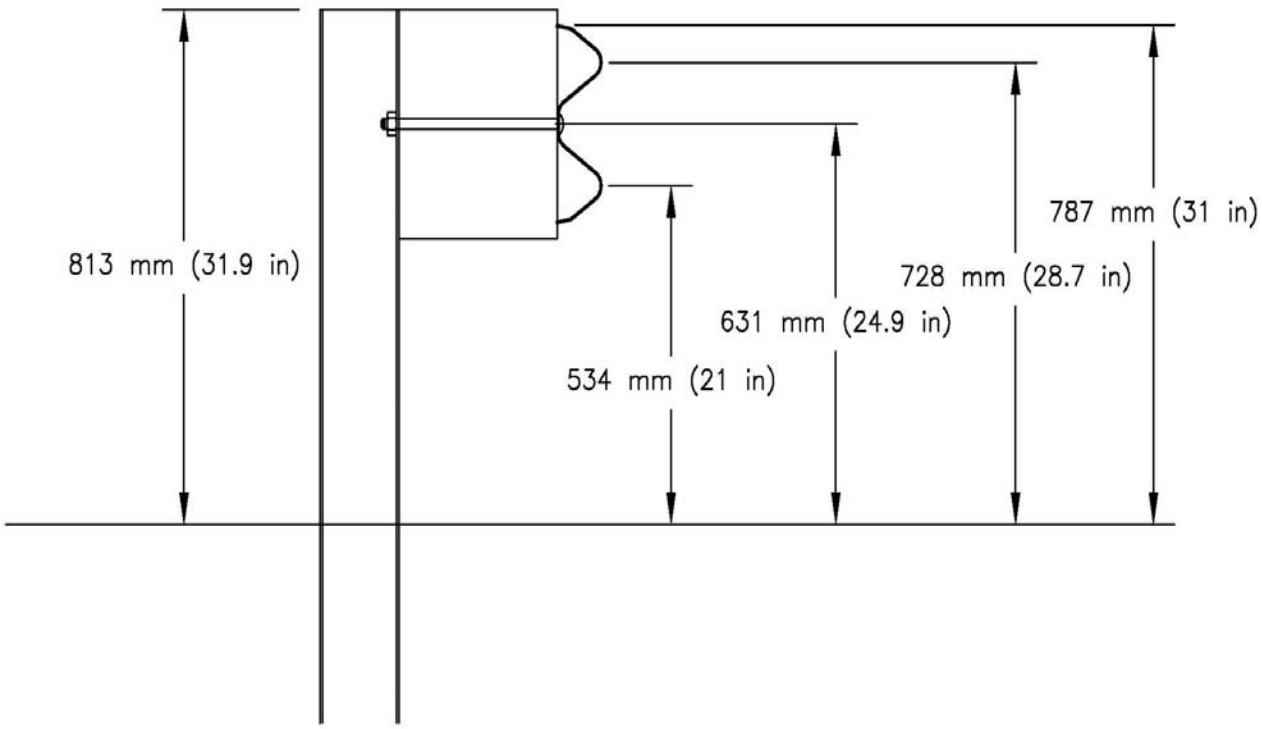

Figure 110. Geometric Dimension of Standard MGS Guardrail

Table 5. Height Comparison of Bumper Top Edge and W-beam Top Corrugation

Test No. (Pickup Model)	Top Edge of Front Bumper	Centerline of W-beam Top Corrugation	Test Result
NPG-2 (4X4 Drive)	781 mm (30.7 in.)	728 mm (28.7 in.)	Pickup rode over MGS and rolled over behind MGS
NPG-3 (2000P)	660 mm (26 in.)	728 mm (28.7 in.)	Passed
NPG-4 (2000P)	705 mm (27.8 in.)	728 mm (28.7 in.)	Passed
MIW-1 (2000P)	660 mm (26 in.)	608 mm (23.9 in.)	Pickup rolled over
MIW-2 (2000P)	660 mm (26 in.)	608 mm (23.9 in.)	Pick went airborne and landed on the guardrail
MG-1 (2000P)	635mm (25 in.)	728 mm (28.7 in.)	Passed
MG-2 (2270P)	635mm (25 in.)	728 mm (28.7 in.)	Passed

Figure 111. NPG-2 Bumper Impact Height

Figure 112. NPG-3 Bumper Impact Height

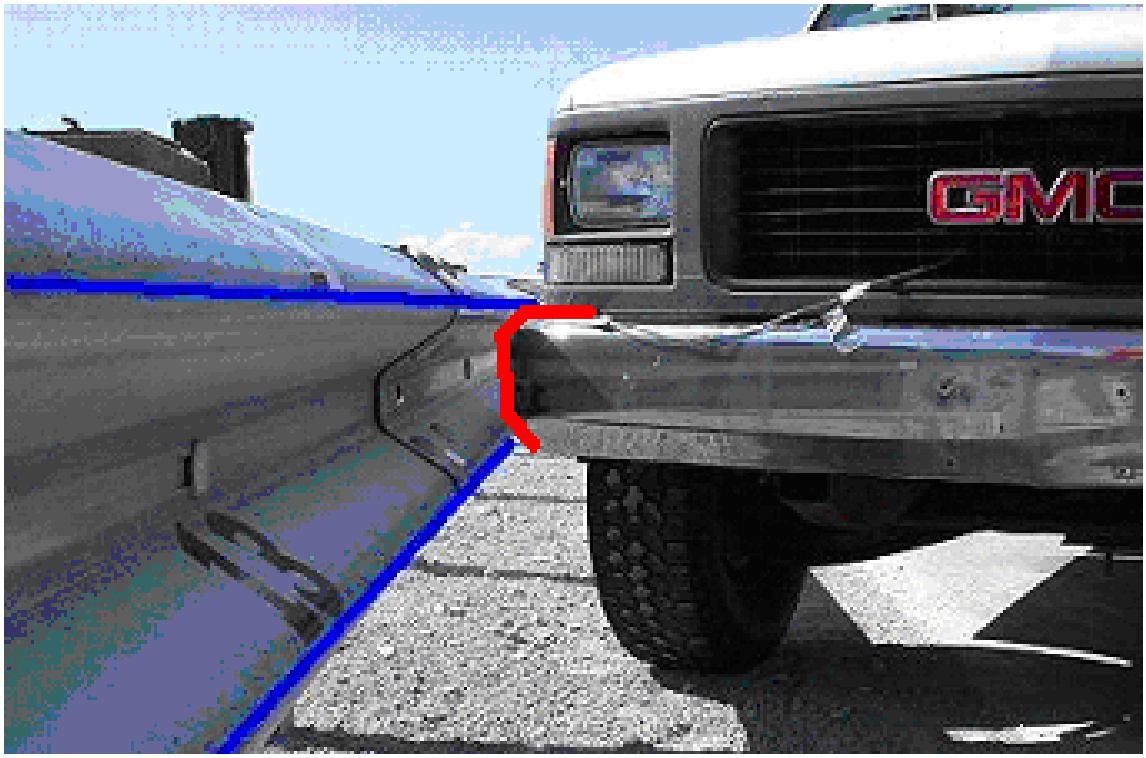

Figure 113. NPG-4 Bumper Impact Height

Figure 114. 2214MG-1 Bumper Impact Height

Figure 115. 2214MG-2 Bumper Impact Height

Figure 116. MIW-1 Bumper Impact Height

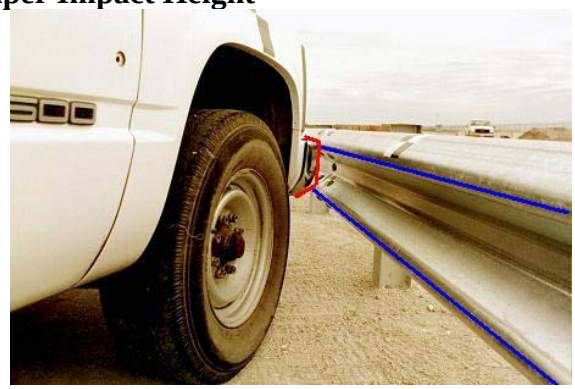

Figure 117. MIW-2 Bumper Impact Height

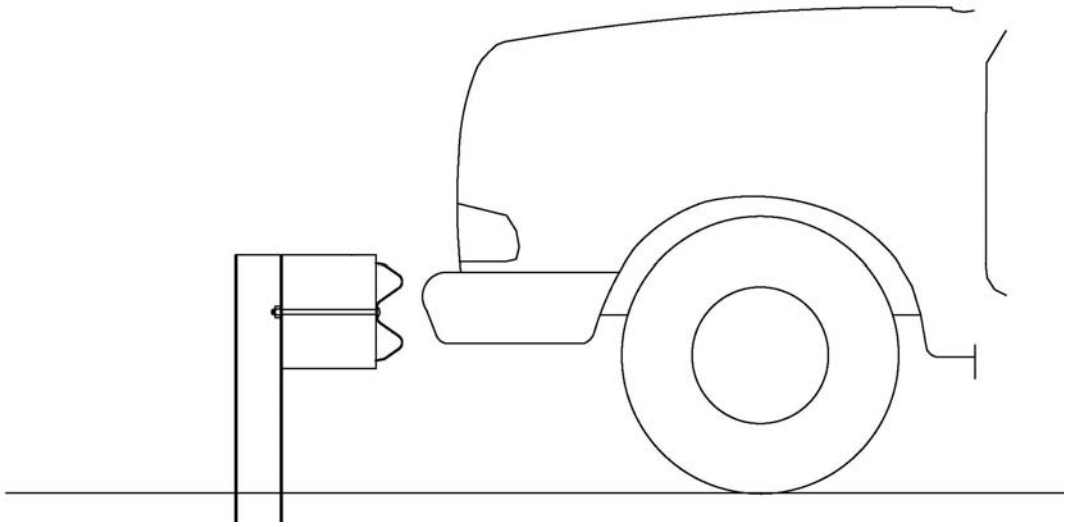

Figure 118. Pickup-MGS Critical Override Impact Height

10.2.3 Analysis of Pickup and W-beam Critical Impact Height

The external forces applied on a bumper during a guardrail impact are illustrated in Figure 119. When the bumper first contacts the guardrail, the force (P1) between the guardrail and the bumper is in the lateral direction; this is the force that redirects the vehicle. The guardrail post is then pushed backward and rotated due to this force, as shown in Figure 120. The post rotation causes the W-beam rail to rise up and generates an resultant force (P2) to the vehicle. The force P2 lifts the vehicle and causes the vehicle to potentially vault over the guardrail. To prevent the vehicle from vaulting the guardrail, there has to be an opposing force P3 that provides downward resistance and allows for vehicle capture using vehicle-rail interlock. The force P3 can be obtained only if the pickup is engaged by the W beam. This can be accomplished if the bumper is below the W-beam's corrugation, as shown in Figure 118. Otherwise, the pickup's bumper would slip over the W-beam and possibly result in vehicle override. This conclusion is identical to the previous analysis of the full-scale tests. Furthermore, by reviewing the previous full-scale tests, it was noticed that failed test bumpers were mostly deformed on the

bottom and the front faces, which demonstrates that the forces were applied from the bottom and the front during impact, as shown in Figure 121. Additionally, in all the successful tests, bumpers were deformed on the top and the front faces, as shown in Figure 122.

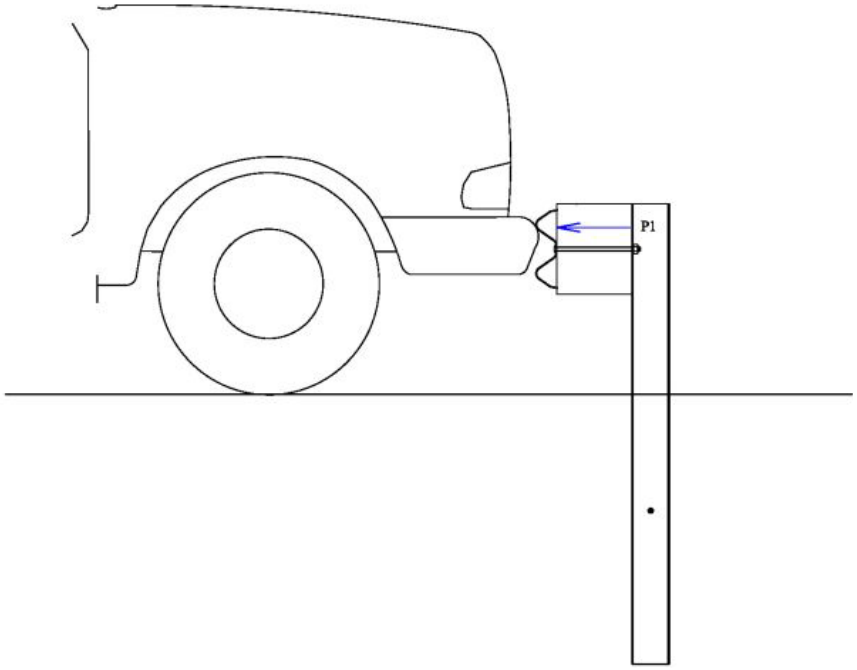

Figure 119. Illustration of Pre-Impact Condition

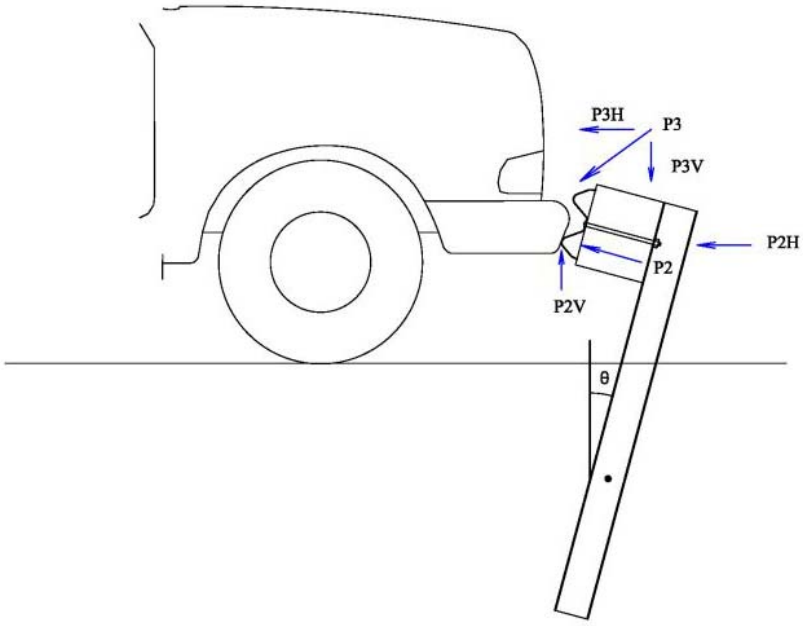

Figure 120. Schematic of Guardrail Rotation during Impact

Figure 121. Bumper Deformation in Test MIW-1 (Failed)

Figure 122. Bumper Deformation in Test NPG-4 (Passed)

10.2.4 LS-DYNA Simulation Verification

LS-DYNA simulations were conducted to verify the critical override impact height of the pickup truck and MGS guardrail. A 2000P pickup truck impacted the MGS guardrail system at an impact speed of 100 km/h (62.1 mph) and at an impact angle of 25 degrees. Two different heights were investigated. First, the top edge of the pickup's bumper top edge was flush with the centerline of the W-beam rail's top corrugation, as shown in the left picture of Figure 123. For this situation, the simulation results showed that the pickup truck was engaged by the MGS and was smoothly redirected. Second, the vehicle was lifted until the top edge of the bumper's vertical surface was aligned with the centerline of the W-beam's top corrugation, as shown in the right picture of Figure 123. In this situation, the simulation results showed that the pickup truck vaulted the MGS guardrail.

From the analysis of the pickup truck impact into the MGS at a 25-degree angle, the critical override impact height of the Chevrolet C2500 ¾ ton pickup truck (2000P) was determined to be the top of the bumper's corner on the impact side, as shown in Figure 124. The critical override impact height of the ½-ton Dodge Ram 1500 Quad Cab pickup truck (2270P) was determined to be the top of the bumper's metal corner on the impact side, as shown in Figure 124. The conclusions are identical to those obtained from both full-scale crash tests (test nos. MGSC-1 and MGSC-2).

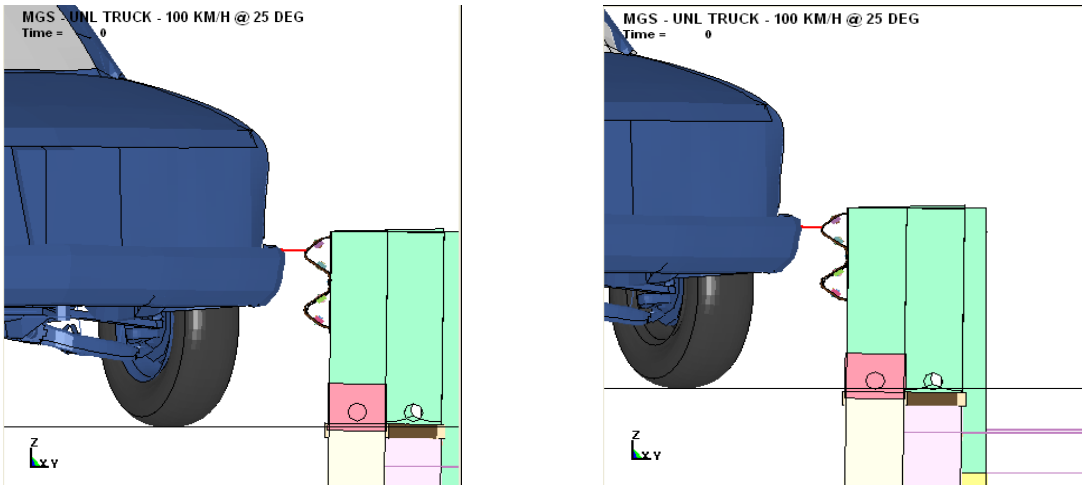

Captured **Vaulted**

Figure 123. LS-DYNA Simulation of the Pickup-MGS Critical Override Impact Point

2000P **2270P**

Figure 124. Pickup-W-beam Guardrail Override Critical Impact Point, 2000P and 2270P

10.3 Discussion

The critical impact height for the pickup and MGS guardrail is the lowest height that can prevent the pickup from overriding the guardrail. Based on the investigation of previous full-scale pickup and W-beam guardrail crash tests, analytical analysis, and LS-DYNA simulation, it is believed that the critical override impact event happens when the top edge of the pickup truck's bumper is flush with the centerline of the top corrugation of the W-beam rail.

However, there is at least one case in which the guardrail can still capture the vehicle without capturing the bumper. In 2006, MwRSF performed a full-scale crash test of the MGS with an approach slope (Test MGSAS-1) (17). A 2000P pickup truck impacted the MGS system on an 8:1 approach slope at a speed of 100.4 km/h (62.4 mph) and at an angle of 25 degrees. The pickup's front bumper slid over the W-beam's top corrugation upon impact, but the pickup was still captured by the guardrail. Normally, the vehicle's front suspension is compressed due to gravity on the flat ground. However in this case, the pickup's front suspension was extended because of the slope. Therefore, the clearance between the top of the right-front tire and the bottom of the bumper was increased, as shown in Figure 125. Although the bumper went above the W-beam, the W-beam rail was trapped between the bumper and the tire, and it captured the vehicle, as shown in Figure 126. This result also explained why the tire was ripped off during the crash, as shown in Figure 127. This result is very similar to the case when the pickup's front suspension was extended after curb impact. Although, under some situations, the vehicle can be contained without engaging the bumper, the bumper height was used to assist the pickup-MGS impact analysis as a conservative consideration.

Figure 125. Vehicle's Front Suspension Extended Due to the Slope

Figure 126. W-beam Rail Trapped Between the Front Wheel and the Bumper

Figure 127. Vehicle's Front Wheel Damage

10.4 Small Car-MGS Critical Impact Point

The critical impact height for the small passenger car and MGS guardrail is the highest point that can prevent the small passenger car from underriding the guardrail. Due to the insufficient crash samples and the complexity of small car and W beam interaction, it is difficult to determine a specific critical impact point for the small passenger car. However, in 2004, MwRSF performed a small passenger car and MGS crash test (Test No. 2214MG-3), which proved the MGS system can contain and redirect the Kia Rio sedan (1100C) at an impact speed of 97.8 km (60.8 mph) and at an impact angle of 25.4 degrees on flat ground (18). Thus, test 2214MG-3 was used as a reference to evaluate the small car and MGS critical impact. To be consistent with the pickup-MGS analysis, the top-front corner of the Kia Rio's bumper was also chosen for critical underride impact analysis.

In the 2214MG-3, the centerline of the bottom corrugation of the W-beam rail was 560 mm (22 in.) above the ground, which was 89 mm (3.5 in.) higher than the small passenger car front bumper corner, as shown in Figure 128. Since the 2214MG-3 system safely redirected the small passenger car, a small car-MGS impact condition is deemed safe as long as the bumper corner is less than 89 mm (3.5 in.) below the bottom corrugation centerline of W-beam; otherwise, there might be a possibility for the small car to underride the MGS.

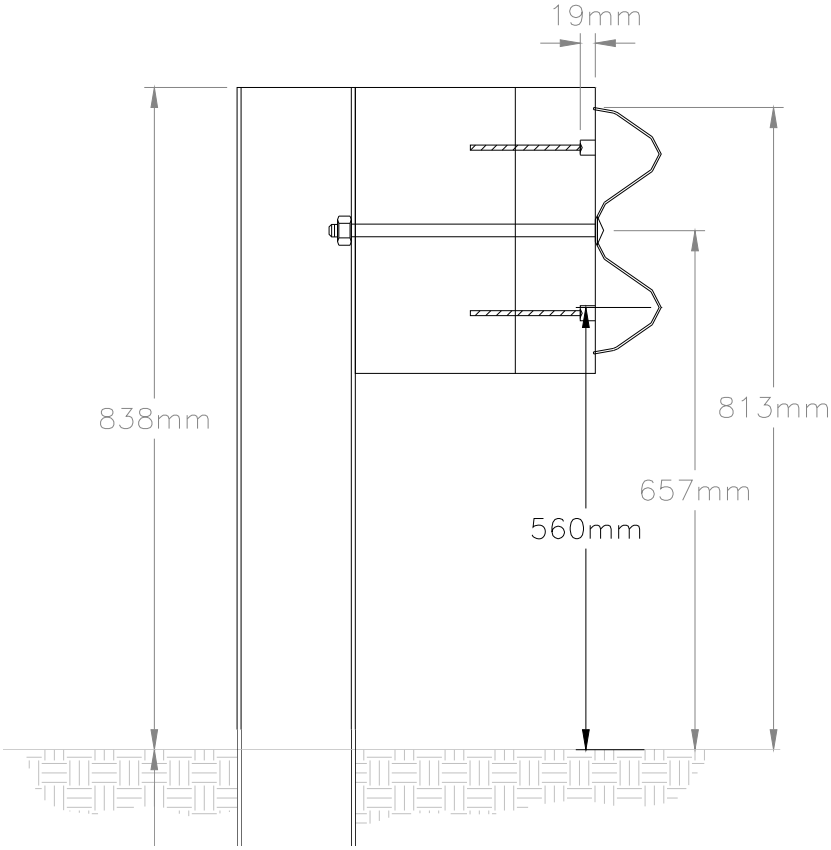

Figure 128. Small Passenger Car and MGS Impact, Test 2214MG-3

11 DETERMINATION OF MGS CRITICAL OFFSET BEHIND CURB

11.1 Introduction

Based on the analysis in Chapter 10, the impact corner of the bumper's top edge was determined to be the critical impact point during vehicle-MGS interaction. An MGS installation was deemed to provide acceptable performance during impacts when the top corrugation of the W-beam rail was positioned above the pickup's top edge of the bumper, and its bottom corrugation was at most 89 mm (3.5 in.) above the top edge of the small car bumper. Thus, the critical override/underride offset for placing the MGS behind the curb was determined by comparing the trajectories of the critical bumper impact points against the MGS top/bottom corrugation heights. However, no target was placed on the critical bumper impact points in the physical tests. Thus, the trajectory of the critical bumper impact points had to be transformed from the existing target trajectories.

11.2 Trajectory of Critical Bumper Impact Point

Based on an existing bumper target trajectory, a critical bumper impact point trajectory was transformed by coupling the bumper target trajectory with a vehicle's pitch motion from the rate transducer. All of the transformations were performed in the PLD coordinate system. Then, each PLD data set was converted into the CLD coordinate system to show the lateral offset distance behind the curb. The side view of a vehicle bumper is shown in Figure 129. The trajectory of the target center was tracked as a part of the high-speed video analysis. With the distance between the target center and the bumper corner (d), the initial angle with respect to the horizontal (α), and the pitch angle (Θ_p), the trajectory of the critical bumper impact point could be obtained from the target trajectory using Equations 11-1 and 11-2 and Table 6.

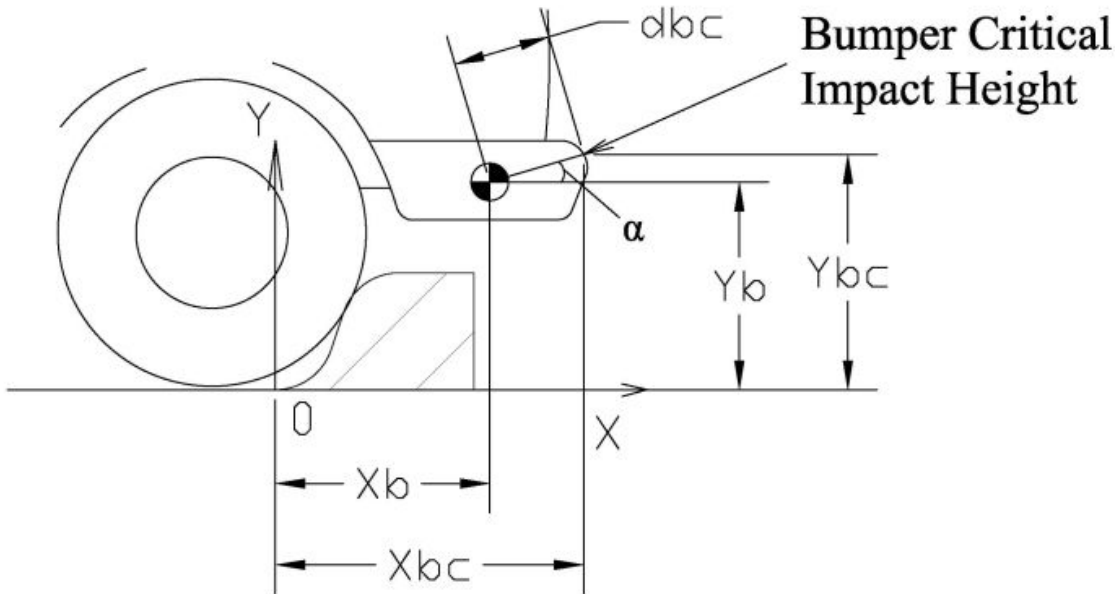

Figure 129. Illustration of the Transformation of the Bumper Critical Impact Point Trajectory from the Bumper Target Trajectory

$$X_{bc} = X_b + d * \cos(\alpha + \Theta_p) \quad \text{Eq. 11-1}$$
$$Y_{bc} = Y_b + d * \sin(\alpha + \Theta_p) \quad \text{Eq. 11-2}$$

X_{bc}= X coordinate of Bumper critical point
Y_{bc}= Y coordinate of Bumper critical point
X_b = X coordinate of Bumper target center
Y_b = Y coordinate of Bumper target center
d_{bc} = Distance between bumper critical point and bumper target center
α = Initial angle between the critical impact point and the Bumper target center
Θ_p = Pitch Angle

Table 6. Summary of Parameters for Bumper Critical Point Trajectory Transition

Test No.	MGSC-1	MGSC-2	MGSC-3	MGSC-4
α (degrees)	14.04		10.30	12.41
d_{bc}	288 mm (11.34 in.)		284 mm (11.18 in.)	325 mm (12.8 in.)

To ensure the reliability of the critical impact point trajectory transformation, the trajectory of a critical bumper impact point was also transformed from the C.G. target trajectory as a double check; details are provided in Appendix D.

11.3 MGS Critical Offset Behind Curb

After the transformation, the trajectories of each pickup's critical bumper impact point were plotted against the centerline height of the MGS's top W-beam corrugation in the CLD coordinate system. When used in conjunction with a curb, the MGS could have two possible installation options. The first option (Option I) has the normal 787 mm (31 in.) height relative to the roadway, while the other option (Option II) has the normal 787 mm (31 in.) height relative to the ground behind the curb, which is 152 mm (6 in.) higher than Option I. Therefore, both MGS installation options are plotted, as shown in Figures 130 and 131. English-unit details are provided in Appendix E.

For the Option I installation, the 2000P bumper's critical impact point was above the W-beam's top corrugation between 1.14 m (3.71 ft) and 4.75 m (15.6 ft) behind the curb. The 2270P bumper's critical impact point was above the top corrugation centerline beyond 1.29 m (4.23 ft) behind the curb in test MGSC-1, while the 2270P bumper's critical impact point was above the top corrugation centerline beyond 1.13 m (3.71 ft) behind the curb in test MGSC-2, as shown in Figure 130. The 1100C bumper's critical impact point was above the safe height all the way after curb impact, which meant the small passenger car will not underride the normal height MGS system behind a 152-mm (6-in.) AASHTO Type B curb, as shown in Figure 131.

For the Option II installation, the 2000P bumper's critical impact point is always below the W-beam's top corrugation after the impact with curb. The 2270P bumper's critical impact point was above the top corrugation centerline between 2.53 m (8.3 ft) and 5.03 m (16.5 ft) behind the curb in test MGSC-1 and beyond 1.87 m (6.11 ft) behind the curb in test MGSC-2, as shown in Figure 130. The 1100C bumper's critical impact point was below the safe height before 0.98 m (3.14 ft) and beyond 4.6 m (15.1 ft), as shown in Figure 131.

The safe lateral MGS offset for each vehicle type is summarized in Figures 132 and 133. To prevent bumper overriding and underriding when using MGS W-beam rail with Option I installation, the MGS should be installed either less than 1.13 m (3.71 ft) or greater than 4.93 m (16.2 ft) behind the curb. Similarly, the MGS with Option II installation should to be installed either between 0.98 m (3.14 ft) and 1.81 m (5.94 ft) or greater than 4.91 m (16.1 ft) behind the curb.

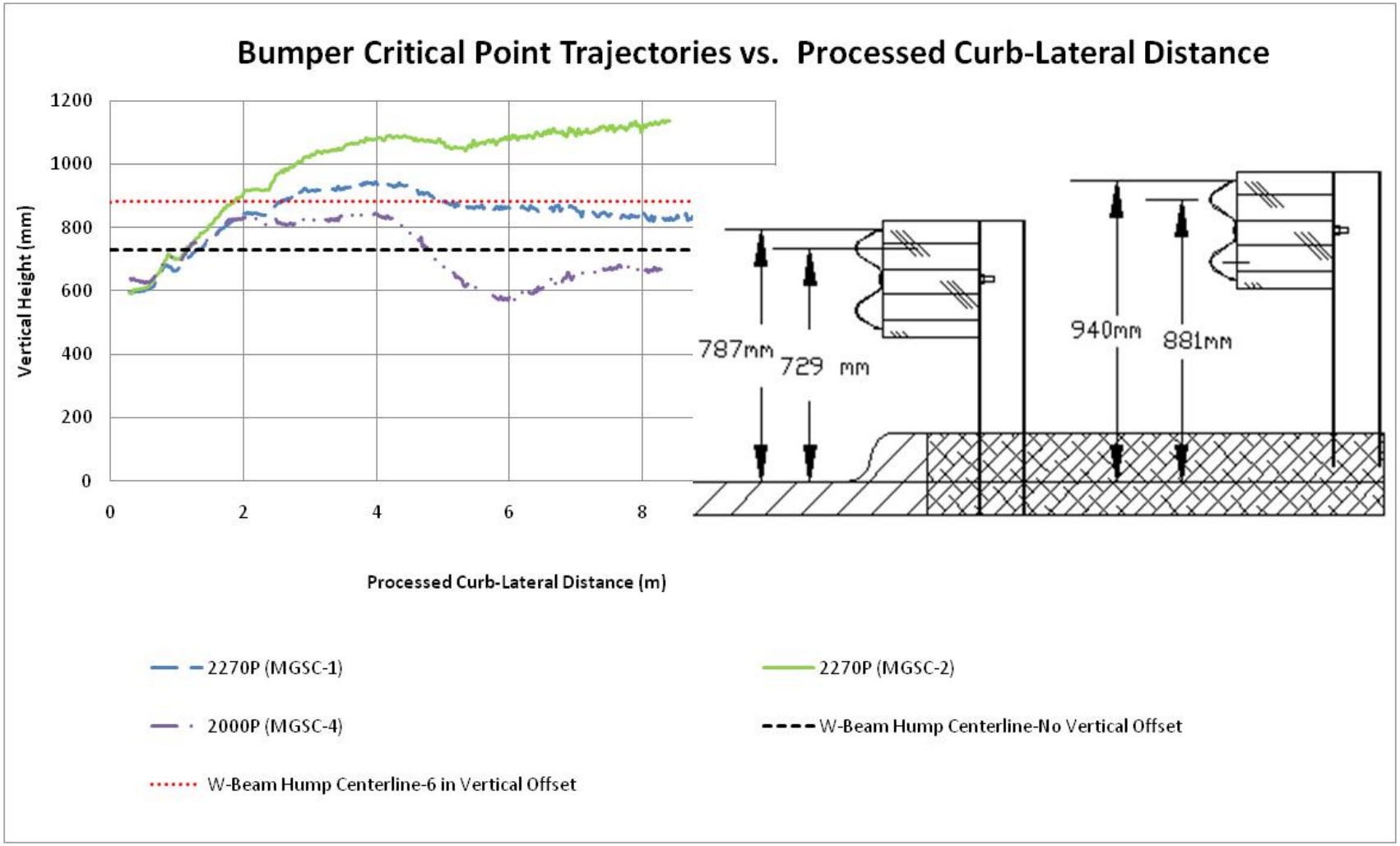

Figure 130. Pickup Bumper Critical Override Impact Point Trajectories

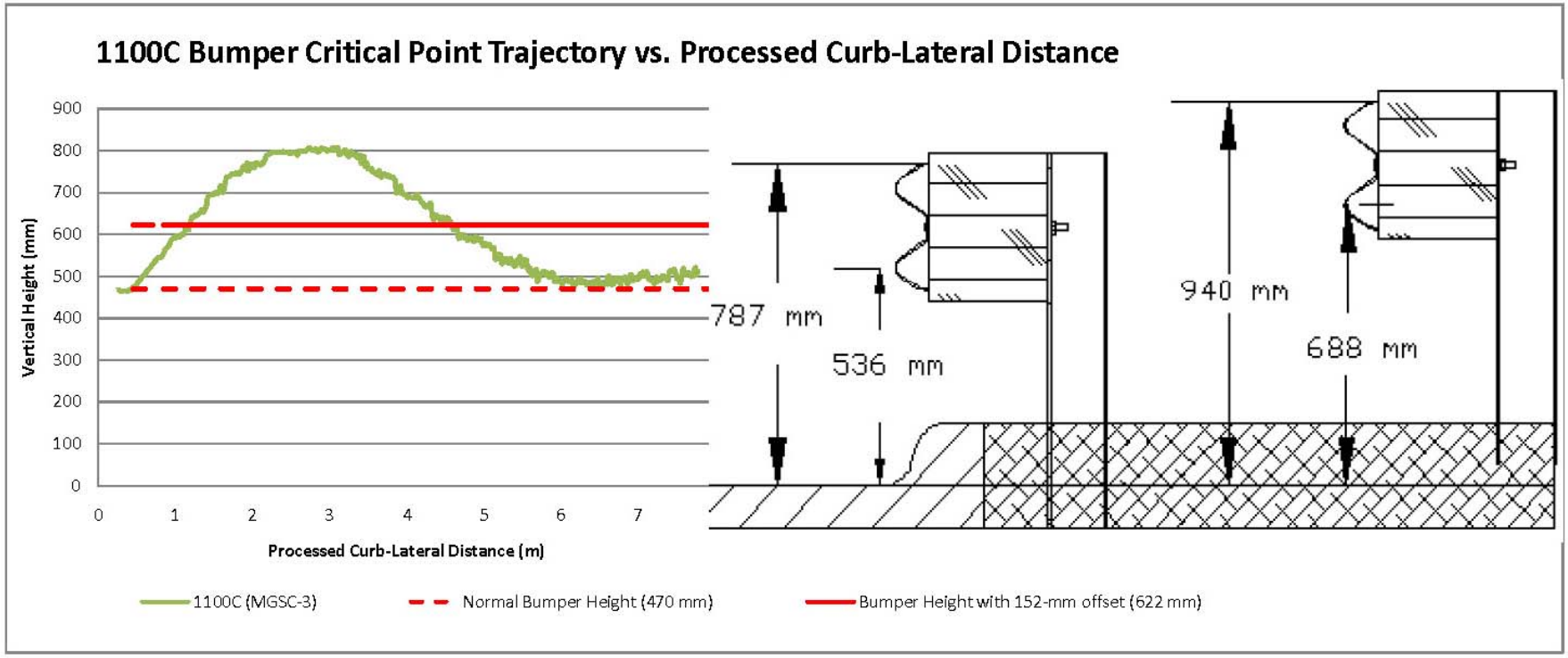

Figure 131. Small Passenger Car Critical Underride Impact Point Trajectory

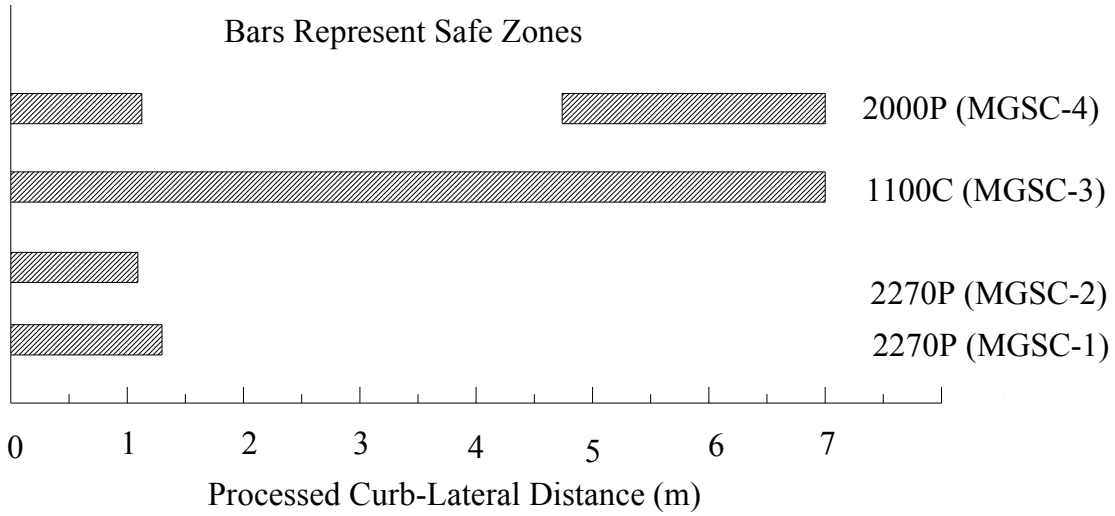

Figure 132. Safe Zone Illustration for MGS Option I Installation behind Curb

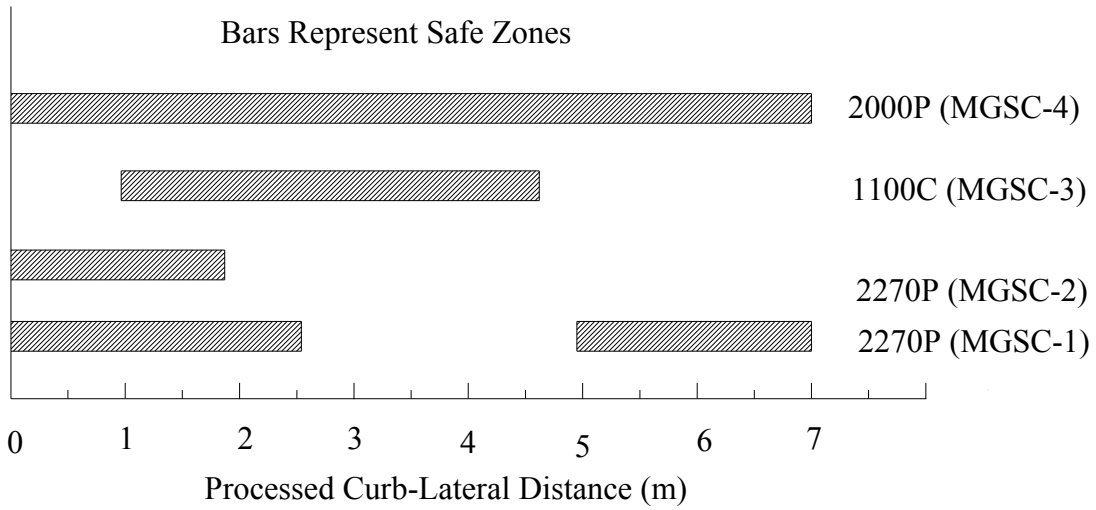

Figure 133. Safe Zone Illustration for MGS Option II Installation behind Curb

12 MGS-CURB COMBINATION LS-DYNA SIMULATION

To investigate the critical lateral offset distance for MGS placement behind AASHTO Type B curb, a series of LS-DYNA MGS-Curb-vehicle crash simulations were performed. The baseline model was setup using the previous vehicle-curb model with an added MGS model placed behind the curb. Based on the previous vehicle-curb simulation result and to ensure the reliability of the MGS-Curb model, the MGS offset distance investigation was only conducted within the range of 0.0 m (0.0 ft) to 2.24 m (7.35 ft) behind the curb.

A 2000P pickup truck impacted the MGS-Curb combination system at an impact speed of 100 km/h (62.1 mph) and an impact angle of 25 degrees, as shown in Figure 134. The curb was a 152-mm (6-in.) AASHTO Type B curb. The MGS was mounted at the normal height with the top of the W-beam rail being 787 mm (31 in.) above the ground relative to the roadway, as shown in Figure 130.

First, the test location was selected at 1.22 m (4 ft) where the 2270P's bumper trajectory was below the top corrugation of the W-beam rail, while the 2000P's bumper trajectory was above it, as shown in Figure 130. According to the previous bumper trajectory analysis, the 2000P pickup truck has the potential to vault over the MGS guardrail at this distance. If this conclusion is confirmed by the simulation, the next point is to be selected at 1.1 m (3.61 ft) where the 2000P's bumper trajectory was slightly below the W-beam top corrugation height. If this location fails, more simulations are to be conducted to locate the critical point that can safely contain the vehicle. The simulation test procedure is shown in Figure 135.

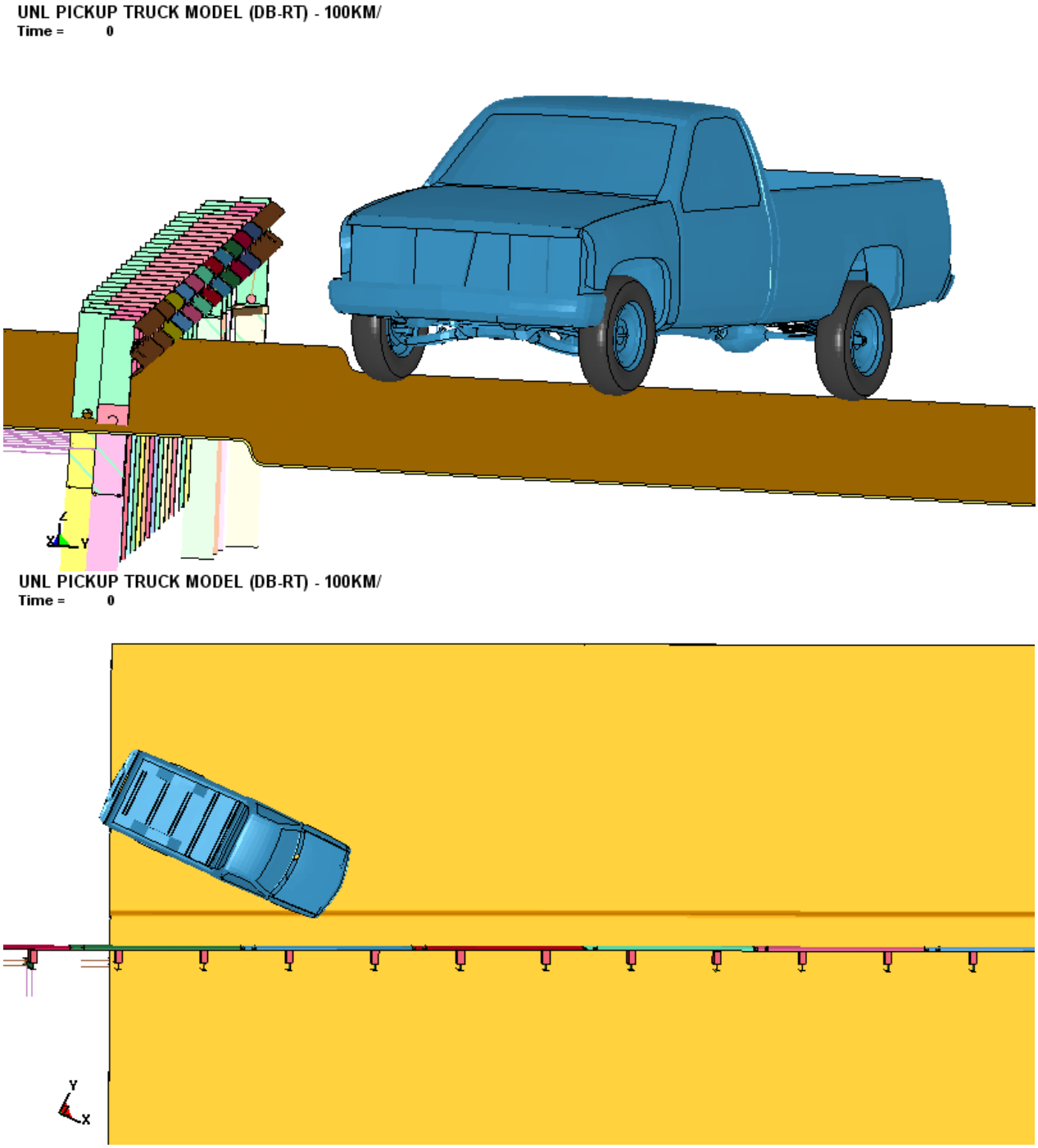

Figure 134. MGS-Curb and 2000P Crash Simulation Setup

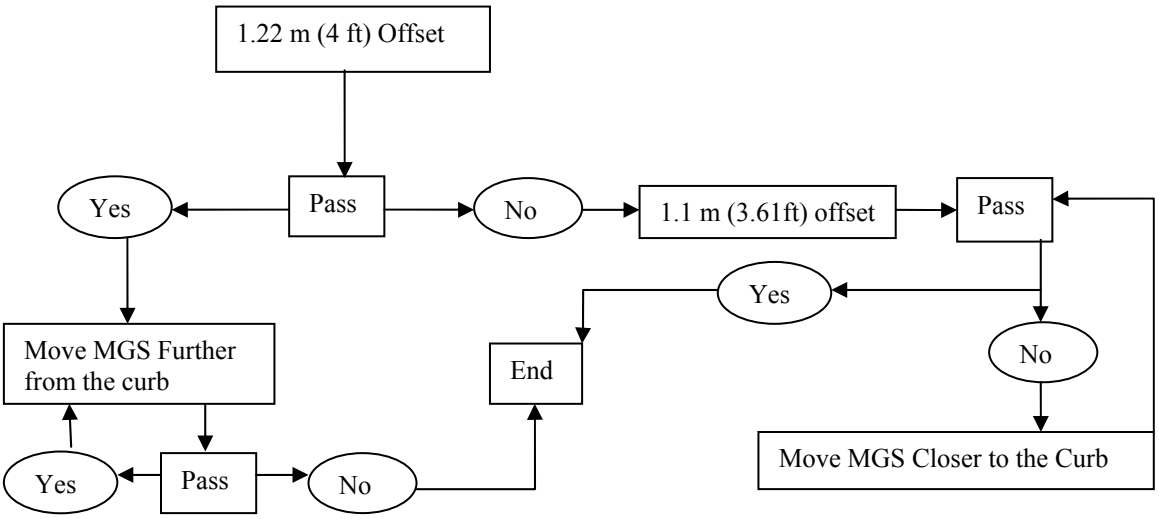

Figure 135. MGS-Curb Simulation Procedure Illustration

12.1 Simulation No. 1

The offset of 1.22 m (4 ft) was selected for the first simulation; the results are shown in Figures 136 through 140. For this offset, the top edge of the pickup's bumper was slightly higher than the W-beam's top corrugation upon impact, as shown in Figure 137. Upon impact, the pickup's bumper skipped over the W-beam rail, and the vehicle kept rising after the first impact. Then, the front tires became airborne and came into contact with the W-beam rail. The W-beam rail was deformed, and the posts were rotated backward due to the impact. The deformed W-beam rail, as well as the rotated posts, formed a ramp, which caused the pickup truck to vault over the guardrail. Thus, at the location of 1.22 m (4 ft) behind the curb, the MGS-curb system failed to capture the 2000P pickup truck, which agreed with the previous test data analysis. In addition, the simulation results implied that the 2000P might override the MGS earlier than the 2270P truck.

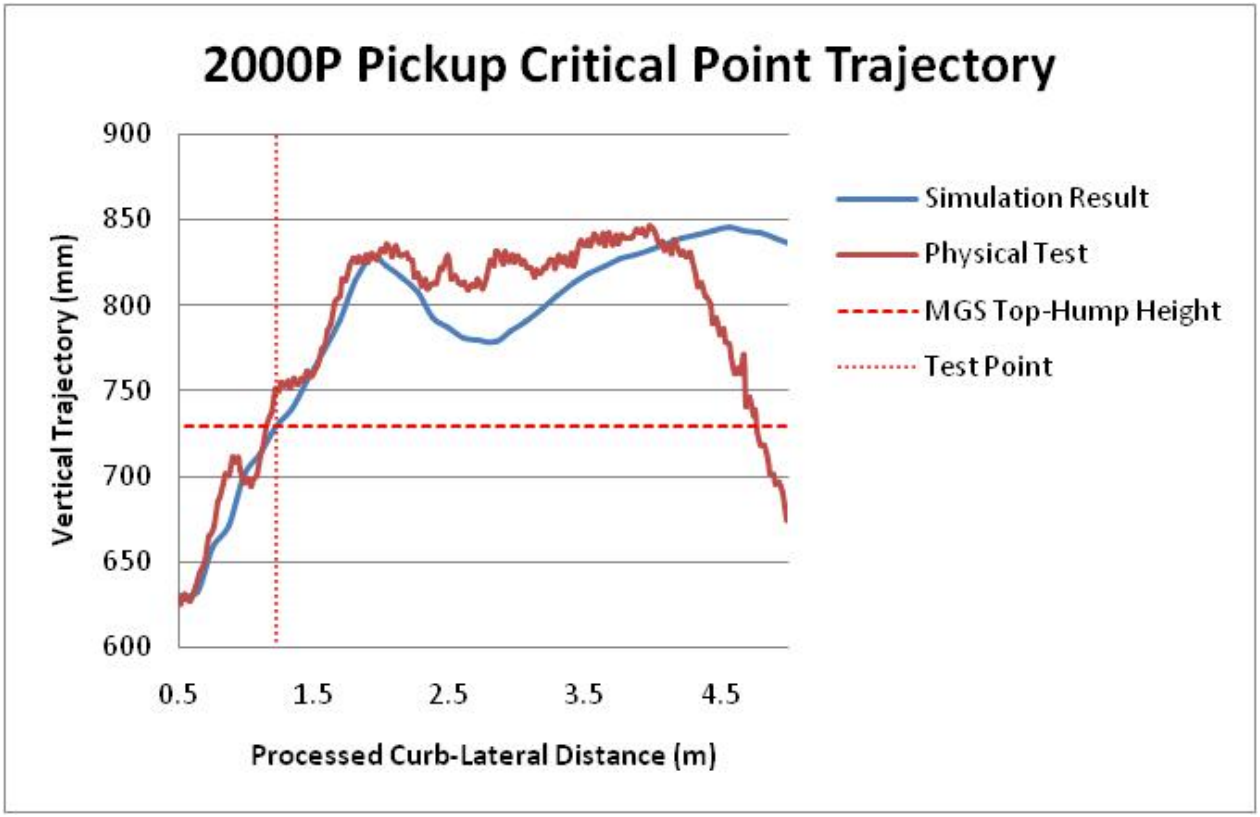

Figure 136. Simulation No. 1 Test Location - 1.22m (4 ft)

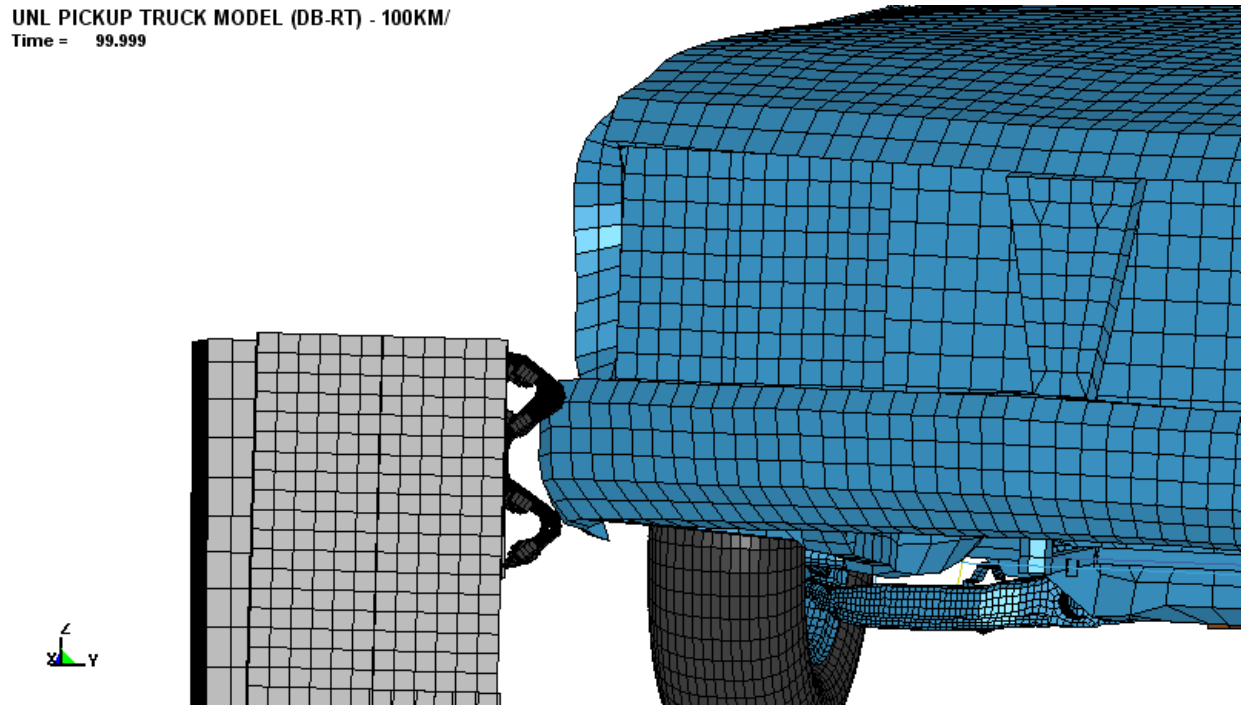

Figure 137. Vehicle-MGS Impact Position, Simulation No. 1

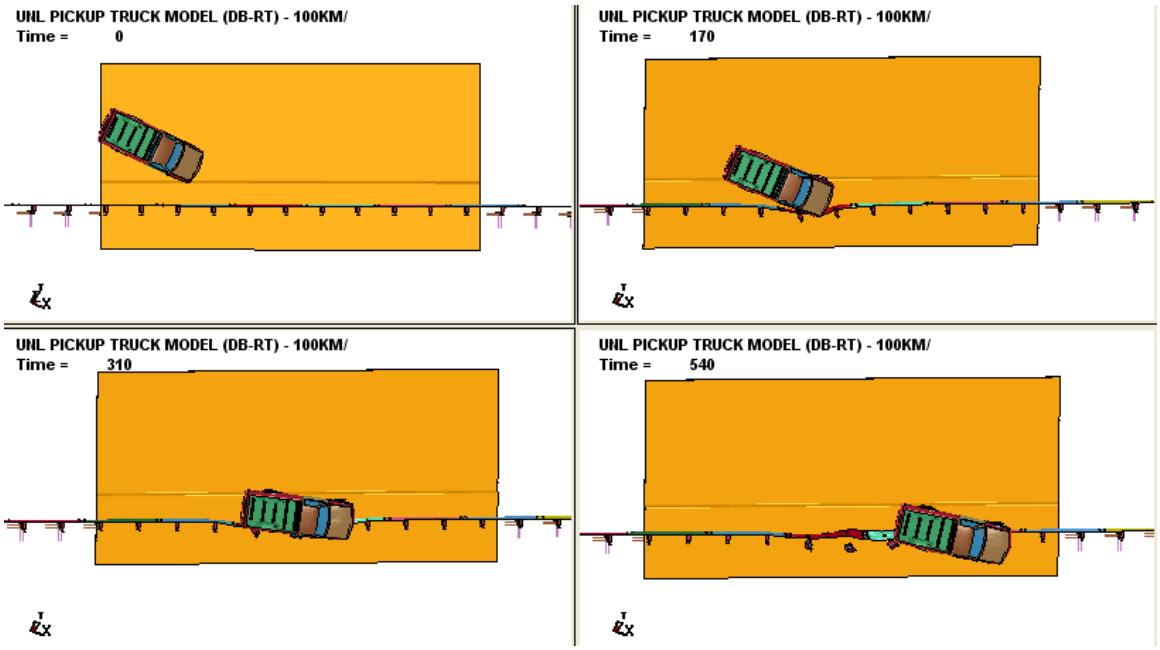

Figure 138. 2000P and MGS-Curb Impact Overhead Sequential, Simulation No. 1

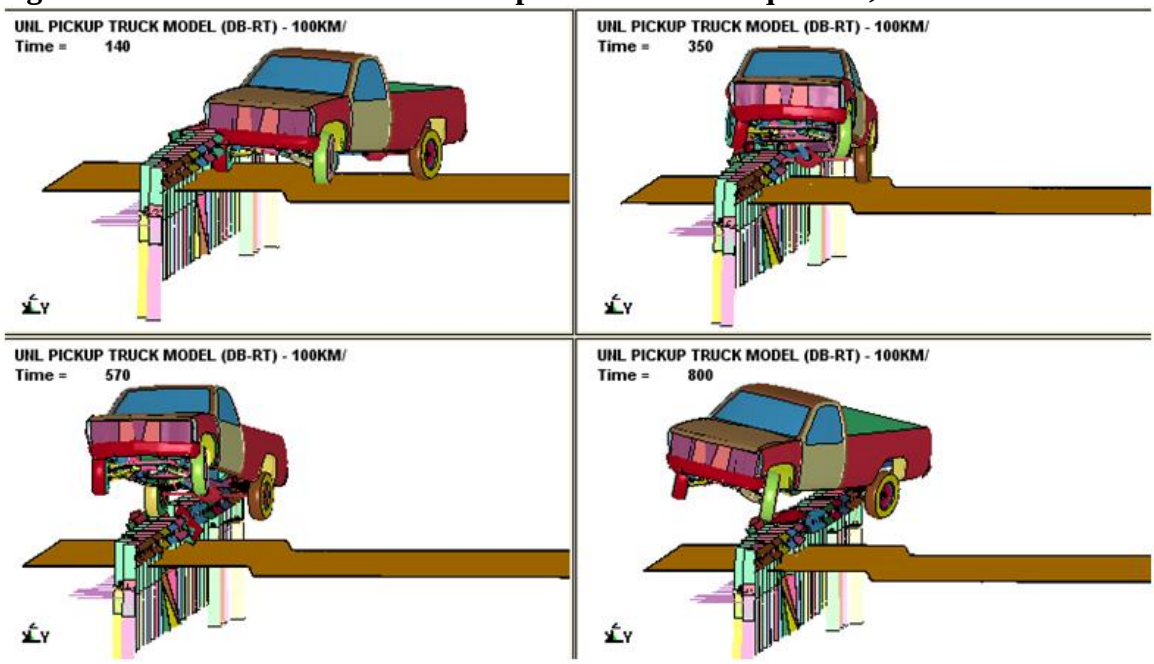

Figure 139. 2000P and MGS-Curb Impact Downstream Sequential, Simulation No. 1

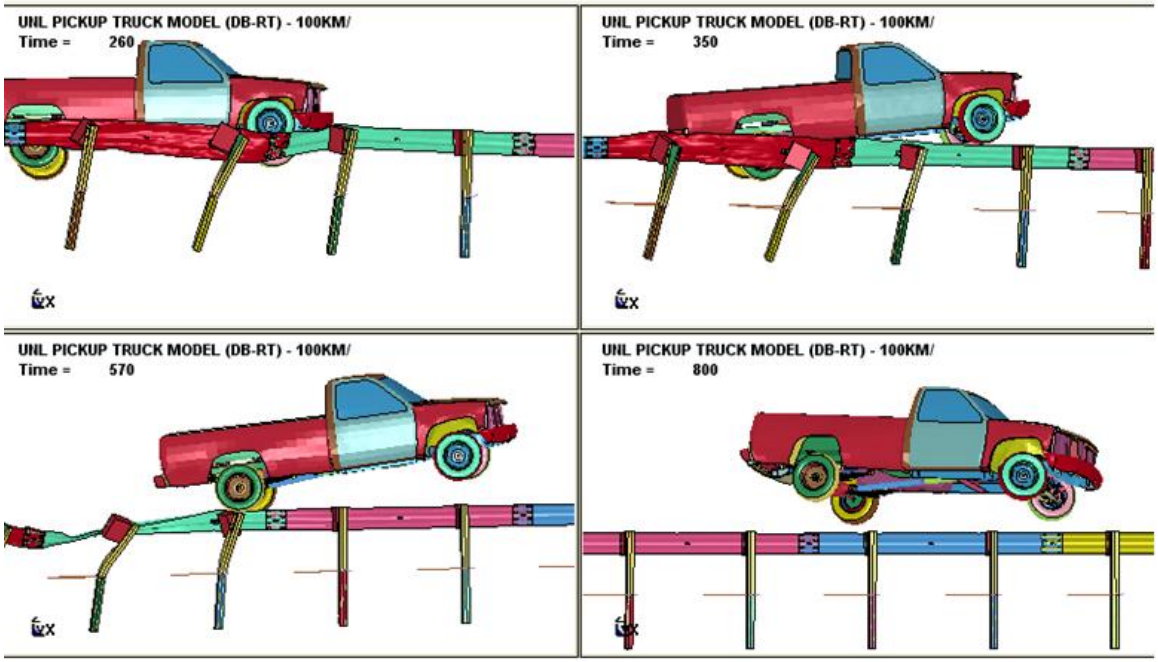

Figure 140. 2000P and MGS-Curb Impact Side Sequential, Simulation No. 1

12.2 Simulation No. 2

Next, an offset of 1.1 m (3.61 ft) was selected for the second simulation. According to the previous bumper trajectory analysis, the pickup's bumper was slightly below the centerline of the W-beam's top corrugation at this point and should have been engaged by the guardrail. The results of simulation no. 2 are shown in Figures 141 through 146.

At the 1.1-m (3.61-ft) offset location, the pickup's bumper was below the centerline of the W-beam's top corrugation upon impact with the rail. After the first impact, the vehicle moved forward, causing the W-beam to deform ahead of the vehicle. The deformation of the rail pushed the posts backward before the vehicle actually impacted them, as is seen in physical tests. Due to the backward rotation of the posts, the actual height of the W-beam rail, ahead of the vehicle, was lowered during impact. Thus, the pickup's bumper moved above the W-beam's top corrugation after the first impact. The W-beam rail did not engage the bumper. The vehicle

became airborne during the impact with the guardrail, but it did not vault over the guardrail. The vehicle was contained on the traffic side and was redirected by the MGS system. After the vehicle was redirected, the right-rear tire side-slapped the guardrail in the air. The impact force on the right-rear tire from the guardrail caused the pickup to yaw clockwise and to roll over, as shown in Figures 145 and 146. Thus, the MGS-Curb system failed to safely contain a 2000P pickup truck at this offset location according to the simulation. However, the simulation indicates that the 2000P pickup truck may not override the guardrail at this location. Furthermore, it was noticed in this simulation that the rebound force from the side impact of the vehicle's right-rear tire and the guardrail was somewhat unrealistic. It was difficult to determine if the system's failure resulted from the unrealistic rear side impact at this point.

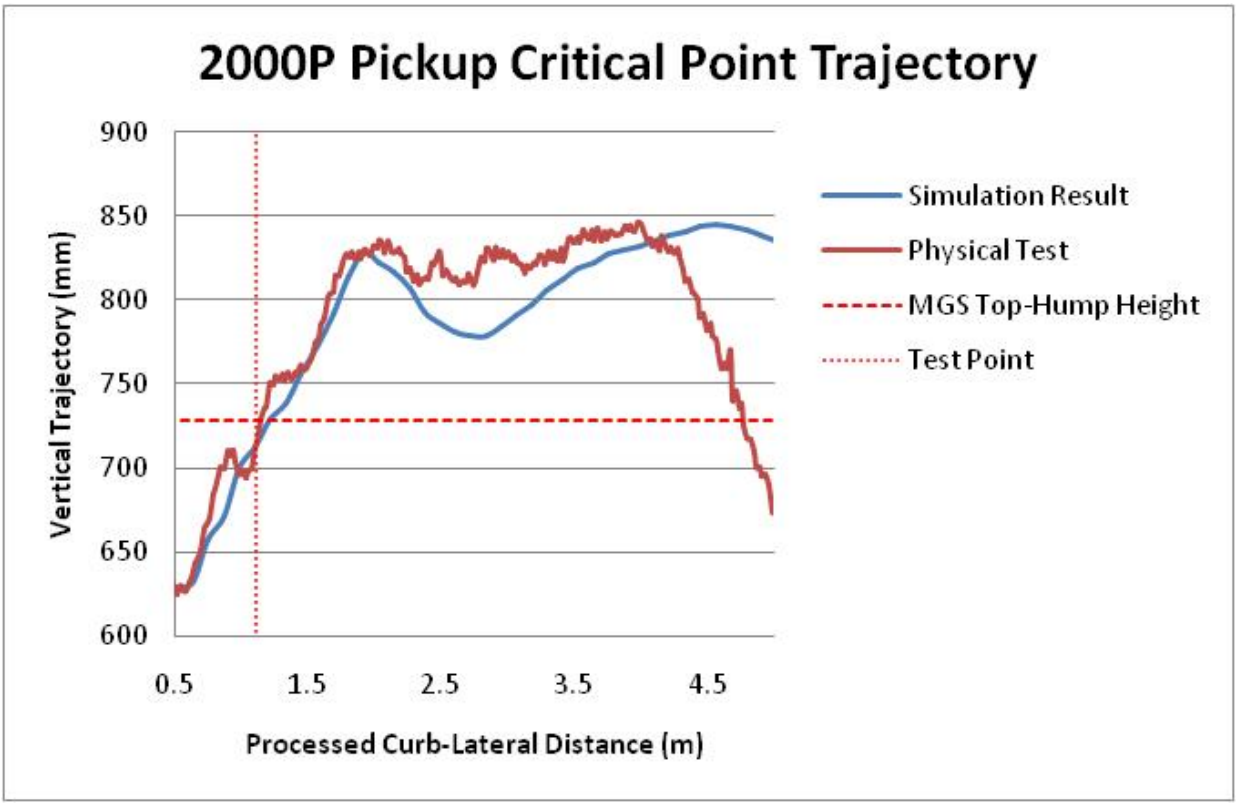

Figure 141. Simulation No. 2 Test Location—1.1m (3.61 ft)

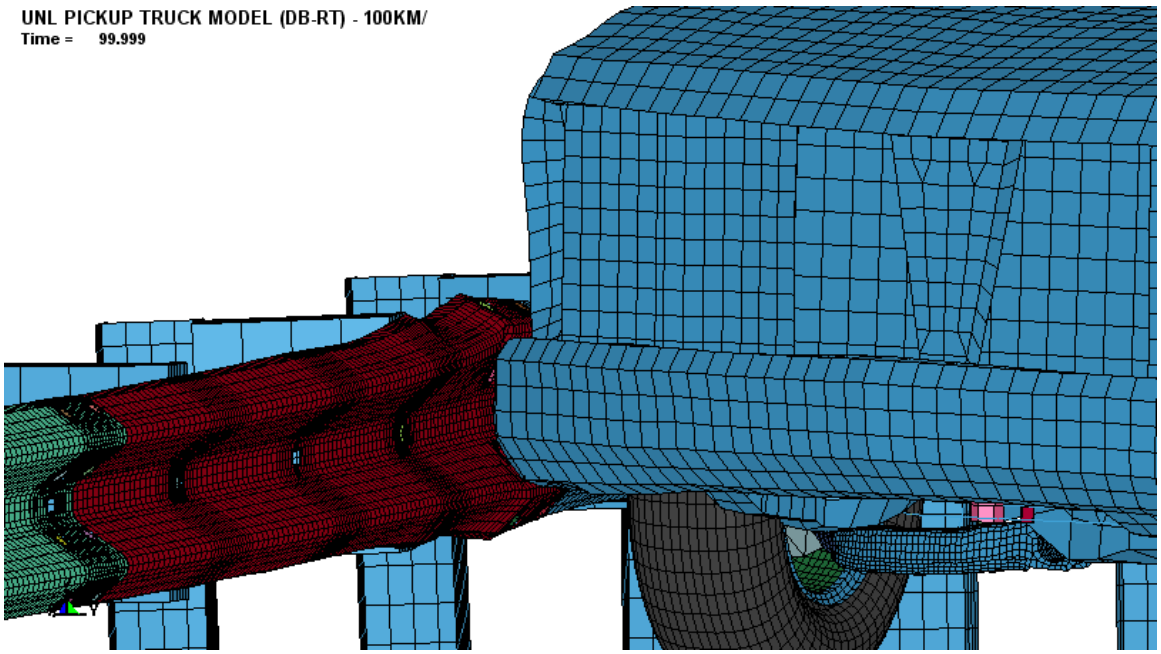

Figure 142. Vehicle-MGS Impact Position, Simulation No. 2

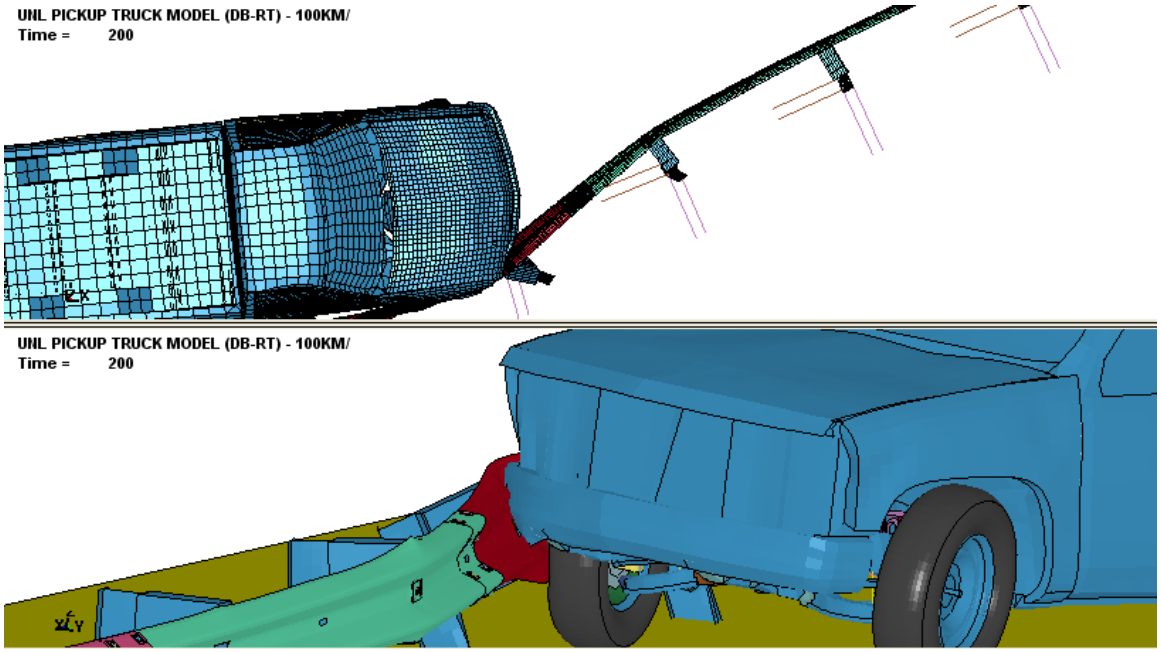

Figure 143. Guardrail Deformed Ahead of Vehicle

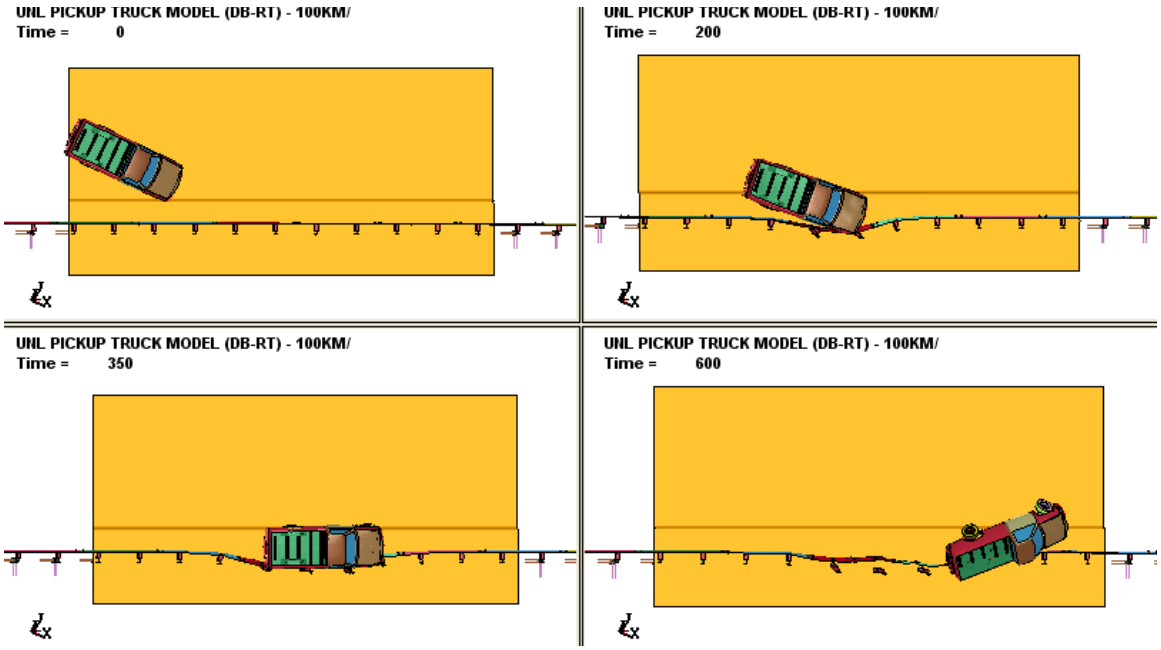

Figure 144. 2000P and MGS-Curb Impact Overhead Sequential, Simulation No. 2

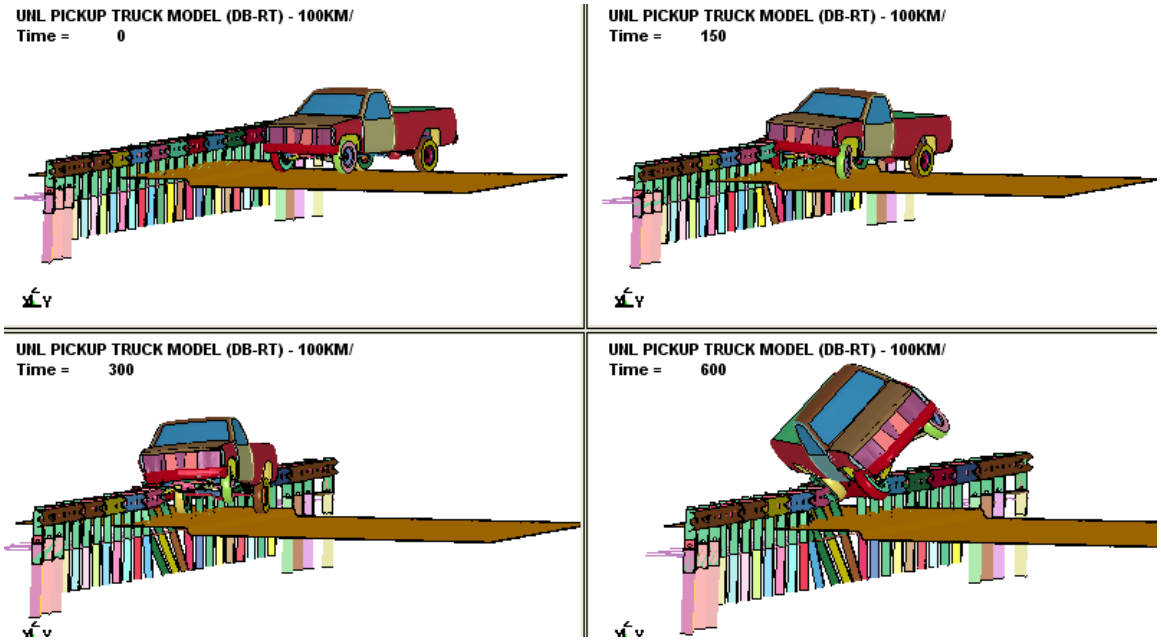

Figure 145. 2000P and MGS-Curb Impact Downstream Sequential, Simulation No. 2

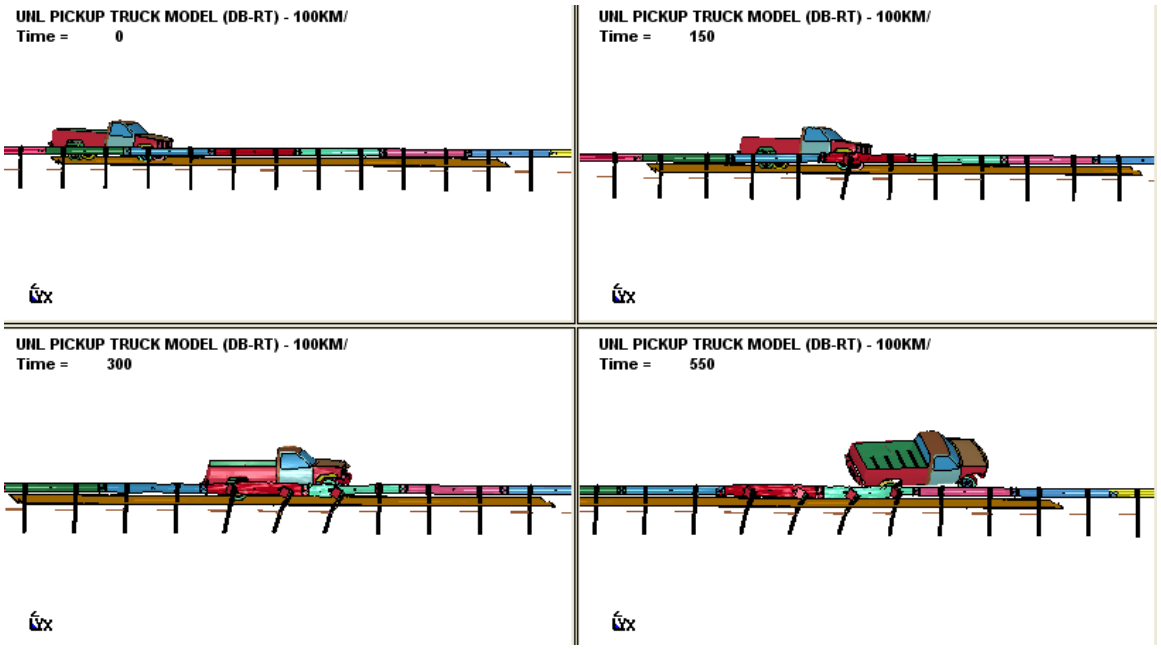

Figure 146. 2000P and MGS-Curb Impact Side Sequential, Simulation No. 2

12.3 Simulation No. 3

To further investigate the critical offset of the MGS behind the curb, another simulation was performed with the MGS offset of 0.8 m (2.63 ft) behind the curb. According to the critical location analysis, this location assures that the pickup's bumper is engaged by the W-beam. The results of simulation no. 3 are shown in Figures 147 through 151.

As expected, the simulation results clearly showed the pickup's bumper was lower than the W-beam's top corrugation and was engaged by the W-beam guardrail. The vehicle was contained on the traffic side and was redirected by the MGS system. The truck's front tires kept contact with the ground during the redirection, while the rear tires became airborne after hitting the curb. The right-rear tire impacted the guardrail later from the side. Upon the side impact between the vehicle's right-rear tire and the guardrail, the vehicle immediately bounced off the guardrail and started a significant clockwise rotation in the air. Finally, the vehicle rolled over.

Although the MGS-Curb system failed to safely contain the 2000P pickup truck in the simulation, it did not mean that the real system would fail too. The vehicle was smoothly contained and redirected by the MGS system in the simulation until the rear tire side impact occurred.

12.4 Additional Simulations

More simulations were conducted with offset distances of 1.0 m (3.3 ft), 0.9 m (3.0 ft), and 0.7 m (2.3 ft). In all the simulations, the vehicle was contained and redirected with the bumper engaged by the W-beam rail, but all of the vehicles rolled over after the right-rear tire slapped the guardrail. In all of these simulations, the roll movements of the vehicle after the rear-tire side impact seemed unrealistic. It was believed that the pickup model's rear tire and rear suspension did not replicate the side impact correctly. Further investigation is needed to improve the pickup truck model.

12.5 Simulation Summary

A series of LS-DYNA simulations on the MGS-Curb combination system was conducted to verify the previous bumper trajectory analysis.

The first simulation was performed with an MGS offset of 1.22 m (4 ft) behind the curb. According to the previous trajectory analysis, the 2270P pickup truck should be engaged by the guardrail at this point, while the 2000P pickup truck will override the guardrail. The simulation result showed that the 2000P truck vaulted over the MGS guardrail at this location behind the curb, which verified the previous trajectory analysis.

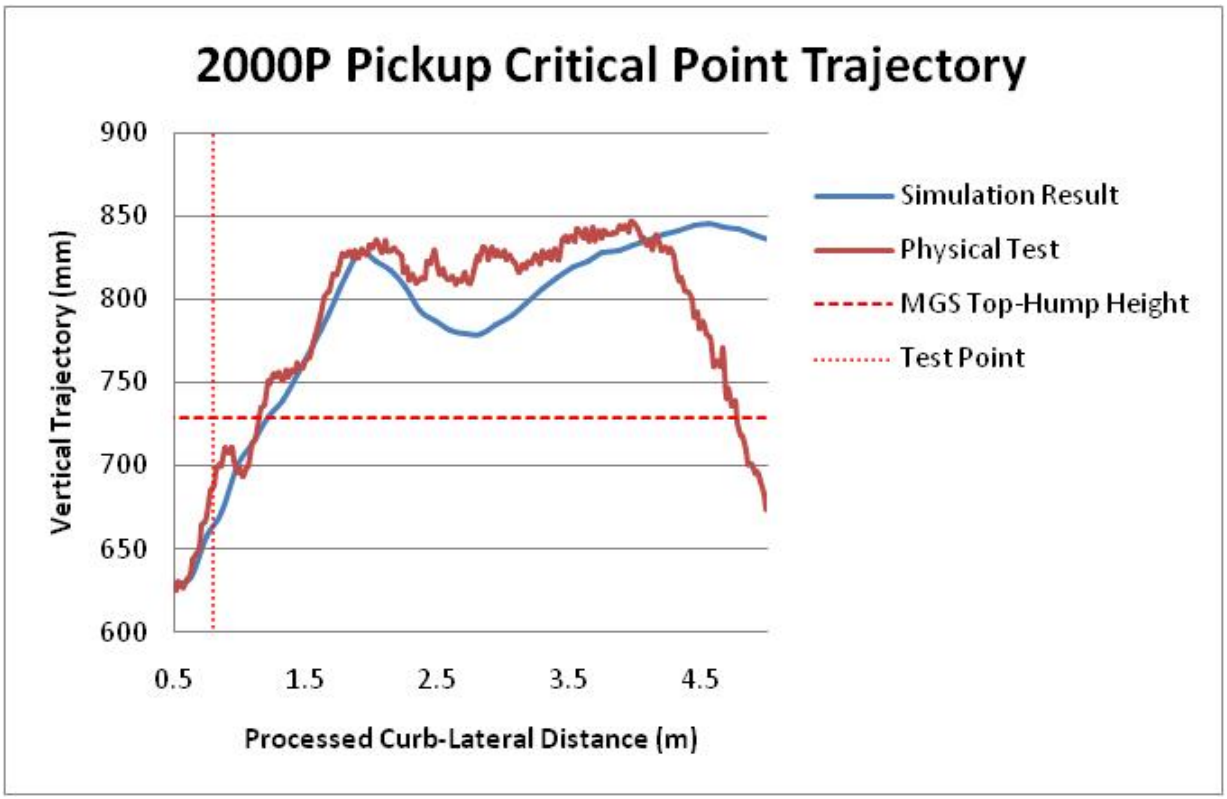

Figure 147. Simulation No. 3 Test Location - 0.8 m (2.63 ft)

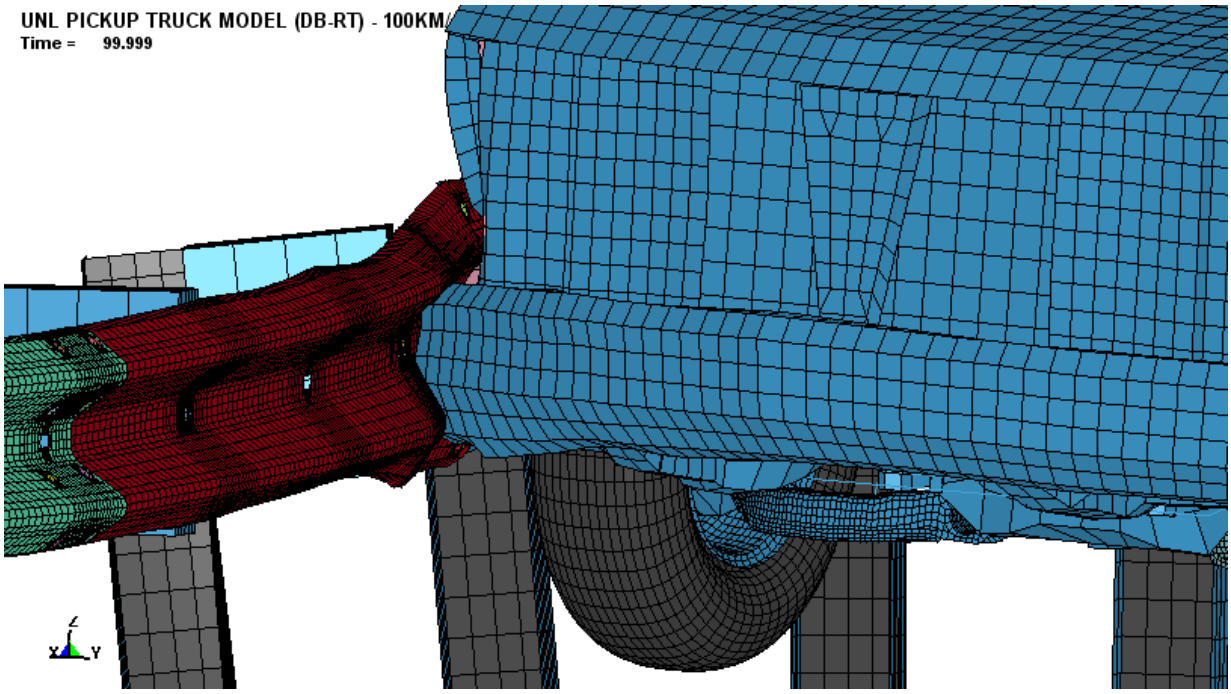

Figure 148. Pickup-MGS Impact Position, Simulation No. 3

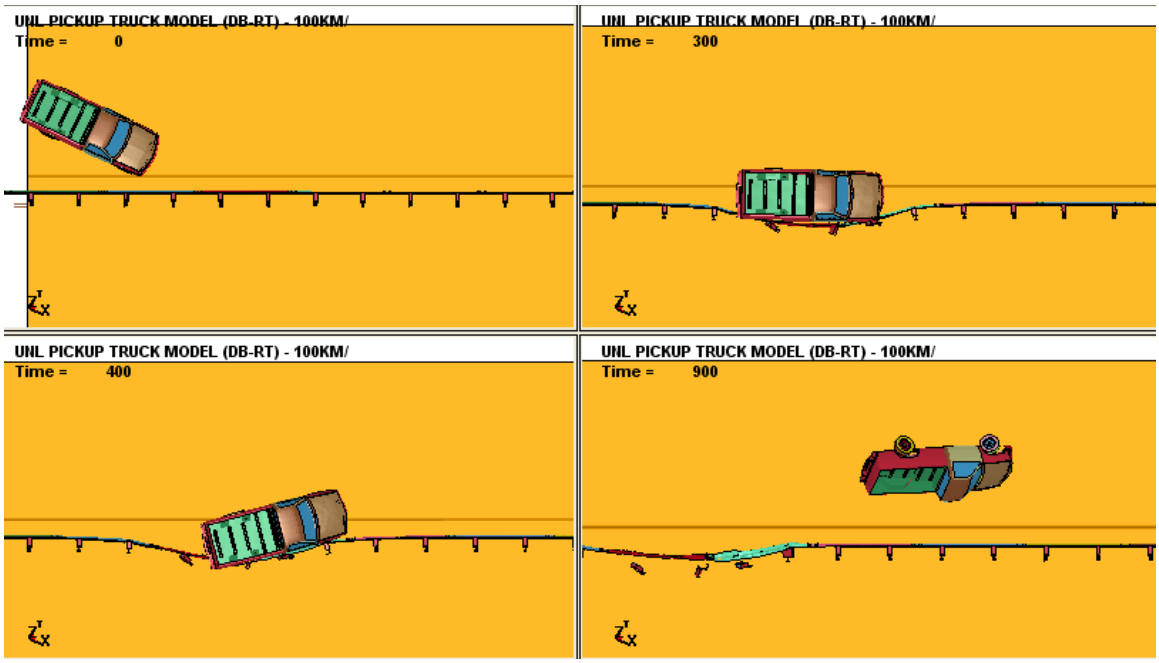

Figure 149. 2000P and MGS-Curb Impact Overhead Sequential, Simulation No. 3

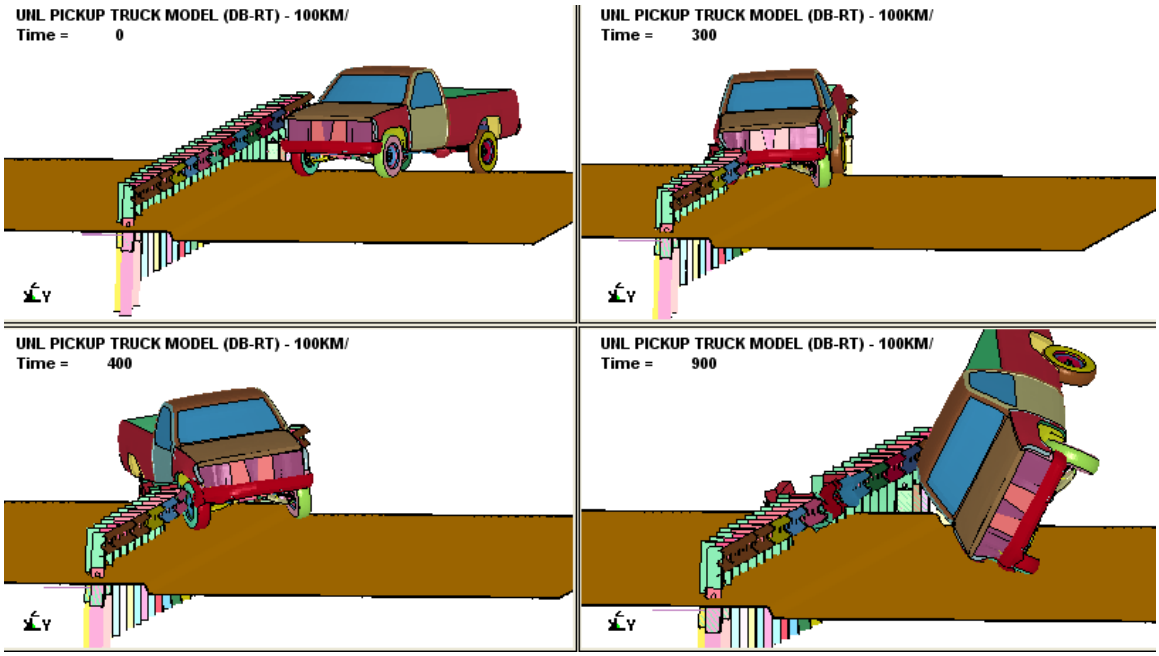

Figure 150. 2000P and MGS-Curb Impact Downstream Sequential, Simulation No. 3

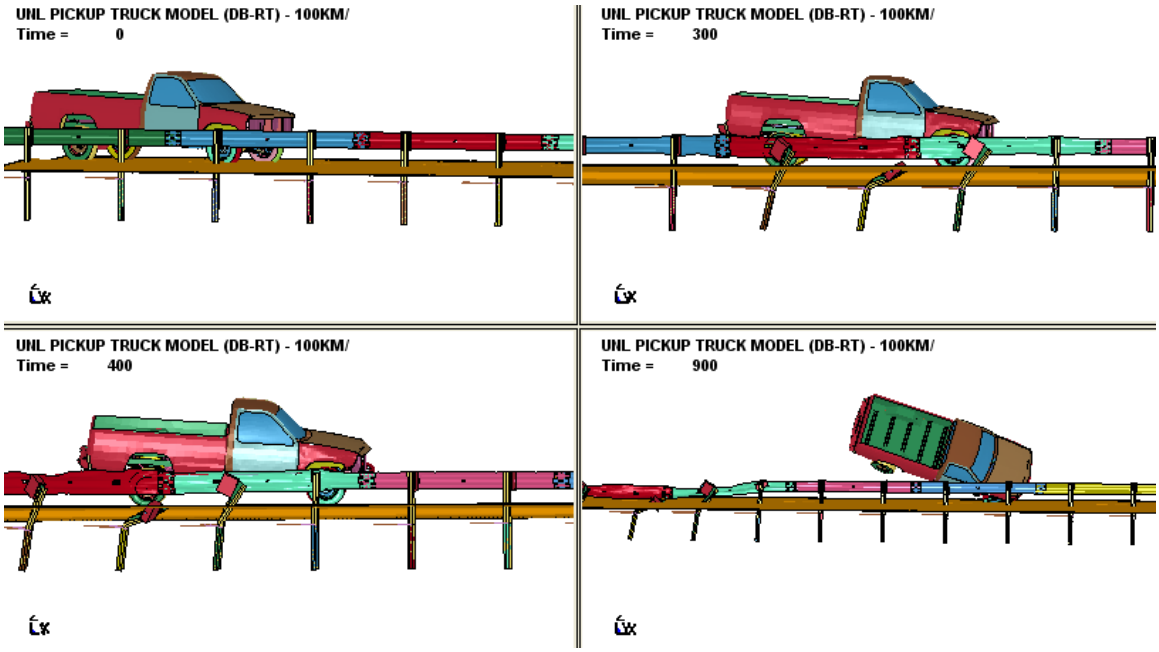

Figure 151. 2000P and MGS-Curb Impact Side Sequential, Simulation No. 3

The second simulation was performed with an MGS offset of 1.1 m (2.61 ft) behind the curb. According to the previous trajectory analysis, the 2000P's bumper top edge trajectory was slightly below the W-beam's top corrugation centerline at this location. Thus, the 2000P's bumper should be engaged by the MGS at this location. The simulation showed the bumper's top edge was below the W-beam's top corrugation upon the impact, but it moved above the top corrugation later due to the rotation of the posts ahead of the vehicle. However, the vehicle was still contained on the traffic side and did not vault over the guardrail at this offset location. A possibly unrealistic roll movement from the rear tire's side impact with the guardrail was observed in this simulation.

More simulations were conducted with closer MGS offsets behind the curb. These simulations showed that at closer offset distances, the pickup's bumper was engaged by the guardrail during impact. The pickup truck was contained and redirected by the MGS in all

simulations. However, increasingly unrealistic vehicle roll movements from the rear-tire side impact were observed in all the close-offset simulations. It is believed the pickup model did not replicate the rear tire/suspension side impact with the guardrail correctly. More investigation is needed to improve the truck model in the future in order to more accurately capture behavior late in the event.

13 SUMMARY AND CONCLUSIONS

Four crash tests were performed to investigate vehicle behavior after impacting a 152-mm (6-in.) high, AASHTO Type B curb. Two tests were conducted with 2270P pickup trucks, one test was conducted with an 1100C small passenger car, and one test was performed with a 2000P pickup truck. A summary of the safety performance evaluation for the four tests is provided in Table 7.

The first test, test no. MGSC-1, consisted of a 2,253-kg (4,966-lb) pickup truck impacting the curb at a speed of 100.0 km/h (62.1 mph) and an angle of 25 degrees. The vehicle ran over the curb without changing heading direction. No damage to the vehicle was observed. The pickup was partially airborne after the impact. Both the C.G. and bumper trajectories showed the vehicle descended after it reached the peak at a certain distance behind the curb.

The second test, test no. MGSC-2, consisted of a 2,253-kg (4,966-lb) pickup truck impacting the curb at a speed of 100.8 km/h (62.6 mph) and an angle of 25 degrees. The vehicle ran over the curb without changing the heading direction. No damage to the vehicle was observed. The pickup was partially airborne after the impact. Both the C.G. and bumper trajectories were higher than test MGSC-1. The C.G. target trajectory had a similar trend as in test MGSC-1, while the bumper trajectory developed quite differently when compared to test MGSC-1. The bumper trajectory in test MGSC-2 kept increasing until it was out of view.

The third test, test no. MGSC-3, consisted of a 1,154-kg (2,254-lb) small passenger car impacting the curb at a speed of 99.1 km/h (61.6 mph) and an angle of 25 degrees. The vehicle's tires and wheel rims were damaged by the impact. No other damage was found on the vehicle. The small passenger car became airborne after the impact.

The final test, test no. MGSC-4, consisted of a 2,032-kg (4,479-lb) pickup truck impacting the curb at a speed of 100.6 km/h (62.5 mph) and an angle of 25 degrees. The vehicle ran over the curb without notable any damage to the vehicle. The pickup was airborne after the impact. Significant pitch-down movement was observed after the vehicle reached its peak height.

Through analysis, the top edge of the pickup's front bumper was determined to be the critical impact height for the MGS impact. The pickup truck was considered safe as long as the bumper's top edge did not pass the centerline of the W-beam's top corrugation. The small car's trajectory was evaluated using the successful impact height of test 2214MG-3. It was considered safe if the small car's impact height was higher than the impact height used in test 2214MG-3.

The vehicle's trajectories were recorded using the high-speed video analysis. To bring them into phase for analysis, the raw trajectory data were transformed into Processed Longitudinal Distance (PLD) coordinates and Processed Curb-Lateral Distance (CLD) coordinates. The processed trajectories were compared against the MGS's height to determine the critical lateral offset behind the curb. The normal MGS installation heights with and without a 152-mm (6-in.) vertical offset were both evaluated. For the MGS height of the Option I installation, the analysis indicated that the 2270P pickup might override the MGS placed greater than 1.13 m (3.71 ft) (from test MGSC-2) and beyond 1.29 m (4.23 ft) (from MGSC-1) behind the curb, the 2000P pickup might override the MGS placed between 1.14 m (3.71 ft) and 4.75 m (15.6 ft) behind the curb, and the 1100C will not underride the MGS. For the MGS height of the Option II installation, the 2270P might override the MGS placed between 1.81 m (5.94 ft) (from test MGSC-2) and 5.03 m (16.5 ft) (from test MGSC-1) behind the curb, the 2000P will not override the MGS, and the 1100C might underride the MGS placed closer than 0.98 m (3.14 ft) and greater than 4.6 m (15.1 ft) behind the curb.

An LS-DYNA simulation was performed to replicate test MGSC-4 using the current 2000P pickup model. Results of the simulation indicated that the current pickup model was fairly accurate to predict the vehicle trajectory within 2.24 m (7.35 ft) behind the curb, and the current tire model could accurately capture the tire deformation upon impact.

Based on the trajectory analysis, a series of LS-DYNA simulations was performed to determine the critical lateral offset of the MGS behind a curb. Results of the simulation indicated that: (1) at 1.22 m (4 ft) behind the curb, where the 2000P bumper was slightly higher than the top corrugation of the MGS, the guardrail did not capture the vehicle and the vehicle vaulted over the guardrail; (2) at 1.1 m (3.61 ft) behind the curb, where the 2000P bumper was slightly lower than the top corrugation of the MGS, the vehicle did not vault over the guardrail, though the bumper was not captured by the MGS due to the post rotation; and (3) at 0.8 m (2.63 ft) behind the curb, where the 2000P bumper was significantly lower than the top corrugation of the MGS, the bumper was captured by the MGS and the vehicle was contained on the traffic side. However, an unrealistic side impact between the right-rear tire and the MGS caused the pickup to roll over. Future investigations need to be performed to improve the current 2000P pickup model.

Table 7. Vehicle-Curb Test Summary

Test No.		MGSC-1	MGSC-2	MGSC-3	MGSC-4
Test Date:		10/11/2007	10/12/2007	10/23/2007	10/23/2007
Test Vehicle:		2003 Dodge Ram 1500 Quad Cab (2270P)		2002 Kia Rio (1100C)	1999 Chevy C2500 (2000P)
Curb Type:		152-mm (6-in.) AASHTO Type B			
Impact Speed:		100.0 km/h (62.1 mph)	100.8 km/h (62.6 mph)	99.1 km/h (61.6 mph)	100.6 km/h (62.5 mph)
Impact Angle:		25 degrees			
Maximum Vertical Displacement	**C.G. Target**	445 mm (17.5 in.)	660 mm (25.9 in.)	236 mm (9.3 in.)	265 mm (10.4 in.)
	Bumper Target:	345 mm (13.6 in.)	548 mm (21.6 in.)	320 mm (12.6 in.)	215 mm (8.5 in.)

14 FUTURE RESEARCH

The current analysis was only based on the vehicle's vertical trajectory, and the curb-MGS combination was deemed safe as long as the vehicle's impact height was within a certain range. This "Height-Safety-Criteria" assumes the vehicle is flat upon impact with the MGS. However, due to the prior curb impact, the vehicle might strike the MGS with different pitch and roll positions. The vehicle's pitch and roll angles upon impact with the MGS are also critical in addition to the vertical impact height. If the pitch and roll angles are beyond certain values, the vehicle might still vault, override, underride, and/or roll over the guardrail, even if the vehicle's impact height met the "Height-Safety-Criteria". Thus, additional investigation is recommended to determine the critical impact pitch and roll angles for vehicle-MGS impacts.

Because the current truck model could not accurately predict the vehicle trajectory after 2.24 m (7.35 ft) behind the curb, full-scale tests need to be conducted to determine the critical offset, if the MGS is desired to be installed farther behind the curb. In addition, future investigations of the unloading performance and side impact performance of the rear suspension are recommended to improve the current pickup truck model.

15 REFERENCES

1. Ross, H.E., Sicking, D.L., Zimmer, R.A., and Michie, J.D., *Recommended Procedures for the Safety Performance Evaluation of Highway Features*, National Cooperative Highway Research Program (NCHRP) Report No. 350, Transportation Research Board, Washington, D.C., 1993.

2. Polivka, K.A., Faller, R.K., Sicking, D.L., Reid, J.D., Rohde, J.R., Holloway, J.C, Bielenberg, B.W., and Kuipers, B.D, *Development of the Midwest Guardrail System for Standard and Reduced Post Spacing and in Combination with Curbs.* Research Report TRP-03-139-04, Midwest Roadside Safety Facility, University of Nebraska Lincoln, Lincoln, Nebraska, 2004.

3. Faller, R.K., Polivka, K.A., Kuipers, B.D., Bielenberg, B.W., Reid, J.D., Rohde, J.R., and Sicking, D.L., *Midwest Guardrail System for Standard and Special Applications*, Paper No. 04-4778, Transportation Research Record No. 1890, Transportation Research Board, Washington D.C., January 2004.

4. Sicking, D.L., Mak, K.K., Reid, J.D., and Rohde, J.R., *Recommended Procedures for the Safety Performance Evaluation of Highway Feature, Draft Report,* Presented to the Transportation Research Board, Prepared by the Midwest Roadside Safety Facility, University of Nebraska-Lincoln, February 2007.

5. *A Policy on Geometric Design of Highways and Street,* American Association of State Highway and Transportation Officials, Washington, D.C., 2001.

6. *Roadside Design Guide*, American Association of State Highway and Transportation Officials, Washington, D.C., 2002.

7. Olson, R.M., Weaver, G.D., Ross, H.E. and Post, E.R., *Effect of Curb Geometry and Location on Vehicle Behavior,* National Cooperative Highway Research Program (NCHRP), Report No. 150, Transportation Research Board, Washington, D.C., 1974.

8. Holloway, J.C., *Safety Performance Evaluation of Vehicular Impacts on Mountable Curbs,* Master's Thesis, University of Nebraska-Lincoln, 1993.

9. Holloway, J.C., Sicking, D.L., and Rosson, B.T., Performance Evaluation of NDOR Mountable Curbs, Final Report to the Midwest States' Regional Pooled Fund Program, Transportation Research Report No. TRP-03-37-94, Project No. RES1(0099) P464, Midwest Roadside Safety Facility, University of Nebraska-Lincoln, June 1994.

10. Ross, H.E., Perera, Sicking, D.L. and Bligh, R.P., *Roadside Safety Design for Small Vehicles,* National Cooperative Highway Research Program (NCHRP) Report No. 318, Transportation Research Board, Washington, D.C., 1989.

11. Plaxico, C.A., Ray, M.H., Weir, J.A., Orengo, F., and Tiso, P., *Recommended Guidelines for Curb and Curb-Barrier Installations*, National Cooperative Highway Research Program (NCHRP) Report No. 537, Transportation Research Board, Washington, D.C., 2005.

12. Hinch, J., Yang, T-L, and Owings, R., *Guidance Systems for Vehicle Testing*, ENSCO, Inc., Springfield, Virginia, 1986.

13. *Center of Gravity Test Code – SAE J874 March 1981*, SAE Handbook Vol. 4, Society of Automotive Engineers, Inc., Warrendale, Pennsylvania, 1986

14. Reid, J.D., Boesch, D.A., and Bielenberg, R.W., *Detailed Tire Modeling for Crash Applications*, International Journal of Crashworthiness, Vol. 12, No. 5, 2007.

15. Plaxico, C.A., *Design Guidelines for the Use of Curbs and Curb/Guardrail Combinations along High-Speed Roadways*, Doctoral Dissertation, Worcester Polytechnic Institute, Worcester, Massachusetts, 2002.

16. Paulsen, T.J., *Improvements to the Suspension and Modularization of the C2500 Pickup Truck Finite Element Model*, Master's Thesis, University of Nebraska-Lincoln, Lincoln, Nebraska, 2003.

17. Johnson, E.A., Lechtenberg, K.A., Reid, J.D., Sicking, D.L., Faller, R.K., Bielenberg, R.W., and Rohde, J.R., *Approach Slope for Midwest Guardrail System*, Research Report TRP-03-188-08, Midwest Roadside Safety Facility, University of Nebraska Lincoln, Lincoln, Nebraska, 2008.

18. Polivka, K.A., Faller, R.K., Sicking, D.L., Rohde, J.R., Bielenberg, B.W., and Reid, J.D., Performance Evaluation of the Midwest Guardrail System - Update to NCHRP 350 Test No. 3-10 (2214MG-3), Final Report to the National Cooperative Highway Research Program (NCHRP), Transportation Research Board, Transportation Research Report No. TRP-03-172-06, Midwest Roadside Safety Facility, University of Nebraska-Lincoln, October 11, 2006.

APPENDIX A

VEHICLE-CURB TEST SETUP (ENGLISH UNITS)

Figure A-1. System Layout (English Units)
Figure A-2. Curb Detail (English Units)
Figure A-3. Bill of Bars (English Units)

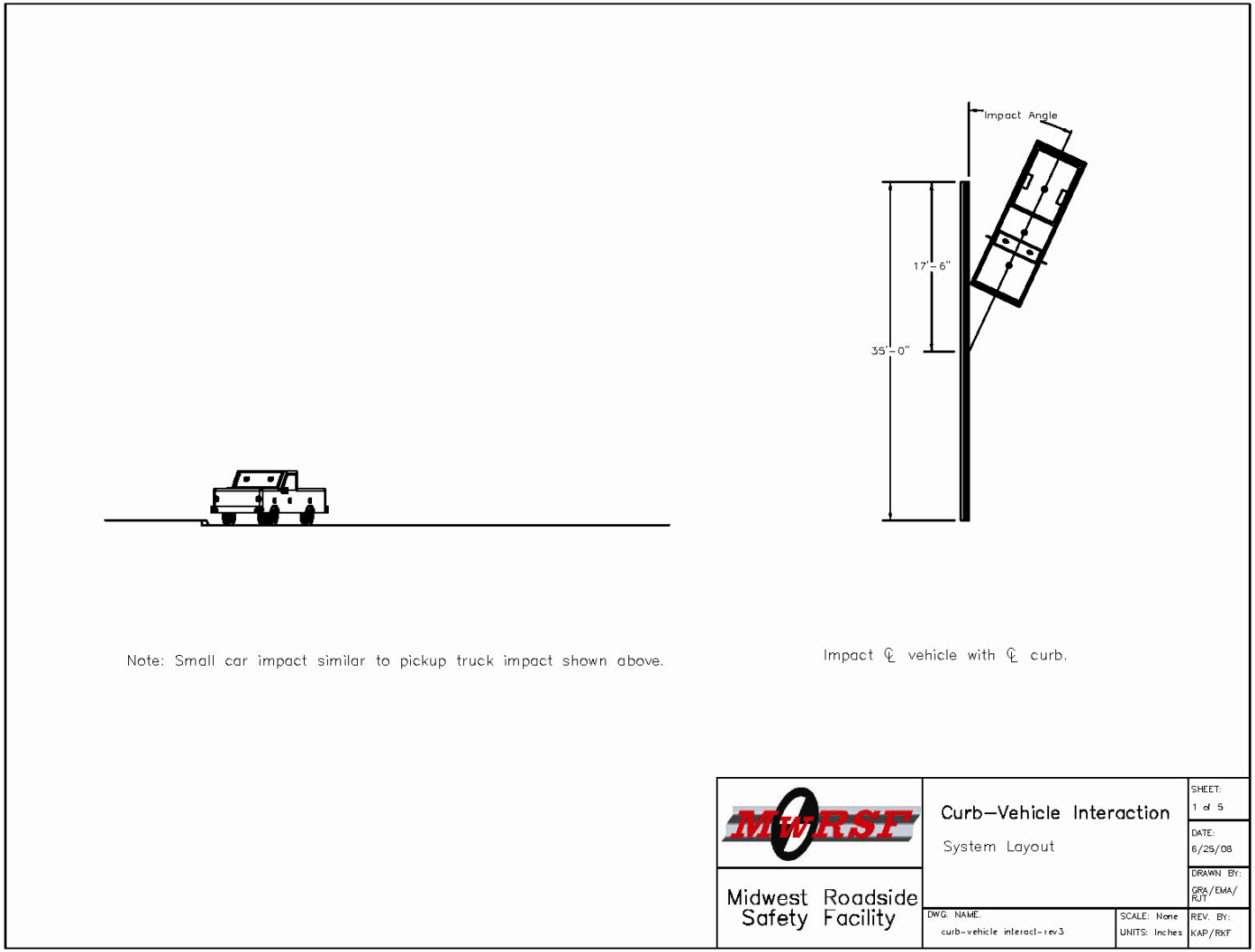

Figure A-1. System Layout (English Units)

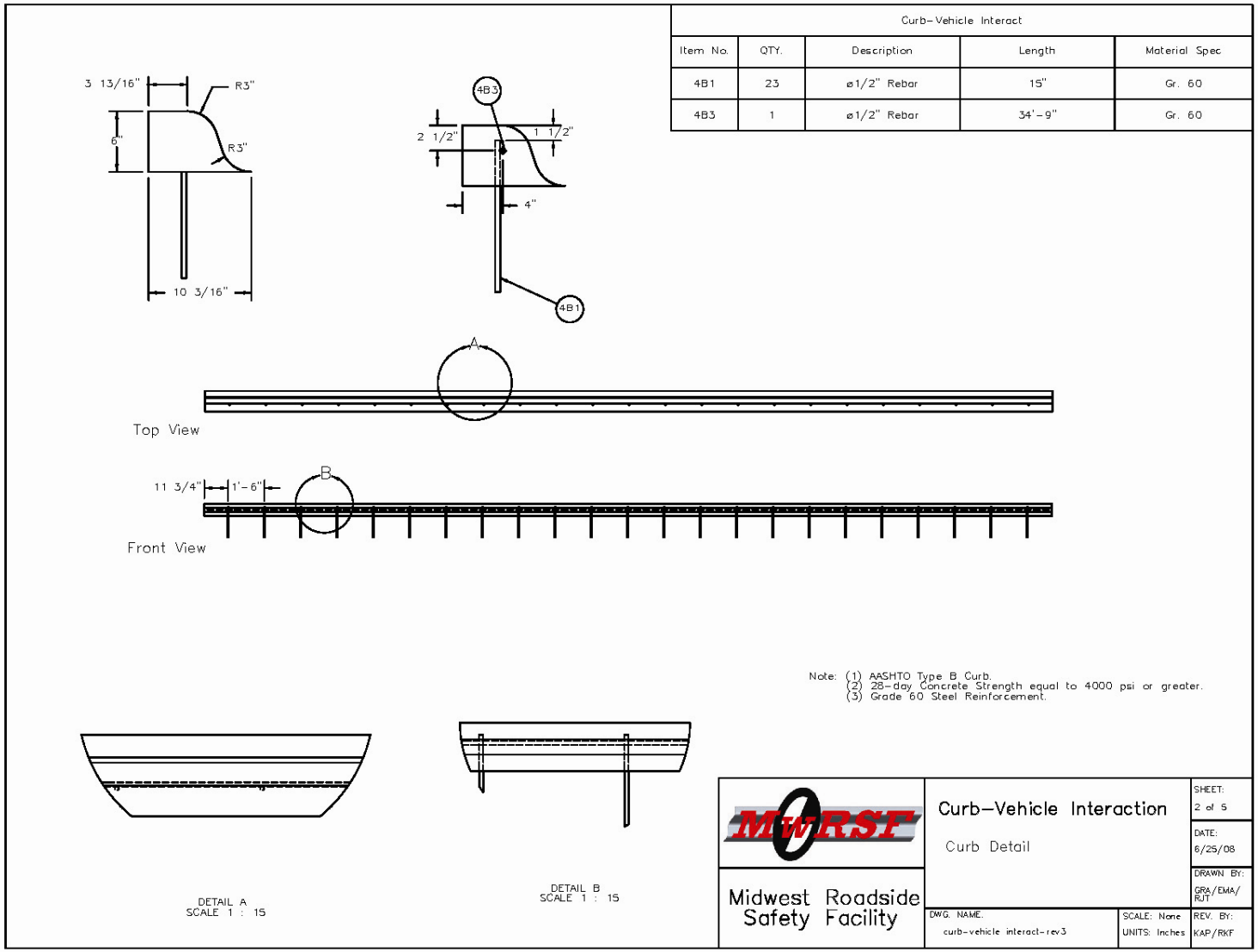

Figure A-2. Curb Detail (English Units)

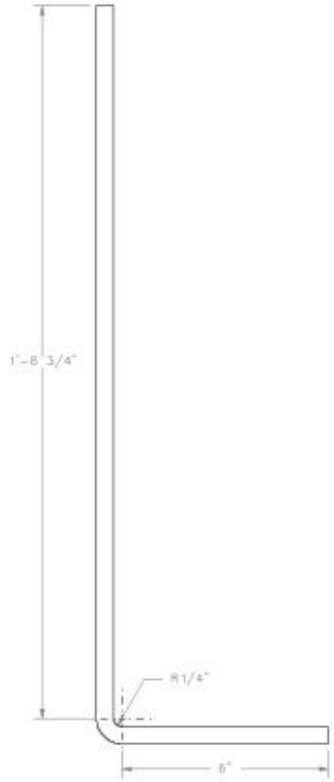

482

Curb-Vehicle Interact					
Item No.	Bend Dia.	Quantity	Length	Material Spec.	Bar Size
481	–	32	15"	Gr. 60	1/2"
482	1/4"	32	28"	Gr. 60	1/2"
483	–	3	34'-9"	Gr. 60	1/2"

MwRSF Midwest Roadside Safety Facility	Curb–Vehicle Interaction Bill of Bars	SHEET: 6 of 6 DATE: 6/11/07 DRAWN BY: GRA
	DWG. NAME: curb-vehicle interact-rev2 SCALE: None UNITS: Inches	REV. BY: KAP/RKF

Figure A-3. Bill of Bars (English Units)

APPENDIX B

RAW TEST RESULTS (ENGLISH UNITS)

Figure B-1. C.G. Target Vertical Displacement vs. Time, Test MGSC-1 (2270P)
Figure B-2. C.G. Target Vertical Displacement vs. Raw Longitudinal Distance, Test MGSC-1 (2270P)
Figure B-3. Bumper Target Vertical Displacement vs. Time, Test MGSC-1 (2270P)
Figure B-4. Bumper Target Vertical Displacement vs. Raw Longitudinal Distance, Test MGSC-1 (2270P)
Figure B-5. C.G. Target Trajectory vs. Raw Longitudinal Distance, Test MGSC-1 (2270P)
Figure B-6. Bumper Target Trajectory vs. Raw Longitudinal Distance, Test MGSC-1 (2270P)
Figure B-7. C.G. Target Vertical Displacement vs. Time, Test MGSC-2 (2270P)
Figure B-8. C.G. Target Vertical Displacement vs. Raw Longitudinal Distance, Test MGSC-2 (2270P)
Figure B-9. Bumper Target Vertical Displacement vs. Time, Test MGSC-2 (2270P
Figure B-10. Bumper Target Vertical Displacement vs. Raw Longitudinal Distance, Test MGSC-2 (2270P)
Figure B-11. C.G. Target Trajectory vs. Raw Longitudinal Distance, Test MGSC-2 (2270P)
Figure B-12. Bumper Target Trajectory vs. Raw Longitudinal Distance, Test MGSC-2 (2270P)
Figure B-13. C.G. Target Vertical Displacement vs. Time, Test MGSC-3 (1100C)
Figure B-14. C.G. Target Vertical Displacement vs. Raw Longitudinal Distance, Test MGSC-3 (1100C)
Figure B-15. Bumper Target Vertical Displacement vs. Time, Test MGSC-3 (1100C)
Figure B-16. Bumper Target Vertical Displacement vs. Raw Longitudinal Distance, Test MGSC-3 (1100C)
Figure B-17. C.G. Target Trajectory vs. Raw Longitudinal Distance, Test MGSC-3 (1100C)
Figure B-18. Bumper Target Trajectory vs. Raw Longitudinal Distance, Test MGSC-3 (1100C))
Figure B-19. C.G. Target Vertical Displacement vs. Time, Test MGSC-4 (2000P)
Figure B-20. C.G. Target Vertical Displacement vs. Raw Longitudinal Distance, Test MGSC-4 (2000P)
Figure B-21. Bumper Target Vertical Displacement vs. Time, Test MGSC-4 (2000P)
Figure B-22. Bumper Target Vertical Displacement vs. Raw Longitudinal Distance, Test MGSC-4 (2000P)
Figure B-23. C.G. Target Trajectory vs. Raw Longitudinal Distance, Test MGSC-4 (2000P)
Figure B-24. Bumper Target Trajectory vs. Raw Longitudinal Distance, Test MGSC-4 (2000P)

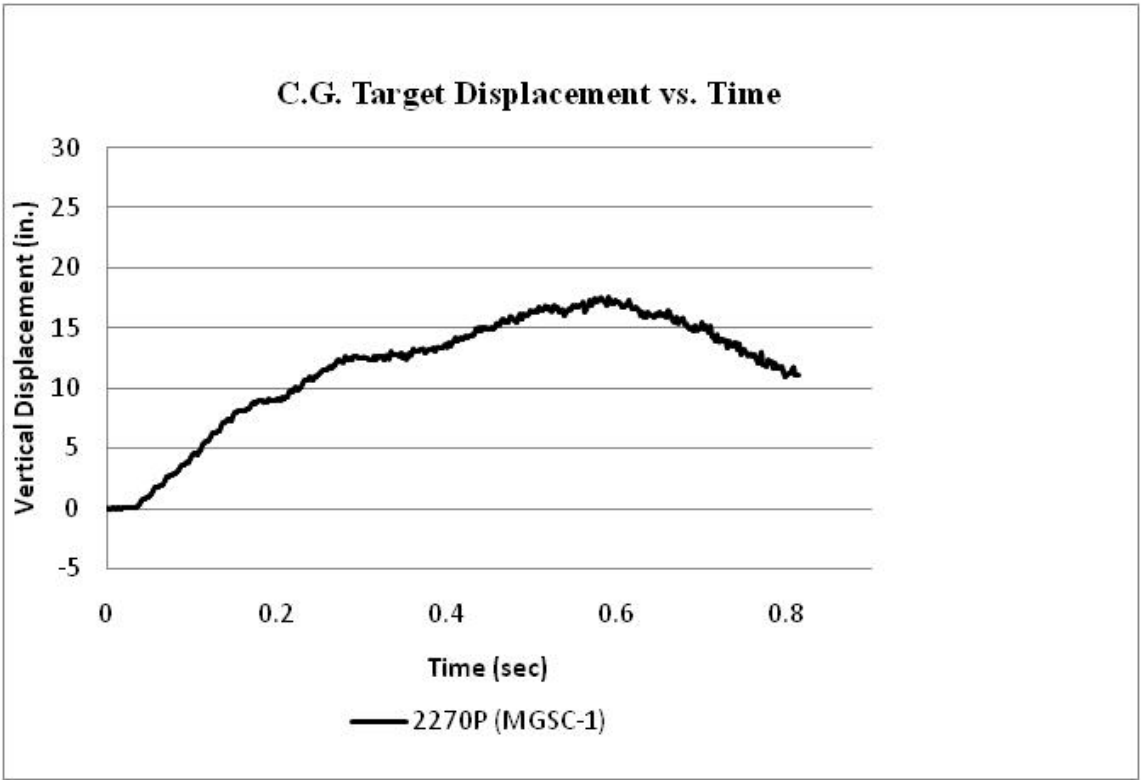

Figure B-1. C.G. Target Vertical Displacement vs. Time, Test MGSC-1 (2270P)

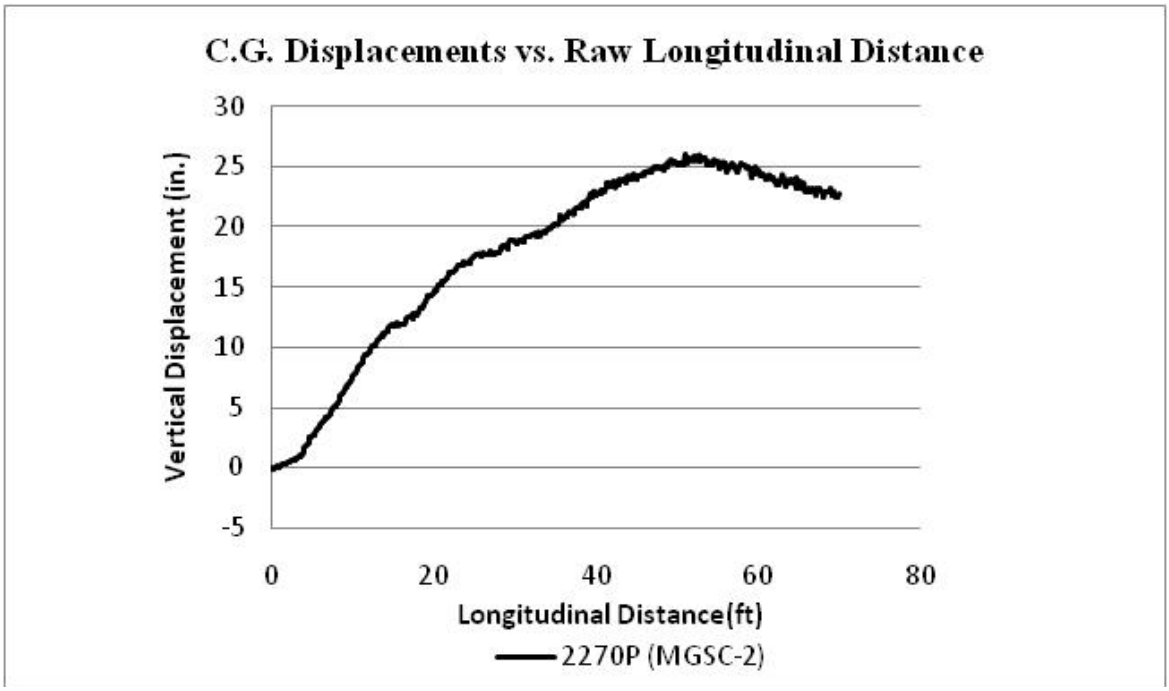

Figure B-2. C.G. Target Vertical Displacement vs. Raw Longitudinal Distance, Test MGSC-1 (2270P)

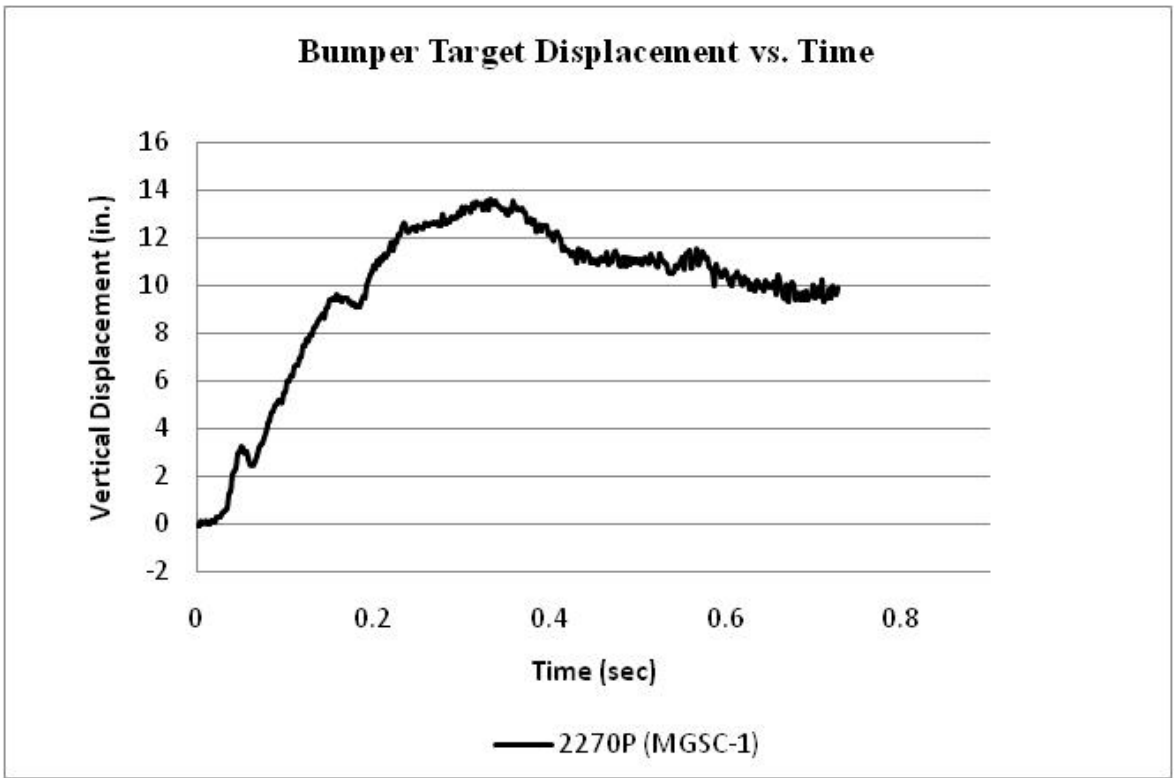

Figure B-3. Bumper Target Vertical Displacement vs. Time, Test MGSC-1 (2270P)

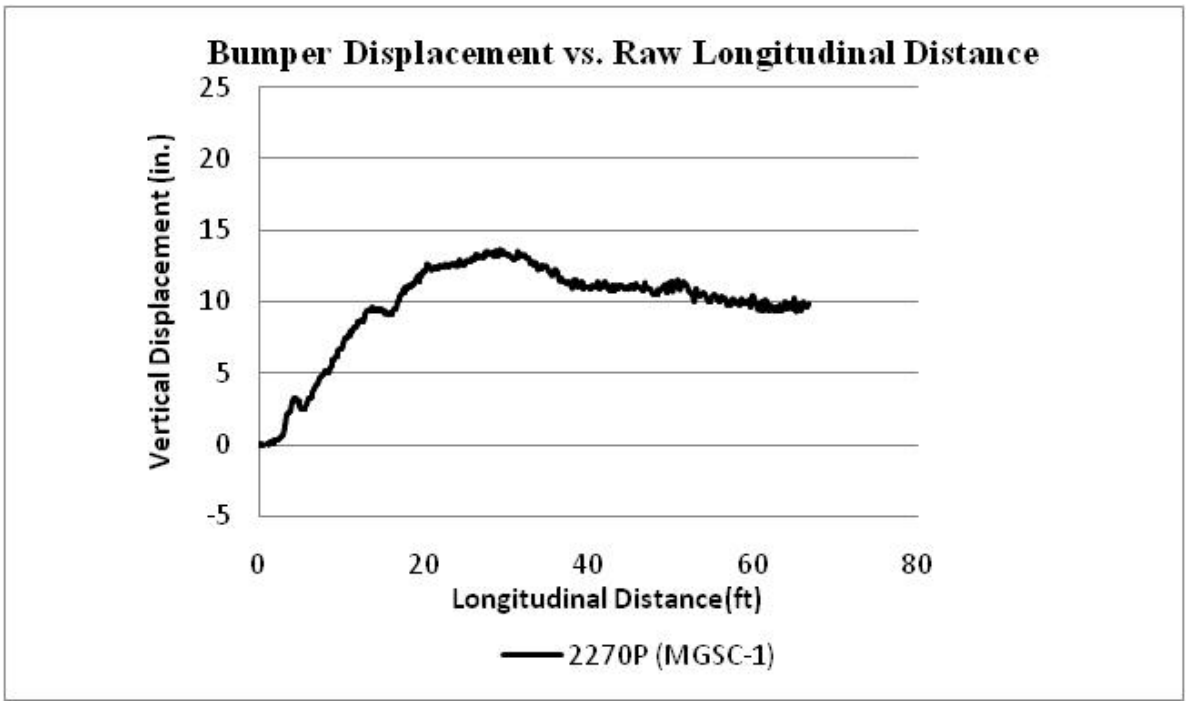

Figure B-4. Bumper Target Vertical Displacement vs. Raw Longitudinal Distance Test MGSC-1 (2270P)

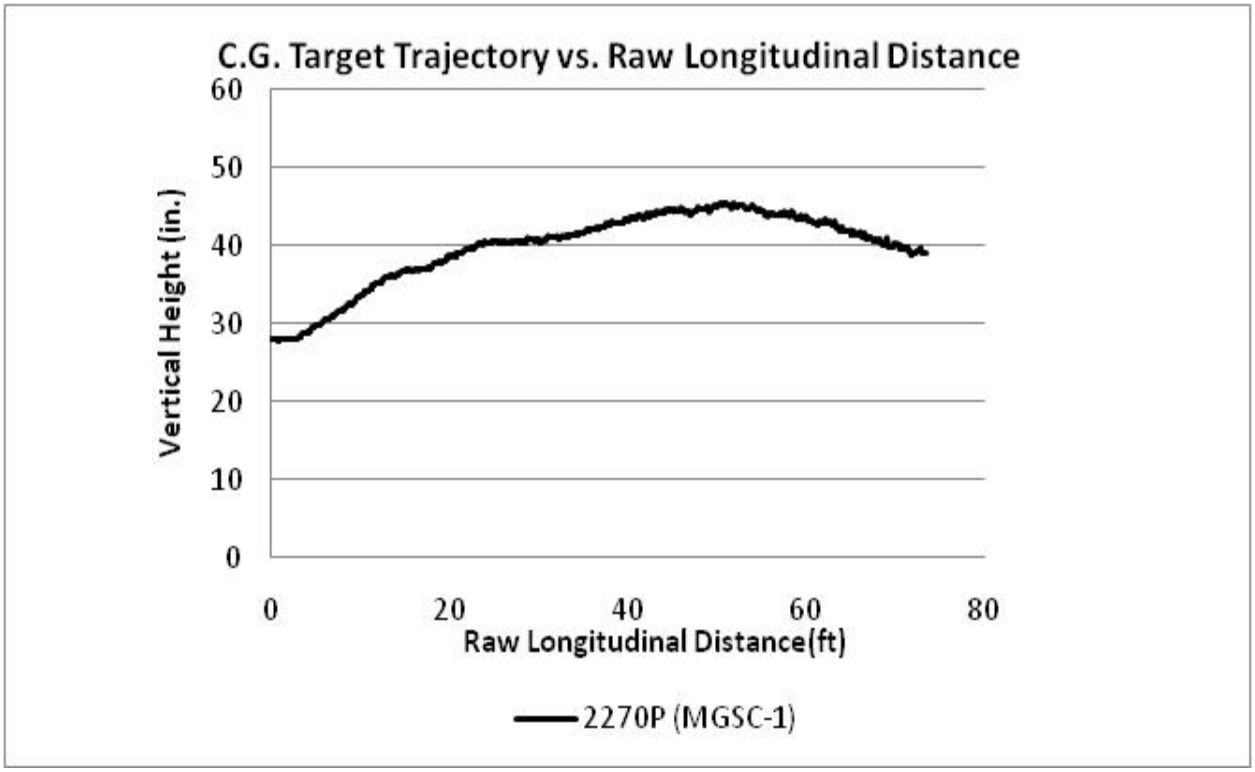

Figure B-5. C.G. Target Trajectory vs. Raw Longitudinal Distance, Test MGSC-1 (2270P)

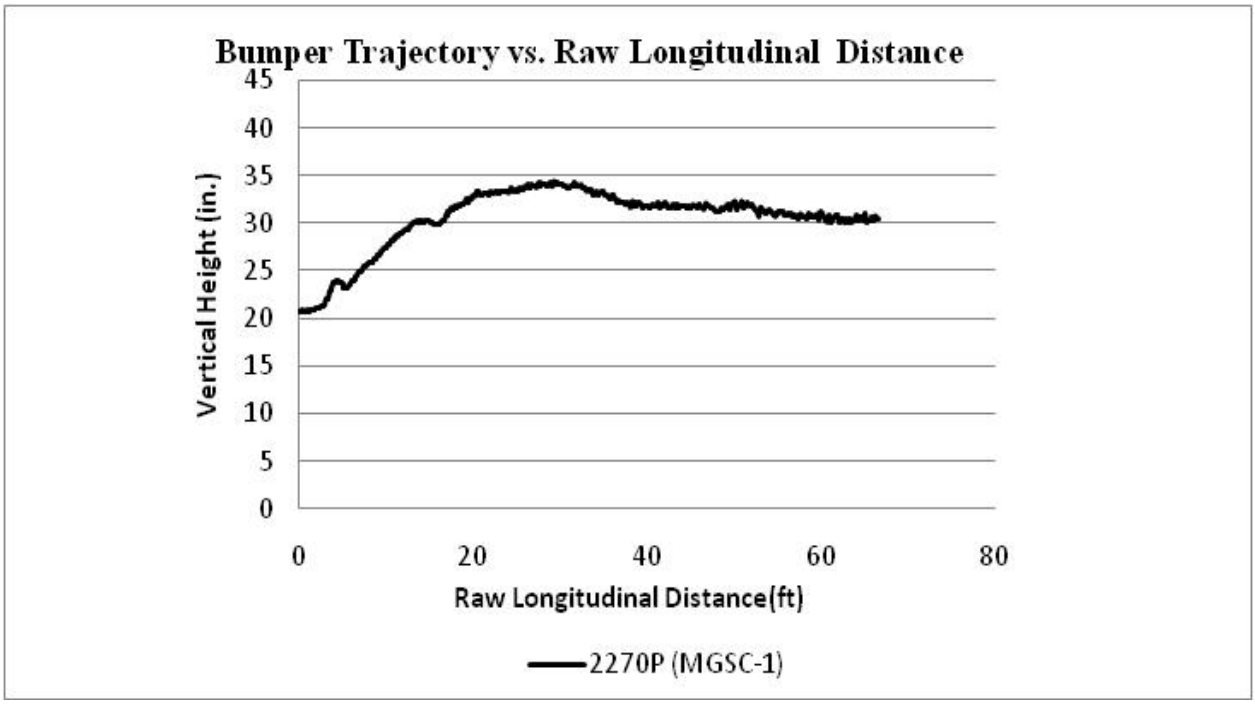

Figure B-6. Bumper Target Trajectory vs. Raw Longitudinal Distance, Test MGSC-1 (2270P)

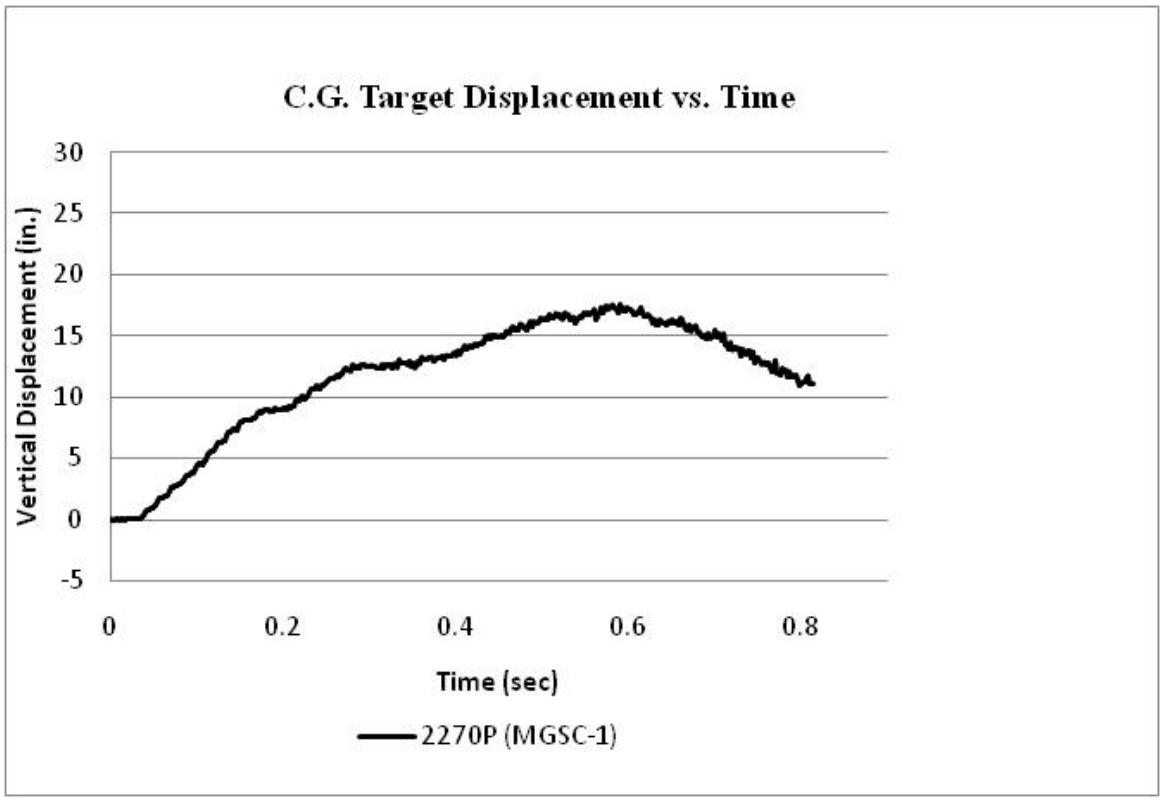

Figure B-7. C.G. Target Vertical Displacement vs. Time, Test MGSC-2 (2270P)

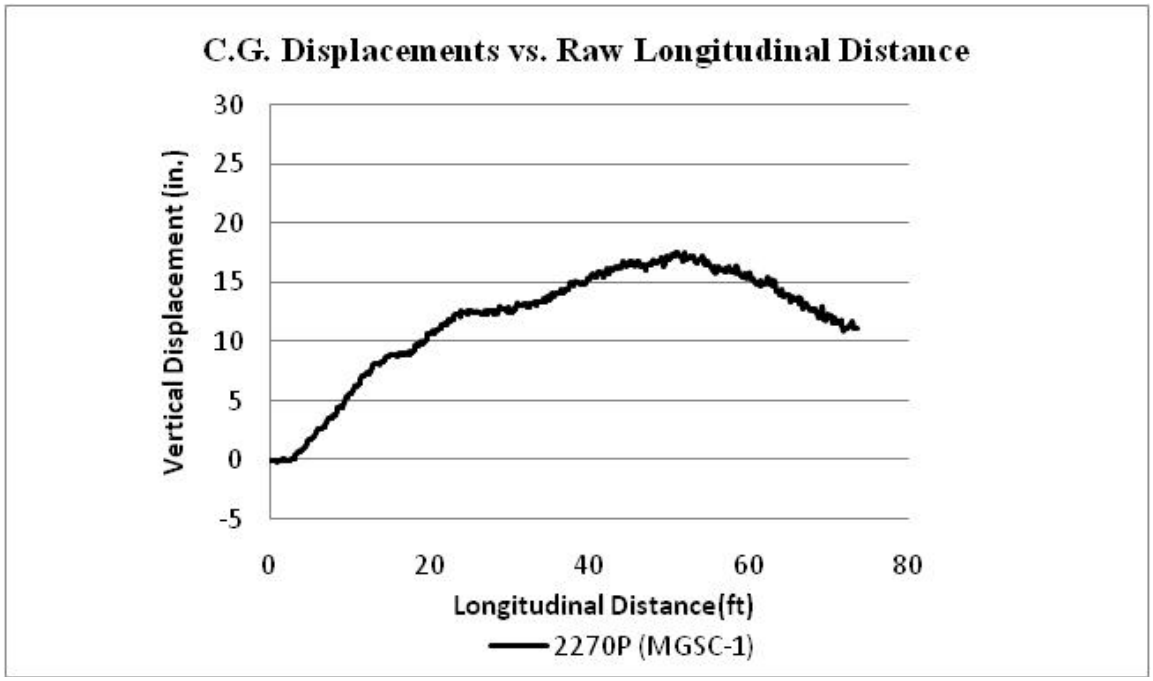

Figure B-8. C.G. Target Vertical Displacement vs. Raw Longitudinal Distance, Test MGSC-2 (2270P)

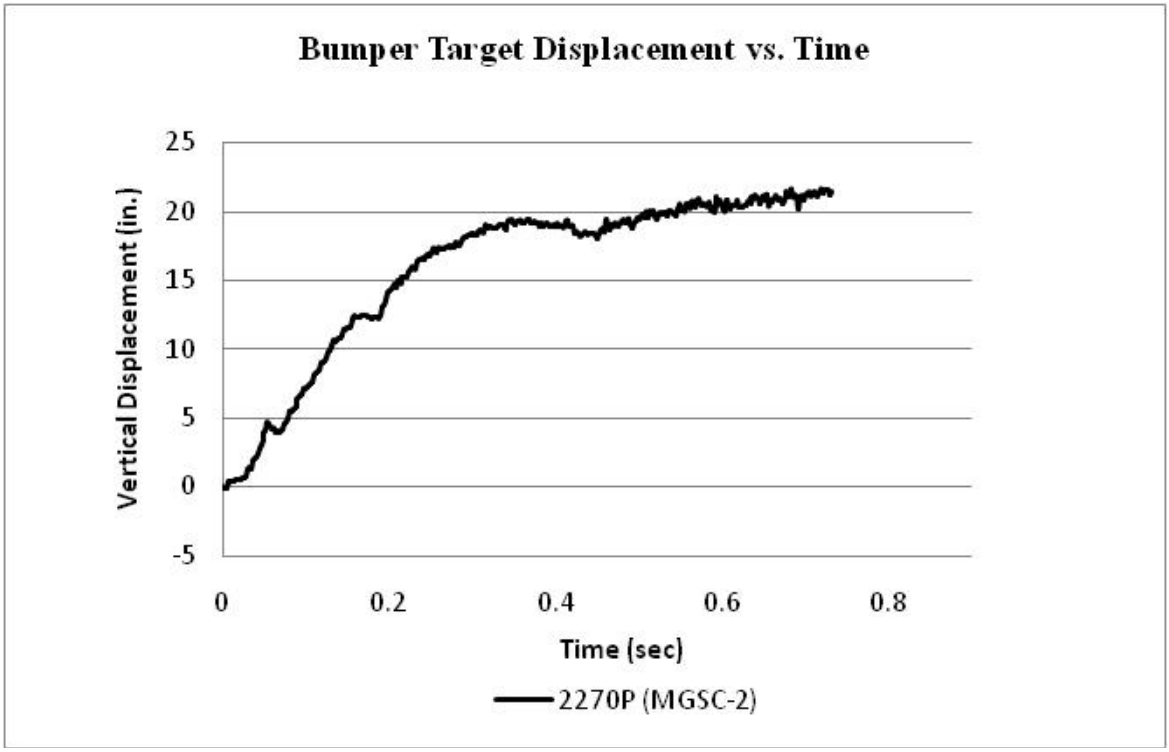

Figure B-9. Bumper Target Vertical Displacement vs. Time, Test MGSC-2 (2270P)

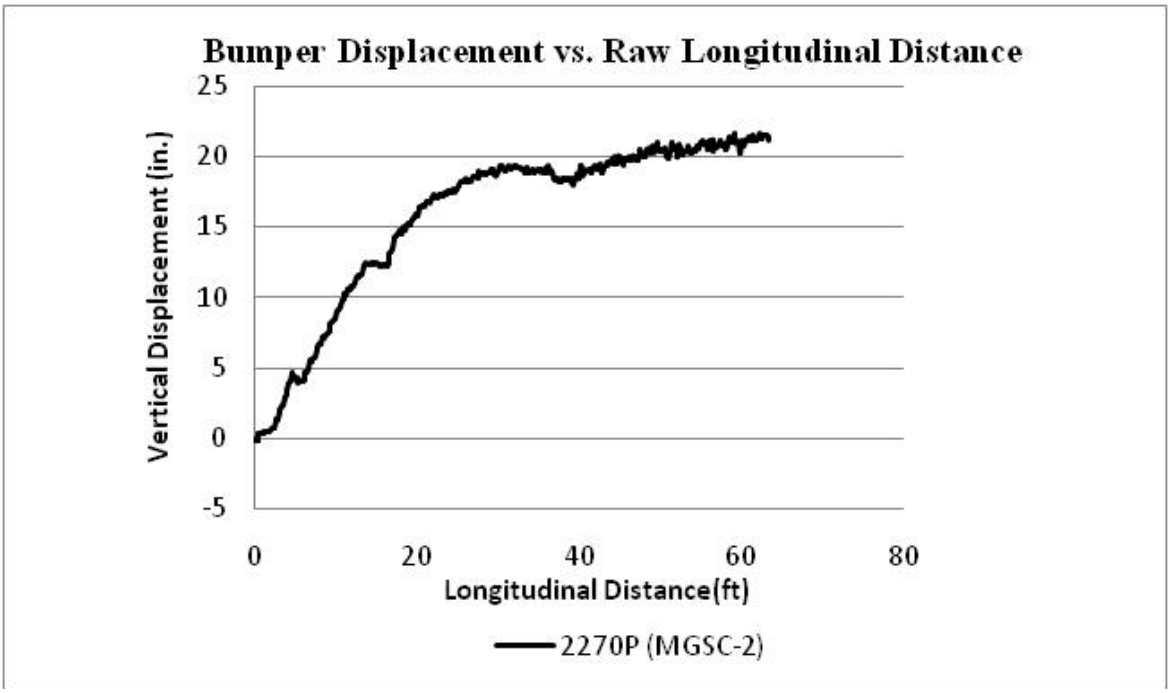

Figure B-10. Bumper Target Vertical Displacement vs. Raw Longitudinal Distance, Test MGSC-2 (2270P)

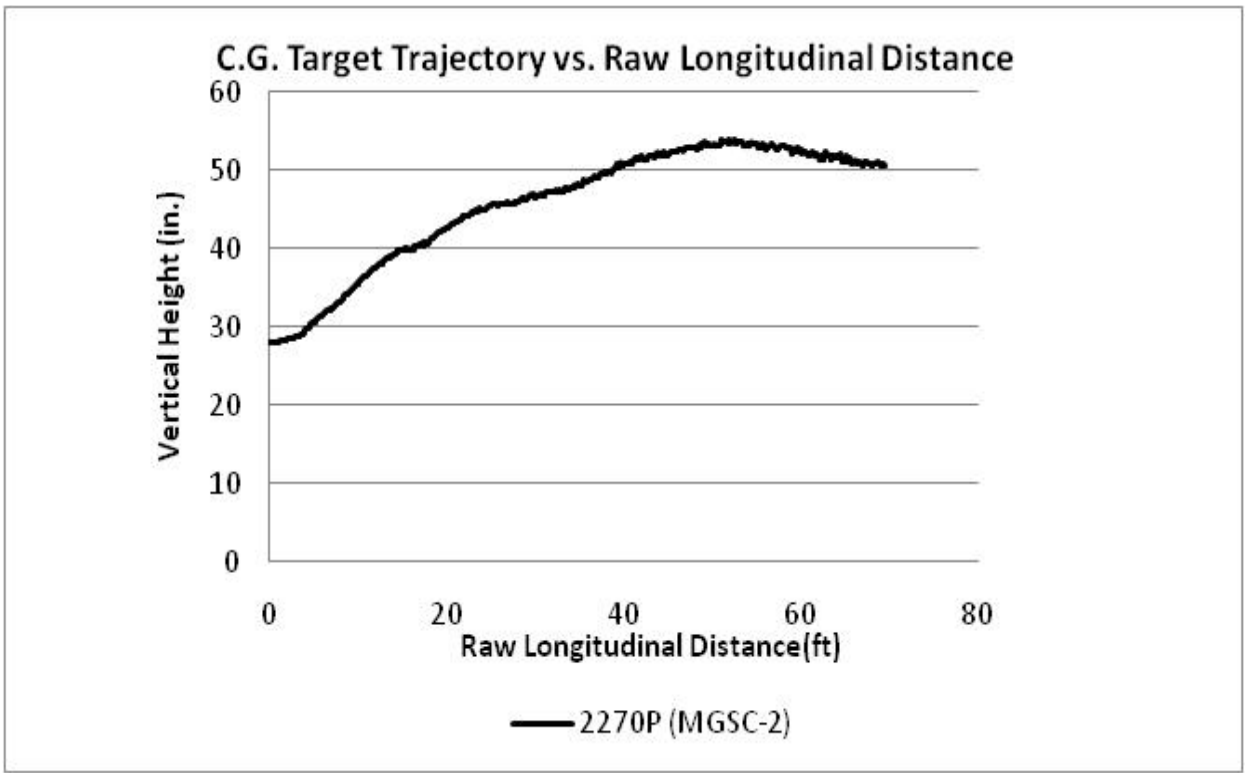

Figure B-11. C.G. Target Trajectory vs. Raw Longitudinal Distance, Test MGSC-2 (2270P)

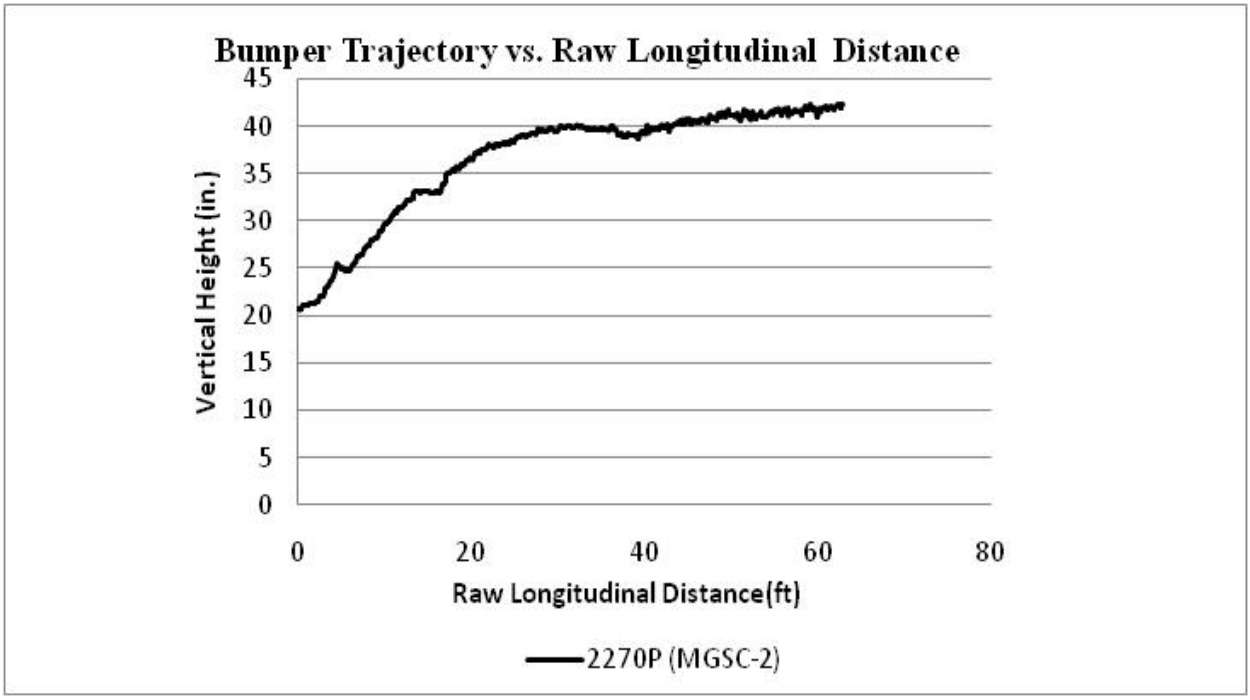

Figure B-12. Bumper Target Trajectory vs. Raw Longitudinal Distance, Test MGSC-2 (2270P)

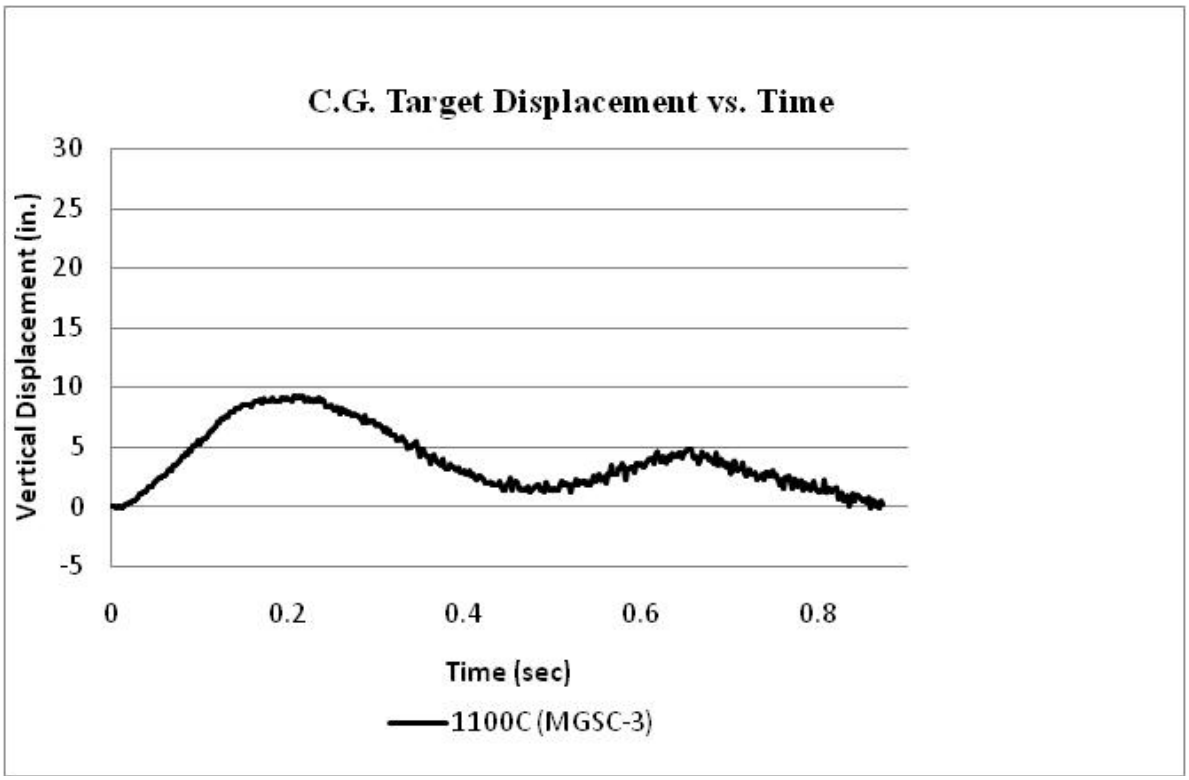

Figure B-13. C.G. Target Vertical Displacement vs. Time, Test MGSC-3 (1100C)

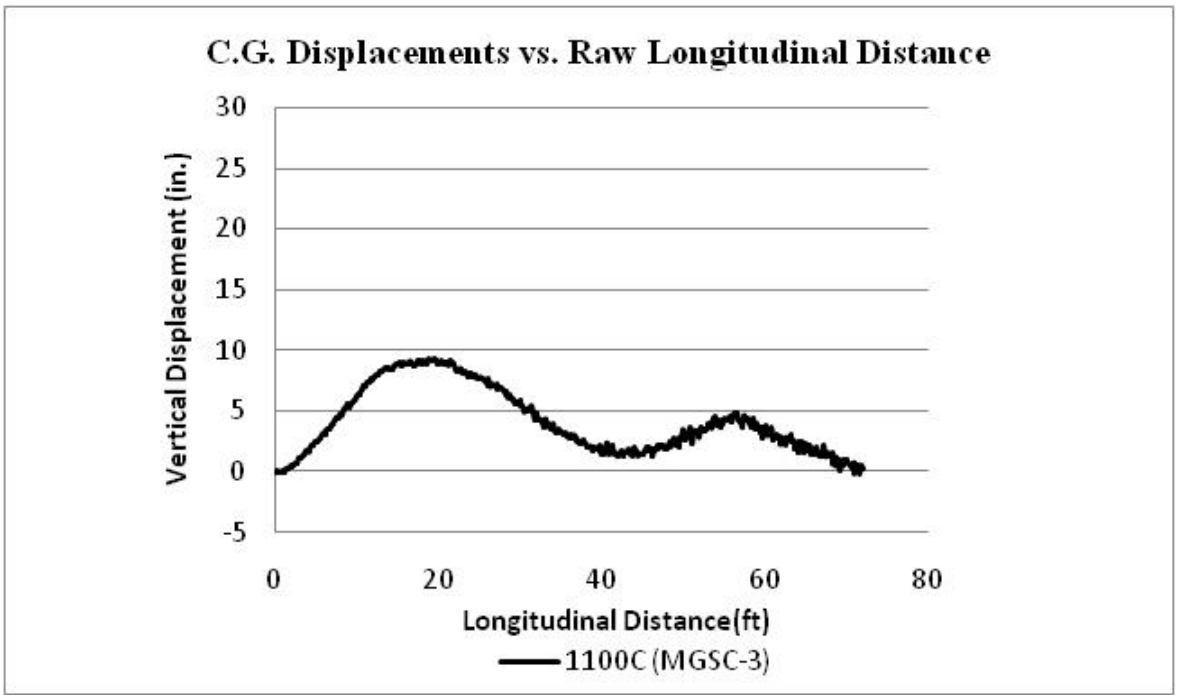

Figure B-14. C.G. Target Vertical Displacement vs. Raw Longitudinal Distance, Test MGSC-3 (1100C)

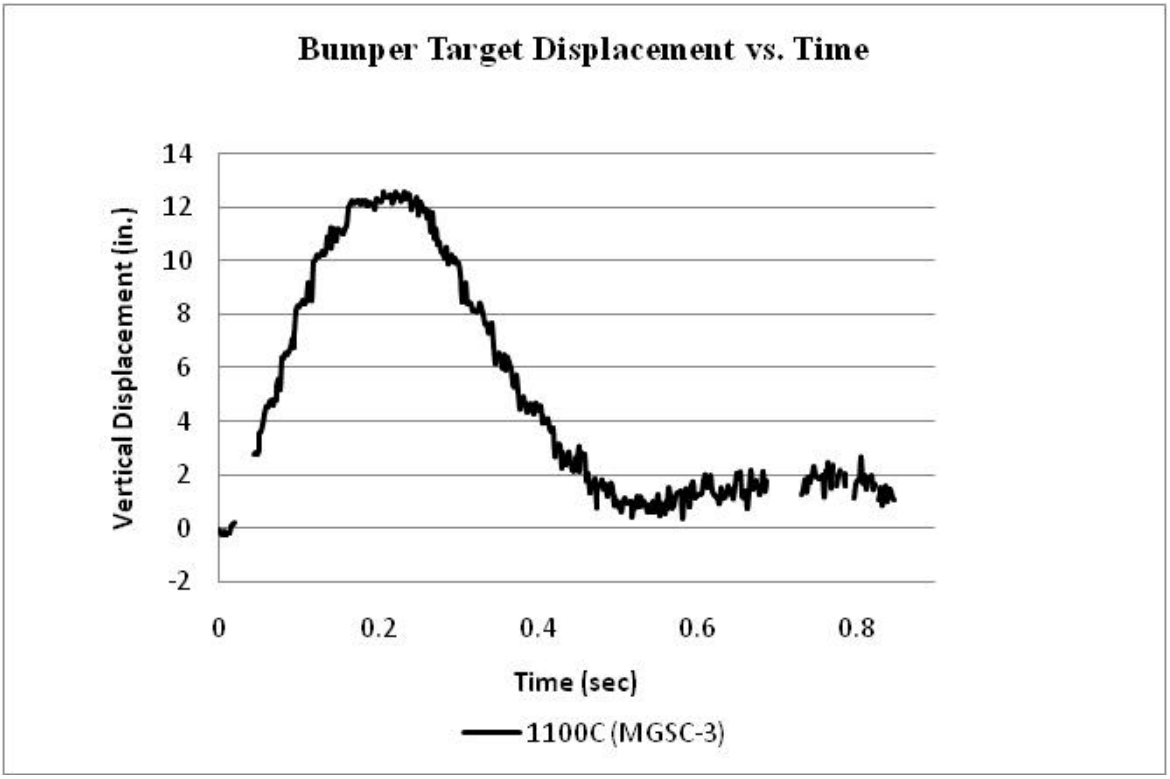

Figure B-15. Bumper Target Vertical Displacement vs. Time, Test MGSC-3 (1100C)

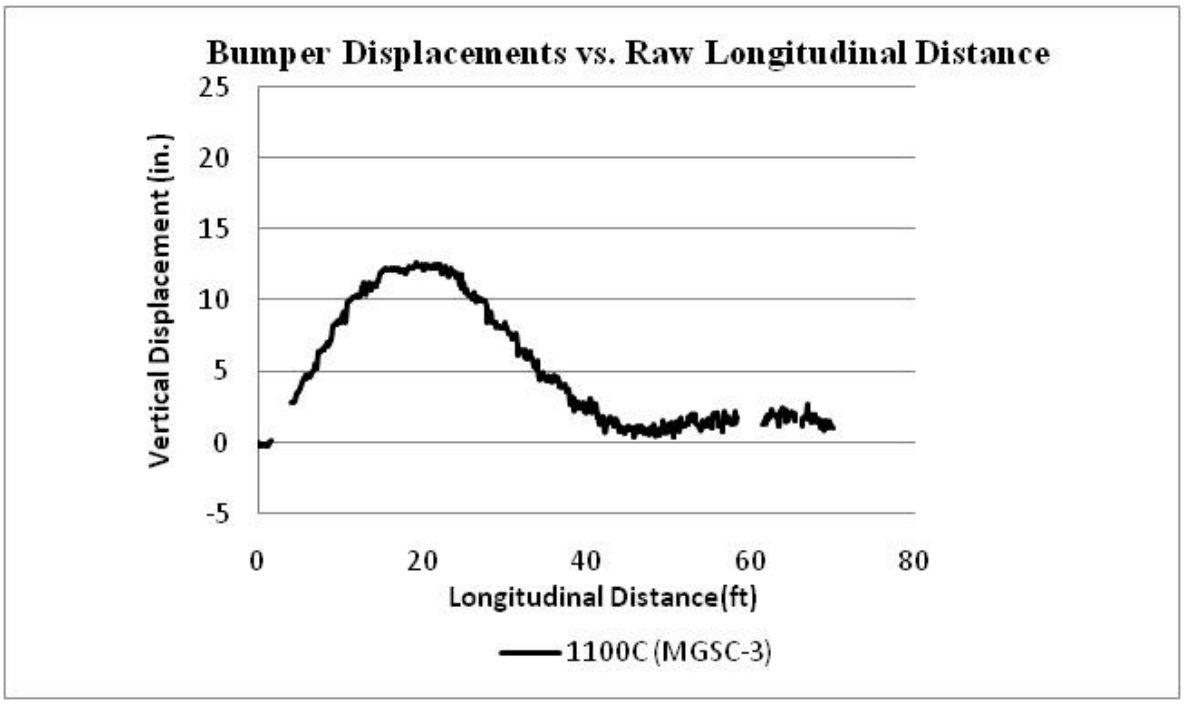

Figure B-16. Bumper Target Vertical Displacement vs. Raw Longitudinal Distance, Test MGSC-3 (1100C)

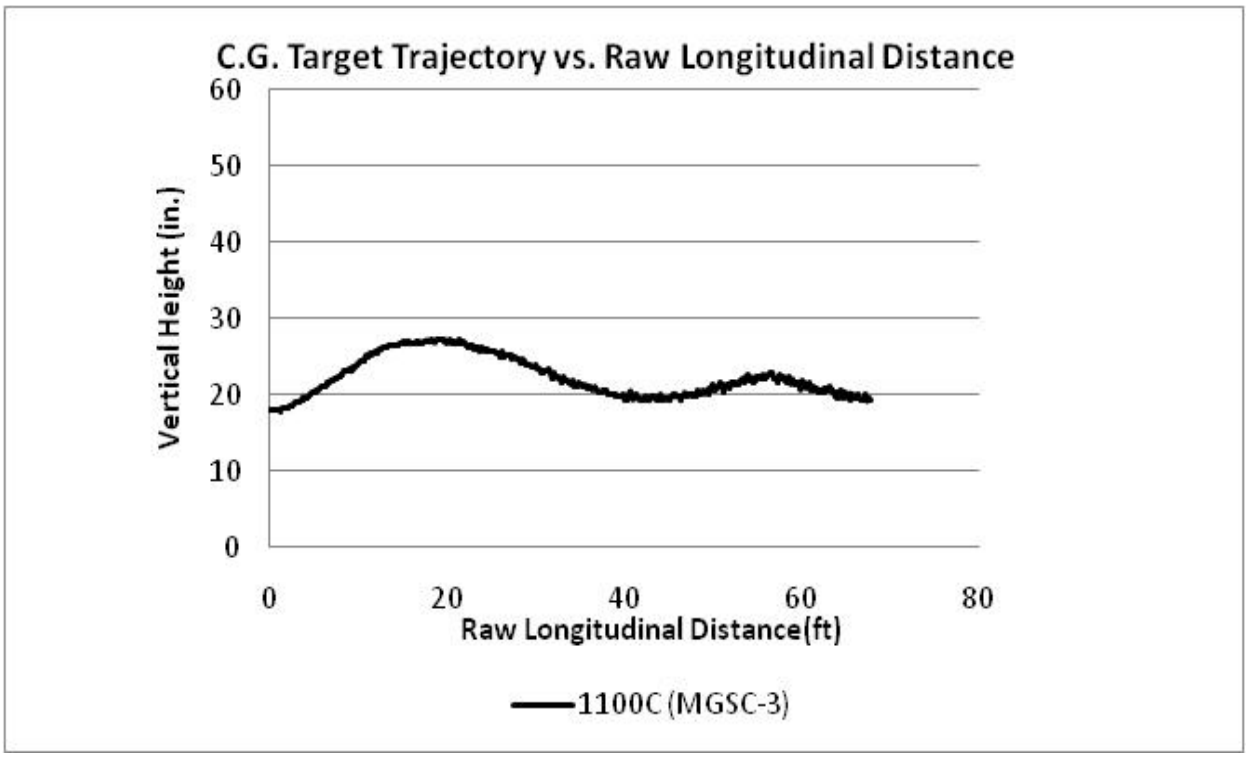

Figure B-17. C.G. Target Trajectory vs. Raw Longitudinal Distance, Test MGSC-3 (1100C)

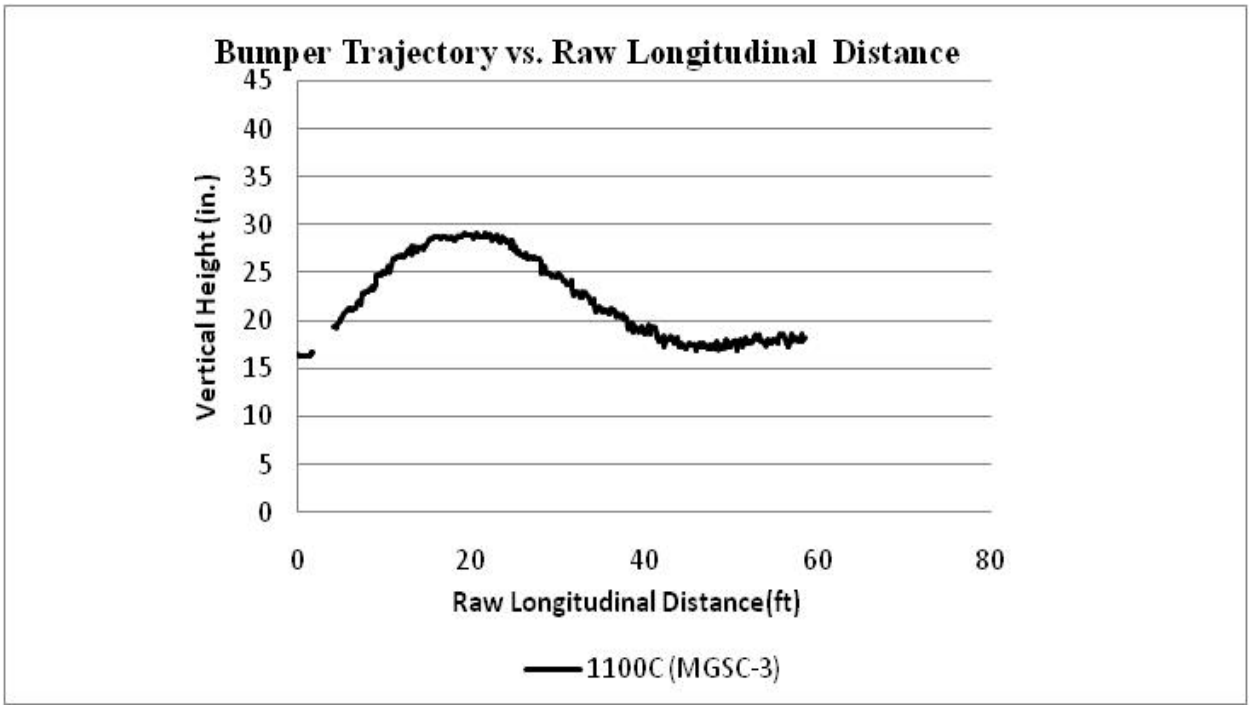

Figure B-18. Bumper Target Trajectory vs. Raw Longitudinal Distance, Test MGSC-3 (1100C)

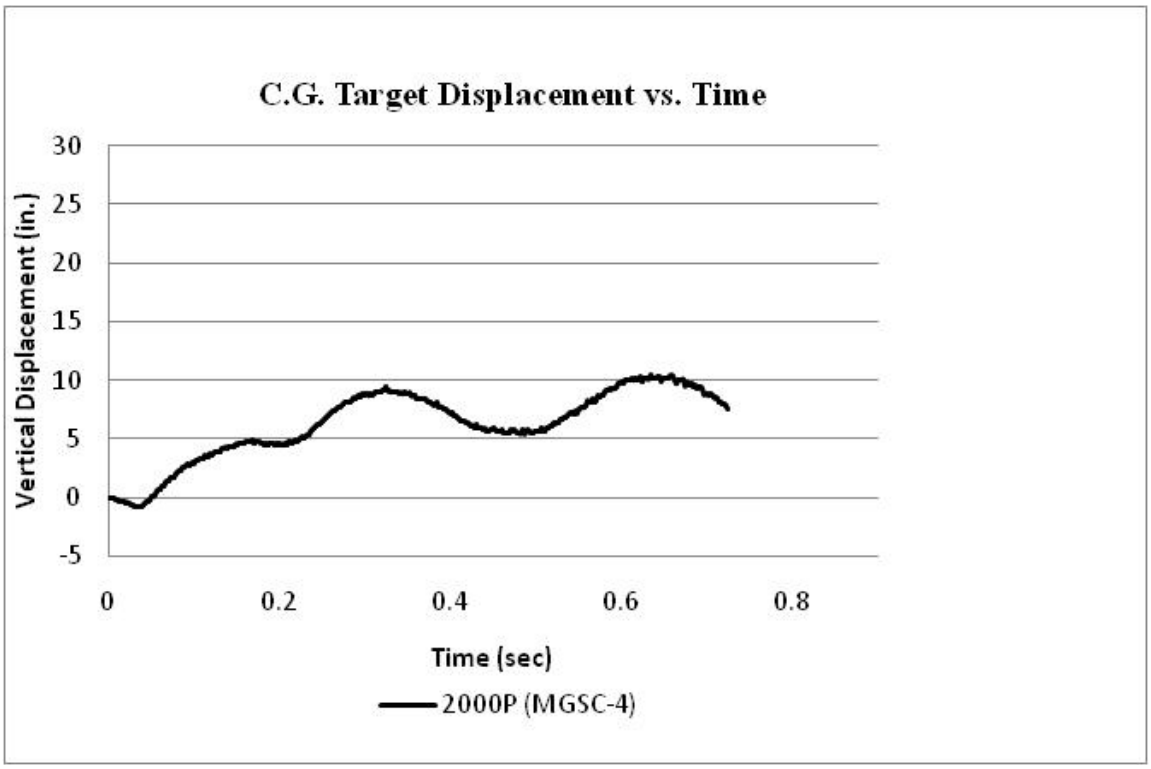

Figure B-19. C.G. Target Vertical Displacement vs. Time, Test MGSC-4 (2000P)

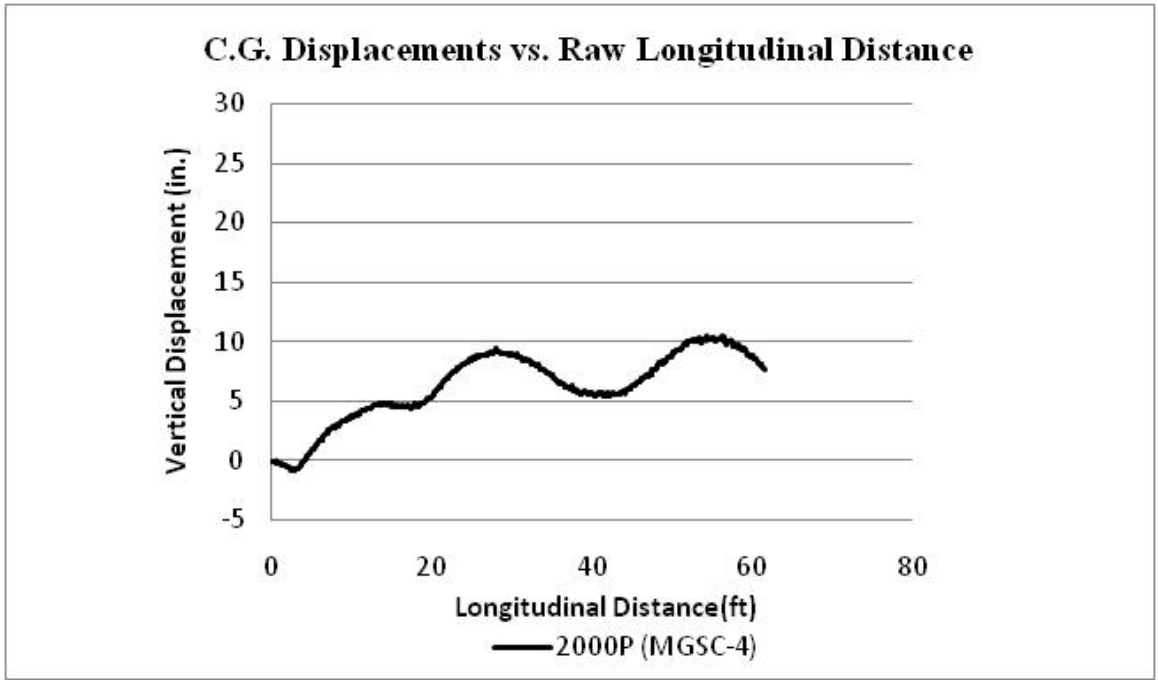

Figure B-20. C.G. Target Vertical Displacement vs. Raw Longitudinal Distance, Test MGSC-4 (2000P)

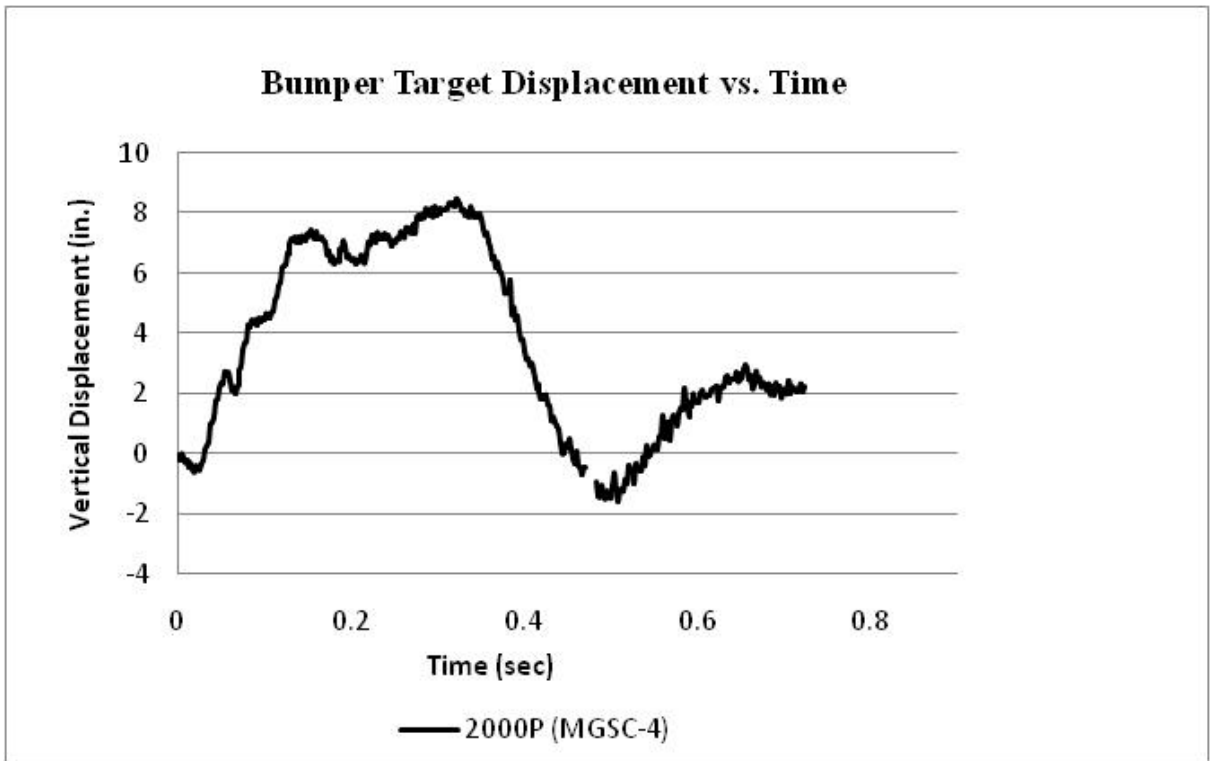

Figure B-21. Bumper Target Vertical Displacement vs. Time, Test MGSC-4 (2000P)

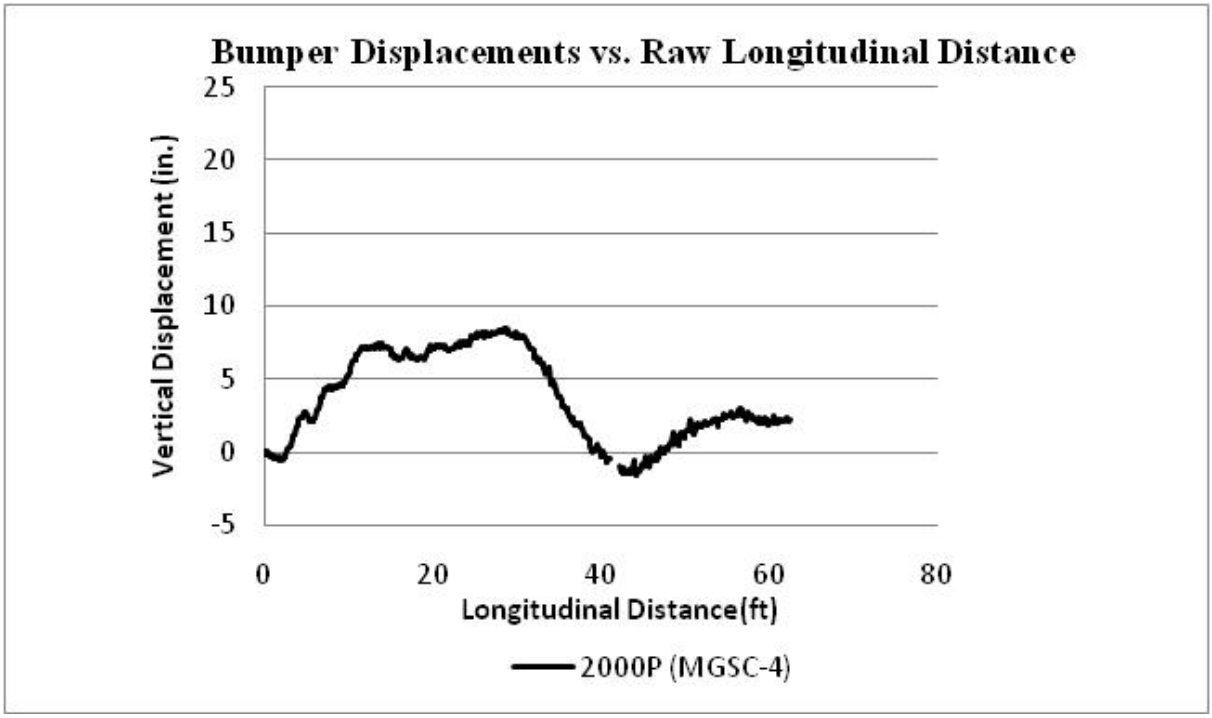

Figure B-22. Bumper Target Vertical Displacement vs. Raw Longitudinal Distance, Test MGSC-4 (2000C)

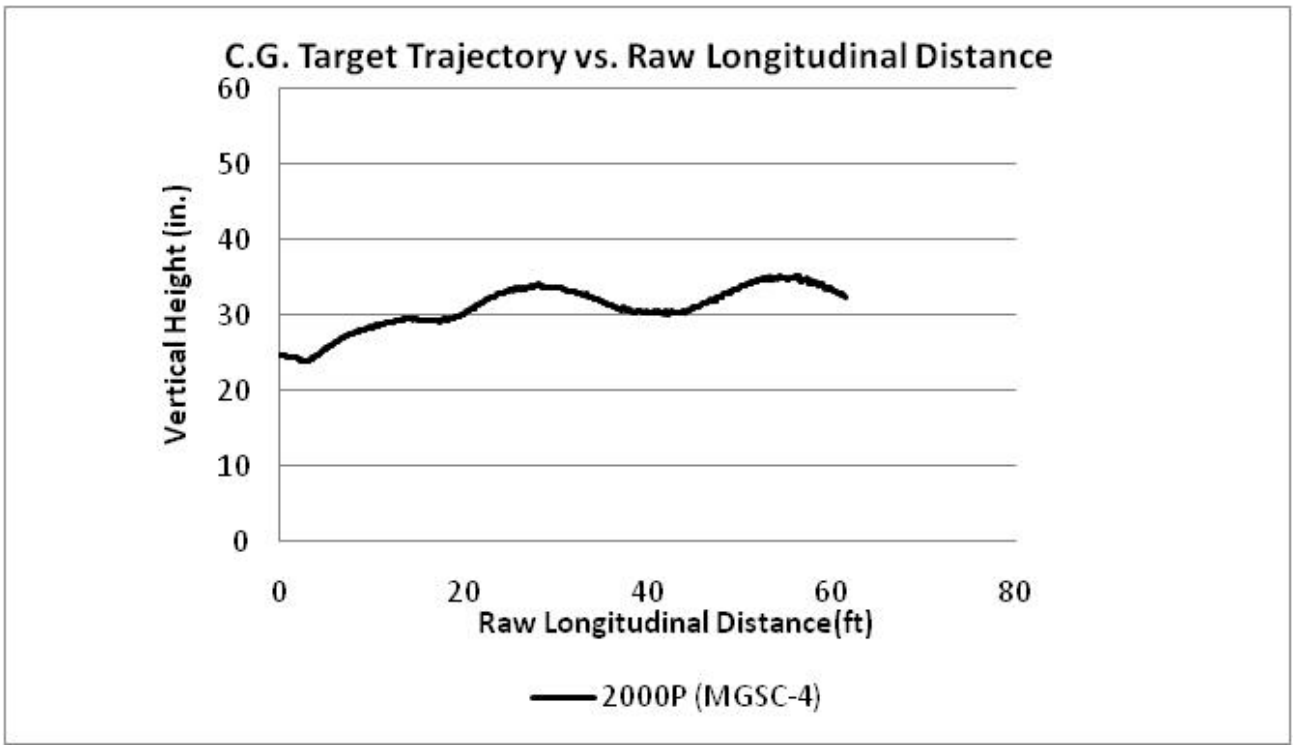

Figure B-23. C.G. Target Trajectory vs. Raw Longitudinal Distance, Test MGSC-4 (2000P)

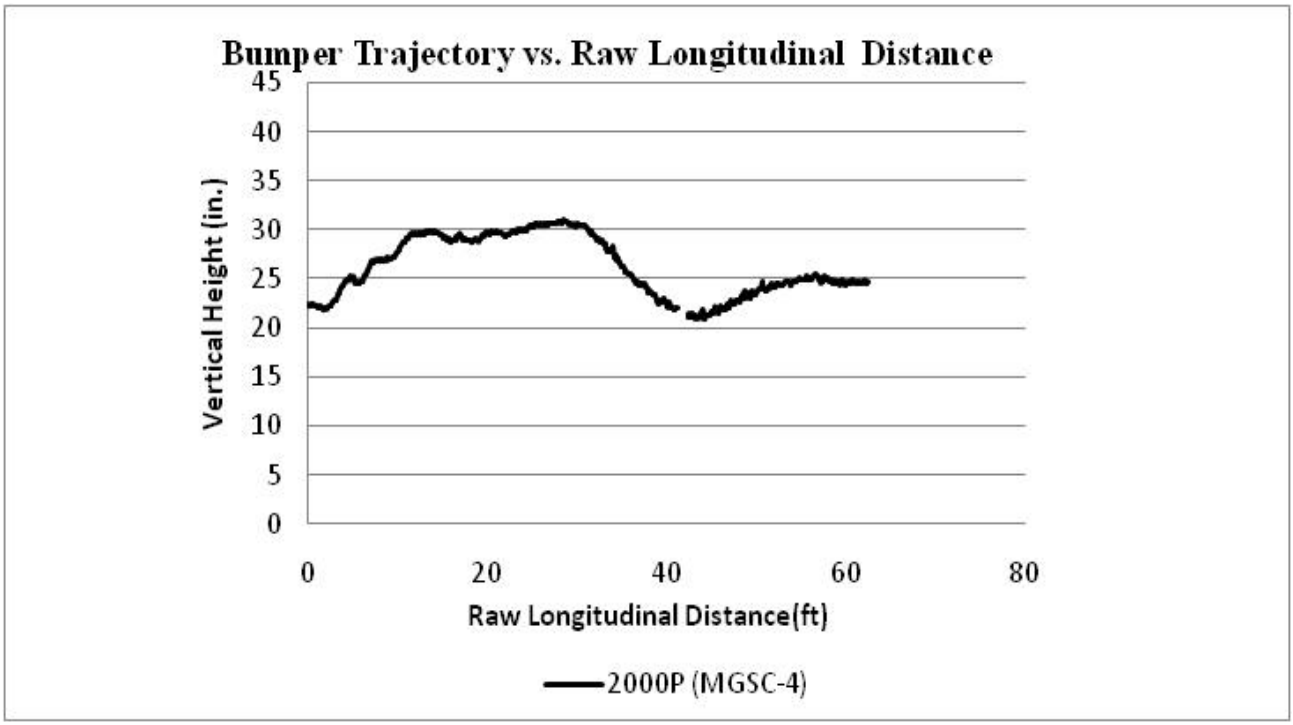

Figure B-24. Bumper Target Trajectory vs. Raw Longitudinal Distance, Test MGSC-4 (2000P)

APPENDIX C

ACCELOROMETER AND RATE TRANSDUCER DATA

Figure C-1. Graph of Longitudinal Deceleration, Test MGSC-1 (2270P)
Figure C-2. Graph of Longitudinal Occupant Impact Velocity, Test MGSC-1 (2270P)
Figure C-3. Graph of Longitudinal Occupant Displacement, Test MGSC-1 (2270P)
Figure C-4. Graph of Lateral Occupant Impact Velocity, Test MGSC-1 (2270P)
Figure C-5. Graph of Lateral Deceleration, Test MGSC-1 (2270P)
Figure C-6. Graph of Lateral Occupant Displacement, Test MGSC-1 (2270P)
Figure C-7. Graph of Roll, Pitch, and Yaw Angular Displacements, Test MGSC-1 (2270P)
Figure C-8. Graph of Longitudinal Deceleration, Test MGSC-1 (2270P)
Figure C-9. Graph of Longitudinal Occupant Impact Velocity, Test MGSC-1 (2270P)
Figure C-10. Graph of Longitudinal Occupant Displacement, Test MGSC-2 (2270P)
Figure C-11. Graph of Lateral Occupant Impact Velocity, Test MGSC-2 (2270P)
Figure C-12. Graph of Lateral Deceleration, Test MGSC-2 (2270P)
Figure C-13. Graph of Lateral Occupant Displacement, Test MGSC-2 (2270P)
Figure C-14. Graph of Roll, Pitch, and Yaw Angular Displacements, Test MGSC-2 (2270P)
Figure C-15. Graph of Longitudinal Deceleration, Test MGSC-3 (1100C)
Figure C-16. Graph of Longitudinal Occupant Impact Velocity, Test MGSC-3 (1100C)
Figure C-17. Graph of Longitudinal Occupant Displacement, Test MGSC-3 (1100C)
Figure C-18. Graph of Lateral Occupant Impact Velocity, Test MGSC-3 (1100C)
Figure C-19. Graph of Lateral Deceleration, Test MGSC-3 (1100C)
Figure C-20. Graph of Lateral Occupant Displacement, Test MGSC-3 (1100C)
Figure C-21. Graph of Roll, Pitch, and Yaw Angular Displacements, Test MGSC-3 (1100C)
Figure C-22. Graph of Longitudinal Deceleration, Test MGSC-4 (2000P)
Figure C-23. Graph of Longitudinal Occupant Impact Velocity, Test MGSC-4 (2000P)
Figure C-24. Graph of Longitudinal Occupant Displacement, Test MGSC-4 (2000P)
Figure C-25. Graph of Lateral Occupant Impact Velocity, Test MGSC-4 (2000P)
Figure C-26. Graph of Lateral Deceleration, Test MGSC-4 (2000P)
Figure C-27. Graph of Lateral Occupant Displacement, Test MGSC-4 (2000P)
Figure C-28. Graph of Roll, Pitch, and Yaw Angular Displacements, Test MGSC-4 (2000P)

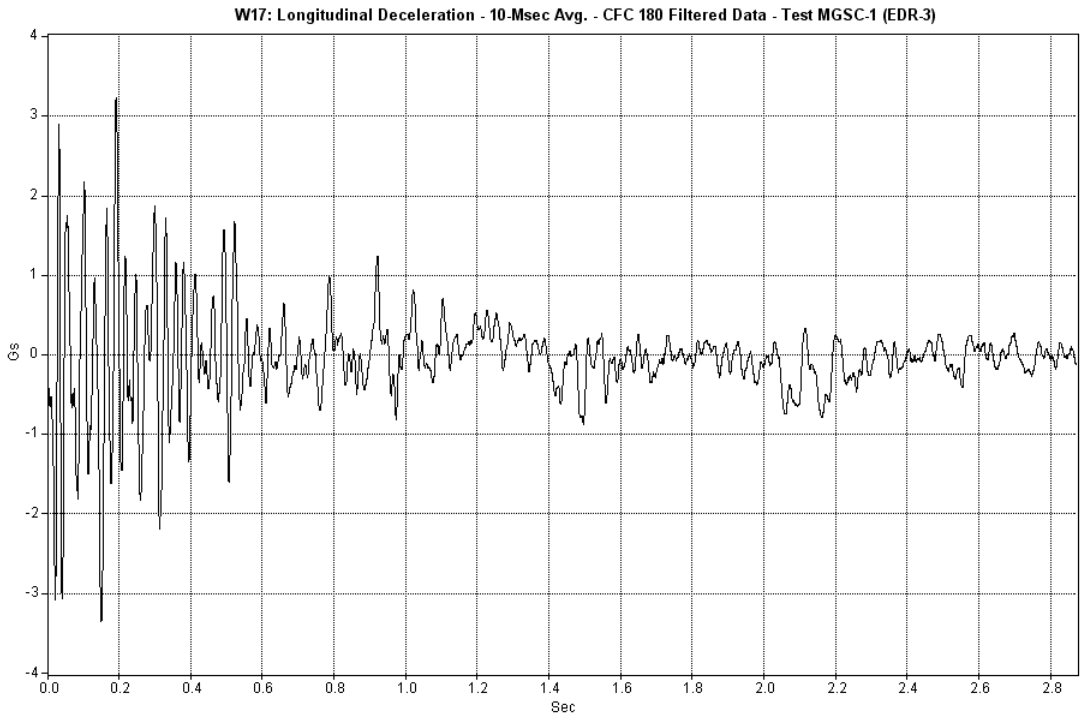

Figure C-1. Graph of Longitudinal Deceleration, Test MGSC-1 (2270P)

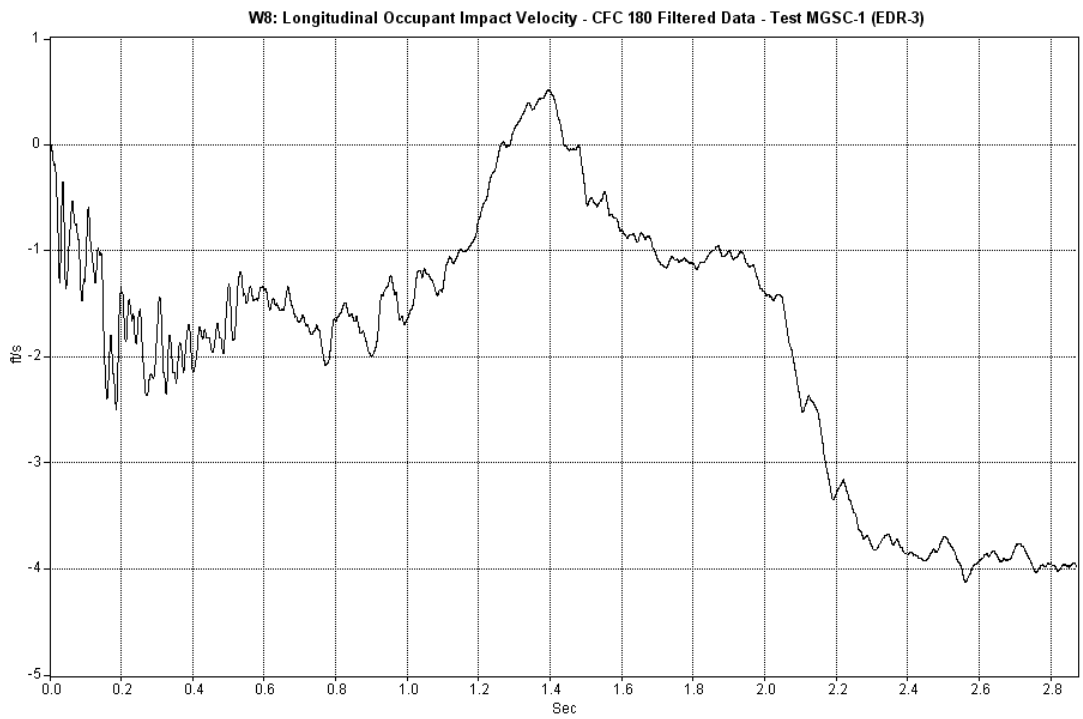

Figure C-2. Graph of Longitudinal Occupant Impact Velocity, Test MGSC-1 (2270P)

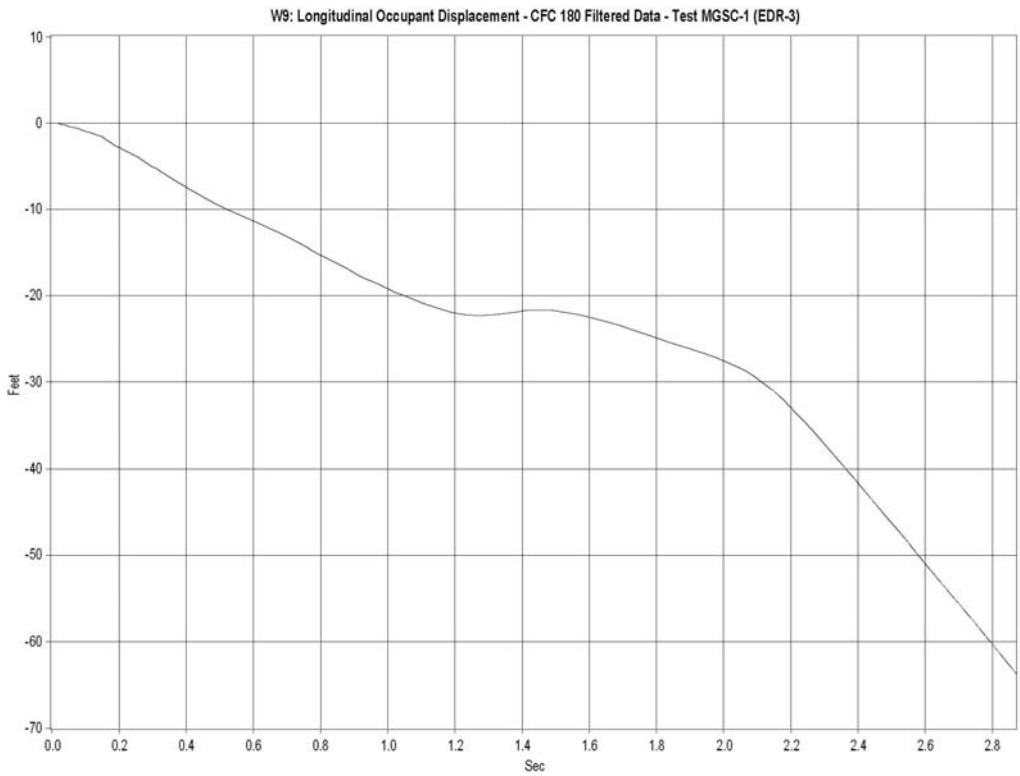

Figure C-3. Graph of Longitudinal Occupant Displacement, Test MGSC-1 (2270P)

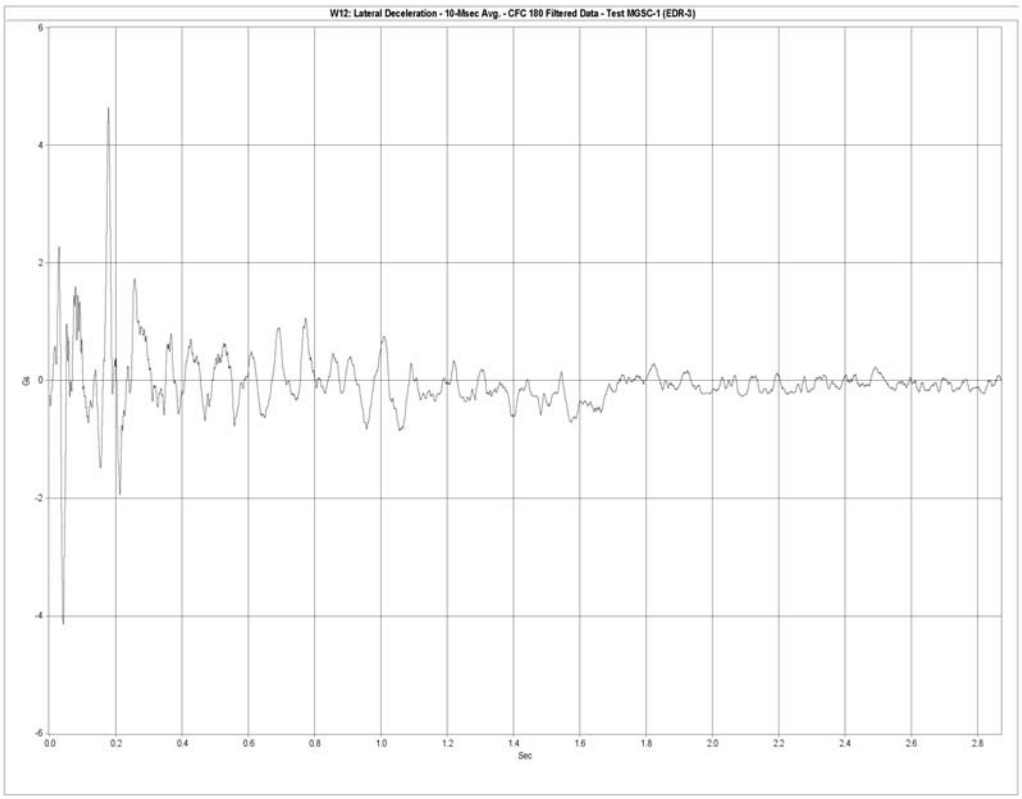

Figure C- 4. Graph of Lateral Deceleration, Test MGSC-1 (2270P)

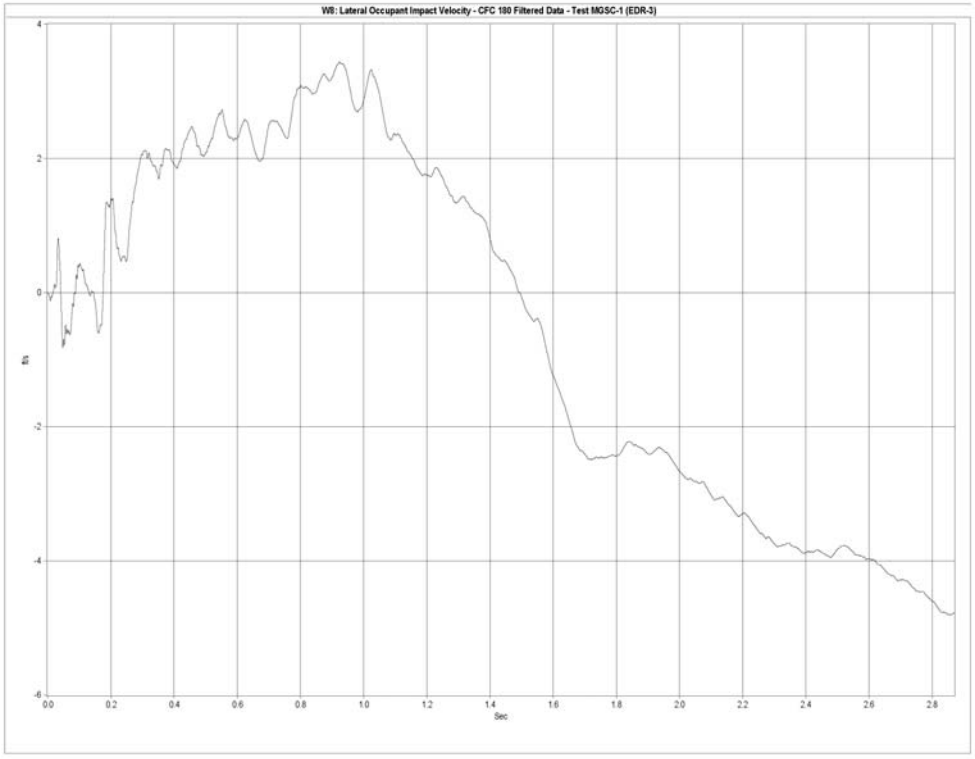

Figure C-5. Graph of Lateral Occupant Impact Velocity, Test MGSC-1 (2270P)

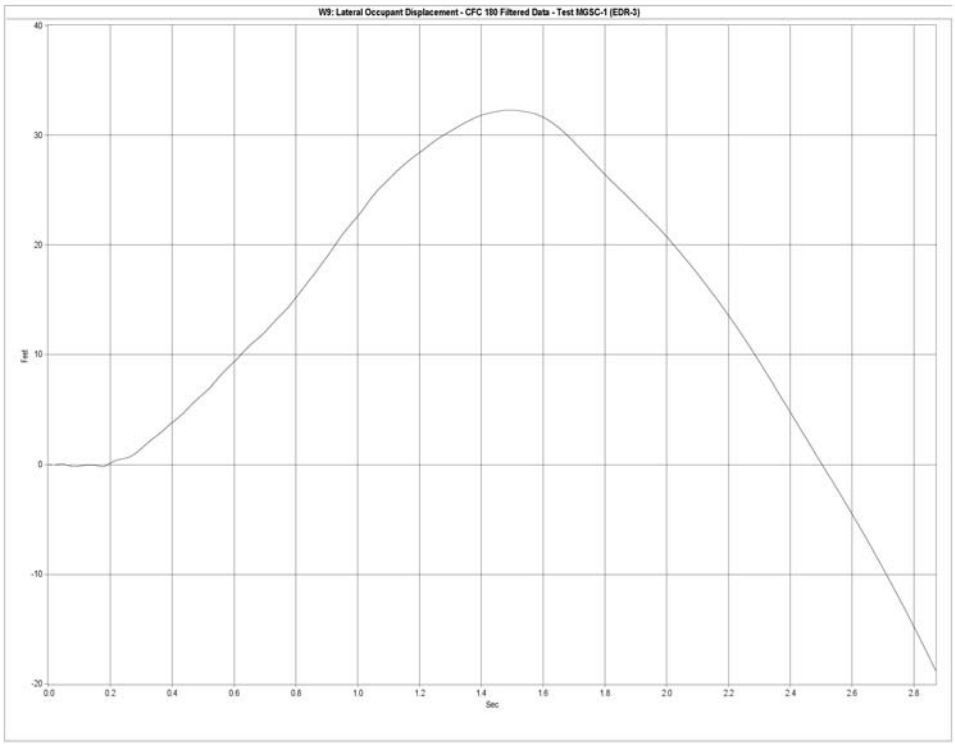

Figure C-6. Graph of Lateral Occupant Displacement, Test MGSC-1 (2270P)

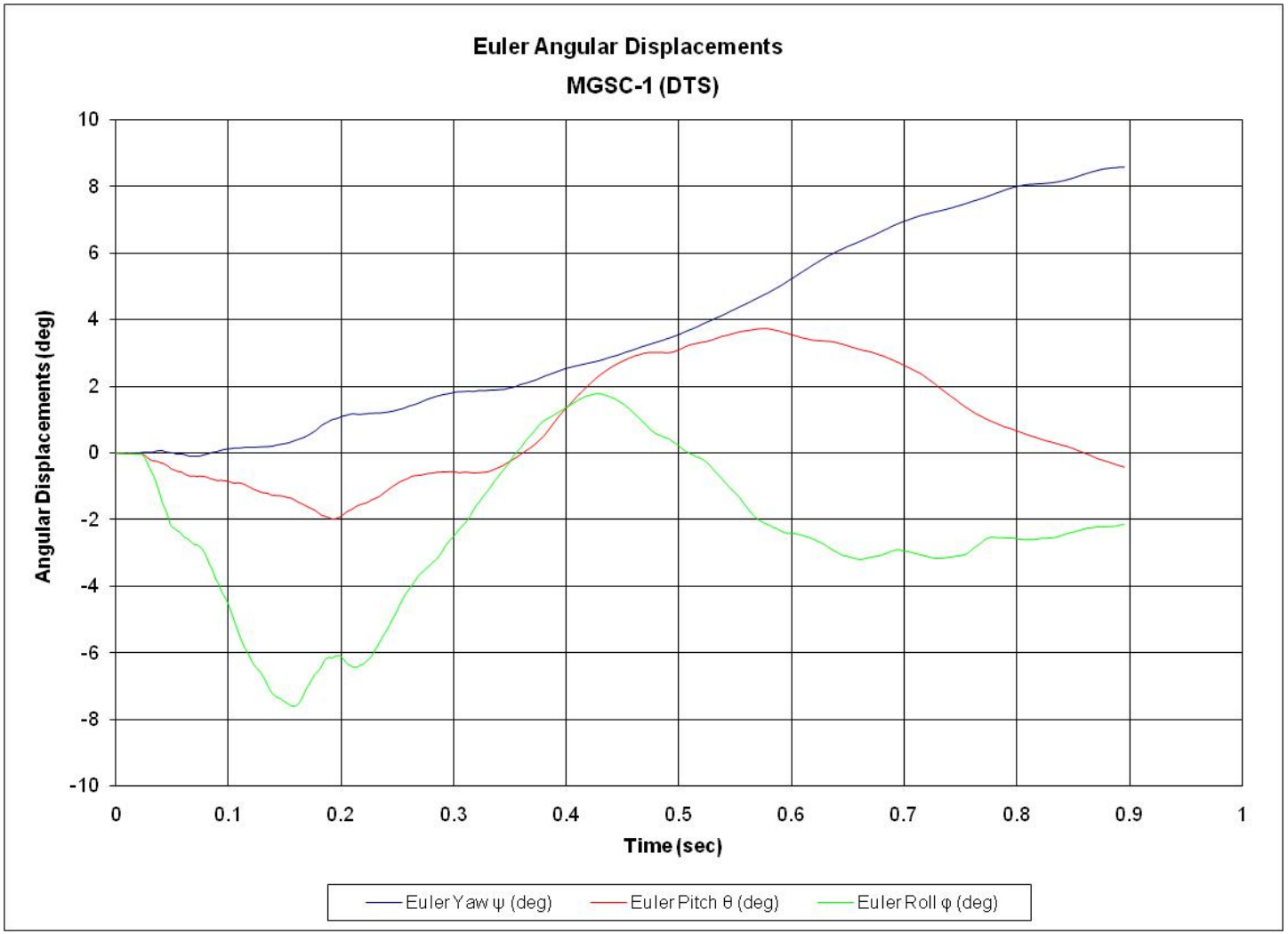

Figure C-7. Graph of Roll, Pitch, and Yaw Angular Displacements, Test MGSC-1 (2270P)

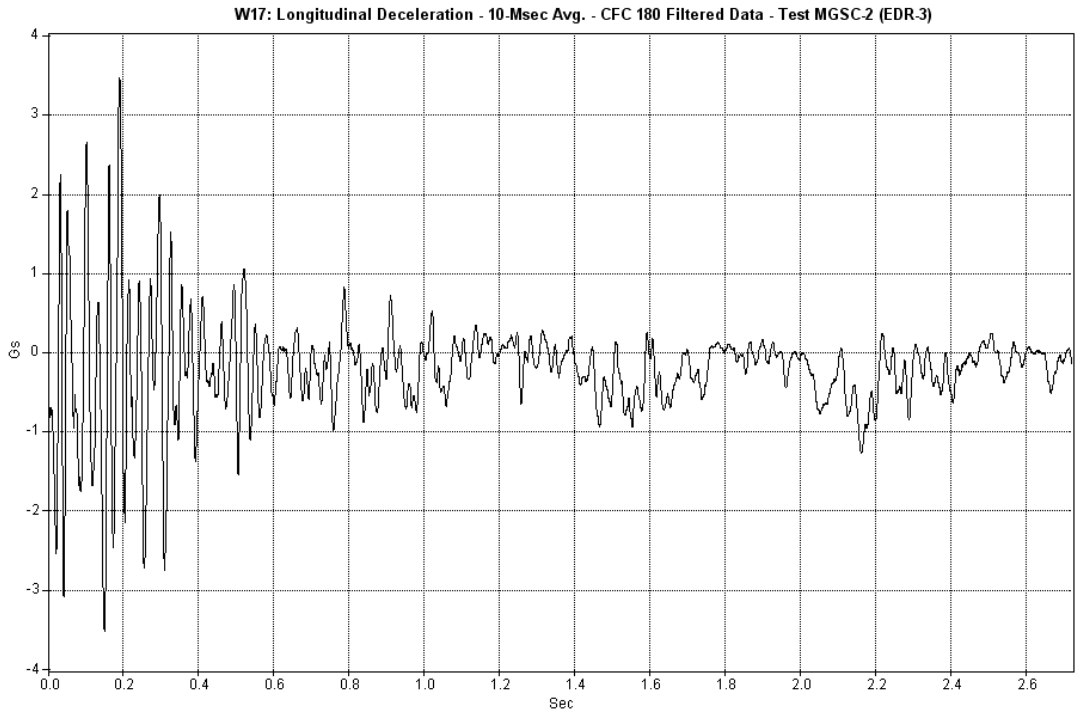

Figure C-8. Graph of Longitudinal Deceleration, Test MGSC-2 (2270P)

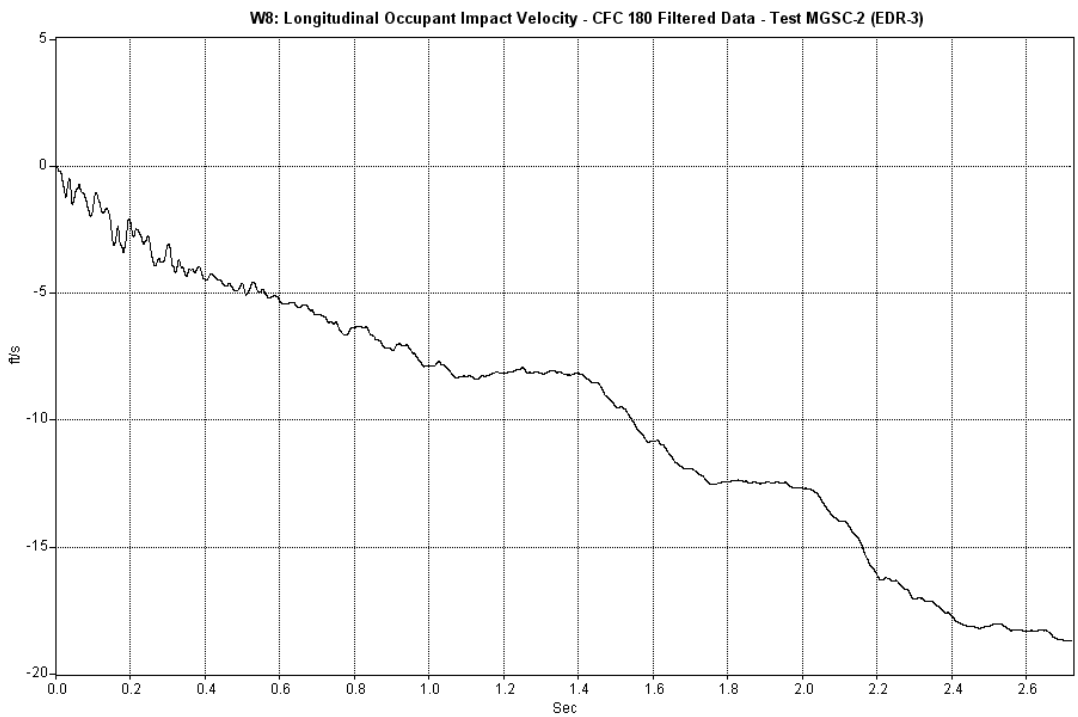

Figure C-9. Graph of Longitudinal Occupant Impact Velocity, MGSC-2 (2270P)

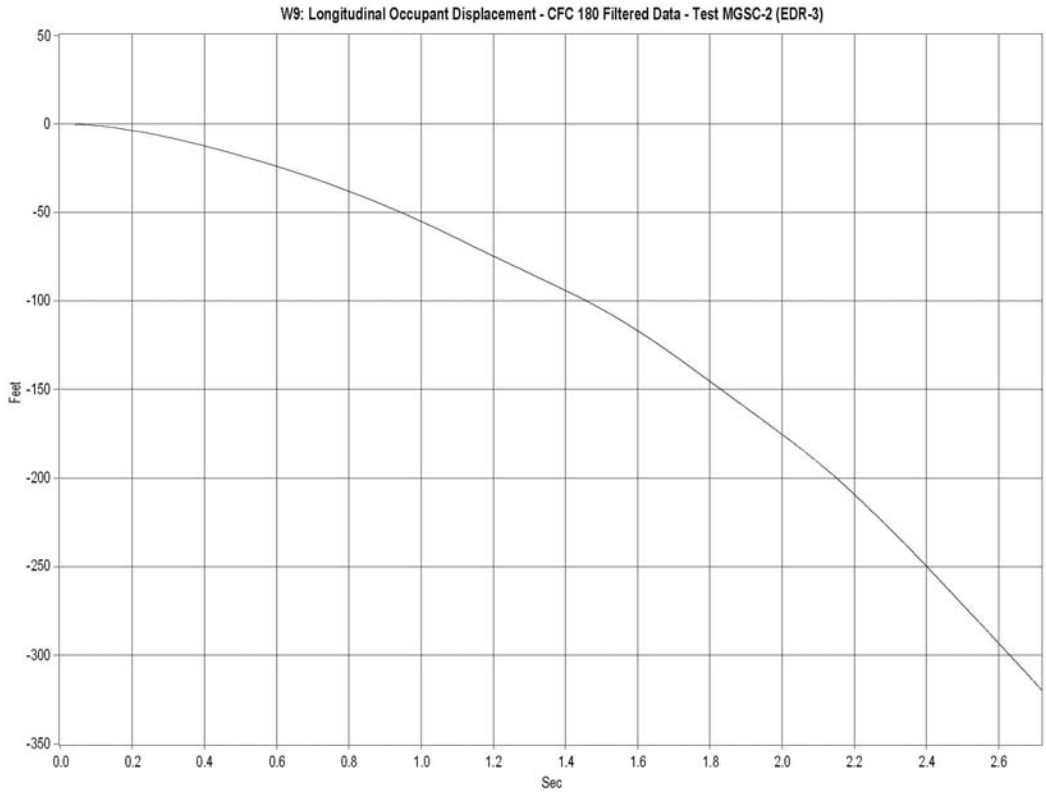

Figure C-10. Graph of Longitudinal Occupant Displacement, Test MGSC-2 (2270P)

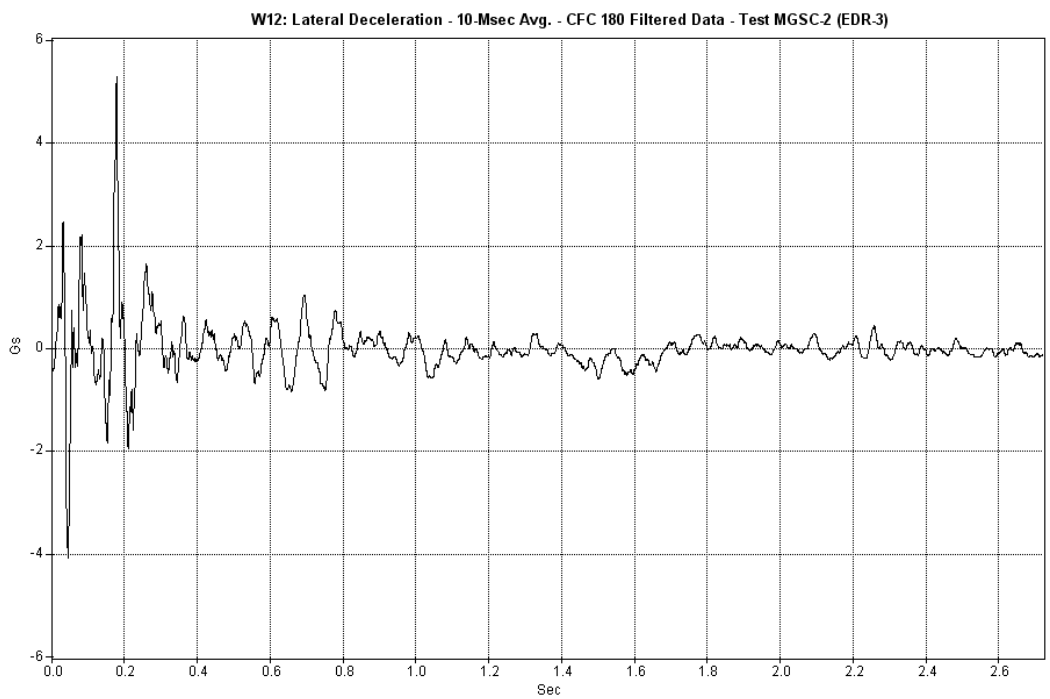

Figure C-11. Graph of Lateral Deceleration, Test MGSC-2 (2270P)

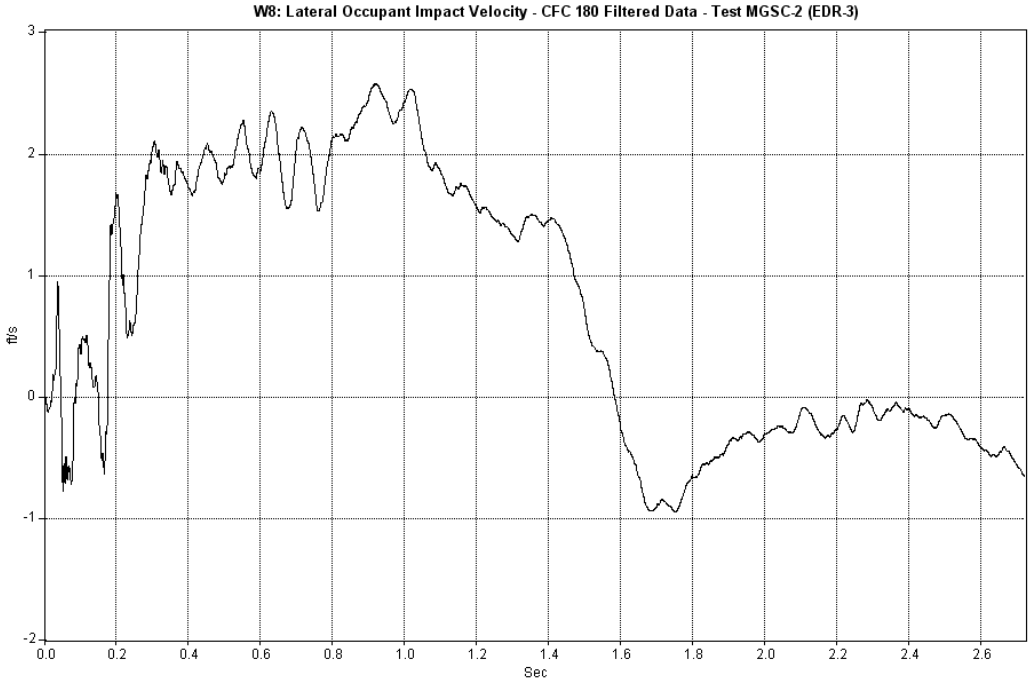

Figure C-12. Graph of Lateral Occupant Impact Velocity, Test MGSC-2 (2270P)

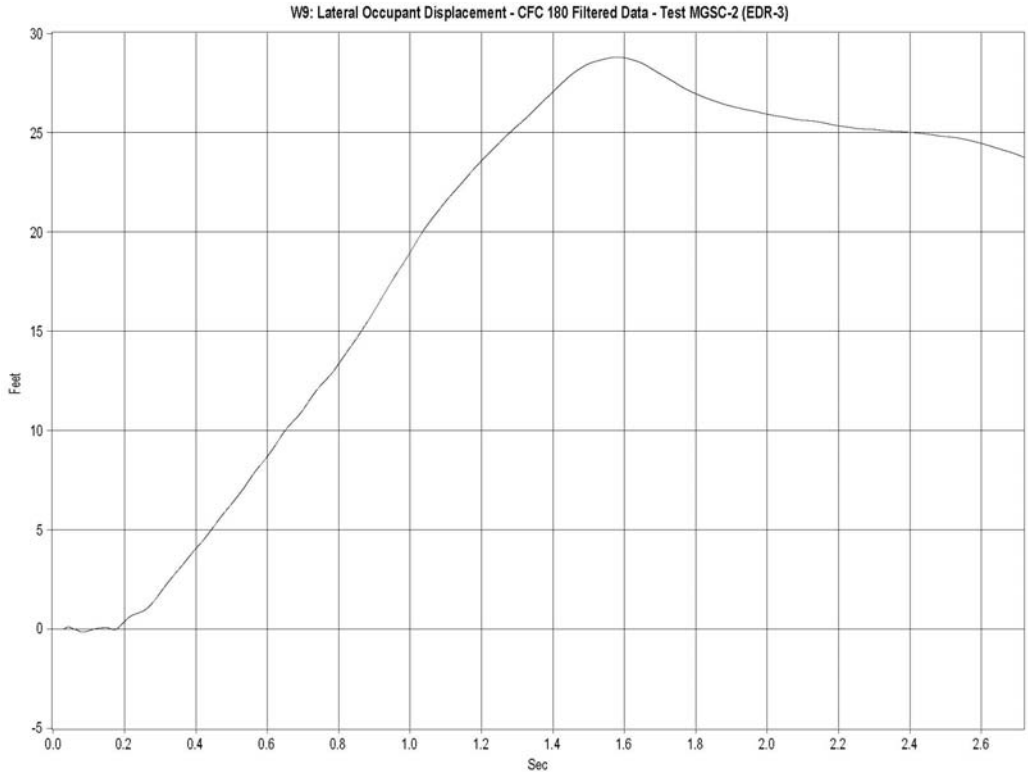

Figure C-13. Graph of Lateral Occupant Displacement, Test MGSC-2 (2270P)

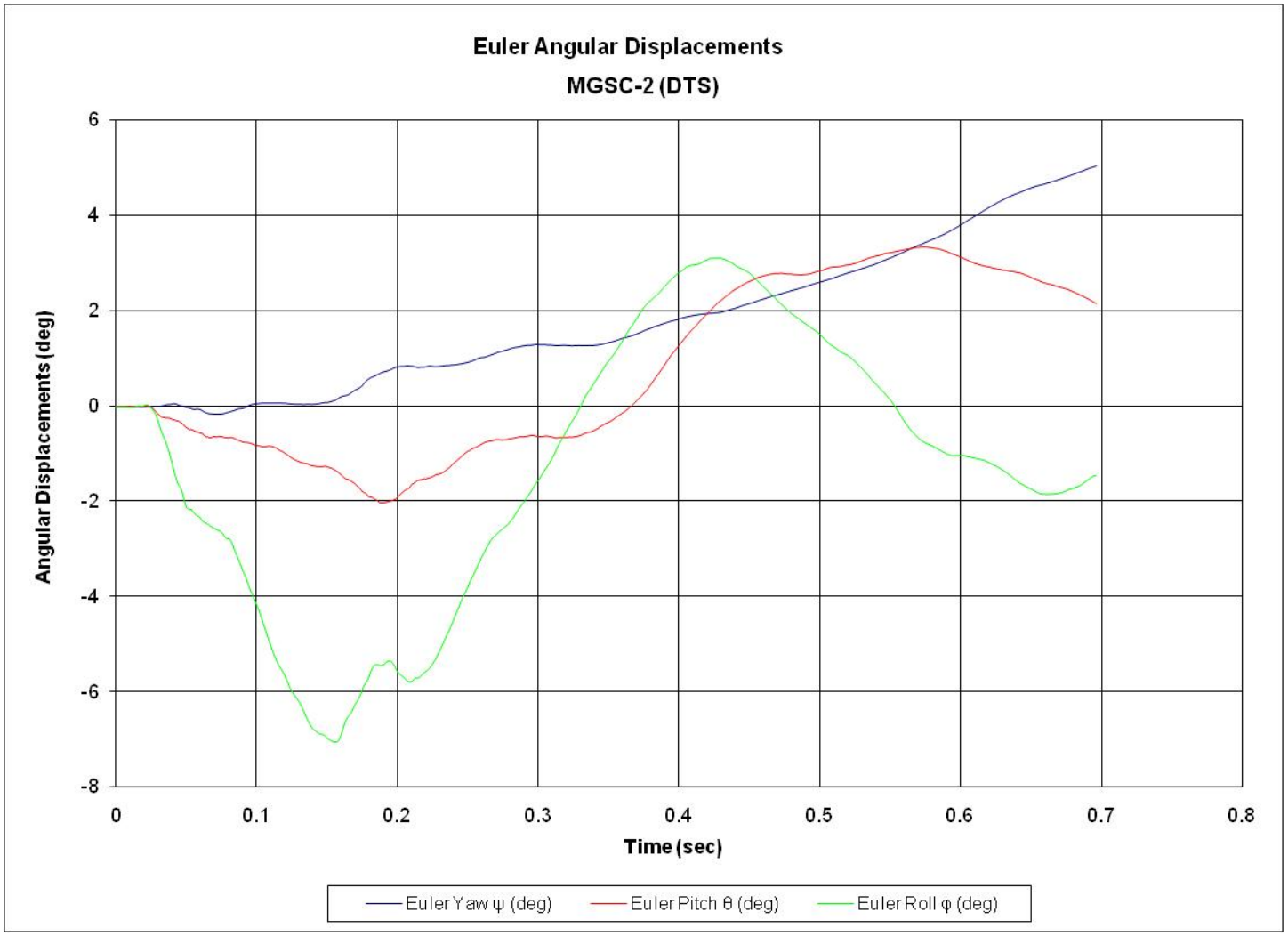

Figure C-14. Graph of Roll, Pitch, and Yaw Angular Displacements, Test MGSC-2 (2270P)

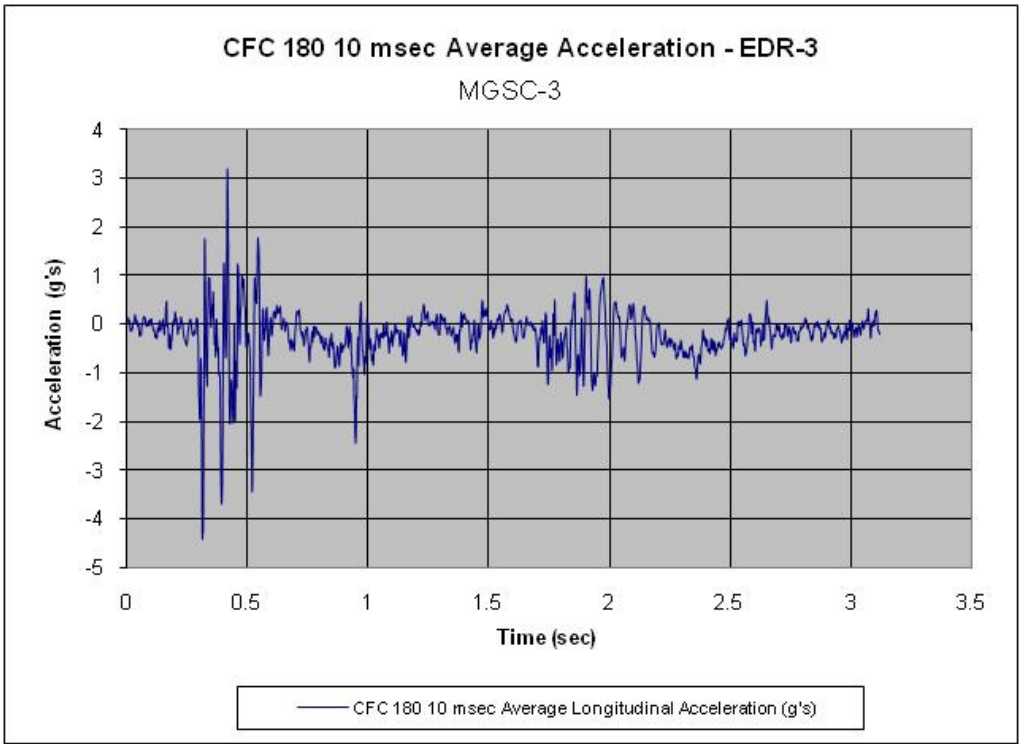

Figure C-15. Graph of Longitudinal Deceleration, Test MGSC-3 (1100C)

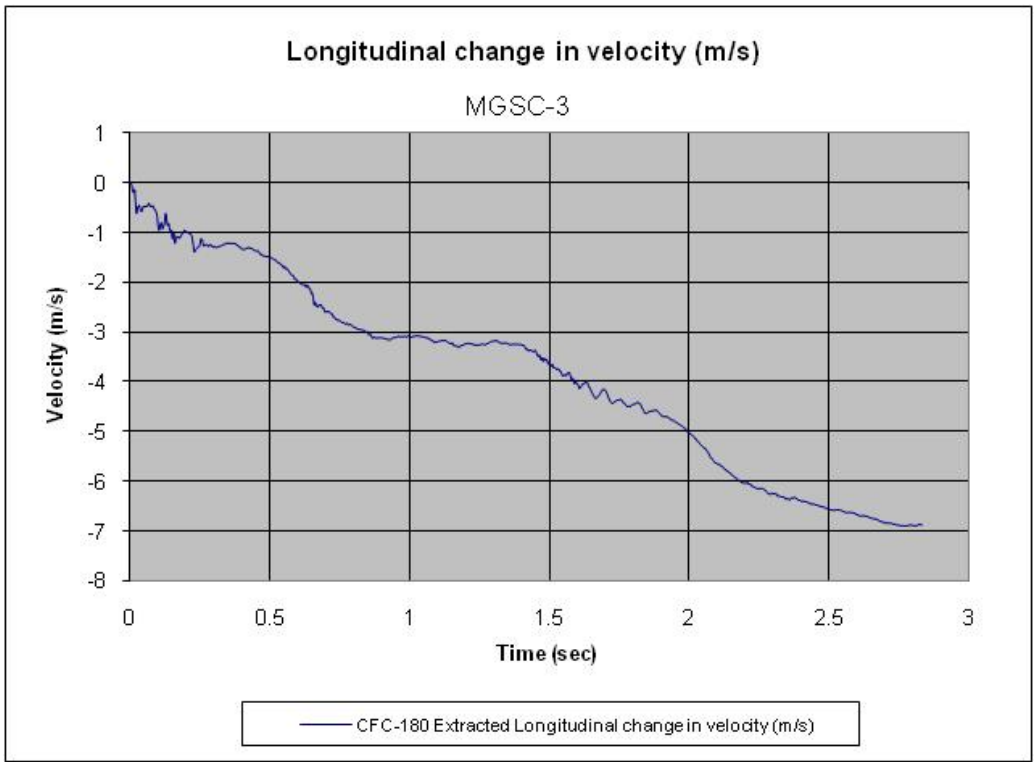

Figure C-16. Graph of Longitudinal Occupant Impact Velocity, Test MGSC-3 (1100C)

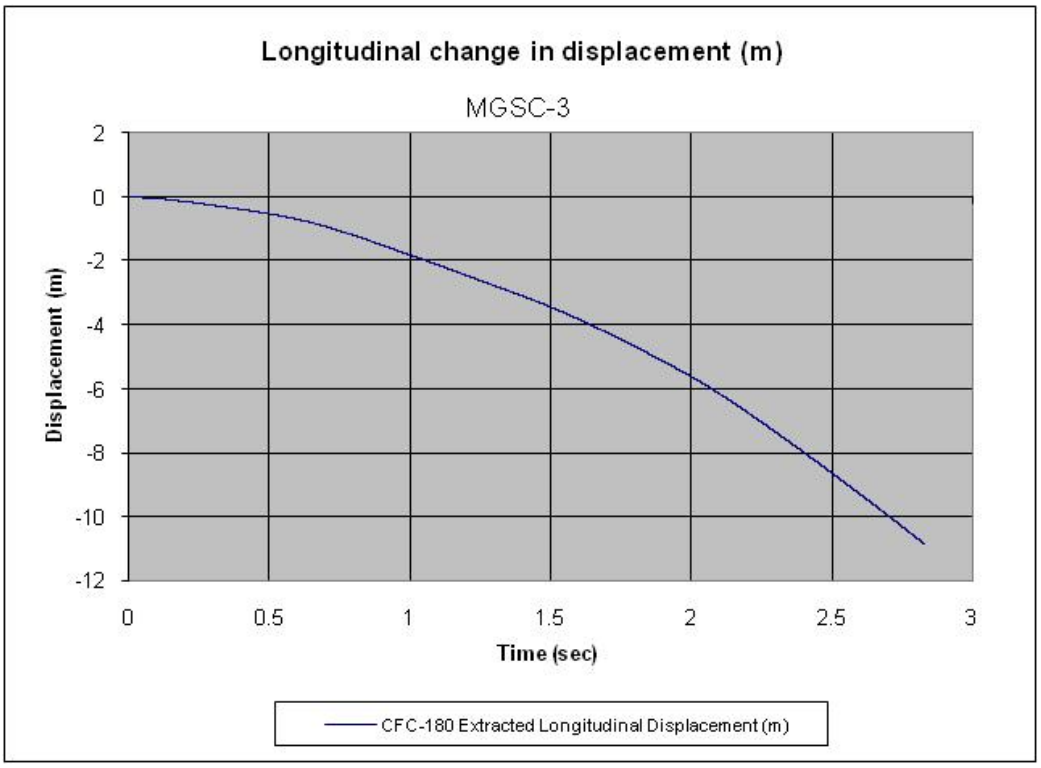

Figure C-17. Graph of Longitudinal Occupant Displacement, Test MGSC-3 (1100C)

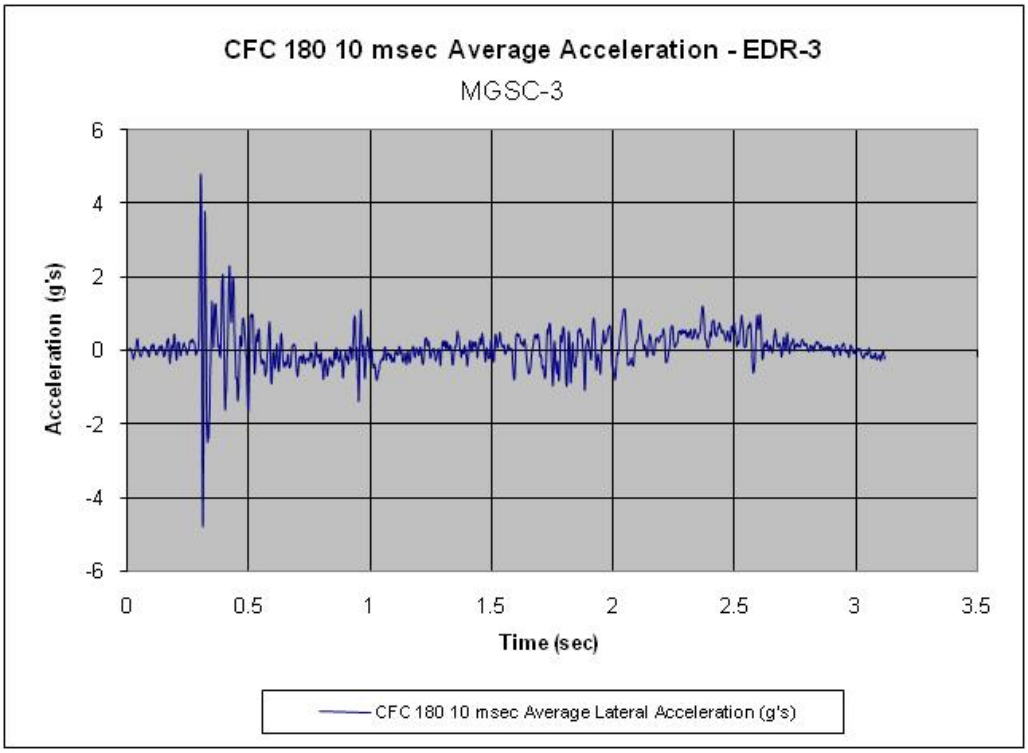

Figure C-18. Graph of Lateral Deceleration, Test MGSC-3 (1100C)

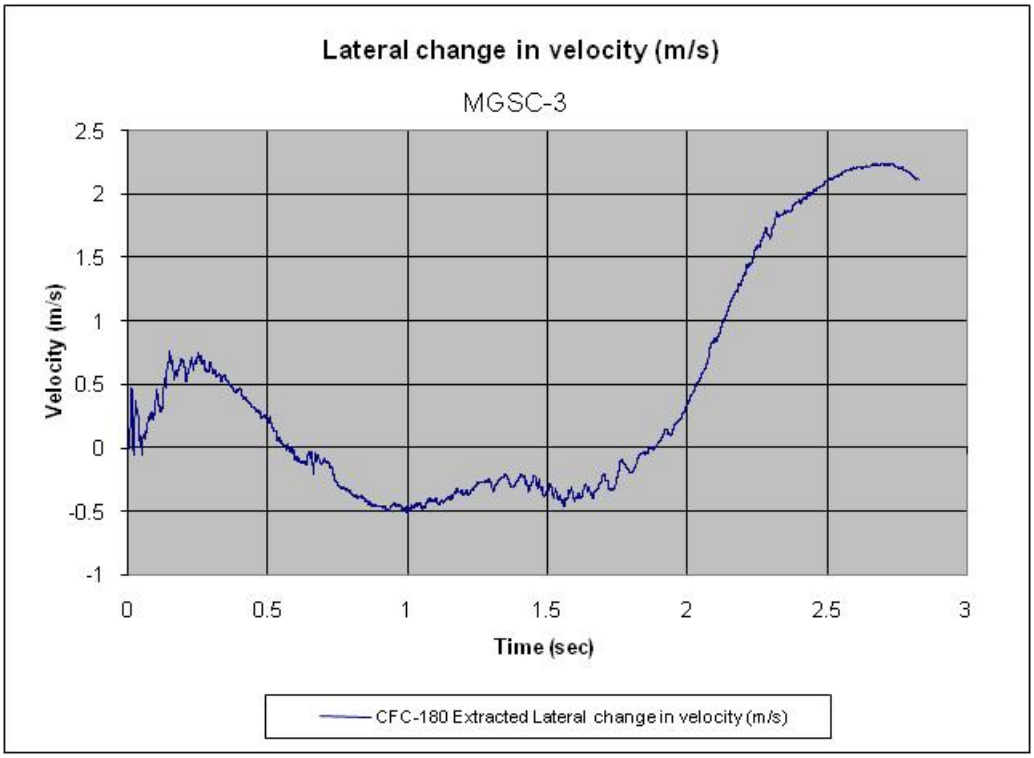

Figure C-19. Graph of Lateral Occupant Impact Velocity, Test MGSC-3 (1100C)

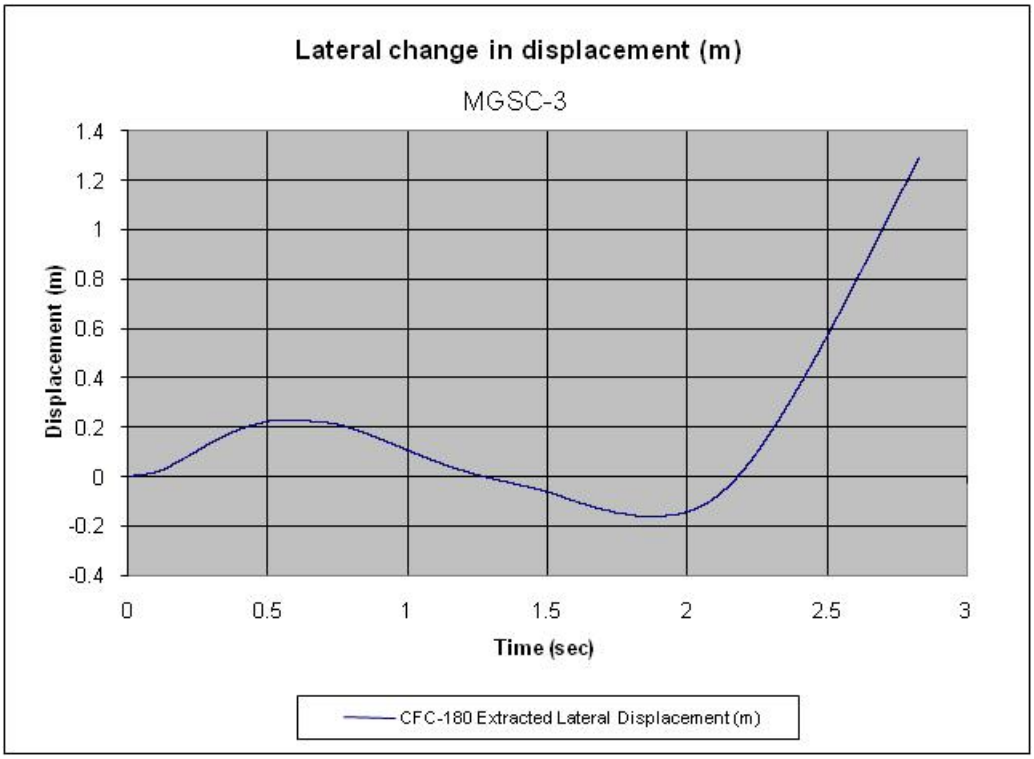

Figure C-20. Graph of Lateral Occupant Displacement, Test MGSC-3 (1100C)

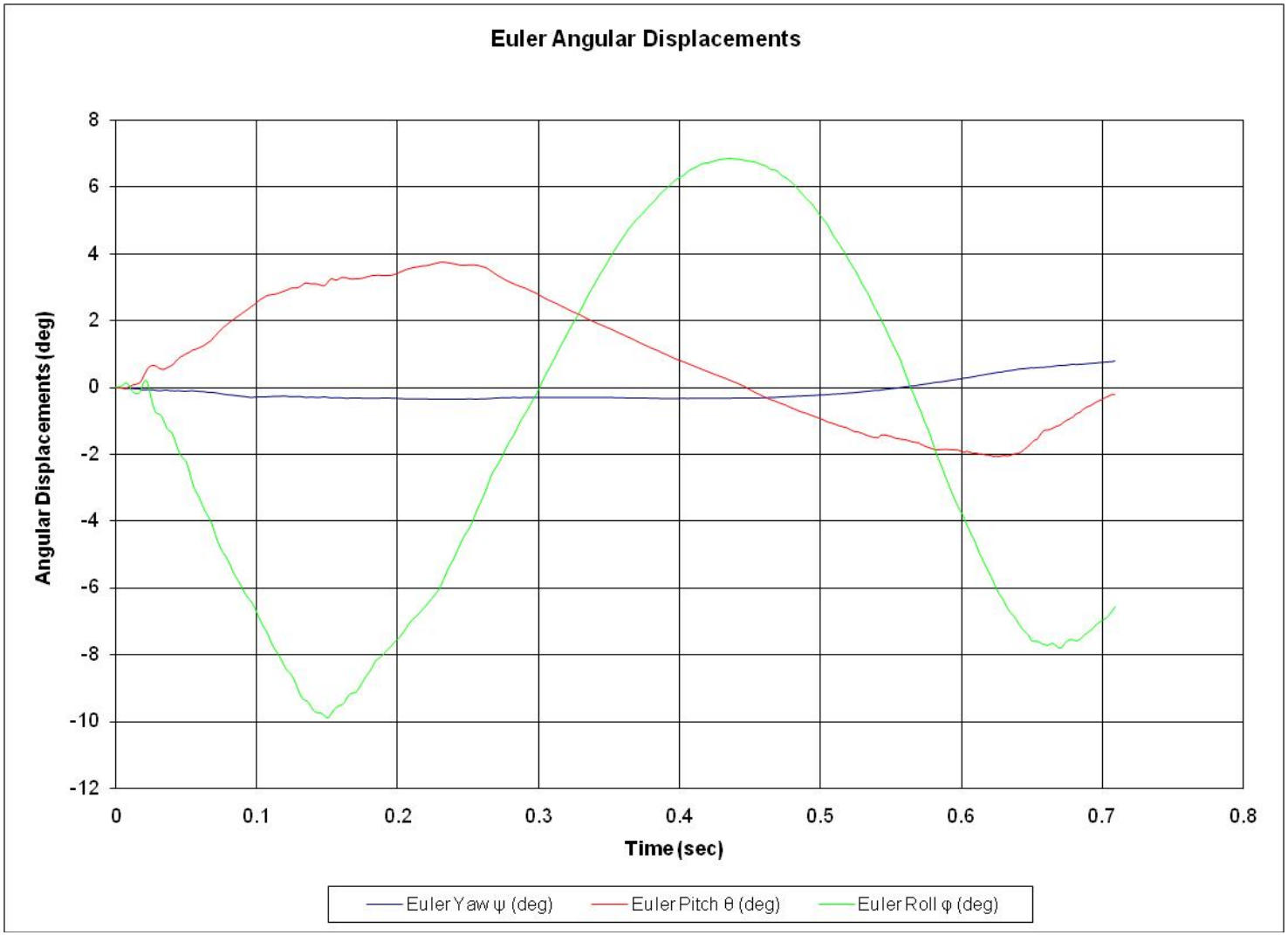

Figure C-21. Graph of Roll, Pitch, and Yaw Angular Displacements, Test MGSC-3 (1100C)

196

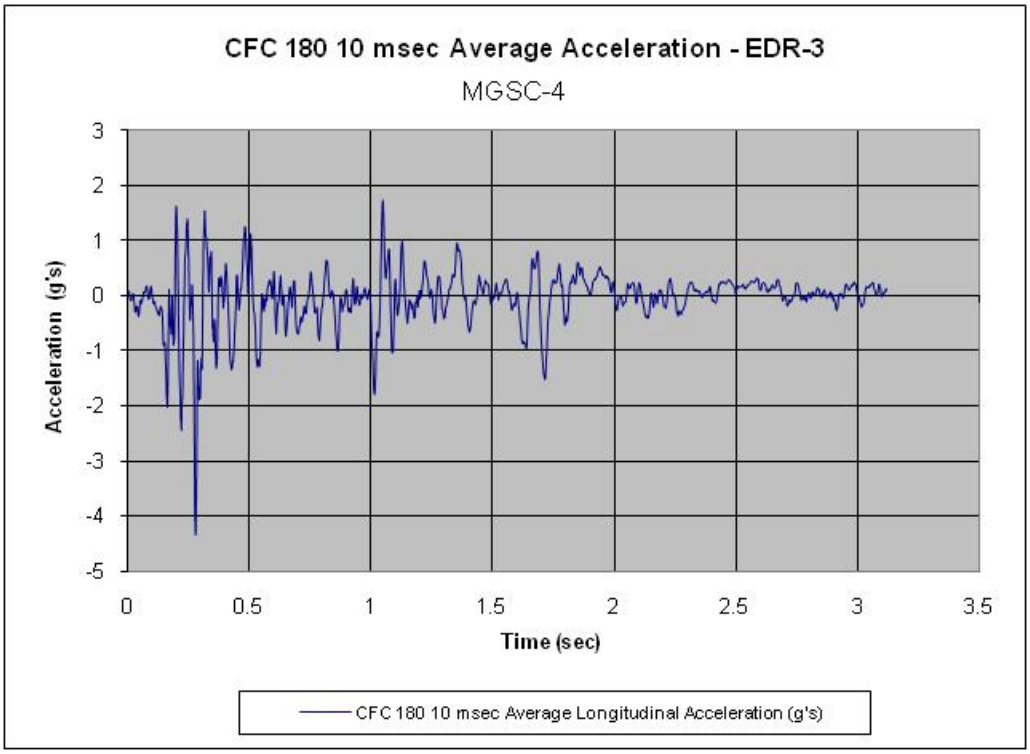

Figure C-22. Graph of Longitudinal Deceleration, Test MGSC-4 (2000P)

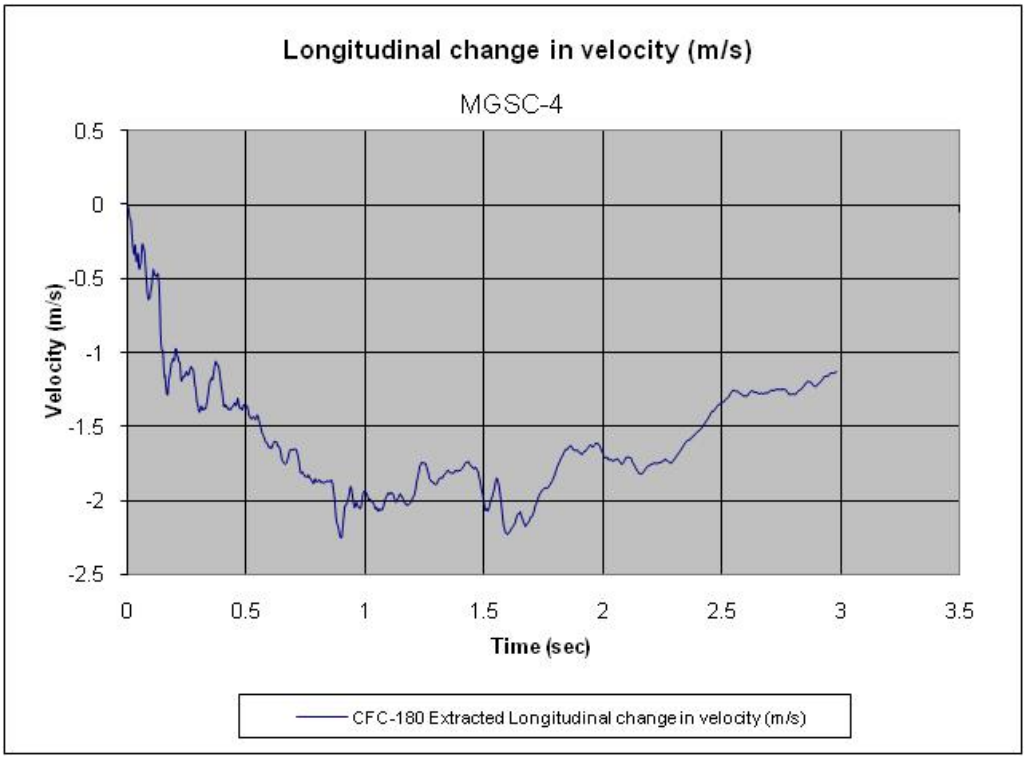

Figure C-23. Graph of Longitudinal Occupant Impact Velocity, Test MGSC-4 (2000P)

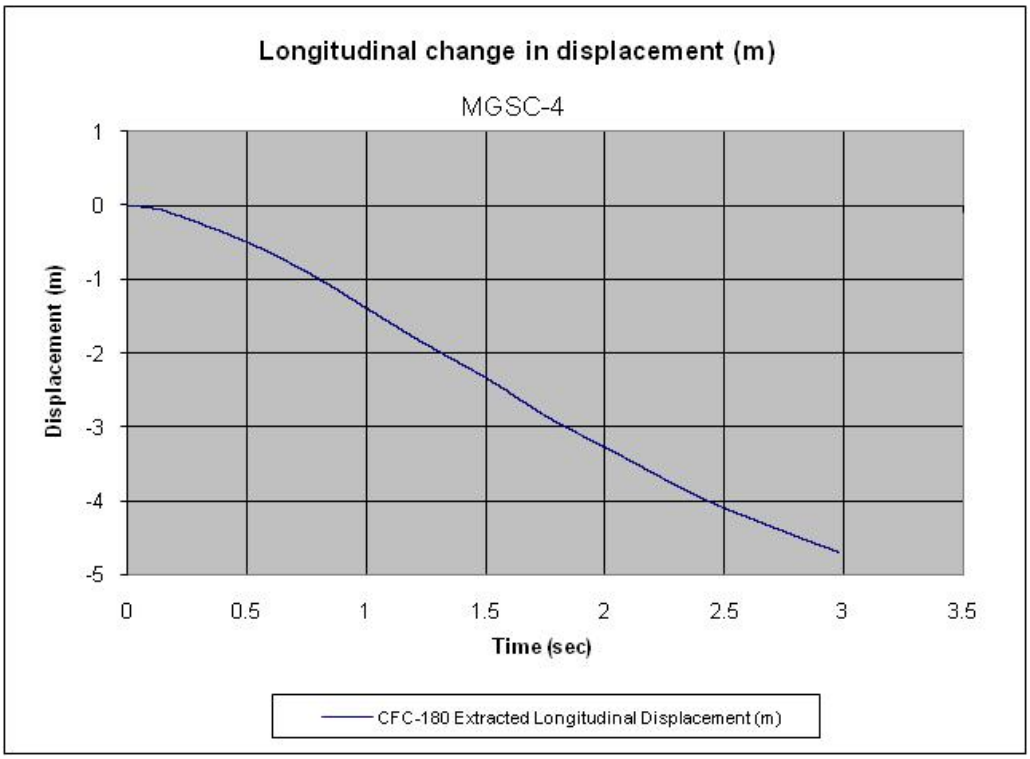

Figure C-24. Graph of Longitudinal Occupant Displacement, Test MGSC-4 (2000P)

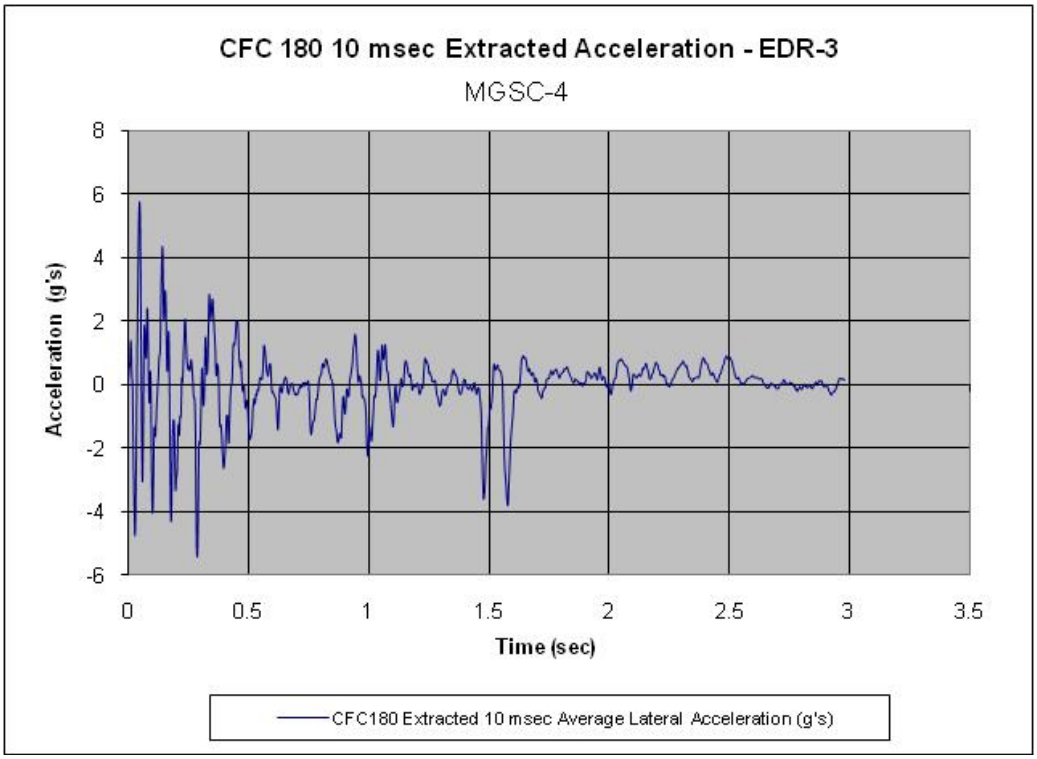

Figure C-25. Graph of Lateral Deceleration, Test MGSC-4 (2000P)

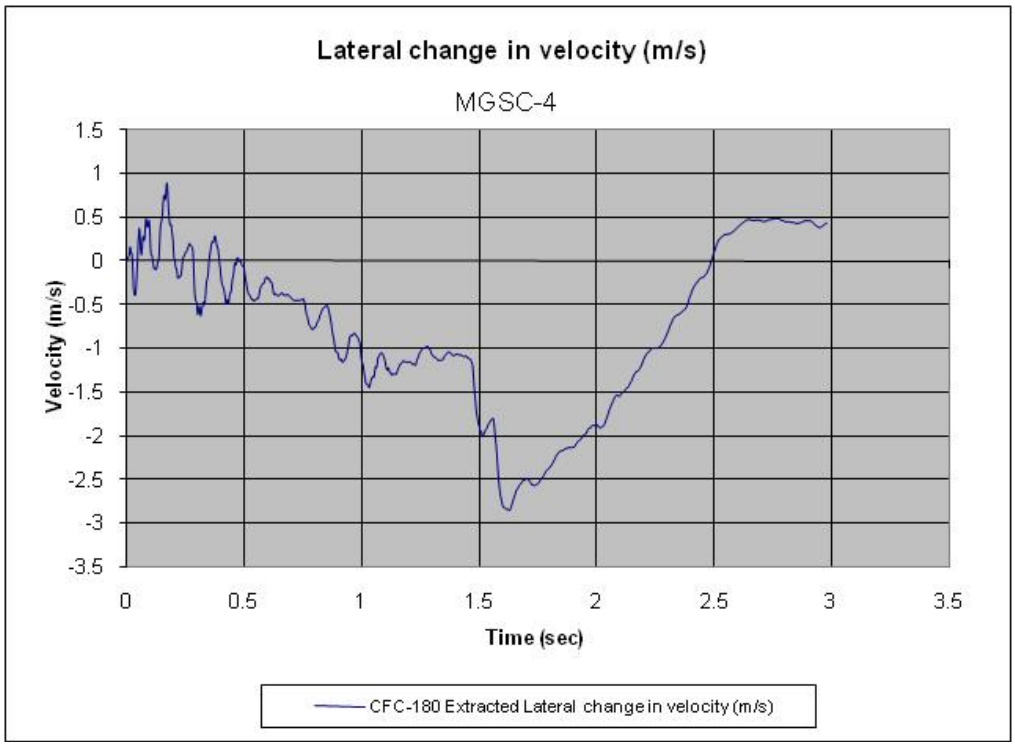

Figure C-26. Graph of Lateral Occupant Impact Velocity, Test MGSC-4 (2000P)

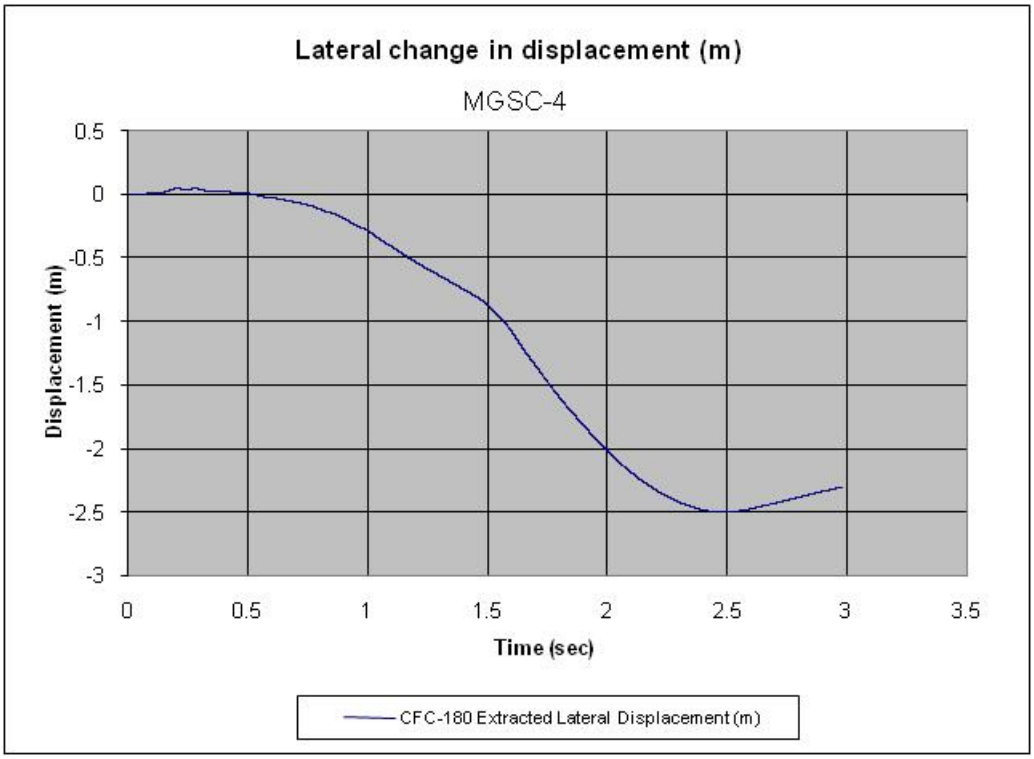

Figure C-27. Graph of Lateral Occupant Displacement, Test MGSC-4 (2000P)

Figure C-28. Graph of Roll, Pitch, and Yaw Angular Displacements, Test MGSC-4 (2000P)

APPENDIX D

TRANSFORMATION OF BUMPER CRITICAL IMPACT POINT TRAJECTORY FROM C.G. TARGET TRAJECTORY

The critical point trajectory was transformed from the C.G. target trajectory as a double check of the transformation from the bumper target trajectory. The transformation was conducted by coupling the C.G. target trajectory from the video analysis with the vehicle's pitch movement from the rate transducer using Figure D-1, Equations D-1 and D-2, and Table D-1. All of the transformations were first performed in the PLD coordinate system. Then, the PLD data were converted into CLD coordinate system to show the offset distance behind the curb. Due to the availability of measurement data, the transitions were only performed on the three pickup tests. The transition results were compared with the previous transitions from the bumper targets, as shown in Figures D-2 through D-4. Since it presented a good agreement with the transition from the bumper target, it proved the reliability of the previous transitions.

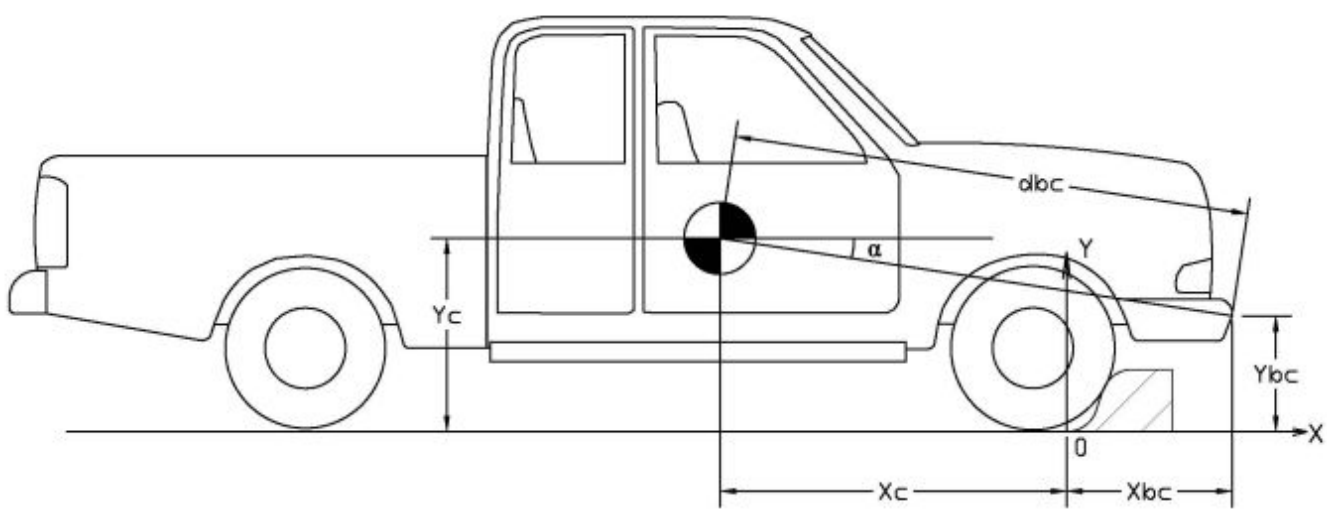

Figure D-1. Illustration of the Transition of bumper Critical Point Trajectory for C.G. Target Trajectory

$$X_{bc} = X_c + d_{bc} * \cos(\alpha + \Theta_p) \quad \text{Eq. D-1}$$
$$Y_{bc} = Y_c + d_{bc} * \sin(\alpha + \Theta_p) \quad \text{Eq. D-2}$$

X_{bc}= X coordinate of Bumper critical point
Y_{bc}= Y coordinate of Bumper critical point
X_c = X coordinate of C.G. target center
Y_c = Y coordinate of C.G. target center
d_{bc} = Distance between bumper critical point and C.G. target center
α = Initial angle between the critical impact point and the C.G. target center
Θ_p = Pitch Angle

Table D-1. Summary of Parameters for Bumper Critical Point Trajectory Transition

Test No.	MGSC-1	MGSC-2	MGSC-3	MGSC-4
α (degrees)	-2.71		NA	0.295
d_{bc}	2463.8 mm (97 in.)		NA	2415.7 mm (95.1 in.)

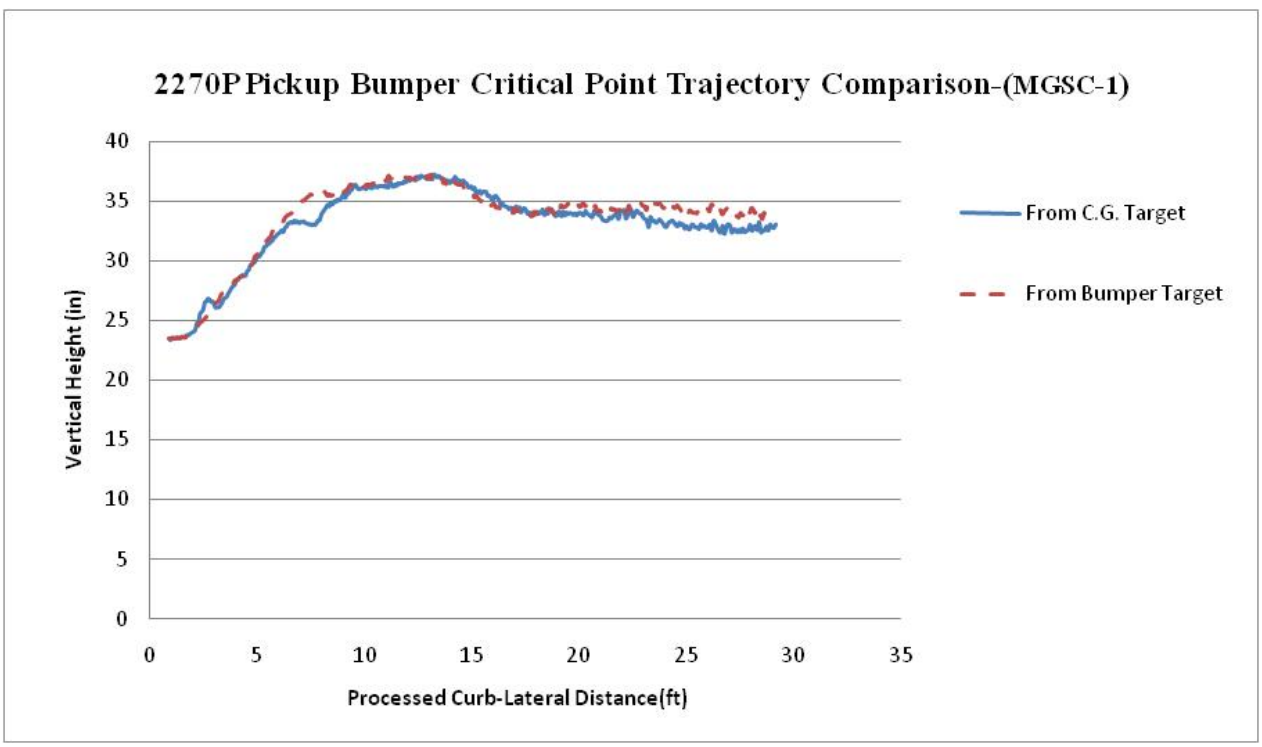

Figure D-2. Transition Comparison of the 2270P Pickup Critical Point Trajectory, Test MGSC-1

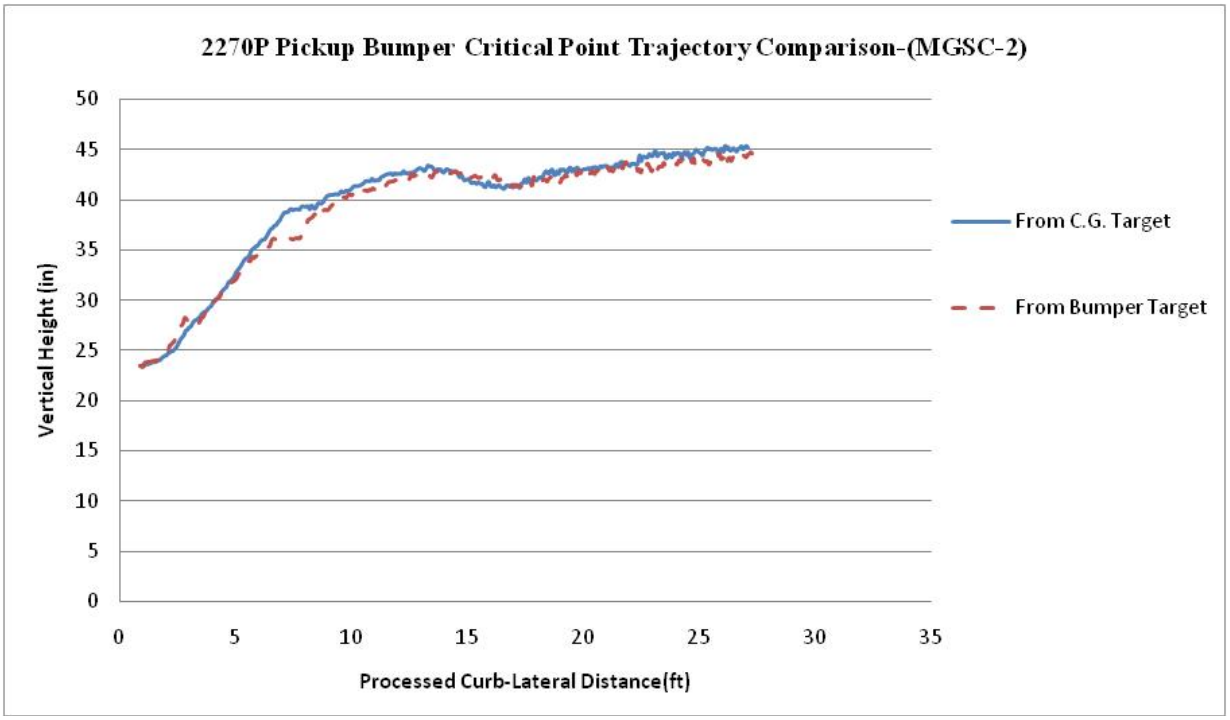

Figure D-3. Transition Comparison of the 2270P Pickup Critical Point Trajectory, Test MGSC-2

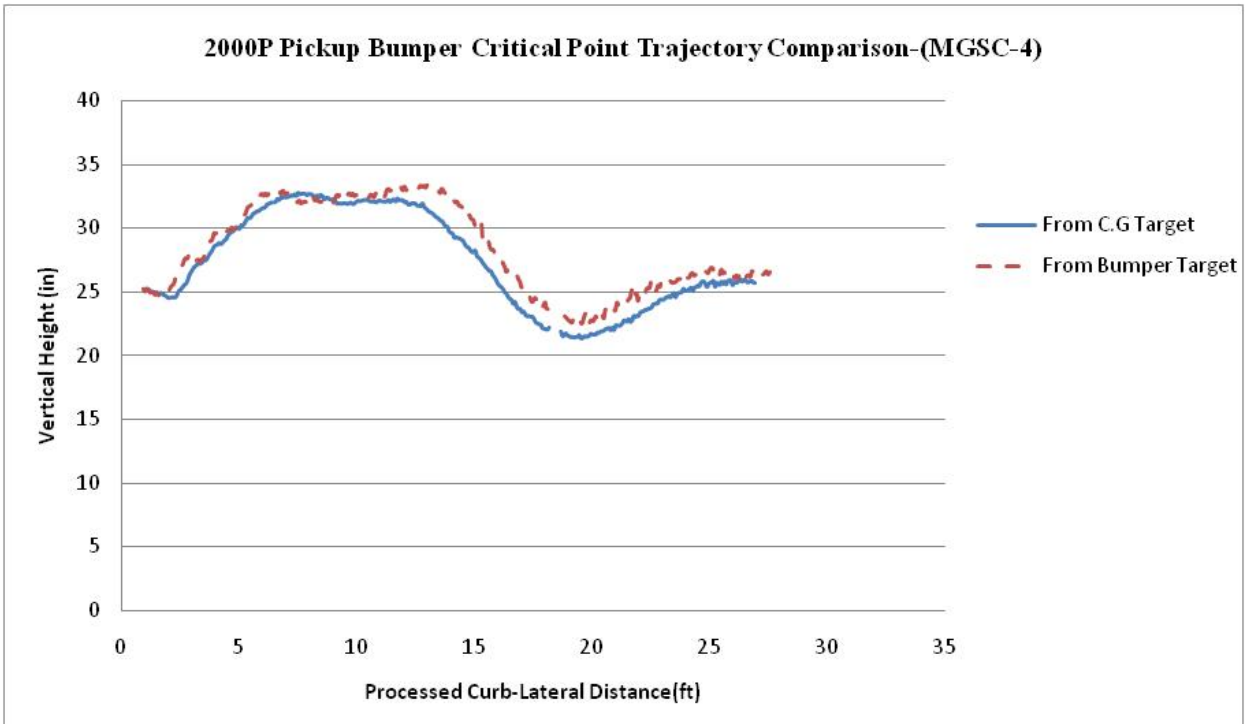

Figure D-4. Transition Comparison of the 2000P Pickup Critical Point Trajectory, Test (MGSC-4)

APPENDIX E

VEHICLE BUMPER CRITICAL IMPACT POINT TRAJECTORIES (ENGLISH UNITS)

Figure E-1. Pickup Bumper Critical Override Impact Point Trajectories (English)
Figure E-2. Small Passenger Car Critical Underride Impact Point Trajectory (English)
Figure E-3. Safe Zone Illustration for MGS Option I Installation behind Curb (English)
Figure E-4. Safe Zone Illustration for MGS Option II Installation behind Curb (English)

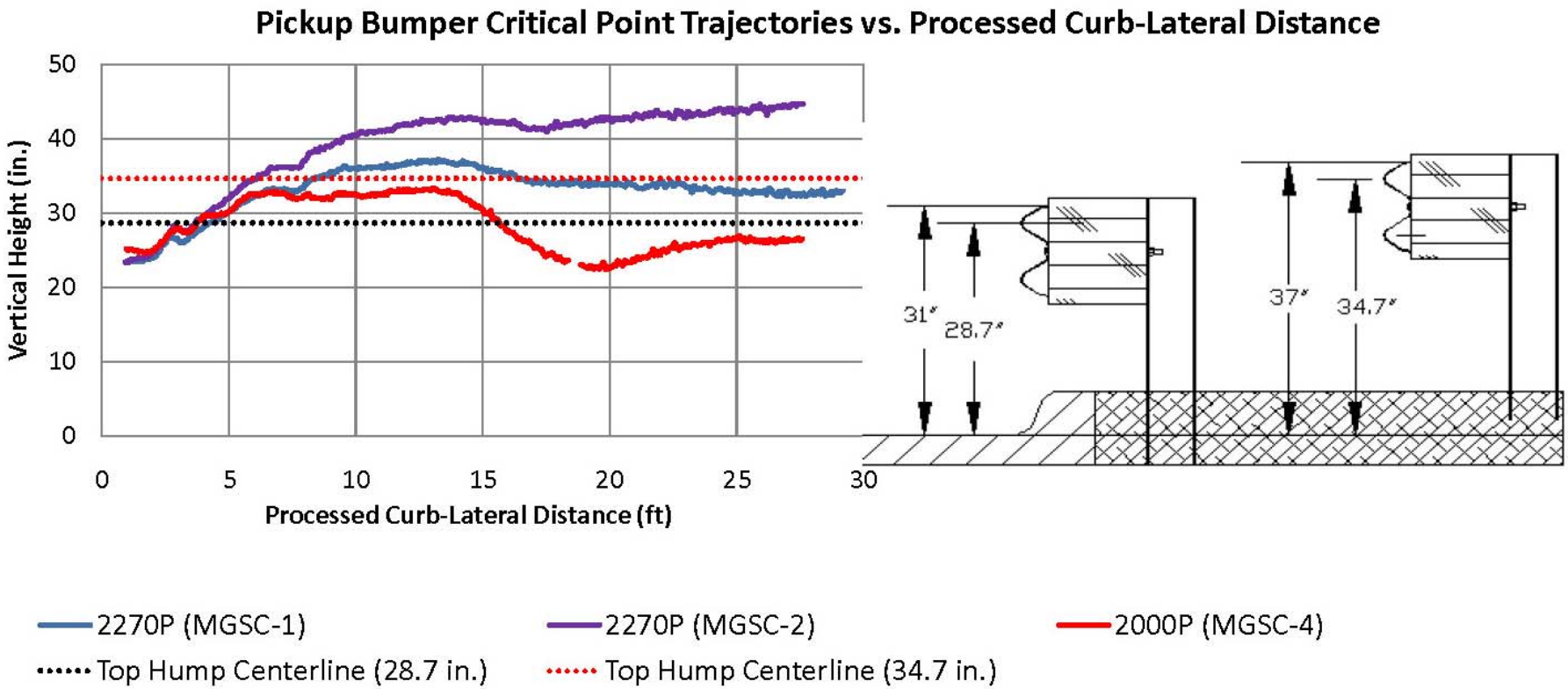

Figure E-1. Pickup Bumper Critical Override Impact Point Trajectories

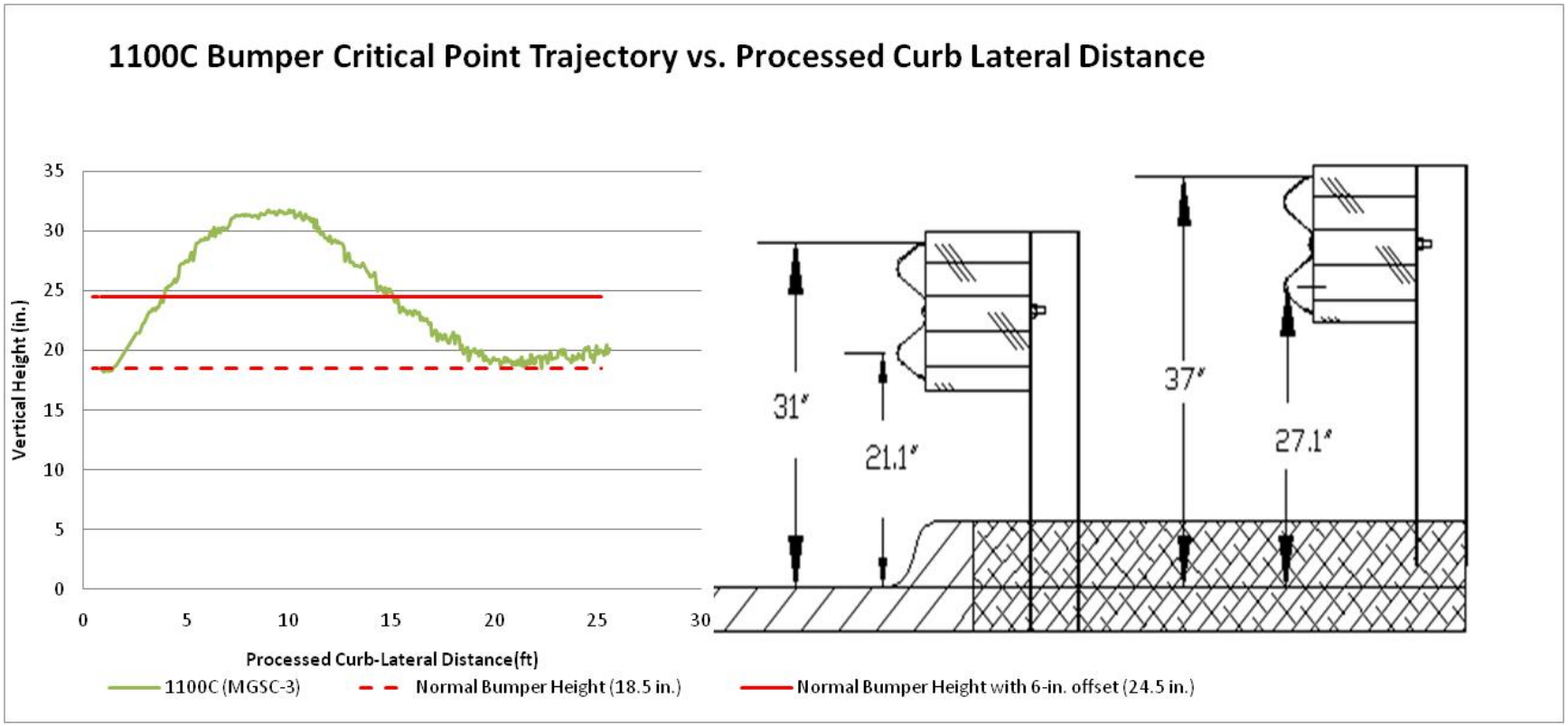

Figure E-2. Small Passenger Car Critical Underride Impact Point Trajectory

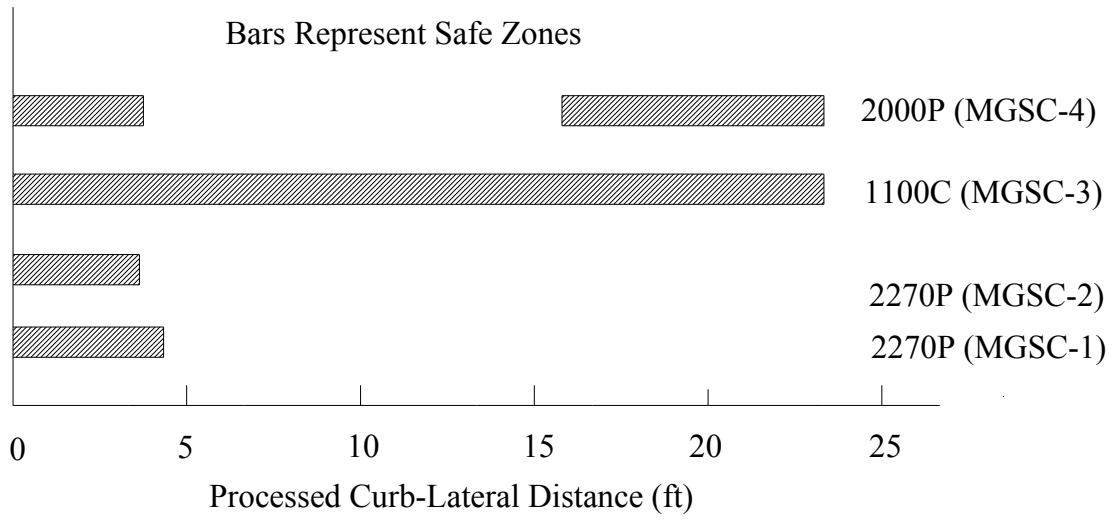

Figure E-3. Safe Zone Illustration for MGS Option I Installation behind Curb

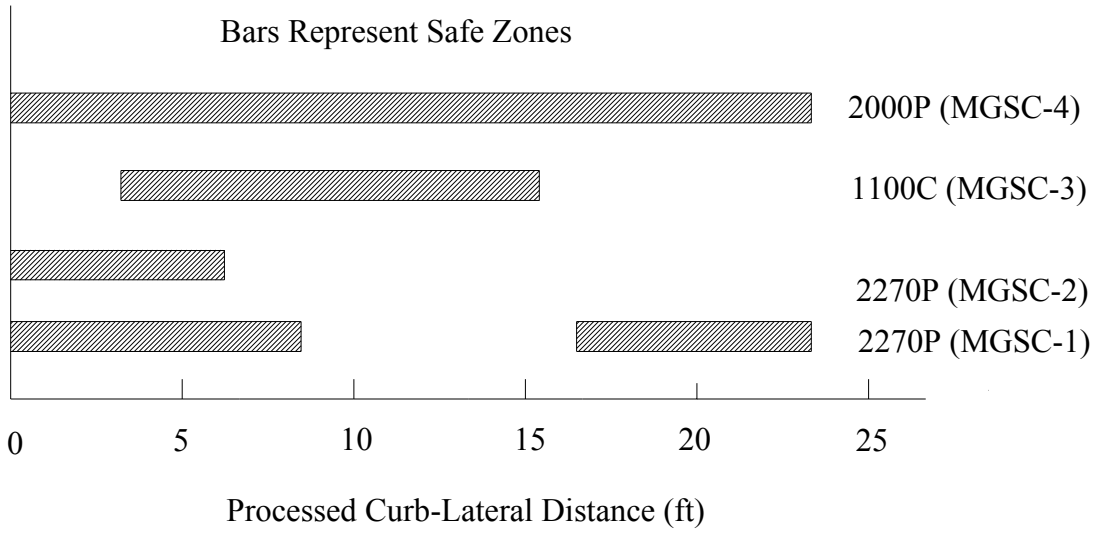

Figure E-4. Safe Zone Illustration for MGS Option II Installation behind Curb